CHEMICAL AND SPECTROSCOPIC STUDIES

OF COMPLEX ORGANIC MOLECULES

by

MICHAEL ALEC BERNSTEIN

B.Sc. (Hons.), University of Cape Town, 1977

A THESIS SUBMITTED IN PARTIAL FULFILLMENT OF

THE REQUIREMENTS FOR THE DEGREE OF

DOCTOR OF PHILOSOPHY

in

THE FACULTY OF GRADUATE STUDIES

(Department of Chemistry)

We accept this thesis as conforming

to the required standard

THE UNIVERSITY OF BRITISH COLUMBIA

July, 1983

In presenting this thesis in partial fulfilment of the requirements for an advanced degree at the University of British Columbia, I agree that the Library shall make it freely available for reference and study. I further agree that permission for extensive copying of this thesis for scholarly purposes may be granted by the head of my department or by his or her representatives. It is understood that copying or publication of this thesis for financial gain shall not be allowed without my written permission.

Department of _CHEMISTRY_____

The University of British Columbia
1956 Main Mall
Vancouver, Canada
V6T 1Y3

Date _22nd SEPT., 1983_____

ABSTRACT

This thesis concerns itself mainly with carbohydrates--
particularly their physical properties and structural elucidation by
spectroscopic methods. Within this broad area a variety of topics are
pursued. The findings are divided into two sections; the first deals
with several spectroscopic approaches applicable to the study of
carbohydrates attached to proteins (glycoproteins) and the second
concentrates on the use of recently devised NMR experiments which assist
in the determination of molecular structure and conformation.

The studies in Section I depend on methods for "activating"
specific loci in glycoprotein glycans. These materials were then
"tagged" with nitroxide spin-labels, which reported on the motional
flexibility of the glycans, which were found to be relatively mobile,
and hydrated. These data were corroborated in an analogous ^{2}H NMR
relaxation study, and this (superior) method reported very similar
motional behavior to that derived from ESR. Finally in this section,
the utility of synthetic glycoproteins in the analysis of ^{13}C NMR
spectra of glycoproteins was studied. First a useful method for
neoglycoprotein synthesis was devised, and proteins bearing homogeneous
and known sugars were prepared. It was determined that the ^{13}C chemical
shifts of the pendant sugars are comparable with those of the
corresponding glycoside. Enzymic oxidation studies suggested that this
approach may also greatly assist with the assignment of such
carbohydrate molecules.

The second section begins with a detailed survey of recent advances in high-resolution NMR spectroscopy which may be useful in organic chemistry. The experiments are explained in a simple conceptual fashion with illustrative data for trideuteriomethyl 2,3,4,6-tetra-O-(trideuterioacetyl)-α-D-glucopyranoside given throughout. This chapter is intended to be of assistance to the practicing organic chemist who has little experience in the areas of two-dimensional (2D) and other multi-pulse NMR procedures. A limited number of these experiments are used extensively in later chapters.

Chapter II.3 details a new procedure whereby an oligosaccharide may be characterized using NMR spectroscopy, only. The method is "de novo" in that little need be known about the molecule prior to analysis; it relies on the characterization of all coupling pathways within each constituent monosaccharide and the determination of linkage order by inter-residue nuclear Overhauser enhancements (nOe's). To increase the chemical shift dispersion, the molecule is derivatized – here as a per-O-acetate.

The ^{13}C and ^{1}H NMR spectra of the plant alkaloid, brucine, were then studied. The emphasis here was on the choice and utilization of selected 1- and 2D NMR methods to determine the molecular structure and conformation of a complex organic molecule in the minimum of time. Elucidation of the final conformational detail required a strong emphasis to be placed on nOe experiments.

Chapter II.4 details an NMR study on a cardenolide glycoside, digoxin. Using the strategies devised earlier, the molecule was studied at 500 MHz with the aim of complete spectral assignment. The spectrum is complicated by extensive signal overlap and the molecule's self-associative properties. For this reason, the lipophilic (steroidal) moiety displays broader lines which resist analysis by spin-echo experiments. The homonuclear and heteronuclear chemical shift correlation experiments performed well under these conditions, allowing the assignment of all sugar and some steroidal protons/carbons. The genin resonances proved relatively intractable, even with the powerful nOe experiment.

TABLE OF CONTENTS

LIST OF TABLES

LIST OF FIGURES

ACKNOWLEDGEMENT

SECTION I

CHAPTER I.1

MOTIONAL STUDIES ON GLYCOCONJUGATES

I.1.1 Background

It has been known for some time that carbohydrates are found in Nature covalently linked to proteins and lipids;[1] such molecules are commonly called "glycoproteins" and "glycolipids", respectively and collectively called glycoconjugates. Owing to the important part they play in life processes, a tremendous effort has been placed in the characterization and determination of the function and structure of such molecules. In what follows here we will concentrate on glycoproteins; spectroscopic studies have already played an important part in the understanding of their function, and part of the purpose of the work described in this chapter is to develop methods for chemically "tagging" specific carbohydrates to act as "reporters" on their microenvironment.

The literature on glycoproteins will not be reviewed in any great detail. Recent reviews by Montreuil,[2] and Wagh and Bahl[3] are highly recommended to the interested reader. Although somewhat dated now, a book by Sharon[4] covers most topics in an "easy to read" style. Membrane glycoproteins' structure and function are insightfully reviewed by Hughes.[5]

Glycoproteins have been found in virtually all forms of life, from microorganisms to man. They serve a wide range of functions, some of which we will soon high-light. The contribution of carbohydrate to the total mass of a glycoprotein varies considerably; thus, lysozyme has no detectable carbohydrate, and some blood-group substances are more

than 80% carbohydrate. An important class of structural molecules, the "proteoglycans",[6] is predominantly polysaccharide with a small proportion of protein. Three classes of monosaccharides are commonly found in mammalian glycoproteins:- (1) neutral sugars, such as D-galactose (gal), D-mannose (man), D-glucose (glc), and L-fucose (fuc), (2) N-acetyl amino sugars, N-acetyl glucosamine (glcNAc) and N-acetylgalactosamine (galNAc), and (3) acidic sugars such as the N-acetylneuraminic acids (NANA). The neuraminic acids may be O-acetylated. Plant and microbial glycoproteins may contain deoxy sugars: D-xylose, L-arabinose and L-rhamnose.

Although this diverse selection of monosaccharides in glycoproteins can, in principle, be joined in an almost infinite number of ways, consideration of the carbohydrate units and the nature of their linkage to the protein allows for a certain degree of classification.

The glycans may be conjugated to the protein in two ways,[7] and this is the first basis for classification. (1) The O-glycoproteins are O-glycosidically linked to L-serine or L-threonine units in the protein back-bone; (2) the N-glycoproteins are N-glycosidated to L-asparagine. With O-glycoproteins, the sugar residue involved in the linkage is often galNAc, and the glycan can be detached from the protein by alkali treatment, through a β-elimination reaction. N-glycoproteins involve so far only glcNAc attached to L-asparagine, and the glycan is usually isolated as a glycopeptide, following extentensive proteolysis; they are more abundant than O-glycoproteins. A proposed classification scheme has been put forward by Montreuil,[2] where he draws comparisons between

glycoprotein glycans and the immunoglobulins; in the glycoproteins he identifies certain non-specific "invariable", or "core" arrangements to which are attached additional carbohydrates coding the "variable" fraction.

The existance of certain "core" structures suggests a limited number of biosynthetic pathways. A key step in biosynthesis must be the attachment of the glycan to the protein. Thus, the amino-acid sequence around the glycan attachment has been extensively studied. N-Glycoproteins invariably are linked to the peptide sequence Asn*-X-Thr (Ser), where Asn is asparagine, Thr, is threonine and Ser is serine. But the presence of this sequence does not guarantee glycosylation, nor does the polarity of "X" determine the nature of carbohydrate units attached. Such an invariant amino-acid sequence is not clear with O-glycoproteins. Many details of the biosynthesis of glycoproteins are known and the elegant results are reviewed.[8,9]

Structure determination methods have developed considerably. Classical "wet" chemical methods are now augmented with GLC-MS (of methylated derivatives), enzymic (glycosidase) methods and NMR (^{13}C and ^{1}H). The interested reader is referred to the literature[10] for further details, and discussions in Ch. II.3.

Whilst the fundamental aspects of glycoproteins, outlined above, have concerned some workers, others have asked why such molecules even exist. Glycoproteins were initially thought to be metabolic accidents playing no important biological role. In fact, glycoproteins play two major roles. The first is physico-chemical. Glycoproteins such as the

"mucins" lubricate the gastro-intestinal tract, protecting it from mechanical abrasion and proteolytic attack. Such viscous glycoproteins also lubricate the eye-socket and form a barrier at the cervix, preventing bacteria from entering the uterus (and abdominal cavity). Upon ovulation, the mucin changes its physical properties so as to permit spermatazoa to enter the uterus and effect conception. The freezing point of certain Arctic fish's serum is depressed by special "anti-freeze" glycoproteins.[11] With all these glycoproteins, the integrity of the glycan is essential for proper activity. (With the enzyme ribonuclease B, however, the glycoprotein has the same activity as the carbohydrate-free counterpart, ribonuclease A).

The second major role of glycoproteins concerns molecular interactions. Here the carbohydrate units play a very important role. For example, the ABO and Lewis blood-group classification results from the constituent sugar residues of the glycan.[12] These glycans have received wide interest and an understanding of their properties has benefitted greatly from synthetic and conformational studies performed by Lemieux[13] and co-workers. The influenza virus is known to agglutinate red blood-cells, unless sialic acid is removed from the cell membranes.

The removal of the carbohydrate from the hormone, human chorionic gonadotropin, attenuates its biological activity, but does not affect its immunological activity. The former implies a contribution of the carbohydrate to the biological activity, in either an active or passive way. The latter is in accord with the well-known fact that glycan

moieties of glycoproteins are usually weakly immunogenic - the obvious
exception being the blood-group substances.

Glycan termini, often sialic acids, serve as determinants of
recognition for the clearance of some plasma glycoproteins. Ashwell and
Morell showed[14] that desialized ceruloplasmin, now bearing terminal
galactose residues, is rapidly removed from circulation by the liver.
Although this clearance mechanism is believed to be fairly general,
asialo-transferrin appears to have an alternative catabolic pathway.
Similarly, the presence of sialic acid on circulating mammalian
erythrocyte membranes is essential for their survival.[15]

The glycoproteins on cell-surfaces are believed to play an
important role in the way the cell interacts with both small molecules
in its surroundings and, indeed, other cells.[16] The importance of
cell-surface glycoproteins is perhaps exemplified by the changes
occuring upon malignant or viral transformation. The evidence for the
involvement of glycoproteins in cell-cell interactive phenomena is far
less detailed, but this topic still must be regarded as pivotal to the
understanding of how cells grow to form tissues, and what processes can
result in the loss of contact inhibition and the onset of uncontrolled
cancerous growth.

Most studies on glycoprotein functions have been phenomeno-
logical. For example, Ashwell and Morell[14] labelled ceruloplasmin with
a radionuclide and injected (a) the intact (sialo-) compound, and (b)
the asialo-compound into an animal, and measured the plasma half-life*

---

*The time required to reduce the plasma concentration by 50%.

in each case. In that the asialoceruloplasmin had a much shorter plasma half-life, it was obviously being cleared from circulation faster than the intact glycoprotein and this indicated that the sialic acid guarantees the glycoprotein's circulatory survival. The radioactivity accumulated in the liver, from whence the receptors for asialoceruloplasmin were later purified.

The work of Ashwell and Morell is now considered a "classic" in studies on the role of the carbohydrate moiety of glycoproteins. Others, however, have focussed their attention on the ways in which these phenomena occur at the molecular level; the purpose of this section of the thesis is to investigate some of the "tools" available for these studies, and the chemistry required to make them feasible. Such studies involve spectroscopy,[17] and nitroxide ESR (electron spin resonance) and NMR (nuclear magnetic resonance) spectroscopy will be used here.

A variety of methods and procedures have been investigated, and each chapter in this section will be introduced later in this discussion. First, we briefly discuss each spectroscopic method, to define its potential information content, and state the underlying prerequisites for its use.

The principal useful spectroscopic techniques available are fluorescence studies, ESR and NMR. Fluorescence and ESR studies invariably require chemical attachment ("labelling") of the macromolecule with a reporter probe; NMR may utilize naturally occuring nuclides (e.g. ^1H, ^{13}C or ^{31}P), or isotopic incorporation (e.g. ^2H, ^{19}F, or isotope enrichment of ^{13}C).

How do these methods provide information with atomic detail? The ESR of spin-labels has been used to yield different types of information, but we concentrate on just two. Firstly, the "g-value" of a nitroxide spin-label - analogous to chemical shift in NMR - is an indication of the polarity of the microenvironment in which the probe is resident. For this information to be of any value, site-specific incorporation is essential. This introduces an important concept underlying the studies in this chapter: chemical or enzymic methods are necessary to activate unique sites in a complex macromolecule for the derived data to be of significance.

Secondly, ESR, NMR relaxation and fluorescence studies share a common feature in that they can potentially provide the "correlation time", τ_c - a measure of the motional libration of the reporter group. Roughly, the correlation time is the time the probe takes to rotate in solution through one radian, and typical values encountered here range between 10^{-12} (fast rotation) and 10^{-9} s. (medium rotation).

Rather than placing too much significance on actual derived numbers, most studies rely on comparisons of τ_c upon perturbation of the system. For example, preparation of a range of fatty acids bearing reporter groups at different positions along the acyl chain, incorporation into a model membrane system and measurement of τ_c might allow one to come to some conclusions regarding the relative mobility of different points of the chain. Incorporating the previous concept of

site-specific modification, a person wishing to study the interacion between a specific carbohydrate residue and a macromolecule to which it is bound might label that residue specifically and monitor any changes in τ_c as the binding protein is added.

One advantage of attaching a spin-, fluorescent- or isotope-probe to a molecule is that the remainder of the molecule will be spectroscopically "silent" and interpretation of data may be greatly simplified. Still, a good case can be made for the observation of a glycoprotein's NMR spectrum at natural abundance. With proton spectra, the problem lies in the very large number of protein resonances overlapping with those of carbohydrate origin, and their assignment. Concerning the latter, a rich legacy of experimental data stems from the efforts of Vliegenthart's group in Holland, where the focus has been on the sequencing of glycopeptide carbohydrates.[19] With carbon spectra, the carbohydrate resonances fall into a "window" of the spectrum having very few protein resonances. Thus, the resonances are easily detectable (within the usual constraints of low inherent sensitivity), but assignment is still a problem.

Although the topics of this section easily fall into three distinct categories, it should be emphasized that the overlap is considerable, at the conceptual level. In fact, many concepts share elements in common with those described in Section II.

Chapter I.2 deals with nitroxide spin-label studies on intact and isolated glycoproteins. Methods were developed to specifically label

carbohydrate termini of sialo- and asiologlycoproteins,* and

correlation time measurements made. Similarly, red blood cell surface

glycoproteins and glycolipids were tagged in the same way and the data

compared.

Whilst the spin-labelling technique has many advantages, it is

also fraught with uncertainties.[20] Deuterium NMR is recognized as a

reliable source of correlation times, and in Ch. I.3 the synthetic

scheme was altered for the site-specific introduction of deuterons, and

correlation time measurements were made. This study was the first of

its kind in this area and, in addition to proving feasibility of the

technique, provided motional correlation times which compared favourably

with those from the ESR studies in Ch. I.2.

Next, the question of the observation of ^{1}H and ^{13}C NMR spectra

of glycoprotein glycans was addressed (Ch. I.4). Since most isolated

glyco-proteins bear a variety of different glycans on a single protein

core, it was decided that "synthetic glycoproteins" - neoglycoproteins[22]

- would be useful in that one could attach any (predetermined) sugar and

so simplify the analysis. Several schemes for neoglycoprotein synthesis

existed in the literature which failed to meet all the criteria we

considered necessary for a useful protocol, and we therefore developed

our own. Some of these materials were analysed by ^{1}H NMR, where a

multi-pulse experiment was used to assess the possibility of

differentially observing carbohydrate resonances under the broad protein

_____

*It is these carbohydrate residues which are responsible for the
recognition phenomena involved in the clearance of some plasma
glycoproteins and cells.

envelope. With ^{13}C NMR, assignments were made by comparisons of chemical shifts of the attached and unattached sugar glycoside, and chemical shift changes induced by enzymic modification. This also provided some interesting information on the requirements of the enzyme.

It will become evident in the following chapters that a variety of methodologies exist for the study of glycoproteins by spectroscopic methods, each with its particular benefits and shortcomings. The handling of biological materials also provides new technical challenges for most spectroscopists and organic chemists, but the restriction to relatively simple systems still allows conceptually important hypotheses to be tested.

REFERENCES

1. N. Sharon. Scientific American. 230 (5), 78-86 (1974); Ibid. 243 (5), 90-116 (1980).

2. J. Montreuil. Adv. Carbohydr. Chem. Biochem. 37, 157-223 (1980).

3. P.V. Wagh and O.P. Bahl. CRC Crit. Rev. Biochem. 10, 307-377 (1981).

4. N. Sharon. Complex carbohydrates: their chemistry, biosynthesis and functions. Addison-Wesley Publishing Co., Mass. 1975.

5. R.C. Hughes. Membrane glycoproteins: a review of structure and function. Butterworths, London, 1976.

6. V.C. Hascall. Biology of carbohydrates, Vol. 1. Edited by V. Ginsburg and P. Robbins. John Wiley and Sons, New York. 1981. pp 1-49.

7. N. Parthasarathy and S.M. Bose. J. Scient. Ind. Res. 37, 305-316 (1978).

8. A.P. Cornfield and R. Schauer. Biol. Cellulaire. 36, 213-226 (1979).

9. H. Schachter. The glycoconjugates, Vol. 2. Edited by M.I. Horowitz and W. Pigman. Academic Press, New York. 1978. pp 87-181.

10. Relevant references may be found in the review by Wagh and Bahl.[3]

11. R.E. Feeney. Amer. Scientist. 62, 712-719 (1974).

12. See Chaps 12 and 13 in Ref. 4.

13. R.U. Lemieux. Chem. Soc. Rev. 7, 423-452 (1978).

14. G. Ashwell and A.G. Morell. Adv. Enzymol. 41, 99-128 (1974).

15. D. Aminoff, W.C. Bell, and W.G. Vorder Bruegge. Prog. Clin. Biol. Res. 23, 569-581 (1978).

16. K.M. Yamada and J. Pouyssegur. Biochimie. 60, 1221-1233 (1978).

17. See, for example, H.C. Anderson. Ann. Rev. Biochem. 47, 359-383 (1978), and Ref. 3.

18. See, for example, A.D. Keith, M. Sharnoff, and G.E. Cohn. Biochim. Biophys. Acta. 300, 379-419 (1973), and other reviews cited in Ch. I.2.

19. J.F.G. Vliegenthart, H. van Halbeek, and L. Dorland. <u>Pure Appl. Chem.</u> 53, 45-77 (1981).

20. S. Schreier, C.F. Polnaszek, and I.C.P. Smith. <u>Biochim. Biophys. Acta.</u> 515, 375-436 (1978).

21. A. Allerhand, K. Dill, and W.J. Goux. <u>NMR Biochem., Symp.</u> Edited by S.J. Opella and P.Lu. Marcel Dekker, New York. 1978 (Pub. 1979). pp 31-50.

22. J.D. Aplin and J.C. Wriston, Jr. <u>CRC Crit. Rev. Biochem.</u> 10, 259-306 (1981).

CHAPTER I.2

ELECTRON SPIN RESONANCE STUDIES ON SPIN LABELLED GLYCOCONJUGATES

I.2.1 The ESR Spin Label Method

Electron Spin Resonance* (ESR) is an important spectroscopic tool

for the study of biological systems; some systems naturally have

unpaired electrons (e.g. those having some transition metals), while

other require incorporation of a paramagnetic reporter group such as a

"spin label". ESR spin labelling studies hae contributed enormously to

the understanding of such biological systems as membranes and enzymes,

and a number of excellent reviews and monographs cover many aspects of

the theory, applications and practical problems associated with the

technique.[1-11] Spin labels can be considered as probes, or reporter

groups designed to be specifically placed in a molecule, whose spectra

would detail the environment of the probe and, hopefully, that of the

molecule to which it is attached. Early work in our laboratory[12,13]

sensitized us to the many problems and difficulties associated with the

approach. Discussions later in the chapter will high-light some of

these in the context of this study.

Spin labels have the basic structure given below, where R_1 and R_2

are chosen to protect the nitroxide functionality from

disproportionation, and provide a means of attachment to the molecule

under study.

---

*Also called Electron Paramagnetic Resonance (EPR).

R₁\ /R₂
  N.
  |
  O
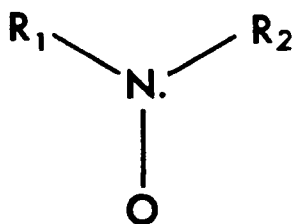
The basic resonance equation defines the large interaction of the electron spin with the laboratory magnetic field, and provides the central resonance frequency:-

$$h\nu = g_0 \, \beta \, \underline{B}_0 \qquad [I.2.1]$$

h is Planck's constant and ν the microwave frequency of the ESR spectrometer (of the order of GHz). β is the a constant for the electron, the Bohr magneton, $\underline{B}_0$ is the applied magnetic field (e.g. 0.34 T) and g_0 is the isotropic g-value of the system.

The unpaired electron in a spin label is largely confined to the N–O group, and largely resides in a π-orbital on the nitrogen. In that ^{14}N has a nuclear spin quantum number, $\underline{I} = 1$, it will have three nuclear spin quantum states ($\underline{m} = 1, 0, -1$) with which the unpaired electron may interact. This is called the electron–nuclear hyperfine interaction, and results in a three-line spectrum being observed, with the lines having equal intensity and separated by the hyperfine coupling, $\underline{a}_0$ (ca. 0.17 mT). Fig. I.2.1 shows a typical ESR spectrum of a nitroxide tumbling rapidly in solution, and shows the measurements of g_0, $\underline{a}_0$ and peak-to-peak line widths, $\underline{W}_0$, $\underline{W}_1$ and $\underline{W}_{-1}$ (corresponding to the three

labelled transitions). The recorded lines are first-derivative and require integration to yield absorption spectra.

The spectrum in Fig. I.2.1 represents isotropically averaged values of $\underline{a}$ and g. By "doping" a crystal of the diamagnetic analogue (reduced) of a spin label with the paramagnetic molecule and orienting it in the applied magnetic field, an angular dependence is observed in the g-value and coupling constant ($\underline{a}$). The extremes in g and $\underline{a}$ lie
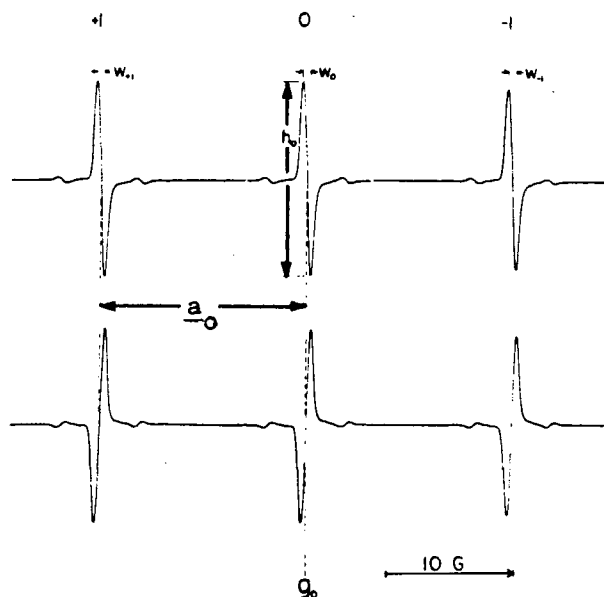
Fig. I.2.1.   Solution ESR spectrum of a rapidly tumbling nitroxide spin label illustrating the measurement of parameters. (From Ref. 10).

along the principal molecular x, y and z axes, where the x-axis lies parallel to the N-O bond, and the z-axis along the nitrogen 2p (π) orbital. For each nitroxide, the three values of g and $\underline{a}$ can be measured; $\underline{a}_{zz} > \underline{a}_{xx}$, $\underline{a}_{yy}$, and $\underline{a}_{xx} \approx \underline{a}_{yy}$.

The principal uses of nitroxide spin labels pertinent to this

chapter lie in their ability to report on (a) polarity (by means of $\underline{a}_0$) and (b) molecular motion (by mean of line widths and heights). In solution, the nitroxide can be considered to be made up of the following resonance forms, with the zwitterion species favoured in a polar environment:-

$$N \text{———} O \cdot \quad \longleftrightarrow \quad {}^+N \cdot \text{———} O^-$$

Fig. I.2.2 illustrates the basic changes in line-shapes as the motion of a spin label is restricted. We have seen that a freely tumbling nitroxide spin label in a non-viscous solvent displays a symmetrical pattern of three lines of equal intensity (Fig. I.2.1). As the motion is further restricted (here, by increasing the solvent viscosity) it is seen that first the high-field line broadens, then the low-field and, finally, the central line. Additionally, spectral features begin to appear at frequencies distant from the original ones ("outer extrema"). Ultimately, a "glass" spectrum is observed, and any further restriction of motion will not be apparent in the spectrum: the ESR spin labelling technique selectively reports on motions ("correlation times") between 10^{-11} and 10^{-8} s rad^{-1} - a useful range for most biological studies.

The derivation of accurate correlation times from such spectra is difficult,[9] and only totally convincing when substantiated by spectral simulations. However, an approximate value is often all that is necessary when two spectra are to be compared where the introduction of a pertubation induces large changes in probe mobility. For such cases, simplified equations may be derived[12] and these have been used in this chapter:-
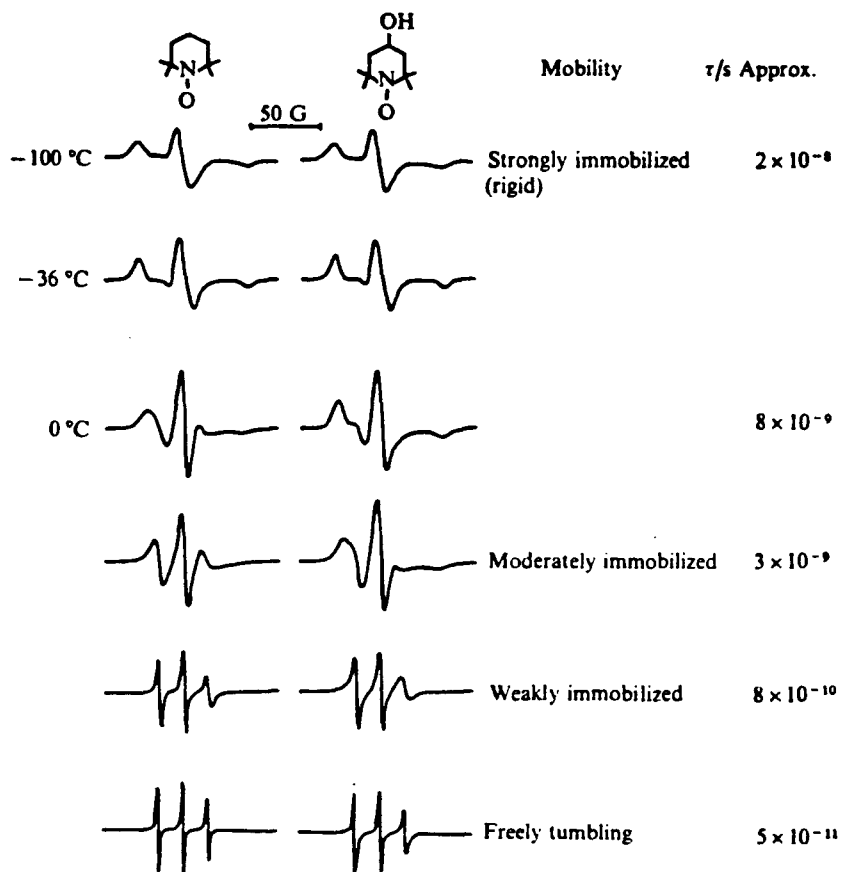
Fig. I.2.2. Solution ESR spectra of a nitroxide spin label as a
function of molecular motion, controlled by altering
solvent viscosity. (Most mobile, bottom spectrum;
least mobile, top spectrum. From Ref. 3).

$$\tau_c = \underline{W}_1 * 6.6 * 10^{-10} \left[\left[\frac{h_1}{h_{-1}} \right]^{1/2} - 1 \right] \qquad [I.2.2]$$

$$\tau_c = \underline{W}_0 * 6.8 * 10^{-10} \left[\left[\frac{h_0}{h_{-1}} \right]^{1/2} - \left[\frac{h_0}{h_1} \right]^{1/2} \right] \qquad [I.2.3]$$

$$\tau_c = \underline{W}_0 * 6.7 * 10^{-10} \left[\left[\frac{h_0}{h_{-1}} \right]^{1/2} + \left[\frac{h_0}{h_1} \right]^{1/2} - 2 \right] \qquad [I.2.4]$$

Generally, τ_c was calculated by all three equations and the average reported as the correlation time.

Aside from its high signal-to-noise sensitivity (concentrations between 10^{-5} and 10^{-7} $\underline{M}$ are the lower limit of detectability, depending on the line broadening) a reflection of motion and polarity, nitroxide spin labels have the further benefit that the spin concentration may be determined. Double integration of the spectrum is necessary, as it is the area under the absorption peaks which varies linearly with concentration. By knowing the spin concentration, the efficacy of a chemical coupling procedure may be assessed.

As mentioned previously, the spin label must provide the means for attachment to the biological substrate. Although several basic skeletons exist, the studies in this chapter involve the spin label based on the 2,2,6,6-tetramethylpiperidine-N-oxyl structure, bearing substituents at C-4.
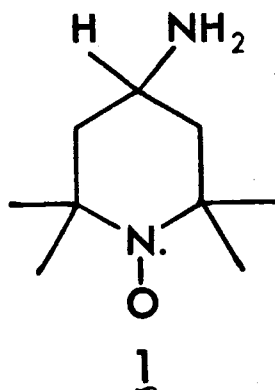
With R representing a secondary amine, the molecule is 2,2,6,6-tetra-methylpiperidine-4-amino-N-oxyl (1)*.

I.2.2 Spin Labelling of Glycoconjugates

In this chapter a modest start is made towards answering the questions of how carbohydrates attached to proteins reorient in solution.

To illustrate[14] the potential of site-specific spin labelling of the carbohydrate portion of glycoconjugates, we chose a plasma glycoprotein, fetuin[15] (isolated from foetal calf serum), a mucin,[16] bovine submaxillary mucin (BSM, isolated from boxine submaxillary glands), and human erythrocytes (red blood cells ≡ RBC's). In all cases, the goal was the labelling of the glycoconjugate sugar termini.

All three materials are known to be rich in sialic acids (N-acetyl neuraminic acid ≡ NANA), usually at the "non-reducing" terminus, attached to gal or galNAc. Fetuin bears O-glycosides and

_____

*This is often called "TEMPAMINE" and indicated in synthetic pathways as SL-NH$_2$.

```
  NANA            NANA            NANA                                          NANA
   │α2→3           │α2→3           │α2→3                                         │α2→3
   ↓               ↓               ↓                                             ↓
  Gal             Gal             Gal                                          Gal
   │β1→4           │β1→4           │β1→4                                         │β1→3
   ↓               ↓               ↓                                             ↓
  GlcNAc          GlcNAc          GlcNAc              NANAα(2→6)GalNAc
   │β1→2           │β1→3(4)        │β1→2(4,6)                                     │α
   ↓               ↓               ↓                                             ↓
  Manα(1→2(6))Manα(1→3)Man(1→4)GlcNAcβ(1→4)GlcNAcβAsn         Ser(Thr)
```
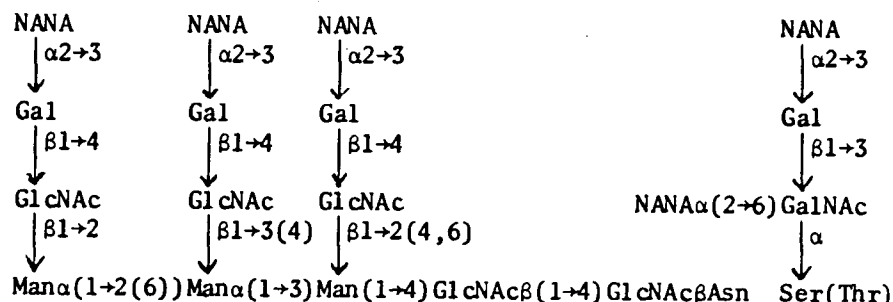
Fig. I.2.3. O- and N-glycosides of fetuin. (From Ref. 17).

N-glycosides of the form depicted in Fig. I.2.3;[17] the outer

trisaccharide structure, NANA-α-(2→3)-gal-β-(1→4)-glcNAc, is common in

animal glycoproteins. The mucins are extensively sialated, and the

following sequence occurs several hundred times in each molecule:[17]

NANA-α-(2→6)-galNAc-α-(1→)-Ser-(or Thr). The exocyclic triol of NANA

may be O-acylated at one or more position. RBC's obviously present a

highly complex and varied carbohydrate code to interacting species. A

major RBC membrane protein is glycophorin A,[18] which is a highly

sialated trans-membrane protein bearing the carbohydrate determinant for

the MN blood-group classification. Although some doubt still exists as

to the detailed structure of the carbohydrate moieties, the terminal

sequence of NANA-α-(2→x)-gal is known (x = 3 or 6).

It has been mentioned that asialoglycoproteins* are an important

sub-set of the sialoglycoproteins, as the terminal galactose marks a

plasma protein for circulatory clearance and catabolism by the liver.

With glycophorin A, terminal sialic acid is essential for the exhibition

---

*Sialoglycoproteins having been desialated in some way.

of MN blood-group activity. Thus, we recognize the need for the labelling of NANA termini of sialoglycoproteins, and galactose termini of the asialo analogues, if their roles at the molecular level are to be monitored.

Precedent exists in the literature for the generation of an aldehyde group either at NANA[19] or gal[20] termini and we considered this to be potentially useful. The reductive amination procedure had been used to chemically modify protein lysyl $6-NH_2$ groups with methanal,[21] using $NaBH_4$ to reduce the intermediate Schiff base; Borch et al. described[22] a superior reductant for this purpose, sodium cyanoborohydride ($NaCNBH_3$).

It was determined by Van Lenten and Ashwell[19] that the exocyclic triol of NANA may be selectively oxidized by periodate under mild conditions.* Strong oxidative conditions could result in the oxidative cleavage of all vicinal diols, thus destroying the integrity of the

---
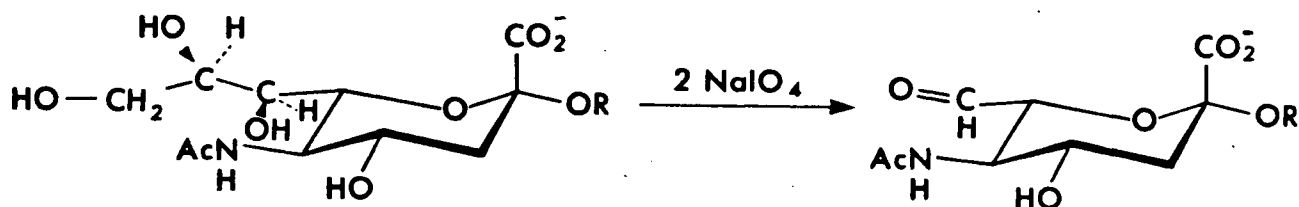
*Periodate is classically used in the "Smith degradation" to determine intersugar linkages in a polysaccharide.[23] Its reactivity towards vicinal diols varies in the order: extracyclic > intracyclic cis- > intracyclic trans-

carbohydrate chain and the specificity of the reaction. The procedure originally called for the addition of 10 moles of $NaIO_4$ per mole of sialic acid, and reaction for 10 min at 0°C and pH 5.6. Later, Jourdian et al. quantified[24] the reaction and it is clear from their data that reaction for 35 min at 0°C yields good selectivity and oxidized NANA for isolated glycoproteins. With RBC's, the total NANA content is difficult to estimate, and the reaction time is accordingly reduced to 15 min. to limit possible oxidation of terminal gal residues (which are the most susceptible to cleavage, after the NANA exocyclic triol).

The oxidation of galactose is best performed enzymatically. Galactose oxidase (E.C. No. 1.1.3.9) effects the oxidation of the 6-CH_2OH to an aldehyde (Fig. I.2.4). The enzyme will act on terminal gal or galNAc residues, and H_2O_2 is produced. Although not done in this spin-label study, it is advisable to remove the H_2O_2 as it is formed (with a second enzyme, catalase), as this inhibits the forward reaction of the enzyme by the classical feed-back control mechanism.
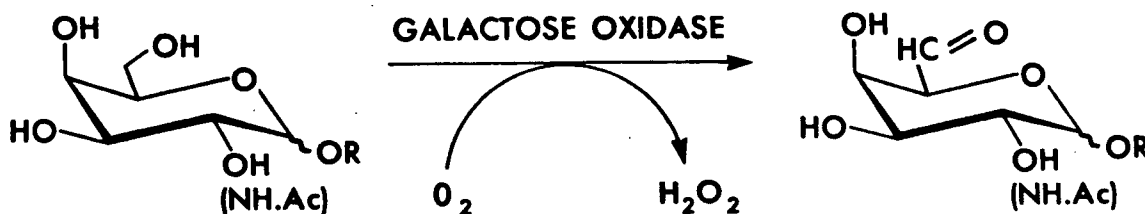
Fig. I.2.4. Oxidation of galactose termini by galactose oxidase.

To expose subterminal galactose residues, it is necessary that NANA be removed; this may be effected by mild acid hydrolysis, or enzymatically using an exoglycosidase specific to NANA - neuraminidase (E.C. No. 3.2.1.18).

Having generated aldehyde functionalities on NANA or gal termini, the spin label TEMPAMINE (1) was reductively aminated onto this point, using NaCNBH₃. Unreacted, low molecular weight components were separated from the glycoprotein by size-exclusion chromatography (Sephadex G-25), and by exhaustive dialysis in the case of RBC's.

$$-C\underset{H}{\overset{O}{\big\backslash}} \quad + \quad \underset{SL}{\overset{NH_2}{|}} \quad \rightleftharpoons \quad \left[-C=N-SL\right] \quad \xrightarrow{NaCNBH_3} \quad -CH_2-NH-SL$$
$$+ H_2O$$
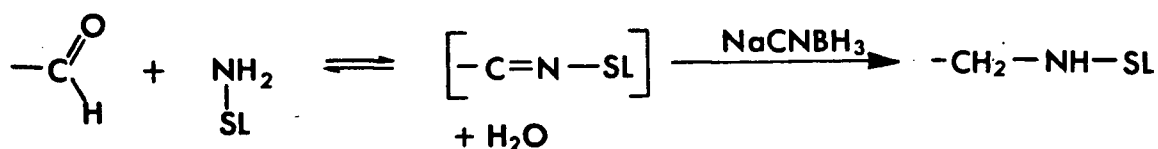
Fig. I.2.5. Reductive amination of an aldehyde with TEMPAMINE, using NaCNBH₃.

Major advantages of the use of NaCNBH₃ over NaBH₄ include its resistance to aqueous hydrolysis and specificity for the intermediate Schiff base over the starting aldehyde.*

─────────────────────

* NaBH₄ will also reduce the aldehyde to a primary alcohol.

I.2.3 Results and Discussion

Fetuin, BSM and RBC's were spin labeled at their NANA termini using the above-mentioned procedure[14] based on specific activation under mild periodate oxidative conditions, and coupling of the amine spin label, TEMPAMINE, by reductive amination using $NaCNBH_3$. Subterminal galactose residues of fetuin and BSM were exposed by neuraminidase treatment, and oxidized by galactose oxidase/catalase action. TEMPAMINE was then attached as before.

Representative ESR spectra are given in Fig. I.2.6. In all cases the level of incorporation was high enough to easily detect an ESR spectrum with milligram quantities of glycoprotein, and a partially immobilized spin label was indicated. Amplification of the high-field region (outer extrema) did not reveal any signal from a rigid component to any spectrum. Motional correlation times were determined from peak heights and widths using Eqns. I.2.2-4. Isotropic hyperfine couplings, a_0, were measured from spectra, and the percentage derivatization determined by double integration of the ESR signal. The relevant data are tabulated (Table I.2.1).

Control experiments involved the incubation of NH_2-SL and $NaCNBH_3$ with the unactivated glycoprotein, and Sephadex separation. Non-specific adsorption was found to contribute < 0.5% of the total signal and was not pH dependent. With the erythrocytes, spin labelling in physiological saline resulted in a minimum of cell lysis, and the spin labels were found exclusively in glycoconjugates associated with the cell wall, after RBC "ghosts" were prepared. The coupling reagents
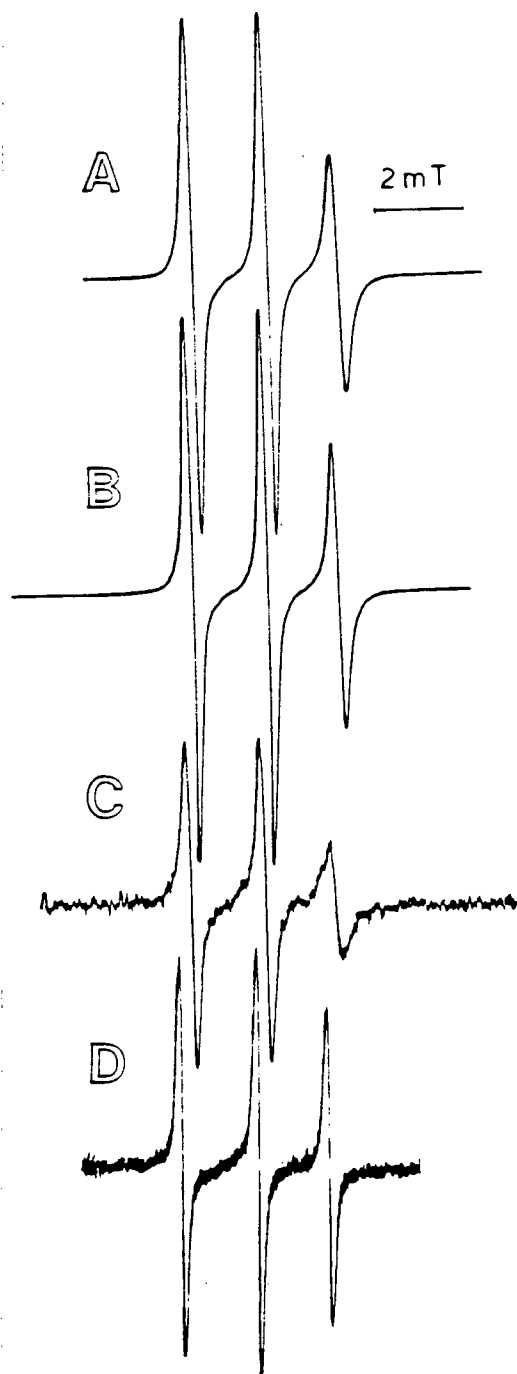
Fig. I.2.6. ESR spectra of nitroxide-labelled materials. Concentration
and relative gain are given in parentheses. A.
Periodate-activated fetuin (3.24 mg in 50 µl H_2O; gain 1).
B. Galactose oxidase-activated asialo-BSM (2.67 µl in 50 µl
H_2O; gain 6.4). C. Periodate-activated, intact
erythrocytes (73 µl packed cells in phosphate-buffered
saline; gain 187.5). D. Fetuin perfused with 1 and $NaCNBH_3$
for 2 h (3.00 mg in 50 µl H_2O; gain 62.5). (From Ref. 14.)

Table I.2.1 Parameters characterizing spin label probes attached to various substrates. [a]Percentage of possible sites spin labelled. N.D.: not determined due to low signal-to-noise.

Material	Activation Procedure	τ_c (ns) (± 0.05 ns)	$\underline{a}_o$ (mT) (± 0.02 mT)	% Activation[a] (± 5%)	Number spins per Molecule
FETUIN	NaIO$_4$, 0°C, 35 min.	0.79	1.68	ca. 20	2.5
ASIALO-FETUIN	Neuraminidase, galactose oxidase	0.52	1.68	50	6.0
BSM	NaIO$_4$, 0°C 35 min.	0.35	1.68	33	115.5
ASIALO-BSM	Neuraminidase, galactose oxidase	0.49	1.67	2	7.0
RBC	NaIO$_4$, 0°C 15 min.	1.0	1.65	N.D.	N.D.

were reacted with the activated glycoconjugate for 2 h at room-temperature – no increase in labelling efficiency was observed by extension of this period.

Turning now to the ESR data, the $\underline{a}_0$ values, around 1.67 mT, indicate a spin label in a polar environment. This is consistent with what one might expect, as the (hydrophilic) sugar residues would be expected to be highly solvated and exposed to the medium. The correlation times indicate a moderately immobilized spin label and it is interesting to note that the correlation times of fetuin (MW 48 000 amu) and BSM (MW 1.3 * 10^6 amu) spin labelled at their sugar termini are quite comparable. This may suggest that the bulk of the contribution to the observed τ_c stems from the mobility about the bonds joining the spin label to the terminal sugar residue, or it could be that, in both cases, the pendant sugar residues are equally mobile with respect to the protein back-bone. Data obtained by ^{2}H NMR (Chapter I.3) support the second hypothesis.

I.2.4 Information Derived from Spin Label Studies of Glycoconjugates

Our studies indicate that NANA or gal termini of complex glycoconjugates may be efficiently activated and spin labelled using the procedures discussed. The spin label exists in a hydroxylated, polar environment and is mobile compared with the glycoprotein as a whole. These additional motional degrees-of-freedom could reflect the enhanced mobility of the pendant sugars resulting from rotation about glycosidic bonds, or could be dominated by motion about the chemical bonds linking the nitroxide spin label to the sugar terminus.

Since the work described here was completed, others found application for this and related procedures to study the role of sugars in binding events. A discussion of these papers is in order as they serve to highlight some of the difficulties with which the technique is fraught.

Grant and co-workers have performed an extensive study[25,26] of the headgroup dynamics and carbohydrate role in lectin binding processes with the transmembrane glycoprotein, glycophorin A (vide supra). When terminal NANA residues are specifically spin-labelled, the probe is confined to a highly polar milieu, and the motion is that of a moderately immobilized spin, even when constituted into a model membrane. That which reduces NANA mobility (as reflected in the ESR correlation time) is a specific binding event. Wheat-germ lectin (WGA) binds to glycophorin A, and the terminal NANA has been implicated in the binding process. As WGA is added, a dramatic increase in τ_c is observed which is a function of the amount of lectin added. This study was extended to gangliosides,[27] labelled in an analogous fashion. Here, upon addition of WGA an initial decrease in τ_c was observed, followed by (the expected) increase as the WGA concentration was further raised. Such observations were explained in terms of randomizing an initial patch-wise distribution of gangliosides, although this was not positively determined as it can be with spin labels.[28]

Studies on a similar system by Butterfield and co-workers[29,30] are in contradiction to those of Grant. These workers used cyanoborohydride to couple spin label with periodate-activated

erythrocyte ghosts, which was found to be more efficient than $NaBH_4$ (used by Grant). Upon addition of lectins which bind glycophorin A (WGA and Phaseolus vulgaris agglutinin, PHA) an increase in mobility was observed[30] which was interpreted in terms of conformational changes exposing the spin label to a less restricted environment upon lectin binding. It is important to note that these two sets of data are not strictly comparable, since Lee and Grant worked with a specifically labelled glycophorin either in solution or a model membrane, while Butterfield and co-workers used intact erythrocyte ghost membranes, where several questions arising from the complexity of the system can be raised. A third study[31] of WGA binding to spin labeled erythrocytes is in accord with the findings of Lee and Grant; special pains were taken to purify the commercial lectins, and the activation was of the intact erythrocytes resulting in very low degree of ganglioside labelling (cf. Butterfield).

Finally on this subject, a French study[32] was concerned with the flexibility of isolated branched glycopeptides; NANA was spin labelled by periodate oxidation and reductive amination. Concanavalin A* was added resulting in a slight immobilization of the spin label – this is not altogether surprising, as the binding site for the lectin is distant from the labelled termini. However, it does suggest a certain rigidity of the oligosaccharide chain in its ability to propagate such effects. Since the inception of the studies presented in this chapter, two other

---

*A lectin with a specificity for mannose, present in the glycan.

groups have reported on the use of similar methods to spin label the carbohydrate moiety of immunoglobulins, and their fractions. Both used non-specific oxidation - 8 hours at room temperature,[33] and 16-24 hours at room temperature or 0° C.[34],[35] One group explicitly states that the selectivity for NANA was only 60%, and it is clear from the pertinent literature reports that the labelling cannot be selective in either case. The Russian group initially reported a highly mobile spin label[34] and then published revised data showing a more immobilized spin label;[35] the initial error was caused through carry over of non-specifically adsorbed label.

The facts emerging from this chapter are that (a) NANA or galactose termini of glycoproteins and erythrocytes can be specifically labelled (b) the spin labels are mobile relative to the protein as a whole, and in a polar environment, and (c) extreme caution should be exercised when drawing conclusions from a complex system, when biological perturbants are introduced. That is not to say that the spin label method is without use, but the experiments should be very carefully designed and controlled.

REFERENCES

1. I.C.P. Smith. Biological applications of electron spin resonance. Edited by H.M. Schwartz, J.R. Bolton, and D.C. Borg. John Wiley, New York. 1972. pp. 483-539.

2. A.D. Keith, M. Sharnoff, and G.E. Cohn. Biochim. Biophys. Acta. 300, 379-419 (1973).

3. R.A. Dwek. Nuclear magnetic resonance in biochemistry: applications to enzyme systems. Clarendon Press, Oxford. 1975. Chapter 12.

4. G.I. Likhtenstein. Spin labeling methods in molecular biology. John Wiley, New York. 1976.

5. B.J. Gaffney and D.C. Lin. The enzymes of biological membranes. Vol. 1. Edited by A. Martonosi. Plenum Press, New York. 1976. pp 71-90.

6. P.M. Vignais and P.F. Devaux. Ibid. pp. 91-117.

7. Spin labeling: theory and applications. Edited by L.J. Berliner. Academic Press, New York. 1976.

8. Spin labeling II: theory and applications. Edited by L.J. Berliner. Academic Press, New York. 1979.

9. S. Schreier, C. Polnaszek, and I.C.P. Smith. Biochim. Biophys. Acta. 515, 375-436 (1978).

10. P.C. Jost and O.H. Griffith. Methods Enzymol. 49, 369-418 (1978).

11. L.J. Berliner. Methods Enzymol. 49, 418-480 (1978).

12. J.D. Aplin. PhD. Thesis. University of British Columbia. 1979, and references therein.

13. M. Yalpani. Ph.D. Thesis. University of British Columbia. 1980, and references therein.

14. J.D. Aplin, M.A. Bernstein, C.F.A. Culling, L.D. Hall, and P.E. Reid. Carbohydr. Res. 70, C9-C12 (1979).

15. E.R.B. Graham. Glycoproteins: their composition, structure and function. Edited by A. Gottschalk. Elsevier, New York. 1972. pp. 716-731.

16. W. Pigman and A. Gottschalk. Ibid. pp. 817-821.

17. N. Sharon. Complex carbohydrates: their chemistry, biosynthesis, and functions. Addison-Wesley, Reading, Mas. 1975.

18. H. Furthmayr. Biology of carbohydrates, Vol. 1. Edited by V. Ginsburg and P. Robbins. John Wiley, New York. 1981. Chapter 4.

19. L. Van Lenten and G. Ashwell. *Methods Enzymol.* 28, 209-211 (1972), and references therein.

20. A.G. Morell and G. Ashwell. *Ibid.* 205-208, and references therein.

21. G.E. Means and R.E. Feeney. Chemical Modification of Proteins. Holden-Day, San Francisco. 1971.

22. R.F. Borch, M.D. Bernstein, and H.D. Durst. *J. Amer. Chem. Soc.* 93, 2879-2904 (1971).

23. P.V. Wagh and O.P. Bahl. *C.R.C. Crit. Rev. Biochem.* 10, 307-377 (1981), and references therein.

24. G.W. Jourdian, L. Dean, and S. Roseman. *J. Biol. Chem.* 246, 430-435 (1971).

25. P.M. Lee and C.W.M. Grant. *Biochem. Biophys. Res. Comm.* 90, 856-863 (1979).

26. P.M. Lee and C.W.M. Grant. *Can. J. Biochem.* 58, 1197-1205 (1980).

27. P.M. Lee, N.V. Ketis, K.R. Barber, and C.W.M. Grant. *Biochim. Biophys. Acta.* 601, 302-314 (1980).

28. L.D. Hall and J.C. Waterton. *J. Amer. Chem. Soc.* 101, 3697-3698 (1979).

29. J.B. Feix and D.A. Butterfield. *FEBS Lett.* 115, 185-188 (1980).

30. J.B. Feix, L.L. Green, and D.A. Butterfield. *Life Sciences.* 31, 1001-1009 (1982).

31. R. Snoek. Personal communication.

32. J. Devoust, V. Michel, G. Spik, J. Montreuil, and P.F. Devaux. *FEBS Lett.* 125, 271-276 (1981).

33. K.J. Willan, B. Golding, D. Givol, and R.A. Dwek. *FEBS Lett.* 80, 133-136 (1977).

34. R.S. Nezlin, V.P. Timofeev, Y.K. Sykulev, and S.E. Zurabyan. *Immunochem.* 15, 143-144 (1978).

35. V.P. Timofeev, I.V. Dudich, Y.K. Sykulev, and R.S. Nezlin. *FEBS Lett.* 89, 191-195 (1978).

CHAPTER I.3

DEUTERIUM MAGNETIC RESONANCE STUDIES ON GLYCOCONJUGATES

Chapter I.2 in this thesis detailed ESR stdies on the carbohydrate moiety of glycoproteins, which provided information on the relative mobility of the glycan. Although the ESR method has advantages - chiefly, sensitivity and the absence of "background" signals from the molecule itself - the physical bulk of the nitroxide probe itself may perturb the system and lead to erroneous conclusions. In addition, where one is interested in the motional correlation time (τ_c) of a sugar to which the spin label is attached, the measured value may largely reflect a high degree of mobility of the probe about the bonds attaching it to the sugar, rather than the sugar per se.

Alternatives exist for the extraction of motional information from such systems - preferably, these should be "non-invasive" in that they do not introduce an extraneous bulky "reporter" group. In this light, NMR relaxation studies are the most promising. To simplify matters, it is desirable to attach a "probe" isotopically enriched in a nuclide with low natural abundance, as such a procedure will obviate complications arising from overlap with signals from the system ("back-ground"). Enrichment in ^{13}C is one possible approach; numerical values for τ_c may be calculated once the relaxation behaviour and the chemical system are known.

An alternative approach is ^{2}H NMR; substitution of a proton with a deuteron is clearly a minor perturbation to the system. Deuterium, having nuclear spin, $\underline{I} = 1$, is quadrupolar, meaning that its nuclear

charge is asymmetrically distributed about the nucleus. This leads to some broadening of the resonances but, most importantly to this discussion, the relaxation mechanism for the deuteron is dominated by this quadrupole effect, and a simplification of the determination of motional information results. Working in its disfavour is the low inherent sensitivity of ^{2}H (< 1% that of ^{1}H): this factor can be partially offset by the use of high magnetic fields ($\underline{B}_0$ 9.4 T in this case), and the Fourier transform method, now so ubiquitous in heteronuclear NMR studies.

The application of high-resolution ^{2}H NMR (and some broad-line studies) was exhaustively reviewed by Mantsch et al.[1] in 1977, and up-dated in 1982.[2] These two treatises are mandatory reading for the applicant of ^{2}H NMR, and the reader wishing a broader view on the subject should consult these. In the carbohydrate area, all related reports have been with isotopically enriched monosaccharides. In 1973, Brewer et al. studied[3] the binding of ^{13}C-enriched α-methyl-$\underline{D}$-glucopyranoside to the lectin,* Concanavalin A. Their mapping of the binding site was found to differ considerably from previous X-ray studies, where an iodophenyl glucoside was used. Few challenge the validity of the NMR data, and this example amply illustrates the difficulties which may arise when large reporter groups are used. Alter and Magnuson used ^{19}F NMR to study the same system,[4] and Neurohr et al. studied[5] the binding of isotopically labelled methyl α-

---

*A lectin is a protein which binds specific carbohydrate(s).

and β-D-galactopyranosides to peanut agglutinin (another lectin) by [13]C

NMR relaxation. The same group[6] studied the molecular dynamics of the

sugar binding process to the lectin, wheat germ agglutinin. In this

case, the sugar was isotopically enriched in ^{2}H and this satisfying

relaxation study includes an analysis for the case where a contribution

to the motion from internal rotation is present in the bound state.

In the case of rapid (where $\omega_o^2 \tau_c^2 \ll 1$) and isotropic motion, the

dominant quadrupole relaxation mechanism is given by:[1]

$$(\underline{T}_1)^{-1} = (\underline{T}_2)^{-2} = \frac{3}{8} (1 + \frac{\eta^2}{3}) (\frac{e^2 qQ}{h})^2 \tau_c \qquad [I.3.1]$$

η is the asymmetry parameter of the field gradient (and may be

neglected), and $e^2 qQ/h$ is the quadrupole coupling constant. Although $\underline{T}_1$

or $\underline{T}_2$ could be measured by multi-pulse methods, it is justifiable to

neglect contributions to the line-width from magnetic inhomogeneities

and [1]H-^{2}H couplings, and assume $\underline{T}_2 = 1/\pi \, \Delta\nu_{0.5}$ (where $\Delta\nu_{0.5}$ is the

peak width at half-height). Equation I.3.1 reduces to:

$$(\underline{T}_2)^{-1} = \pi \, \Delta\nu_{0.5} = \frac{3}{8}(\frac{e^2 qQ}{h})^2 \tau_c \qquad [I.3.2]$$

By measuring $\Delta\nu_{0.5}$ and using a reasonable value for the quadrupole

coupling constant, τ_c may be easily calculated.

In Chapter I.2 we described two methods by which aldehyde

functionalities may be introduced at specific loci in a glycoprotein

glycan. Our approach to the specific incorporation of ^{2}H into

glycoprotein rests on the use of these same procedures to generate the

specific aldehyde, and the regeneration of an alcohol using the ^{2}H-labelled reductant, sodium borodeuteride. The specific deuteration of terminal sialic acid or galactosyl units is illustrated in Figs. I.3.1 and I.3.2, respectively. With sialic acid, the sugar is modified in that the exocyclic triol is shortened by two carbons; with galactose, the labelled sugar matches the native sugar almost exactly. The exocyclic −CHDOH unit is racemic, and this, too, will contribute to the observed line-width.

In light of our previous successes with the reductive amination procedure using sodium cyanoborohydride, it was apparent that proteins could be labelled with deuterons by performing such a reaction with hexadeuterioacetone and lysyl 6-amino groups:

$$6\text{-}NH_2 \; + \; O{=}C \left\langle \begin{array}{l} CD_3 \\ CD_3 \end{array} \right. \quad \xrightarrow{\text{NaCNBH}_3} \quad 6\text{-}N\underset{\text{1 or 2}}{\overset{H}{|}}C H \left\langle \begin{array}{l} CD_3 \\ CD_3 \end{array} \right.$$
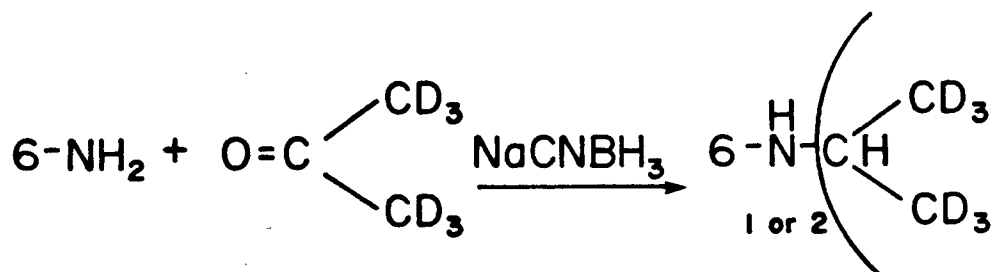
The above-mentioned procedures were used to label the sialic acid termini of bovine submaxillary mucin (BSM), galactose termini of asialofetuin and lysyl groups of fetuin.[7] The ^{2}H NMR spectra were recorded at 61.4 MHz ($\underline{B}_0$ 9.4 T) as solutions in distilled water, and are shown in Fig. I.3.3.* The partial overlap of the sugar signal(s)

_____

*Spectra were recorded by Dr. W.E. Hull of Bruker, West Germany.
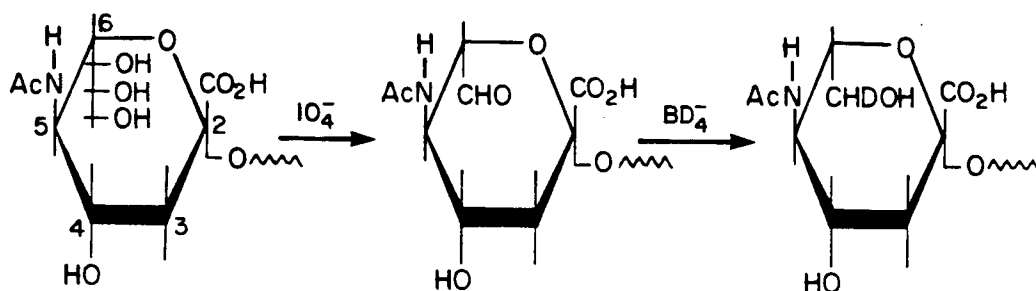
Fig. I.3.1 Procedure for the specific deuteration of sialic acid
termini of glycoproteins at the C-7 position.
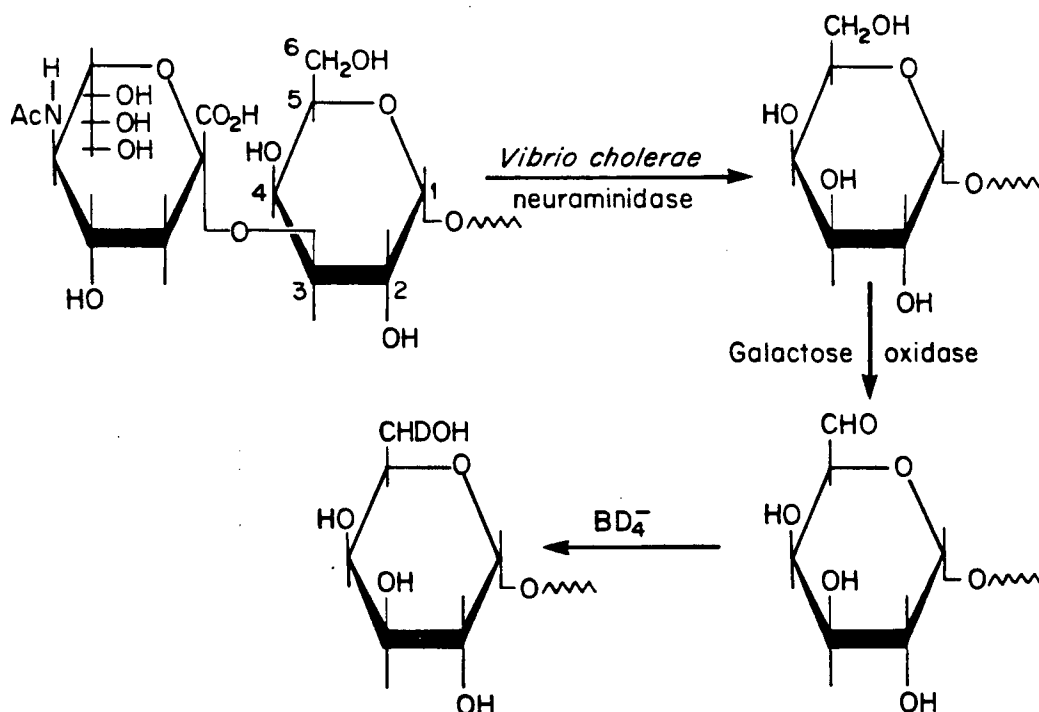
Fig. I.3.2. Procedure for the specific deuteration of galactose
termini of asialo-glycoproteins at the C-6 position.
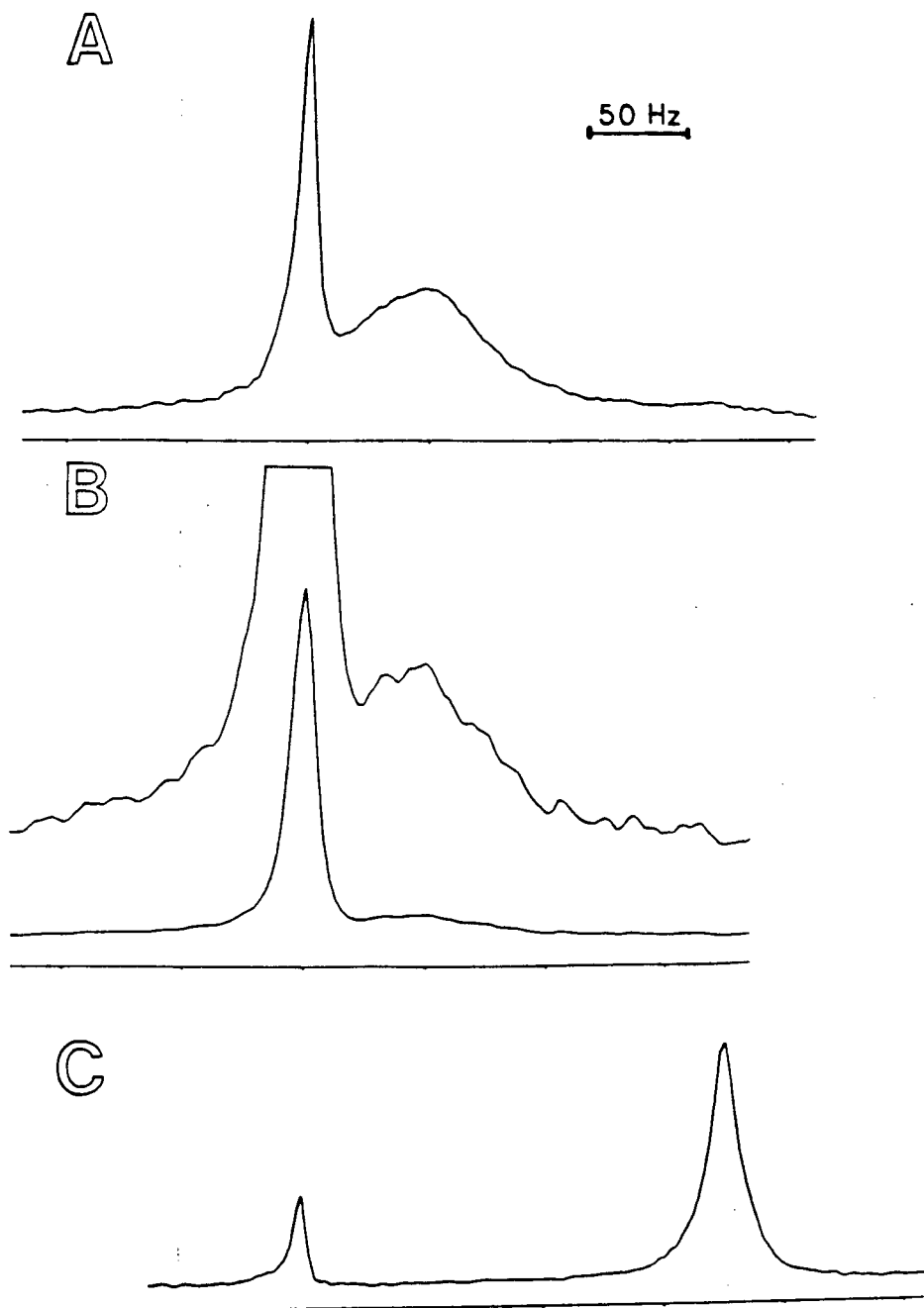
Fig. I.3.3. ^{2}H NMR spectra measurement at 61.4 MHz. Samples were dissolved in ≃ 1.5 ml H_2O. (A) BSM deuterated at C-7 on sialic acid residues (145 mg; 2700 transients). (B) Asialofetuin deuterated at C-6 position on terminal galactose residues (190 mg). (C) Fetuin reductively aminated with hexadeuterioacetone on lysine residues (240 mg; 550 transients). The HOD resonance was arbitrarily assigned a shift of 5 ppm. From ref. 7.

with the residual HOD in distilled water is undesirable and the problem
was largely alleviated by using deuterium-depleted water as a solvent
(data not shown).

For the determination of τ_c, line-widths were measured and
inserted in Equation [I.3.2]. A typical[1] quadrupole coupling constant
(165 kHz) was used throughout. The correlation times from ^{2}H NMR are
compared with those for the analogous molecule from ESR measurements
(Ch. I.2), in Table I.3.1. The quoted errors are that in measuring peak
widths - especially difficult when the signal-to-noise is low and
overlap with the HOD resonance is significant (as in the case with Fig.
I.3.3.B).

The correlation between the measurements is good, and these data
suggest that τ_c values derived from nitroxide ESR studies are
representative in such systems. BSM labelled at sialic acid "appears"
from the ^{2}H NMR measurements to be roughly twice as mobile as from the
ESR, and this should serve to caution the reader not to take the figures
too literally. Indeed, this may be a real effect, reflecting a somewhat
restricted motion of the spin label with BSM, where the glycan is short
(a disaccharide), and the carbohydrate substitution level high. As
mentioned in the previous chapter, useful results may arise from ESR
studies where changes in τ_c resulting from the perturbation of the
system are considered, and this conviction is supported by the
literature.

We conclude that, given ca. 100 milligrams of material, one may
successfully label specific sites on a glycoprotein with deuterons, and

Table I.3.1 Comparison of τ_c determined from ^2H NMR relaxation measurements, and nitroxide ESR. a. τ_c in ns. b. Reductive amination of protein lysyl 6$^{\underline{C}}$amine groups with hexadeuterioacetone, or 2,2,6,6-tetramethylpiperidine -4-keto-$\underline{N}$-oxyl (TEMPONE).

Substrate	Activation Procedure	τ_c^a from ^2H NMR	τ_c from ESR
FETUIN	PERIODATE	0.73 ± 0.13	0.79
ASIALOFETUIN	GALACTOSE OXIDASE	0.57 ± 0.03	0.52
BSM	PERIODATE	0.12 ± 0.07	0.35
ASIALO-BSM	GALACTOSE OXIDASE	Not Determined	0.49
FETUIN	REDUCTIVE AMINATION[b]	0.5	0.77

observe the ^{2}H NMR resonances on a high-field spectrometer.

Measurement of line-widths yields a correlation time for the sugar very

similar to that derived from an analogous nitroxide spin-label study.

While this is interesting and, perhaps, useful information, it should be

cautioned that in neither study have we perturbed the system with, for

example, a molecule which should bind the sugar (i.e. a lectin) to

evaluate the possible effect of the bulky spin label on the binding

process. It is our belief that ^{2}H NMR studies of the kind detailed here

will be useful in understanding molecular interactions and physical

properties of biological macromolecules.

REFERENCES FOR CHAPTER I.3

1. H.H. Mantsch, H. Saito, and I.C.P. Smith. Prog. Nuclear Magn. Reson. Spectrosc. 11, 211-271 (1977).

2. I.C.P. Smith and H.H. Mantsch. NMR spectroscopy: new methods and applications. Edited by G.C. Levy. ACS Symposium Series 191. 1982. pp. 97-117.

3. C.F. Brewer, H. Sternlicht, D.M. Marcus, and A.P. Grollman. Proc. Nat. Acad. Sci. USA. 70, 1007-1011 (1973).

4. G.M. Atler and J.A. Magnuson. Biochemistry. 13, 4038-4045 (1974).

5. K.J. Neurohr, N.M. Young, I.C.P. Smith, and H.H. Mantsch. Biochemistry. 20, 3499-3504 (1981).

6. K.J. Neurohr, N. Lacelle, H.H. Mantsch, and I.C.P. Smith. Biophysical J. 32, 931-938 (1980).

7. M.A. Bernstein, L.D. Hall, and W.E. Hull. J. Amer. Chem. Soc. 101, 2744-2746 (1979).

CHAPTER I.4

NEOGLYCOPROTEINS: SYNTHESIS AND NMR STUDIES

I.4.1 Introduction

At the time when the work described in this chapter was performed (1979/1980), much use had been made of ^{13}C and ^{1}H NMR in the study of oligo- and polysaccharides (see Ch. II.3), but little in a second important class of glycoconjugates, glycoproteins (Ch. I.2). At natural abundance the scarcity of studies can, in part, be attributed to the complexity of the material and the lack of model compounds. In addition to contending with protein resonances (overlapping with carbohydrate peaks to a greater or lesser extent), glycoproteins often display microheterogeneity in their glycans, making it impossible to write a single chemical structure for the carbohydrate moiety.* This added complexity obviously compounds the difficulty of analysis. Glycoproteins cannot always be isolated in appreciable quantities, and this could preclude ^{13}C NMR studies.

One approach to the development of simple model systems for NMR studies is to liberate the glycans from the protein (or perform an enzymic protein digest), separate the fragments, and perform NMR experiments on these purified materials. This solves the problem of microheterogeneity and eliminates the bulk of the protein resonances, and could be a worthwhile first approach. We considered this to be somewhat undesirable, as the low molecular weight fractions were too far

---

*An obvious exception to the rule is the Arctic fish "antifreeze" glycoproteins, which are extremely homogeneous.

from the "real" situation. An alternative exists and we have exploited this: known, characterized sugars can be covalently attached to a (hitherto sugarless) protein to create a "neoglycoprotein". The bulk of protein resonances can potentially be identified by observing the protein before glycan attachment. In essence, one can characterize both the protein and carbohydrate independently of one another, and then observe changes when the neoglycoprotein is studied. This allows one to make assignments of neoglycoprotein glycans and evaluate such concepts as the potential use of chemical shift data of carbohydrate standards. With the purpose of spectral assignment we evaluated the use of enzymic (and, in principal, chemical) perturbations.

We felt that the neoglycoprotein approach had the further advantage that the material is of similar physical form to a glycoprotein, and this was crucial in our ^{1}H NMR studies where use was made of the differential in mobility between the glycan and protein back-bone. The structure and complexity of the glycone would be restricted by the lengths an investigator is prepared to go in oligosaccharide synthesis*. The neoglycoprotein synthetic protocol allows also for flexibility in the nature and linkage length of the glycone to protein, and this could be useful to one interested in differential mobility or enzymic studies (vide infra).

At this time, other groups have proceeded to successfully employ ^{13}C NMR to study a variety of aspects of the structure and form of glycoprotein glycans, and these will be reviewed later in the chapter.

---

*This is, by no means, a trivial task! In this study, monosaccharides and purchasable disaccharides were considered.

I.4.2 Neoglycoprotein Synthesis

The first neoglycoproteins were synthesized by Goebel and Avery[1] in 1929, and their procedure is still popular. A sugar is $\underline{O}$ - glycosylated with para-aminophenol, and the p-aminophenyl glycoside converted into the diazonium salt (nitrous acid, 0°, 15 min.). This is then mixed with the protein, in basic solution for another 15 min.; substitution primarily occurs at histidine, lysine and tyrosine amino acid loci. This procedure has a number of major draw-backs:- the specificity is low, which can cause problems in the interpretation of results, and the introduction of the bulky aromatic group can itself elicit an antibody response, reducing the specificity of the antibody to the sugar hapten.

Literature precedent existed for the selective amination of methanal by lysyl amino acids, at the 6-amine position.[2,3] Reductive amination had been described by Gray and co-workers between lysyl amines and reducing sugars[4] (Fig. I.4.1), using sodium cyanoborohydride as the reductant. Although the reaction is controllable and mild, it has the disadvantages that it introduces a polyol (to which antibodies have been shown to direct), destroys one sugar ring (which is disadvantageous when the attached product is the result of a long synthetic route) and the

R = Sugar
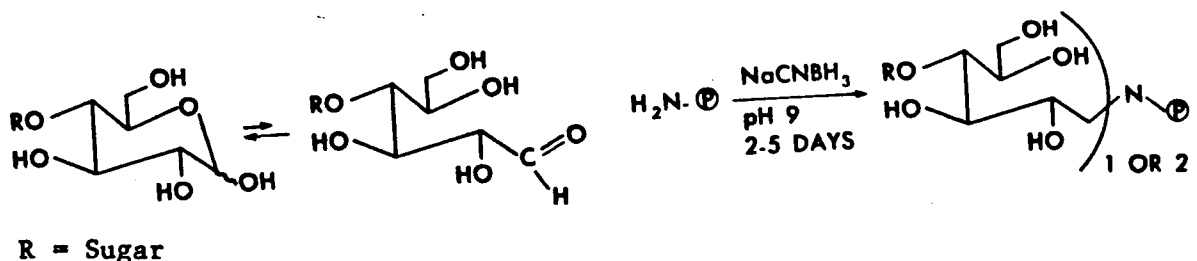
Fig. I.4.1. Gray's procedure for the attachment of a reducing disaccharide to a protein (P) via its lysyl 6-amino groups.

An encyclopaedic review of methods described for neoglycoprotein synthesis is not in order here - two excellent reviews have appeared recently.[5,6] Our survey of these methods for neoglycoprotein synthesis did not point to an ideal procedure, compared with the criteria we considered necessary:-

1. The method should be directly compatible with the reagents and protecting groups used in oligosaccharide synthesis.

2. It should cause no destruction of the integrity of the reducing (terminal) sugar ring.

3. It should have in-built variability of the "spacer" between the terminal sugar and the point of attachment on the protein, in terms of length and hydrophilicity.

4. The coupling reaction should be convenient, and rapid at, or near, physiological pH in aqueous media, using chemically stable reagents.

5. The reaction should give high-yielding coupling to a specific amino acid _via_ a hydrolytically stable, covalent linkage.

6. The surface charge of the protein should not be significantly altered by carbohydrate attachment.

In consideration of the above-mentioned criteria, and the two protocols illustrated above, it seemed that the most obvious route was the glycosidation of a sugar such that an aldehyde could be generated at a specific point on the aglycone. Our (see Ch. I.2) and Gray's

experience with the reductive amination reaction using sodium cyanoborohydride encouraged us to consider this method for the coupling reaction. Further, we wanted a protocol which relied on previously characterized reactions.

Our protocol[7] is illustrated in Fig. I.4.2 for the attachment of α-D-glucose to bovine serum albumin (BSA). The procedure involves three steps:- glycosidation of the parent sugar with an alkenyl alcohol, reductive ozonolysis in methanol to generate an aglycone aldehyde (not isolated), and reductive amination with lysyl 6-amino groups on the protein using sodium cyanoborohydride. All steps have been well characterized in the literature.
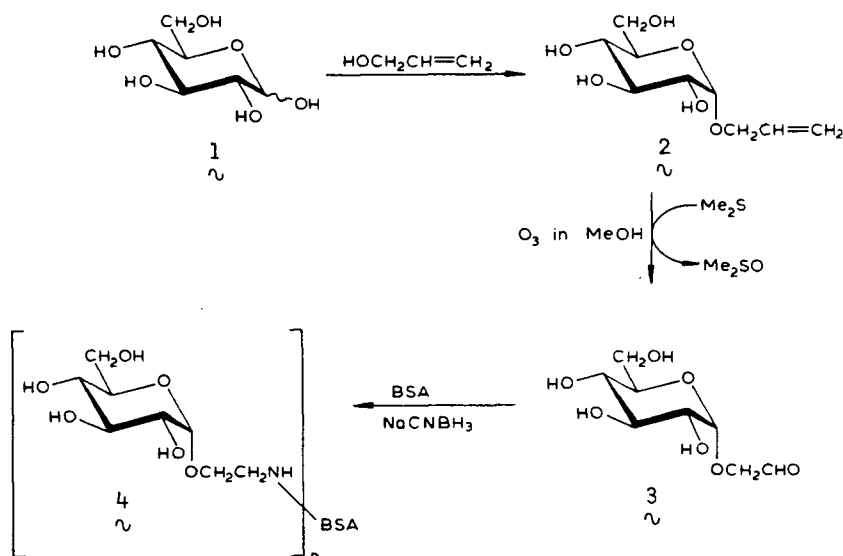
Fig. I.4.2. Neoglycoprotein synthesis protocol. From Ref. 7.

The allyl group is well known for its use as a protecting group in carbohydrate synthesis,[8] and Lee and Lee have described[9] the glycosidation of sugars with allyl alcohol. The glycosidation procedures we used were either those of Lee, or variations.[10] α-Glycosides were generally prepared by heating the free sugar in allyl alcohol under reflux, and β-glycosides prepared from the α-bromo sugar per-acetate and alkenyl alcohol via a Koenigs-Knorr[11] related procedure. To illustrate the versatility of spacer arms, glucose was also glycosidated with undecenyl alcohol - $HO-(CH_2)_9CH=CH_2$, thereby introducing a long (relatively hydrophobic) spacer arm between the "nascent aldehyde" (i.e. the alkene) and the sugar. The prepared allyl glycosides all had melting points in close agreement with the literature, and their NMR spectra were consistent with their structures.[12] They are all stable molecules which can, as far as we know, be stored indefinitely at room temperature.

Although alternate routes exist for the oxidative cleavage of the alkene aglycone (e.g. periodate-ruthenium dioxide oxidation[13]), we found the reductive ozonolysis reaction[14] to be fast, specific, and high-yielding (essentially quantitative in a total of ca. 2 hours). The sugar is dissolved in a methanolic solvent (pure methanol in the case of a free sugar or 4:1 $MeOH-CH_2Cl_2$ with protected sugars) and purged with ozone at reduced temperature (5-10 min./mmole). The reaction is "self-indicating", as excess ozone is manifested by the clear solution turning blue. This step produces the hydroperoxide (8) which is reduced in situ with dimethyl sulphide (DMS). The generally accepted mechanism[15] for the reaction is given in Fig. I.4.3.
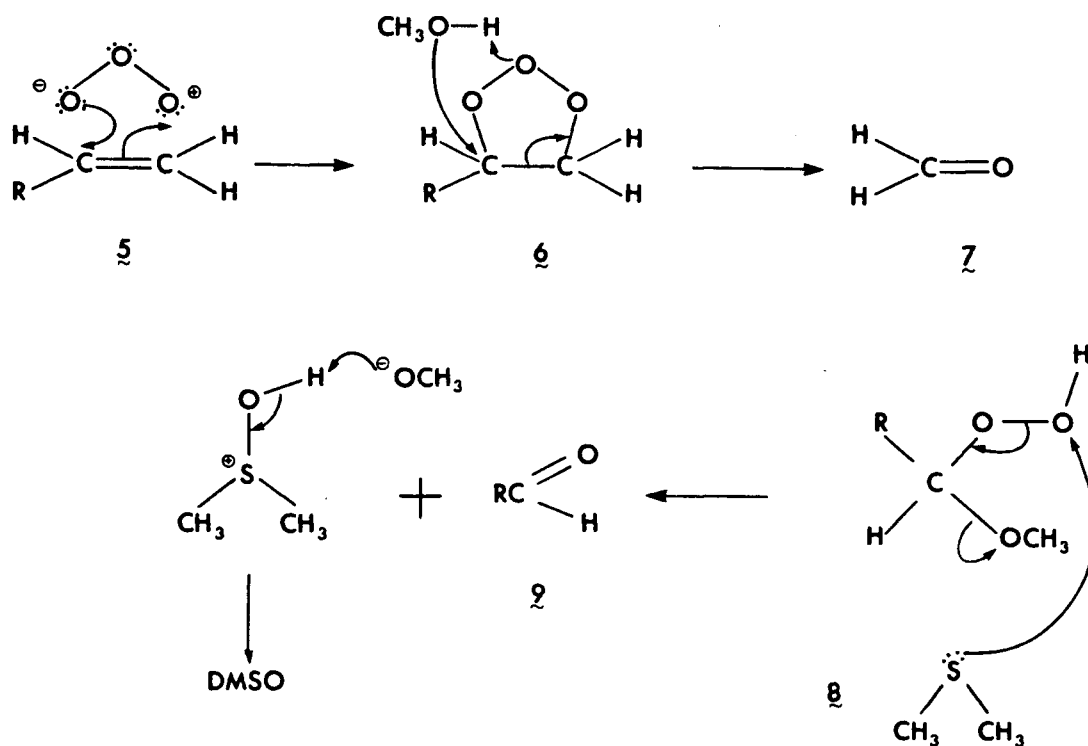
Fig. I.4.3. Reaction mechanism for the reductive ozonolysis of an alkene in methanol, using dimethyl sulphide.

After adding an excess of DMS, the solution is allowed to reach room temperature and left for ca. 2 hours. Methanol, methanal and unreacted DMS can be removed by rotary evaporation under reduced pressure and, in the case of the protected sugar, DMSO removed by repeated washing of a

chloroform solution with water. The aldehydo sugar (3) was only

isolated for the purpose of characterization, and the reaction routinely

monitored for completion by TLC.

The aldehydo sugar was then dissolved with BSA at a molar ratio

of ca. 5 (sugar:lysyl 6-amine). The pH was adjusted to 9.0, and a ca.

20-fold molar excess of $NaCNBH_3$ added. In the case of the coupling of a

blocked sugar, a heterogeneous reaction was performed in a

water/methanol solvent pair (85:15). The mixture was shaken and

coupling allowed to proceed for 18-48 hours, at which time the

neoglycoprotein was isolated. The homogeneous solution was applied to a

Sephadex G-25 column and the excluded volume collected. In some cases

this was further purified by dialysis against running water, and then

the solution was lyophilized.

The solid neoglycoprotein was stored at -4°C. Sugar analyses

were performed on milligram quantities using the standard phenol-

sulphuric acid assay,[16] with a calibration curve prepared from freshly

prepared standard solutions of the appropriate sugar. The protein was

not found to interfere with the assay, and accuracies are within 10%.

Using the above-mentioned procedures, neoglycoproteins (10-17)

were prepared. The coupling conditions chosen were, largely, those of

Schwartz and Gray.[17] The use of ratios of sugar/amine (5:1), should,

based on other workers' experience,[18] result predominantly in 2° amine

formation at the ~35 easily accessible 6-amino groups on BSA. The

higher levels of incorporation observed with the attachment of

acetylated sugars to BSA, in methanolic/aqueous solutions, could either

Table I.4.1 - Table of sugars coupled to BSA and their efficiencies.
BSA bears 55, lysyl 6-amino groups per molecule.

[a]Expressed as mole/mole

	Sugar Glycoside	Aglycone	Coupling Efficiency	Sugars per BSA Molecule[a]
10	α-galactose	allyl	36	20
11	α-glucose	allyl	36	20
12	β-N-acetyl glucosamine	allyl	5	3
13	β-lactose	allyl	24	13
14	α-acetoglucose	allyl	36	20
15	β-acetoglucose	allyl	69-82	38-45
16	β-aceto-N-acetyl-glucosamine	allyl	24	13
17	β-acetoglucose	undecenyl	15	8

result from the "exposure" of formerly inaccessible amines, or 3° amine

formation (i.e. attachment of >1 sugars to each amine) resulting,

perhaps, from a decrease in aldehydrol concentration caused by the

reduced water concentration.

Although extensive pH profile studies were not performed here,

the reaction was found to proceed with greater efficiency in

non-buffered solutions. This could result from the anionic form of the

buffer associating with the cationic lysyl 6-amino group (pH < 10) in an

ion pair, thereby "shielding" it from collision with the aldehyde, and

possible aldimine formation.

Coupling reactions were often performed overnight (18 hrs) but

satisfactory levels of derivatization were possible in 2-4 hrs. Rather

than extensively characterize an already well-studied reaction, we were

content with the levels of substitution and made no attempts to

"fine-tune" the coupling procedure. Similarly, we make no attempt to

interpret the varying coupling levels too closely.

Neutral free sugars appear to give a substitution level of

coupling of ca. 20 sugars per BSA*, and N-acetyl glucosamine appears to

give lower levels. Lactose coupled to BSA at a lower level of

efficiency caused, perhaps, by its greater bulk. The highly efficient

coupling of β-acetoglucose (38-45 sugars/BSA) cannot be explained

without further experiments. The relatively low efficiency of coupling

the long-chain β-acetoglucose molecule could result from its reduced

solubility in aqueous media, and the possibility of its self-association.

---

*With much longer coupling times, up to 32 sugars may be
attached.

In summary, we believe we have developed a useful protocol for neoglycoprotein synthesis. By capitalizing on prior detailed analyses of a similar coupling reaction, such studies were obviated here. The limitations of Gray's procedure are circumvented by using a sugar glycoside bearing a "nascent" aldehyde on the aglycone in the form of an alkene. Protected* or free sugars have been attached to lysyl 6-amine groups of a common test protein, BSA.

It is appropriate to mention related developments which have occurred since the inception of our studies. Lee and Lee have reported[18,19] the synthesis of 1-thioglycosides bearing ω-aldehydo groups, stored as a dimethyl acetal. Acid hydrolysis of the acetal (0.05 $\underline{M}$ HCl, 100°, 20 min.) is required before the coupling stage, and we draw the reader's attention to the possibility that acid-sensitive glycosidic bonds (e.g. fucosyl) may be hydrolysed at this stage, should these sugars be present. Jentoft and Dearborn performed[3] a detailed analysis of the reductive amination reaction with methanal and BSA – a close comparison between their observations and ours is dangerous, due to the very different nature of the aldehyde. Lee and Lee recently described[20] the use of 1-thioaldehydo sugars very similar to ours; they observed that at very high sugar/protein molar ratios (ca. 1000:1) as many as 70 sugars can be attached to each BSA molecule. Obviously, in this case, a large number of 3° amines are formed, and the authors also postulate the existence of ~35 "accessible" lysyl 6-amine groups, and the rest relatively hidden. One might postulate that the latter are perhaps involved in ionic bonds with acidic amino acids, to stabilize the

---

*Neoglycoproteins of this kind can be de-O-acetylated, if required.

protein's tertiary structure. Finally, Friedman et al. have reported the reductive amination of a protein and an aromatic aldehyde;[21] the reaction proceeds in very good yield (ca. 90% of lysyl 6-amines modified), suggesting that this non-polar aldehyde can penetrate the protein to the lysyl amines previously determined "inaccessible". This finding is in accord with ours for the neoglycoprotein (15), where a very high yield was observed when coupling a protected sugar, which is relatively apolar, to a methanolic/aqueous solution of BSA.

I.4.3 ^{13}C NMR of Neoglycoproteins

Literature precedent has established ^{13}C NMR spectroscopy as a useful tool in the study of proteins in solution, within the restraints of the necessary large sample size and high solubility (caused by the low inherent sensitivity of ^{13}C). Comparing the spectra of native and denatured proteins, it became clear in the late 1970's that it would be possible to observe single carbon sites in the native protein.[22]

The relaxation behaviour of ^{13}C nuclei is of great importance as it has the potential to report on the mobility of the protein at a specific site, once the relaxation mechanisms are understood. Therefore, it is common to report T_1, nOe and line-width ($\Delta v_{0.5}$) measurements in an attempt to derive conclusions on this fundamental aspect of protein behaviour in solution (vide infra).

To simplify analysis the protein's spectrum is divided into three regions:- aliphatic region (δ 10-75), aromatic region (δ 105-160) and the carbonyl region (δ 170-185). The 100.3 MHz ^{13}C NMR spectra of native and denatured BSA are shown in Fig. I.4.4.
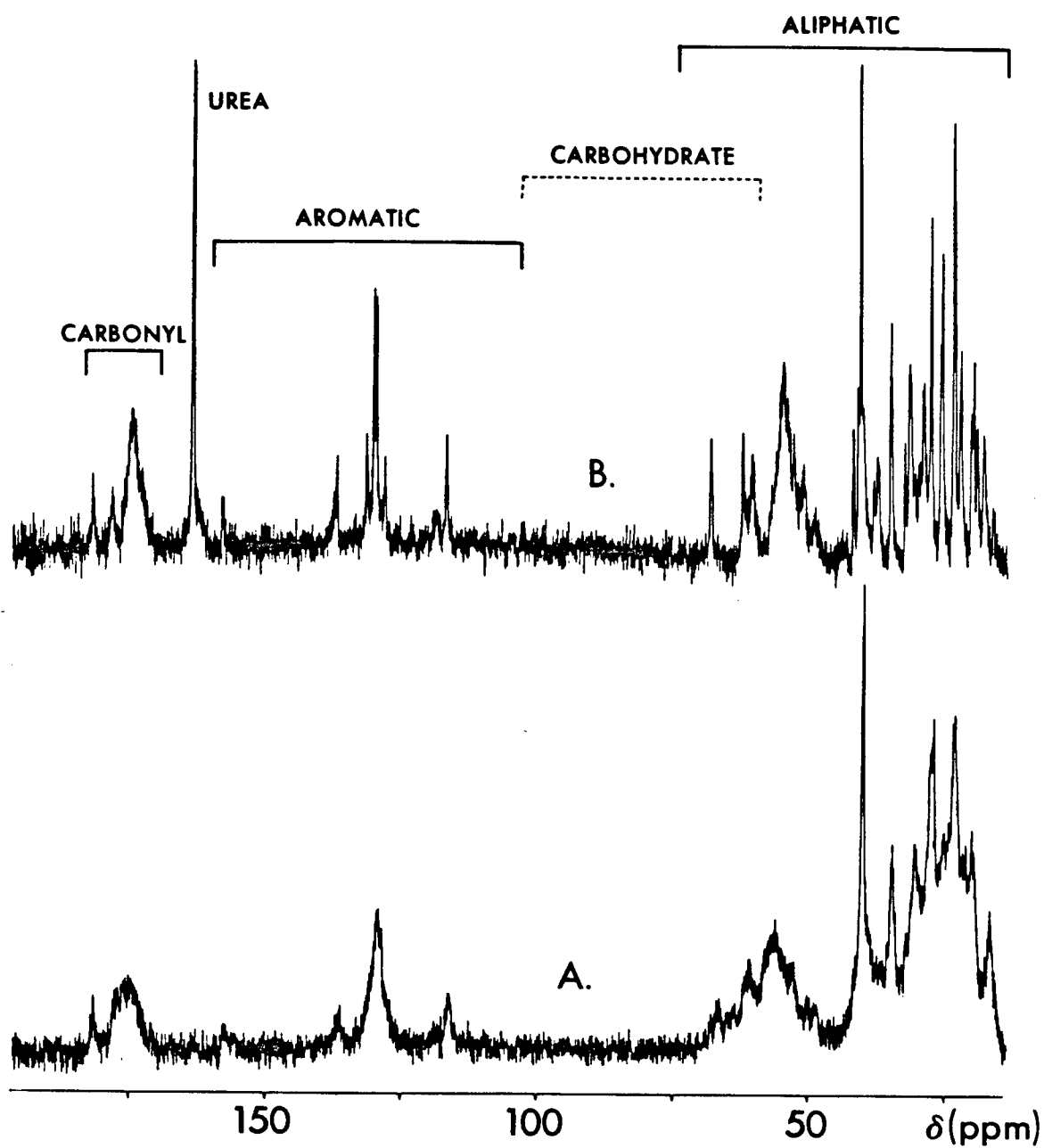
Fig. I.4.4 ^{13}C NMR spectra at 100.3 MHz of (A) native BSA in D_2O, and (B) the denatured protein in 8 $\underline{M}$ urea/D_2O.

It is well known that the ^{13}C NMR spectra of common neutral carbohydrates[23] is divisible into two regions:- the O-glycosidic anomeric carbon region (δ 95-105) and the region in which the rest of the hydroxylated and N-glycosidic anomeric carbons resonate (δ 60-80). Clearly, the anomeric carbons fall into a spectroscopically silent "window" of the protein spectrum, and the other carbohydrate resonances overlap slightly with a few protein aliphatic resonances (mainly, serine and threonine C^β). Hence it would seem reasonable to postulate that anomeric carbons will be uniquely discernible and other carbohydrate carbons somewhat less so, in the ^{13}C NMR spectrum of natural or synthetic glycoproteins.

A possible factor in the assignment of carbohydrate resonances between δ 60-80 might be the relative mobility of the overlapping resonances. Our previous studies (Chs I.2 and I.3) indicate that the terminal sugar has at least an order of magnitude of rotational freedom greater than the protein and this, reflected in their line-widths, could prove sufficient to differentiate the two. To illustrate this point, Fig. I.4.5 shows the result of superimposing the spectrum of native BSA with that of β-O-methyl glucopyranoside. In Fig. I.4.5B, the sugar resonances are broadened by 2 Hz with an Exponential filter, and in Fig. I.4.5C, by 15 Hz; only the "carbohydrate region" (δ 60-110) is plotted, and the carbohydrate peaks assigned.[23] Clearly, a large number of relatively mobile carbohydrate resonances can be readily distinguished from the broader peaks originating from protein carbons, in Fig. I.4.5B.
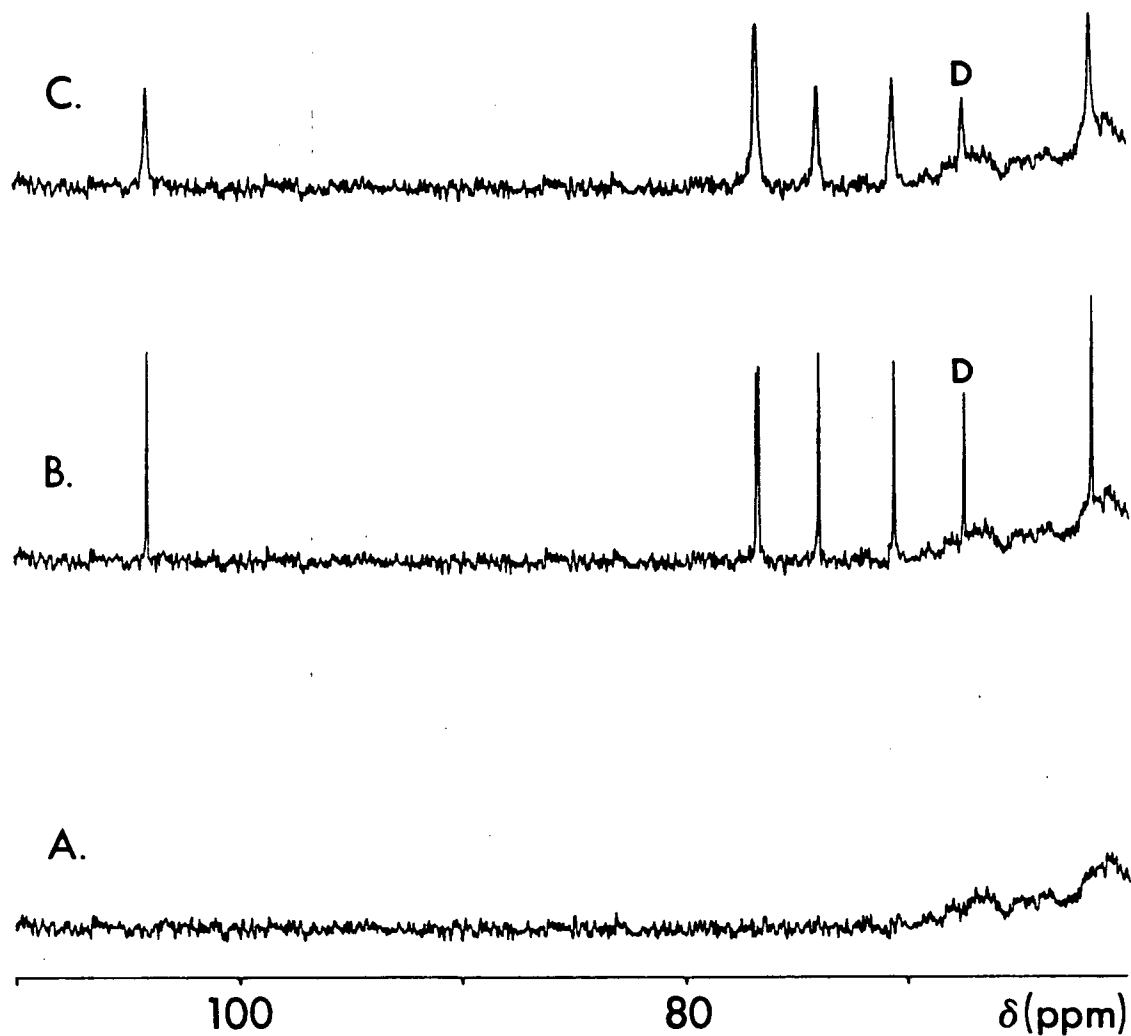
Fig. I.4.5 ^{13}C NMR spectra at 100.3 MHz, showing the "carbohydrate region" only. (A) Native BSA. (B).(A), superimposed with the spectrum of methyl β-D-glucoside, with

line-widths broadened by 2 Hz. (C).(B), with line-widths broadened by 15 Hz. D: internal dioxane reference (δ 67.4).

These elementary "feasibility studies" bode well for the possibility of observing ^{13}C sites on a (neo)glycoprotein, but they cannot predict the possible effects the protein may have on the ^{13}C chemical shifts of the sugar(s). ^{13}C resonances are notoriously difficult to assign and the most common resource is to make comparisons between the chemical shifts of known, assigned molecules and those of the "unknown". Thus, we might consider the methyl glycosides of mono-, di- and oligosaccharides to be useful model compounds in the assignment of (neo)glycoproteins' ^{13}C NMR spectra, and we went about testing this theory. Pfeffer et al. have used deuterium isotope-induced shifts (DIS) to assign the ^{13}C NMR spectra of a range of mono- and disaccharides,[23] and their data was used throughout this study. This was the rationale for studying neoglycoproteins as model glycoproteins: the carbohydrate moieties have been assigned independently of the protein and, by recording the ^{13}C NMR spectra of the (known) same sugar, now attached to the protein, useful generalizations might be derived concerning assignment in the glycoconjugate.

Fig. I.4.6 shows the 100.3 MHz ^{13}C NMR spectrum of a neoglycoprotein comprising β-glucose attached to BSA* (11, having 14 glucose molecules per BSA), comparing it with the spectrum of BSA. The carbohydrate region is expanded above the full spectrum and the chemical shifts of methyl β-D-glucoside indicated above the peaks. We immediately note that the carbohydrate peaks are sharp in comparison

---

*All neoglycoproteins were prepared by the procedure detailed in the previous section (I.4.2).
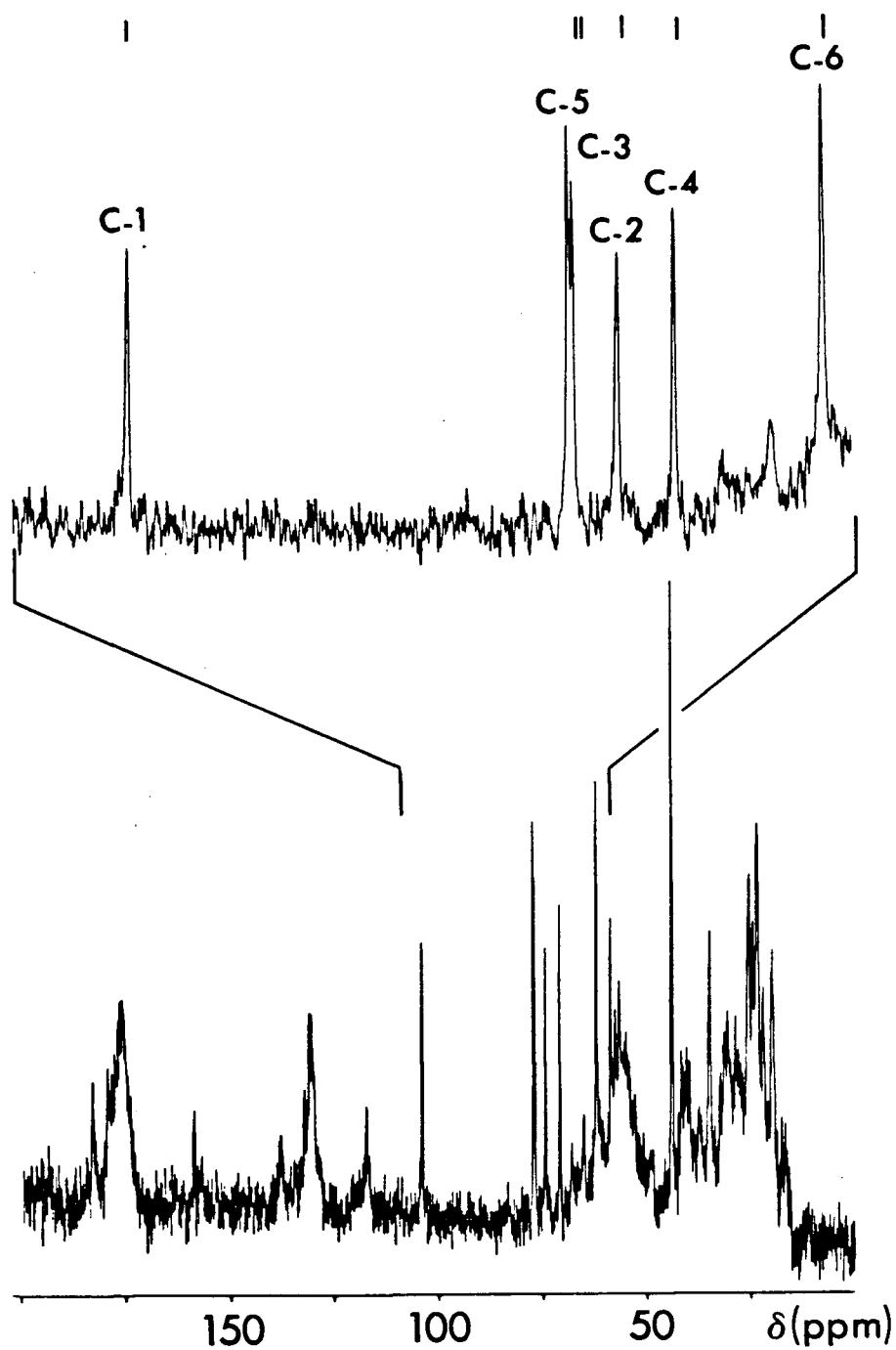
Fig. I.4.6 ^{13}C NMR spectrum of a neoglycoprotein (β-glucose attached to BSA), with the "carbohydrate region" expanded and asigned. Lines aboves the resonances indicate the literature chemical shifts of methyl β-D-glucoside.
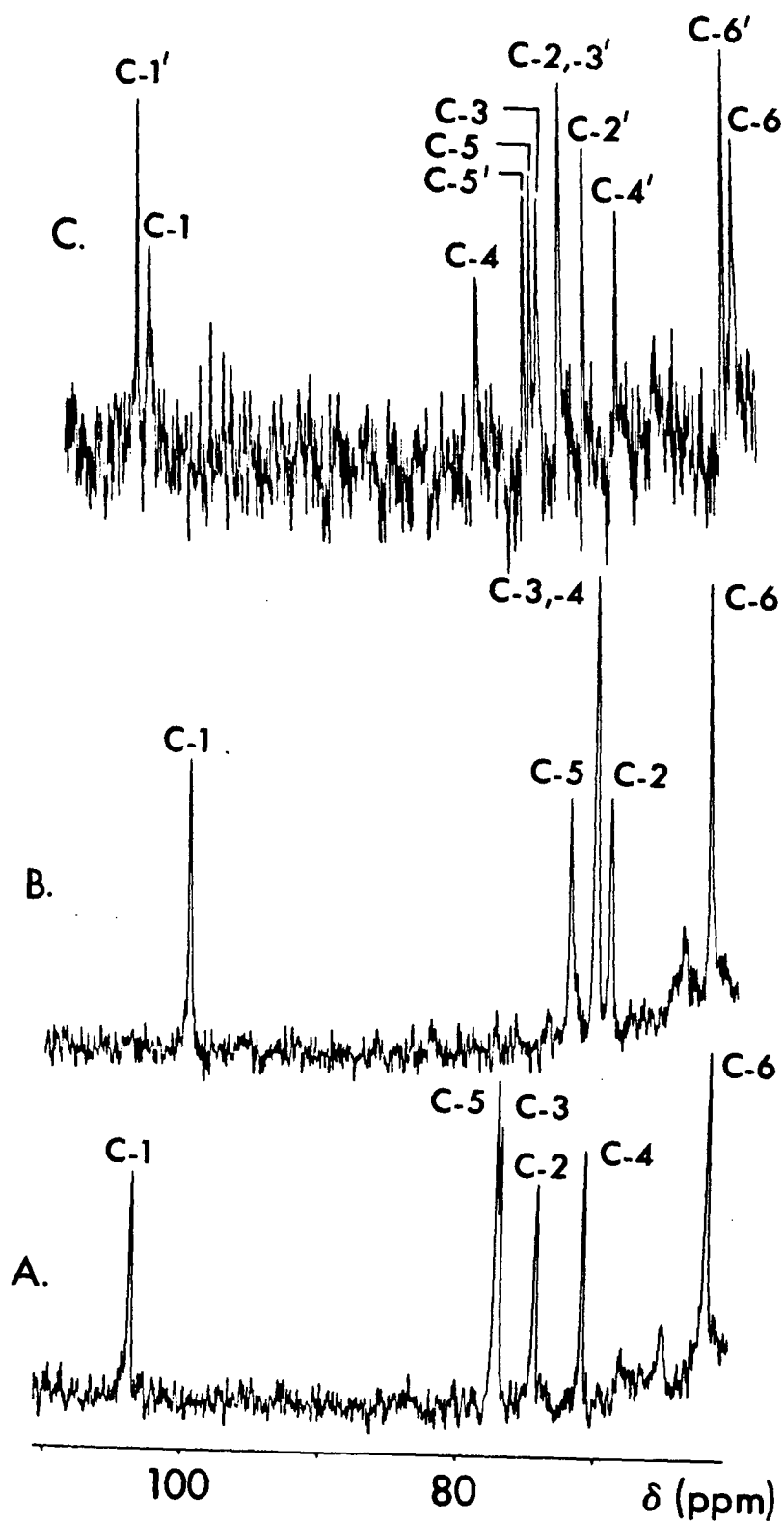
Fig. I.4.7. The "carbohydrate region" of the 100.3 MHz ^{13}C NMR spectrum of three neoglycoproteins: (A) β-glucose, (B) α-galactose, and (C) β-lactose attached to BSA.

Table I.4.2 Comparison of ^{13}C chemical shifts of the carbohydrate resonances of neoglycoproteins with the methyl glycoside of the attached sugar. The chemical shifts of neoglycoproteins are with an error of ± 0.1 ppm. Δδ represents the difference in chemical shift between a sugar resonance of a neoglycoprotein and its corresponding methyl glycoside.

	C-1	C-2	C-3	C-4	C-5	C-6	C-1'	C-2'	C-3'	C-4'	C-5'	C-6'
β-glc-BSA	103.1	74.0	76.6	70.6	76.9	61.7						
β-Me-glc	103.4	74.1	76.8	70.7	76.8	61.8						
Δδ	-0.3	-0.1	-0.2	-0.1	-0.1	-0.1						
α-gal-BSA	99.6	69.2	70.2	70.2	72.1	62.1						
α-Me-gal	100.1	69.2	70.5	70.4	71.6	62.2						
Δδ	-0.5	0.0	-0.3	-0.2	-0.5	-0.1						
β-lac-BSA	103.3	73.8	75.4	79.7	76.0	61.4	104.1	72.1	73.8	69.7	76.4	62.0
β-Me-lac	103.8	73.8	75.3	79.3	75.6	61.1	103.8	71.9	73.5	69.5	76.2	62.0
Δδ	-0.5	0.0	0.1	0.4	0.4	0.3	0.3	0.2	0.3	0.2	0.2	0.3

with those of the protein, and the chemical shift correlation is excellent. Fig. I.4.7 shows the ^{13}C NMR spectrum of the carbohydrate region of the three neoglycoproteins indicated. Sharp resonances are seen in every case and the measured chemical shifts are compared with those of their parent methyl glycosides in Table I.4.2.

Within the limits of ± 0.5 ppm, the agreement in chemical shifts between the methyl glycoside and the corresponding neoglycoprotein sugar resonances is excellent, with the constraints of this statistically small survey. Except for a trend for C-1 to be slightly deshielded (≈0.5 ppm) in the neoglycoprotein compared with the methyl glycoside, the differences in chemical shift (Δδ) are often within the experimental error of the measurement. Hence, we conclude that the methyl glycoside of a sugar may be used to give chemical shifts which can be compared closely (± 0.5 ppm) with the chemical shifts of the sugar attached to a protein. This is an important finding and is analogous to the use of small saccharides' chemical shifts to assign and determine the structure of polysaccharides,[24] which is now a relatively common procedure.

We then decided to extend the study and determine whether some of the technologies used in previous chapter could be applied to these systems to assist in carbohydrate structure determination. Specifically, we considered D-galactose oxidase which catalyses the oxidation of, e.g., methyl α-D-galactose to the molecule having an aldehyde at C-6; in aqueous solution, methyl α-D-galacto-hexodialdo-1,5-pyranoside (19), predominates. This reaction has been studied by ^{1}H NMR by Maradufu and Perlin,[26] and Whyte and Englar.[27] The ^{13}C chemical
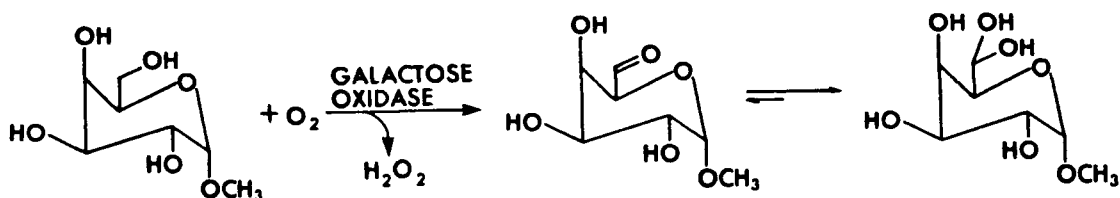
Fig. I.4.8. The action of D-galactose oxidase on methyl
α-D-galactopyranoside.

shift of an aldehydrol may be typified by a study[28] on streptomycins in

D_2O; C-13 (aldehydrol) has a chemical shift of 90-96 ppm. The chemical

shift of the hydrated aldehydic carbon of acetaldehyde is 88.9 ppm.

Hence, we might confidently anticipate that the ^{13}C chemical shift of

C-6 of a terminal galactosyl residue on a glycoprotein might change by

~ 30 ppm after oxidation with galactose oxidase and the aldehydrol

should be easily detectable, as it resonates in a spectroscopically

"silent" region. To test this, and ascertain the effect of oxidation at

C-6 on the other ring carbons' chemical shifts, we subjected a 0.2 M

solution of methyl α-D-galactopyranose to such an oxidation, measuring

the ^{13}C NMR spectrum before and after the reaction (Fig. I.4.9). Fig.

I.4.9A shows the ^{13}C NMR spectrum before, and Fig. I.4.9B after ca. 20%

galactose oxidase oxidation. The shift in resonant frequency (Δδ) is
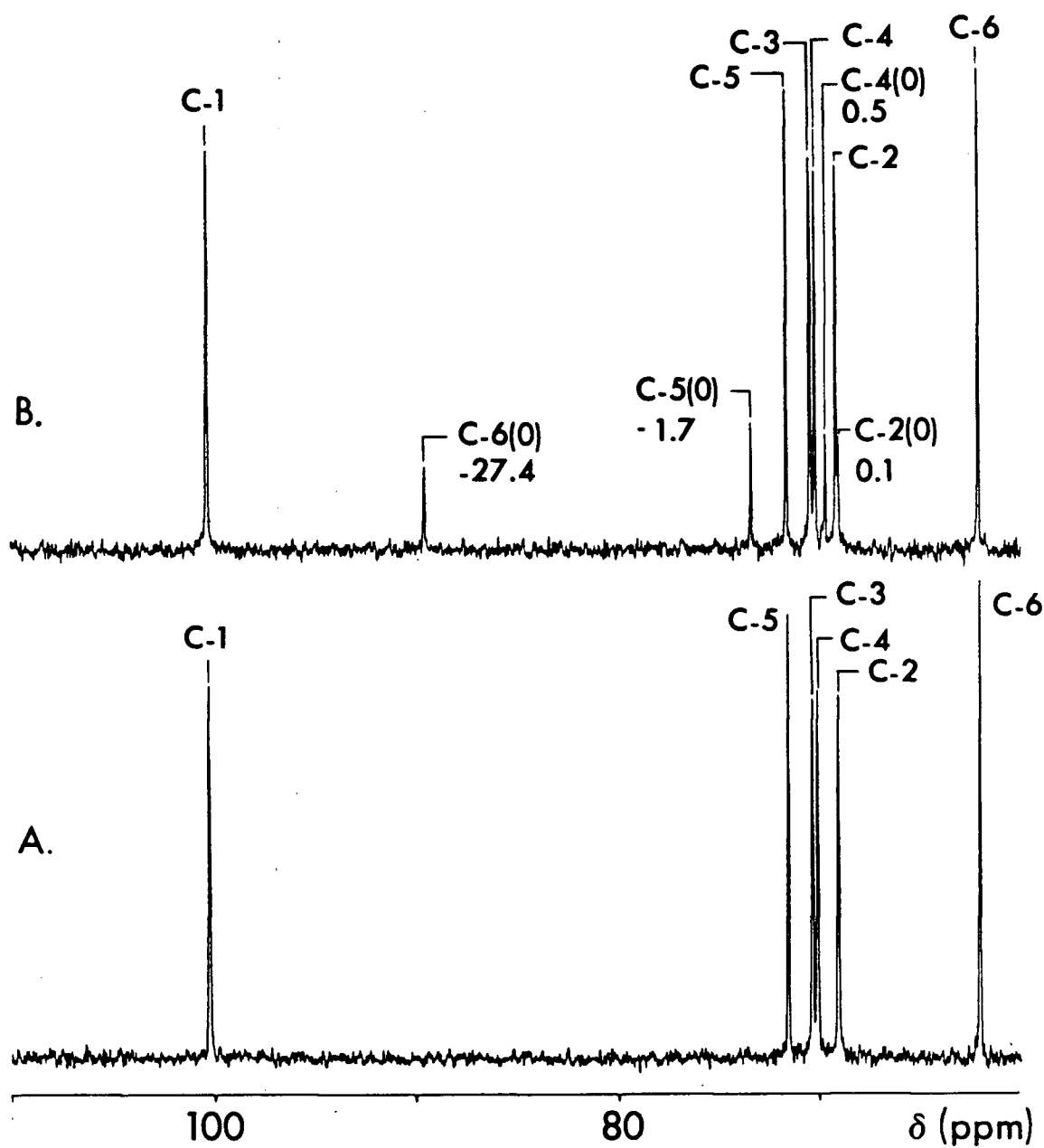
Fig. I.4.9 ^{13}C NMR spectrum (100.3 MHz) of (A) methyl α-galactoside, and, (B), the same after oxidation at C-6 by D-galactose oxidase, at 20% efficiency.

recorded for each carbon. As might be expected, C-6 suffers the largest shift (-27.6 ppm); C-5 and C-4 are also shifted significantly. Only C-1 and C-3 did not shift measurably. It is interesting to note that the relative peaks heights of C-6 and C-3 do not change significantly with oxidation, but the decreased intensity is measurable in peak areas of C-2, C-4, C-5 and C-6. This pilot experiment bodes well for the use of galactose oxidase in the assignment of C-4, -5 and -6 terminal galactosyl residues, especially when an accurate integration is possible.

Galactose-containing neoglycoproteins were then reacted with galactose oxidase. Compound 13 bears terminal galactose residues (lactose bound to BSA) and, after treatment with the enzyme, the spectrum in Fig. I.4.10B was obtained. The aldehydrol C-6' is clear (δ 98.8), but the level of oxidation is low, as the large galactosyl methylene C-6' peak suggests. This peak is narrower, (indicating less area), and so we may only conclude from this experiment that (a) the pendant sugar bears terminal galactose residues, and, (b) the galactosyl C-6 resonates at δ 62.0. Shifts in resonance frequency of other carbon centres are small, overlap with other peaks, or are lost in the noise. Whether this would be the case with complete oxidation is not possible to predict, but the model study with the α-galactoside, above, suggests that significant shifts in the resonance frequencies of C-5' and C-4' would occur, assisting in their assignment, too.

Two control experiments were performed. Firstly, the oxidized sample which gave the spectrum of Fig. I.4.10B was reduced with sodium
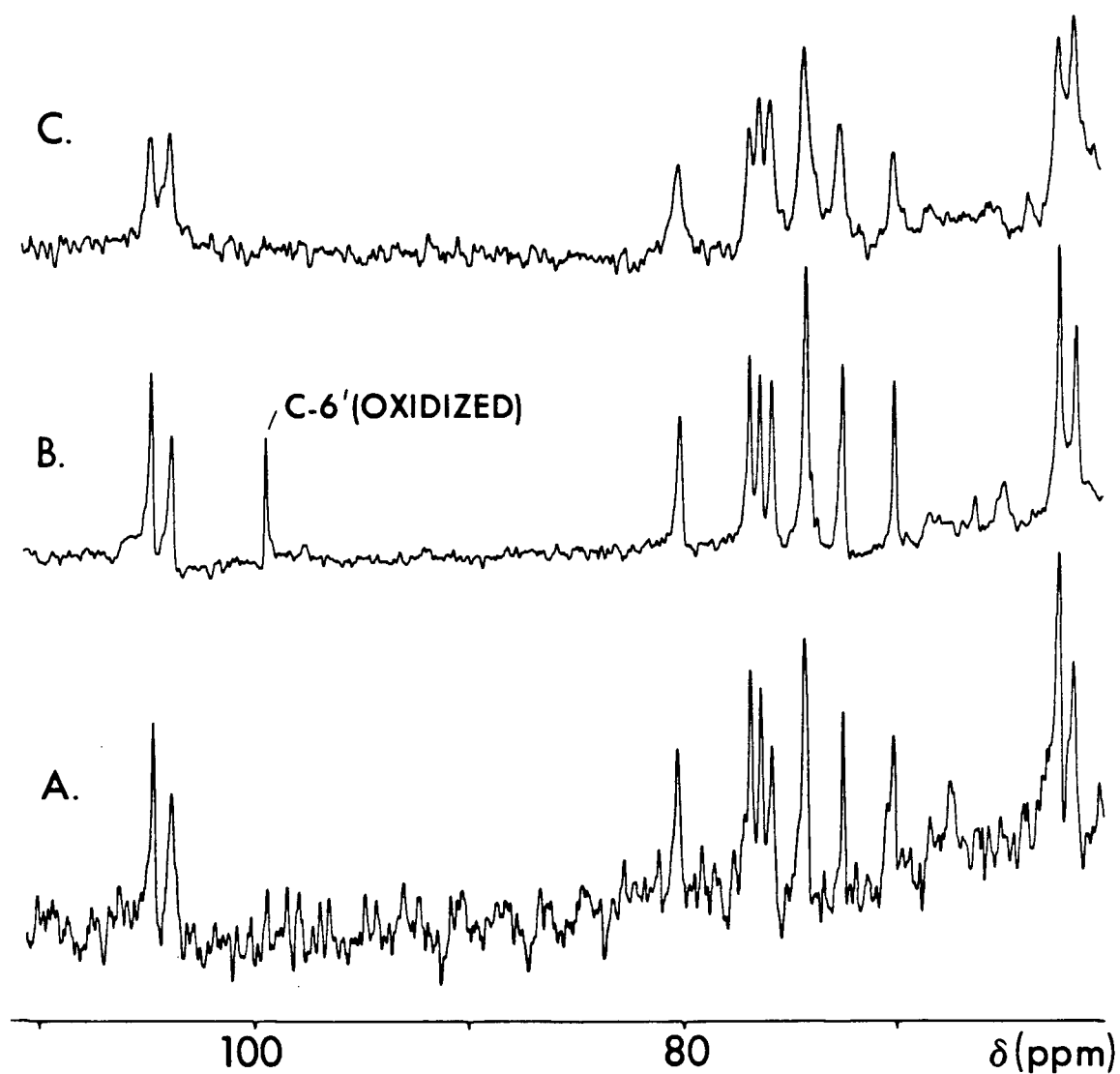
Fig. I.4.10 The 100.3 MHz ^{13}C NMR spectrum of β-lactose attached to
BSA. (A). Unoxidized. (B) After oxidation by galactose
oxidase overnight. (C) After reduction of (B) with
NaBH$_4$.
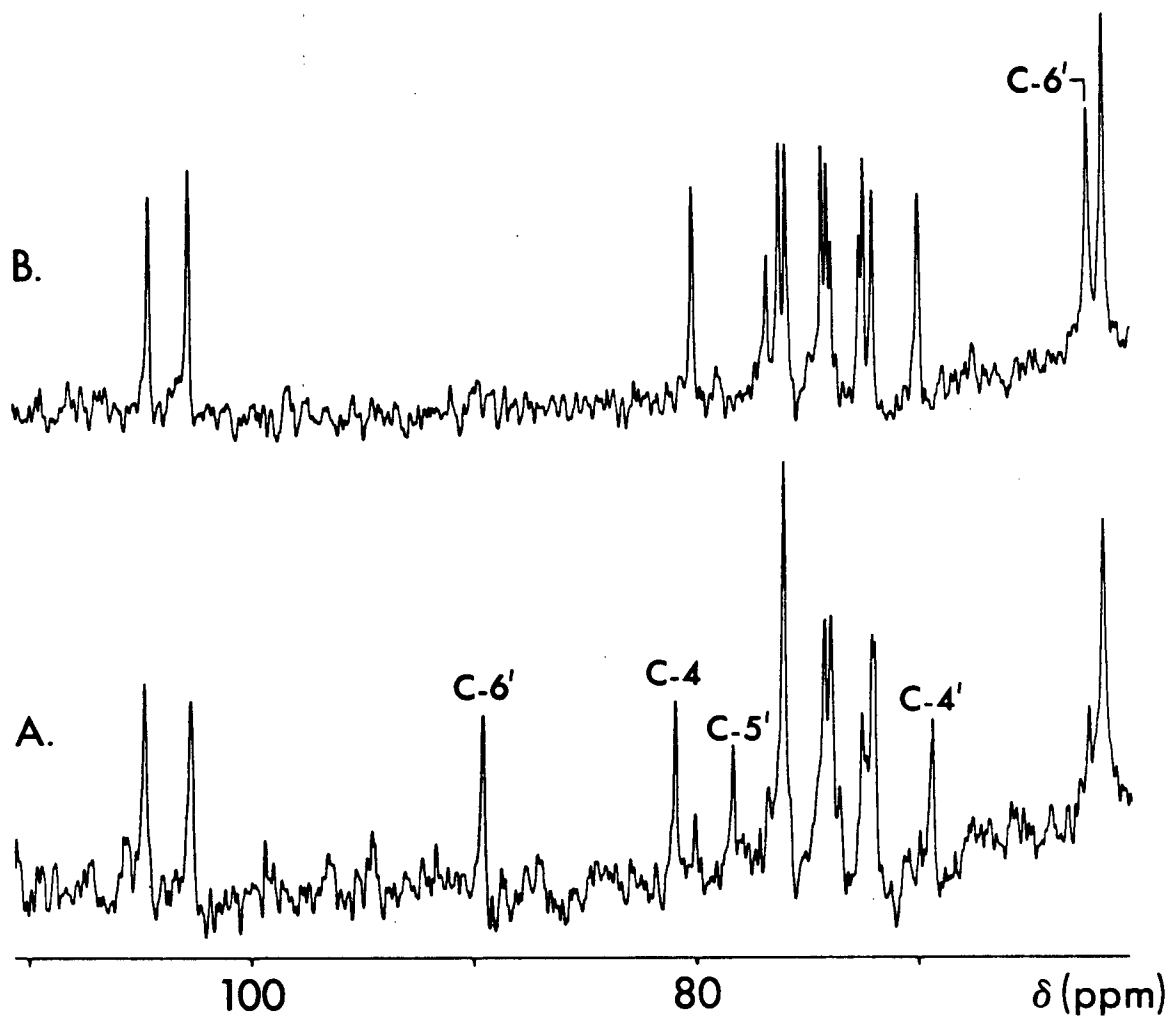
Fig. I.4.11 The 100.3 MHz ^{13}C NMR spectrum of a mixture of BSA and allyl β-lactoside, (A) after enzymic oxidation by galactose oxidase, and (B), after NaBH$_4$ reduction of (A).

borohydride (Fig. I.4.10C). By this time the sample was quite degraded,
and this is evident in the line-widths in Fig. I.4.10C, which reflect
the fact that some sample had precipitated by the end of the
measurement. However, the aldehydrol peak is no longer present and the
spectrum bears the features of that of the starting material, as might
be predicted. To determine whether the protein was in some way
inhibiting the action of the enzyme, allyl β-D-lactoside was mixed with
BSA in a mole ratio comparable with the neoglycoprotein. Galactose
oxidase treatment almost completely oxidized C-6' as indicated by its
large down-field resonance shift (Fig. I.4.11A,B). Similarly with the
monosaccharide, C-5' shifts down-field 1.6 ppm, C-4' up-field 0.8 ppm
and the carbon involved in the glycosidic linkage (C-4) down-field by a
surprisingly large 0.9 ppm. The last observation has important
implications as it suggests that the galactose oxidase treatment gives
information on the point of attachment of the terminal galactose, too.
It is interesting to note the changes in the spectrum between δ 65 and
80 - many extra peaks appear after oxidation; it is possible that some
of these result from side-reactions galactose oxidase is known to
produce.[26]

Again, borohydride reduction resulted in the loss of the
aldehydrol peak, and a reappearance of the galactosyl methylene C-6'.
This second experiment is not a perfect control, but unambiguously shows
that galactose oxidase can oxidize C-6' galactose groups on lactose in
the presence of BSA, and that diagnostically useful chemical shift
changes occur with full oxidation.

Galactose oxidase failed to react with 10, α-galactose attached

to BSA. It is tempting to postulate that the free substrate (allyl

β-$\underline{D}$-lactopyranoside) can easily fit in the enzyme's active site and is

efficiently oxidized. Lactosyl-BSA (13) is partially oxidized due to

somewhat restricted "fit", or accessibility of substrate to enzyme

caused by the proximity of BSA. With galactosyl-BSA (10), the substrate

cannot fit into the active site at all, and no reaction can occur. To

test this hypothesis it would be interesting to synthesize a series of

alkenyl glycosides having spacer arms of varying length, attach each one

to BSA and determine the accessibility of the sugar to oxidation by

galactose oxidase. If our reasoning is correct, an increase in level of

oxidation should occur as the spacer arm is lengthened.

It is interesting to speculate on the effect specific chemical

modifications might have on the ^{13}C NMR spectra of (neo)glycoproteins.

It is probable that such approaches might usefully augment the enzymatic

approach which we have evaluated and found potentially useful.

In summary, studying the ^{13}C spectra of neoglycoproteins might

prove useful in the investigation of glycoproteins. The carbohydrate

resonances are sharper than most protein resonances, reflecting the

influence of their greater mobility on $\underline{T}_2$. The corresponding methyl

glycoside of the attached sugar appears to be a good model for [13]C

assignment. That is to say, if a sugar glycoside is characterized, and

its ^{13}C NMR spectrum assigned, it is reasonable to expect that the

spectrum of the same sugar attached to a protein will have peaks at the

same frequencies (± 0.5 ppm). Finally, except with only galactose

attached to a protein, terminal galactosyl residues present will be

determinable from their susceptibility to oxidation by galactose oxidase. This procedure not only identifies the presence of terminal galactose, but also clearly assigns a number of its resonances, and the attaching carbon in the sub-terminal sugar residue.

Finally, we make mention of the relevant ^{13}C NMR studies of glycoconjugates performed in other laboratories after the inception of our work; much of these come from the laboratory of Allerhand. Harris and Thornton[29] studied carbohydrate head-group dynamics of glycolipids in various phases; only anomeric resonances were assigned and it was concluded that the pentasaccharide had no differential in mobility along its chain, indicating a closely hydrogen-bonded entity. Dill and Allerhand[30] reported the first ^{13}C NMR spectrum of a glycoprotein, glucoamylase. Few specific assignments were possible due to the complex nature of the carbohydrate, but certain generalizations were possible. A study [31] on the highly regular and simple antifreeze glycoproteins yielded beautiful ^{13}C NMR spectra; a differential in mobility is quite clear from the carbohydrate line-widths and explicit assignments were possible by comparison of chemical shifts of low molecular weight analogues. The anomeric carbons were assigned on the basis of $^1J_{CH}$ measurements. Jennings et al. used chemical and enzymic methods to assist in the assignment of the ^{13}C NMR spectrum of a streptococcal polysaccharide.[32]

Ribonuclease (RNA'se) is found in glycosylated (RNA'se B) and non-glycosylated forms (RNA'se A), and both were studied by Allerhand and co-workers.[33] Protein folding was found to have small effects on the chemical shifts of close carbohydrate centres. Comparison of model

oligosaccharides allowed the structure determination of the complex glycoprotein carbohydrate.

Armitage and co-workers[34] characterized the glycopeptide of glycophorin A, a red-blood-cell membrane glycoprotein. Assignments were largely based on procedures common in polysaccharide studies - model compound chemical shifts plus additivity rules. Calcium ion titrations induced shifts in N-acetylneuraminic acid ^{13}C resonances. Several unusual shifts are explained by the involvement of hydrogen bonding in the maintenance of a fixed secondary structure.

Berman and Allerhand[35] studied the hydrolytic action, specificity, and kinetics of an α-mannosidase (endoglycosidase enzyme) on the glycopeptide of ovalbumin, where they found that most information came from a study of the anomeric region. The rationale for their assignments has not, yet, been published.

Goux et al. perfomed[36] a detailed relaxation study on uniformly ^{13}C-enriched galactose, attached by enzymatic methods to the carbohydrate chain of hen ovalbumin. The overall motion of the terminal residue was found to be anisotropic, comprising a slow (23 ns) isotropic contribution (arising from the motion of the glycoprotein as a whole) and a fast (40-80 ps) contribution arising from rotation of the carbohydrate C-H vector rotating at an angle of 30° about the effective axis of rotation.

Finally, Bedford and co-workers[37] have reported the ^{13}C NMR spectra of canine mucins. Purified materials yield reasonably sharp resonances in the carbohydrate region of the spectrum, which further sharpen when the material is treated with β-mercaptoethanol (which

reduces protein cysteinyl disulphide bridges). Their material was found to have a very low sialic acid content, which was surprising.

I.4.4 ^{1}H NMR of Neoglycoproteins

The previous section illustrated ^{13}C NMR as having the potential to be of considerable utility in the study of glycoproteins. Two major difficulties remain:- the large amounts of sample required (> 120 mg) and the difficulty of assigning complex glycans. The first problem may be partially solved by observing a more sensitive nuclide, such as ^{1}H, and in Chapter II.3 we describe how ^{1}H NMR may be used de novo to assign oligosaccharides.

When studying the ^{1}H NMR spectrum of glycoproteins, one major difficulty lies in the extensive overlap of glycan and protein signals. Our previous studies have indicated that the glycans are at least an order of magnitude more mobile than the protein, and this fact was seen to be pivotal in the route to the "spectroscopic factorization" of the sugar resonances. Literature precedent exists for the observation of rapidly tumbling molecules in the presence of immobile ones, where all methods rely on the differential in transverse relaxation times ($\underline{T}_2$) between the two entities. These will be reviewed at the end of the chapter.

All methods for such differentiation come under the heading of "spin-echo" techniques.[38] Essentially, a 90° pulse creating magnetization in the x'-y' plane is followed by a delay τ, and a second pulse is used to induce the spin-echo, having a maximum at 2τ. The choice of the delay is crucial, since this is where the slow and fast tumbling molecules are "sorted". Protons having long $\underline{T}_2$'s (rapidly

tumbling) will still have magnetization after the refocussing pulse (180°), and will, therefore, be observed; those with short T_2's (slowly tumbling) will have lost their transverse magnetization by the time the 180° pulse is applied and, therefore, will not be seen when the receiver is turned on.

The classical experiment is the Hahn spin-echo, comprising a (90°-τ-180°-τ-AQN) pulse-sequence. A spin-echo maximum is generated at 2τ, and the following half-echo is then acquired (see explanation of 2D J-resolved spectroscopy, Ch. II.2.5.2). The amplitude of the refocussed echo is determined by a T_2 term, and in some cases, diffusion rates and magnetic field field gradients will enhance the decay of the spin-echo amplitude. With homonuclear spin-coupled spins, the peaks' phases will be "J-modulated", meaning that the peaks may be partially or fully inverted. In some instances, such as when J is known, this may be of utility for assignment purposes, but this is not often the case. One recourse is to calculate the phase-insensitive spectrum (magnitude, or power mode), but contributing dispersive components lead to broad lines being observed with this approach.

If a high-resolution spin-echo spectrum with no J-modulation is required, one of two approaches may be taken. A train of closely spaced 180° pulses can be used to refocus the magnetization[38] (rather than a single 180° pulse) and this removes the dependencies on J and the diffusion and magnetic field gradient terms.[39] Phase-sensitive display is used and narrow lines are observed. Alternately, one can make use of SEAS[40] (spin-echo absorption spectroscopy), which requires collection of

the full Hahn-echo $(90°_x - \tau - 180°_{\pm x} - AQN)$. With a fully symmetrical echo, Fourier transform (FT) and phase-insensitive display removes J-modulation and gives absorption-like peaks.

Although the two methods were not critically compared in our laboratory, we chose to use SEAS for these studies. The basic experiment was modified slightly to include a solvent null procedure - 3 s presaturation prior to the 90° pulse. A time-domain window function which insured that there was zero intensity at the beginning and end of the acquisition* improved spectral quality.

The first test of the technique was on a D_2O solution of BSA (14 mg/0.4 ml). Fig. I.4.12A shows the normal spectrum, with HOD solvent nulling; only broad spectral features are discernible. The SEAS experiment was then performed, with the indicated τ delays (Fig. I.4.12B-F). Using $\tau = 40$ ms results in very little signal intensity arising from the BSA protons, and so it was decided to perform all subsequent experiments using this delay time.

Results for the SEAS experiment ($\tau = 40$ ms) for a variety of molecules are given in Fig. I. 4.13. The question was: can SEAS be used to yield the spectrum of the glycan portion of a glycoconjugate with sufficient detail for this to be of utility in their assignment?

Firstly, BSA and the β-allyl glycoside of acetylated glucosamine were co-dissolved in D_2O. SEAS ($\tau = 40$ ms) yielded spectrum I.4.13B, which compares favourably with the spectrum of the monosaccharide in D_2O

---

*The Nicolet (NTCFTB) "trapezoidal multiplication" (TM) command was used.
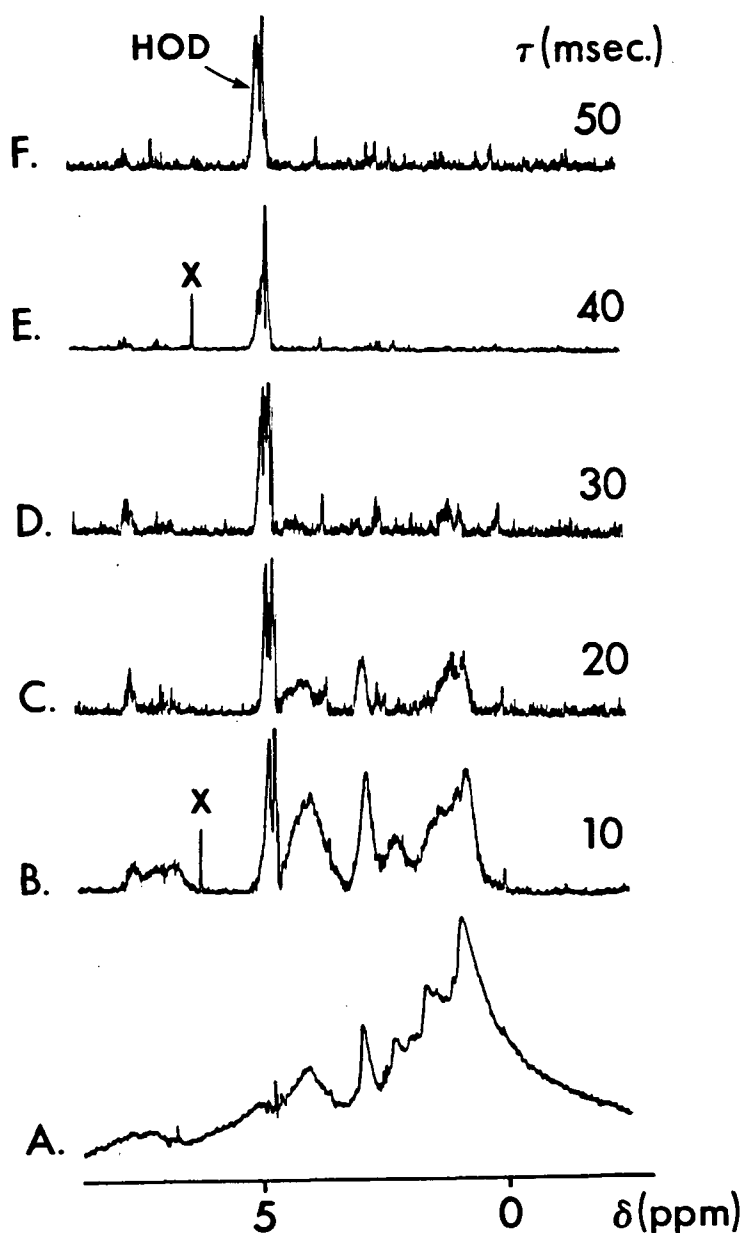
Fig. I.4.12 The 270 MHz ^{1}H spectra of BSA in D_2O (14 mg/6.4 ml). (A)
Single pulse experiment. (B)-(F) SEAS experiments with
the indicated τ values. The HOD was supressed by 3 s
presaturation.
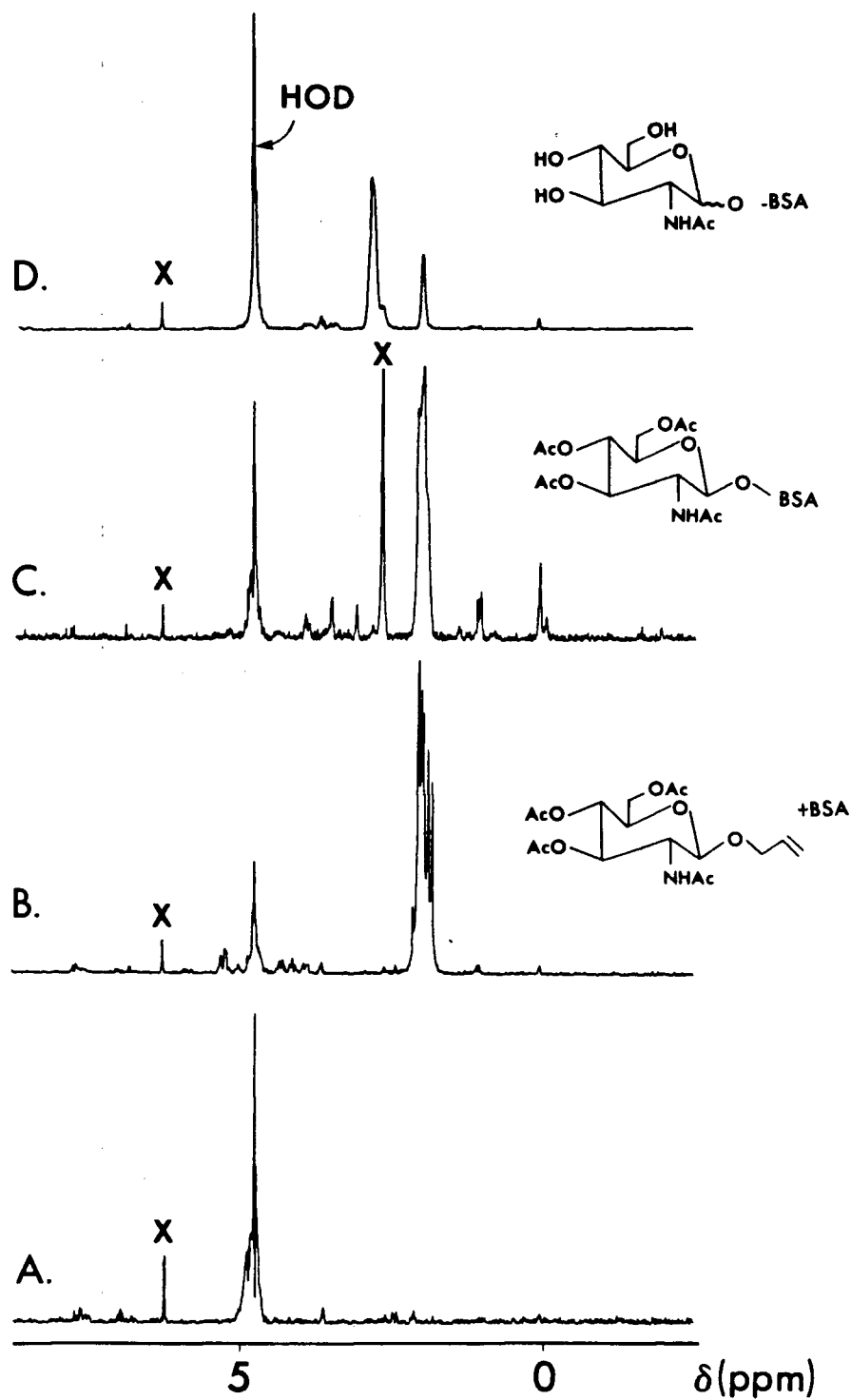
Fig. I.4.13 The 270 MHz ^{1}H SEAS spectra with τ=40 ms. (A) BSA. (B) BSA plus allyl β-acetoglucosamine. (C) β-AcetoglcNAc attached to BSA. (D) α- and β-glcNAc attached to BSA.

(data not shown). The carbohydrate spectrum is still clear even when using τ up to 100 ms. We conclude that SEAS can be used to yield the spectrum of a rapidly tumbling monosaccharide in the presence of a protein macromolecule.

Next, the neoglycoprotein having aceto-glucosamine attached to BSA (12) was studied and its SEAS spectrum is given in Fig. I.4.13C.* A pattern of peaks similar to the monosaccharide is evident, but much of the detail in coupling constants has been lost to the increased intrinsic line-widths. With $\tau > 40$ ms, the carbohydrate ring protons are rapidly lost, leaving only the acetyl peaks. The β-anomeric proton is, as with all these spectra, hidden under the incompletely suppressed HOD peak.

Next, a neoglycoprotein was prepared, bearing a 1:1 mixture of α- and β-N-acetyl glucosamine. The SEAS spectrum of this material is given in Fig. I.4.13D. Broad "humps" are visible in the carbohydrate region, but, again, little detail is evident upon close inspection, and the two anomeric proton signals cannot be detected, as hoped.

Our data indicate that SEAS can be used to obtain a ^{1}H spectrum of the carbohydrate moiety of a neoglycoprotein. The line-widths of the signals appear to be broadened slightly in comparison with the monosaccharide, to the point where they obscure the details of the coupling constants in the sugar spectrum. This is unfortunate, as part of the great strength of ^{1}H NMR as a method of structure determination lies in this information. Whether this situation could be remedied by the application of time-domain resolution enhancement functions[41] was

*Neoglycoproteins were synthesized as described in Ch. I.4.2.

not determined, but might be a possibility. The solvent peak overlap with the anomeric protons was a problem which could probably be partially alleviated by elevation of temperature. This would also increase the mobility (and sharpen the lines of) the carbohydrate molecules, which would be an added bonus. In short, the spin-echo experiments described here bode well for the incorporation of ^{1}H NMR in the scheme of procedures available for the study of glycan components of glycoconjugates. However, much work still has to be done before the utility of the procedure can be accurately assessed.

In 1975, Campbell et al. described[42] the use of spin-echo experiments to simplify protein spectra. Egmond et al. studied the ^{1}H NMR spectrum of the sialo-glycoprotein, glycophorin.[43] The broad, protein component was partially removed by the use of a convolution-difference time-domain function. Several aspects of the molecule's macroscopic behaviour were studied, and some sialo-sugar assignments were possible in the high-field region; the sugars were mobile, relative to the protein.

Several workers have used the Hahn spin-echo to study living erythrocytes. Brown and co-workers[44] assigned some of the unassociated, low molecular weight components of red blood cells (RBC's), and later went on to study RBC membrane transport using NMR.[39,45] Rabenstein[46] in Alberta has reported on several aspects of the chemistry of small molecules inside and out of RBC's.

The SEAS experiment was first described by Bax et al.[47] and later by Hall and Sukumar who applied it to a mixture of carbohydrates, lysozyme[40] and RBC's.[48]

I.4.5 Conclusions

To sum up, we have described an efficient route to the synthesis of artificial glycoproteins (neoglycoproteins). The method is quick and high-yielding, and we anticipate it could be of use, too, in the synthesis of carbohydrate haptens. Our use for this technology has been in NMR studies of conjugated sugars.

The study of neoglycoproteins by ^{13}C NMR is facilitated by the fact that the sugar resonances resonate, largely, in a spectroscopically "silent" region, and, through their enhanced mobility, may be identified. It was determined that the corresponding methyl glycoside of the sugar(s) attached to the protein acts as a good source of reference for assigning ^{13}C resonances, with our neoglycoproteins. No significant shifts in resonance frequency are observed when we compared three neoglycoproteins this way. Oligosaccharides bearing terminal galactose residues can be identified by oxidation with D-galactose oxidase. Significant shifts occur in galactosyl C-6, C-5 and C-4, and the carbon to which the galactosyl anomeric carbon is attached. With an α-galactoside and β-lactoside, the shifts were very similar in their direction and magnitude. This approach would appear to be of great potential in the assignment of sugars bearing terminal galactose, provided a reasonable level of oxidation can be achieved.

^{1}H NMR studies of neoglycoproteins require that special steps be taken to observe the sugar resonances; this can be done by a spin-echo experiment, SEAS. The method relies on differentials in mobilities (and T_2) and can easily give the spectrum of a monosaccharide with a

protein present. When the monosaccharide is <u>attached</u> to the protein, the differentiation is not as dramatic, and line broadening of the sugar resonances occurs to the point where it obscures many <u>J</u>-couplings. Several possibilities exist to remedy this and the other major limitation, <u>viz.</u>, the overlap of the solvent resonance with the anomeric proton, but these were not assessed.

We feel that these studies are, in their own right, of interest, but the hope is that the information derived will ultimately be of use in the study of glycoproteins using NMR.

REFERENCES

1. W.F. Goebel and O.T. Avery. J. Exp. Med. 50, 521-531 (1929).

2. G.E. Means and R.E. Feeney. Biochemistry. 7, 2191-2201 (1968).

3. N. Jentoft and D.G. Dearborn. J. Biol. Chem. 254, 4359-4365 (1979).

4. G.R. Gray. Methods Enzymol. 50, 155-160 (1978), and references cited therein.

5. J.D. Aplin and J.C. Wriston, Jr. CRC Crit. Rev. Biochem. 10, 259-306 (1981).

6. C.P. Lee and Y.C. Lee. Adv. Carbohydr. Chem. Biochem. 37, 225-281 (1980).

7. M.A. Bernstein and L.D. Hall. Carbohydr. Res. 78, C1-C3 (1980).

8. P.A. Gent and R. Gigg. J. Chem. Soc. Perkin Trans. 1. 361-363 (1975), and others in the series.

9. R.T. Lee and Y.C. Lee. Carbohydr. Res. 37, 193-201 (1974).

10. From the series:- Methods in carbohydrate chemistry. Academic Press, New York, Vols. 2 and 5. 1963 and 1965, respectively.

11. K. Igarashi. Adv. Carbohydr Chem. Biochem. 34, 243-283 (1977).

12. J. Balatoni. B.Sc. Thesis. University of British Columia. 1981.

13. H.O. House. Modern synthetic reactions. Benjamin, New York. 1972. Chapter 7, and references cited therein.

14. J.J. Pappas, W.P. Klareney, E. Gancher, and M. Berger. Tetrahedron Lett. 4273-4278 (1966). P.S. Bailey and R.E. Erickson. Org. Synthesis. 41, 41-45 (1961).

15. P.S. Bailey. Chem. Rev. 58, 925-1010 (1958).

16. M. Dubois, K.A. Gilles, J.K. Hamilton, P.A. Rebers, and F. Smith. Anal. Chem. 28, 350-356 (1956).

17. B. Schwartz and G.R. Gray. Arch. Biochem. Biophys. 181, 542-549 (1977).

18. R.T. Lee and Y.C. Lee. Carbohydr. Res. 77, 149-156 (1979).

19. R.T. Lee and Y.C. Lee. Biochemistry. 19, 156-163 (1980).

20. R.T. Lee and Y.C. Lee. Carbohydr. Res. 101, 49-55 (1982).

21. M. Friedman, L.D. Williams, and M.S. Misri. *Int. J. Peptide Protein Res.* 6, 183-185 (1974).

22. A. Allerhand. *Accts. Chem. Res.* 11, 469-474 (1978), and references cited therein.

23. P.E. Pfeffer, K.M. Valentine, and F.W. Parrish. *J. Amer. Chem. Soc.* 101, 1265-1274 (1979); *Ibid.*, 7438 (correction).

24. P.A.J. Gorin. *Adv. Carbohydr. Chem. Biochem.* 38, 13-104 (1981).

25. See Chaps I.2 and I.3, and references cited therein.

26. A. Maradufu and A.S. Perlin. *Carbohydr. Res.* 32, 93-99 (1974).

27. J.N.C. Whyte and J.R. Englar. *Carbohydr. Res.* 57, 273-280 (1977).

28. K. Bock and C. Pedersen. *J. Antibiotics.* 27, 139-140 (1974).

29. P.L. Harris and E.R. Thornton. *J. Amer. Chem. Soc.* 100, 6738-6745 (1979).

30. K. Dill and A. Allerhand. *J. Biol. Chem.* 254, 4524-4531 (1979).

31. E. Berman, A. Allerhand, and A.L. De Vries. *J. Biol. Chem.* 255, 4407-4410 (1980).

32. H.J. Jennings, C. Lugowski, and D.L. Kasper. *Biochemistry.* 20, 4511-4518 (1981).

33. E. Berman, D.E. Walters, and A. Allerhand. *J. Biol. Chem.* 256, 3853-3857 (1981).

34. R. Prohaska, T.A.W. Koerner, Jr., I.M. Armitage, and H. Furthmayr. *J. Biol. Chem.* 256, 5781-5791 (1981).

35. E. Berman and A. Allerhand. *J. Biol. Chem.* 256, 6657-6662 (1981).

36. W.J. Goux, C. Perry and T.L. James. *J. Biol. Chem.* 257, 1829-1835 (1982).

37. K. Barrett-Bee, G. Bedford, and P. Loftus. *Bioscience Reports.* 2, 257-263 (1982).

38. R. Freeman and H.D.W. Hill. Determination of spin-spin relaxation times in high-resolution NMR. Edited by L.M. Jackman and F.A. Cotton. Academic Press, New York. 1975. pp. 131-162.

39. K.M. Brindle, F.F. Brown, I.D. Campbell, C. Grathwohl, and P.W. Kuchel. *Biochem. J.* 180, 37-44 (1979), and references cited therein.

40. L.D. Hall and S. Sukumar. J. Magn. Reson. 38, 559-564 (1980).

41. J.C. Lindon and A.G. Ferrige. Prog. in NMR Spectroscopy. 14, 27-66, 1980.

42. I.D. Campbell, C.M. Dobson, R.J.P. Williams, and P.E. Wright. FEBS Lett. 57, 96-99 (1975).

43. M.R. Egmond, R.J.P. Williams, E.J. Welsh, and D.A. Rees. Eur. J. Biochem. 97, 73-83 (1979).

44. F.F. Brown, I.D. Campbell, P.W. Kuchel, and D.C. Rabenstein. FEBS Lett. 82, 12-16 (1977).

45. F.F. Brown and I.D. Campbell. Phil. Trans. R. Soc. Land. B. 289, 395-406 (1980).

46. D.L. Rabenstein, S.J. Backs, and A.A. Isab. J. Amer. Chem. Soc. 103, 2836-2841 (1981), and others in the series.

47. A. Bax, A.F. Mehlkopf, and J. Smidt. J. Magn. Reson. 35, 373-377 (1979).

48. S. Sukumar. Ph.D. Thesis. University of British Columia. 1980.

CHAPTER I.5

EXPERIMENTAL FOR SECTION I

I.2 ESR Experiments

1. Reagents

All reagents were purchased and used without further purification: fetuin (Type IV, Sigma), BSM (Boehringer Mannheim), sodium periodate (Fisher), sodium cyanoborohydride (Aldrich), TEMPAMINE (Aldrich), Sephadex G-25 medium (Pharmacia), Vibrio cholera neuraminidase (Behringwerke, 500 U/ml), galactose oxidase (Sigma, 227 U/mg protein). Centriflo CF 25 cones (retention limit 25000 amu) were purchased from Amicon.

2. ESR Measurements

ESR spectra were recorded at X-band using a Varian E-3 spectrometer in the derivative absorption mode. Derivative signals were integrated with a Pacific Precision Co. MP-1012A integrator; second derivatives were calculated by cutting out and weighing the peak areas, and comparison with a standardization curve derived from ESR spectra of freshly prepared samples of spin label of known concentration. Spectrometer settings — modulation amplitude, filter time constant and scan rate — were chosen in each case to avoid spectral distortions, and power levels were non-saturating. All aqueous samples (50-73 μl were placed in a flat, high-quality glass cell (J. Scanlon Co. - capacity 73 μl).

3. Fetuin-SL

15 mg of fetuin (4.14 μmoles NANA) was dissolved in 2.7 ml H_2O, to which was added 14.6 μmoles $NaIO_4$ and the solution kept at 0° for 35 minutes. The reaction was quenched with an excess of $Na_2S_2O_3$ and KI. The solution was concentrated using CF 25 membrane cones. A 15 molar excess of SL-NH$_2$ and 100 molar excess of NaCNBH$_3$ were added in 1-2 ml of solution at pH 8-9; this was kept at room temperature for 2 hours. The solution was passed through a Sephadex G-25 column (eluant, 0.02% azide; column dimensions, 2.2 cm (i.d.) * 20 cm) and the excluded volume collected. The sample was freeze-dried and stored at -4°C until spectroscopic measurements were made.

4. Asialofetuin-SL

15 mg of fetuin was dissolved in 5 ml of buffer (pH 6.9, 0.2 $\underline{M}$ NaOAc, 0.15 $\underline{M}$ NaCl, 0.002 $\underline{M}$ CaCl$_2$), to which was added $\underline{ca}$. 20 units of galactose oxidase and 30 units of neuraminidase. The latter was added in equal aliquots, one at the start of the experiment, and the second after 24 hours. The solution was maintained at 37° for 48 hours. After Centriflo CF 25 concentration, the coupling procedure was as for sialo-fetuin (3).

5. BSM-SL

15 mg of BSM (16 μmoles sialic acid) was first saponified (removal of $\underline{O}$-acetyl substituents on NANA extracyclic triol) by exposure to 1.5 ml of 1 $\underline{M}$ NaOH for 30 min. at room temperature, and neutralized with 1 $\underline{M}$ HCl. Desalting was affected by Centriflo CF 25 membranes, and the material exposed to $NaIO_4$ (43 μmoles) for 35 min. at 0°. All other procedures were as for fetuin-SL (3).

6. AsialoBSM-SL

The native BSM was saponified as above (5) and the neuraminidase and galactose oxidase treatment performed as in (4). The coupling of TEMPAMINE proceeded as in (3).

7. Erythrocytes-SL

Freshly drawn venous blood from a healthy donor was packed, and to 7 ml of packed erythrocytes, 0.5 ml of 0.01 $\underline{M}$ NaIO$_4$ was added. The solution was kept at room temperature for 15 min. The oxidation was terminated by the removal of reagents - three washes with physiological saline solution, with RBC precipitation by centrifugation (400 g, 10 min). A 25 fold molar excess of SL-NH$_2$ and 100 fold molar excess of NaCNBH$_3$ were added and the saline solution (pH 7.5-8) kept at room temperature for 2 hours. With centrifugation and washing, some cell lysis was indicated by a slightly red supernatant. The labelled erythrocytes were dialysed against PBS buffer for 3 days at 4° - the buffer was changed daily. The cells were spun down and ESR spectra run on packed erythrocytes.

I.3 ^{2}H NMR

^{2}H NMR spectra were recorded at 61.4 MHz (B$_0$ 9.4 T) on a Bruker WH-400 instrument (Karlsruhe, West Germany, and U.B.C.). Samples were either dissolved in distilled water (spectra in Fig. I.3.3) or deuterium-depleted water (Aldrich). The $\underline{ca}$. 1.5 ml sample, in a 10 mm tube, was run at room temperature without field-frequency lock and proton decoupling. A 25 μs pulse was used and the acquisition time was 0.85 s.

BSM and fetuin were activated by the procedure detaile in

Chapter I.2. Typically, 125 mg of material was used. For the
deuteration, the aldehyde-containing compound was dissolved at pH 9, and
_ca._ 2.5 mg NaBD$_4$ (MSD) added to the solution at 0°. The solution was
allowed to reach room temperature and left for one hour, when the pH was
lowered to _ca._ 5 to decompose unreacted NaBD$_4$. Desalting was performed
either on a Sephadex G-25 (medium) column, or using Centriflo PM 10
size-exclusion membranes (Amicon). With asialofetuin, catalase was not
used in conjunction with galactose oxidase, and this probably accounts
for the rather low signal-to-noise (low level of activation) in this
instance.

Fetuin was labelled at lysine residues with deuterium by
dissolving the glycoprotein in a borate buffer solution (pH 9.0, 0.1 $\underline{M}$)
at a concentration of _ca._ 100 mg/200 ml. Sodium cyanoborohydride (15
moles/mole lysine) was added, followed by a _ca._ 200 fold molar excess of
hexadeuterioacetone, added drop-wise to prevent protein precipitation.
The solution was stirred overnight at room temperature, and unreacted
hexadeuterioacetone removed carefully under reduced pressure. Further
desalting procedures were as described previously.

I.4 Neoglycoproteins

Chemicals were often used as supplied from the chemical
companies. Allyl alcohol (Aldrich) was dried over calcium sulphate and
stored under N$_2$. Chloroform was rendered alcohol-free by washing with
conc. H$_2$SO$_4$, neutralizing with alkali washes and dried over 4 Å
molecular sieves. Mercuric oxide and bromide were from BDH and mercuric
cyanide from ICN. Acid resins were from Bio-Rad. Melting points were
determined on a Fisher-Johns apparatus and are uncorected.

Ozone was generated by a Welsbach Ozonator (90 V with 2 p.s.i.
input O_2 pressure), dimethyl sulphide was from Sigma and sodium
cyanoborohydride from Aldrich. Bovine serum albumin was purchased from
Miles and passed down a Sephadex G-25 column prior to use, to remove low
molecular weight impurities.

All allyl glycosides were prepared by standard methods and
checked for purity by TLC, ^{1}H NMR and melting points. O-Acetylations
were performed with pyridine and acetic anhydride in the cold.
Acetoglycosyl bromides were prepared from the per-O-acetylated sugar
using 30% HBr in acetic acid. Koenigs-Knorr glycosidations were
performed either using silver carbonate (undecenyl
β-D-acetoglucopyranoside), mercuric cyanide (2-acetamido-3,4,6-tri-
O-acetyl allyl-β-D-glycopyranose), or mercuric oxide and mercuric
cyanide (all other allyl β-D-acetoglycosides). De-O-acetylations were
with a methanolic solution of the sugar to which was added a freshly
prepared solution of 0.1 M sodium methoxide in methanol.

For example, allyl α-D-galactopyranose was prepared thus. One
gram of Dowex 50W-X8 (H^+) resin was prepared by washing several times
with methanol (to remove high molecuar weight impurities), and then
washed several times with allyl alcohol. Galactose (1.8 g) was dried
(over NaOH in a vacuum desiccator) and to this was added the resin and
20 ml of dry allyl alcohol. The apparatus was fitted with a reflux
condenser and heated under reflux (B.Pt. 98°) for 20 hours, by which
time all the galactose had dissolved and the reaction judged completed

by TLC (eluant, $CHCl_3/MeOH/HOAc/H_2O$, 25:15:4:2). The allyl alcohol was removed by rotary evaporation at reduced pressure, and the α-glycoside precipitated preferentially from an ethanolic solution of the oil at -4°. The isolated yield was 10%, and the melting point 146-148° (Lit. 143-145°).

The synthesis of a β-glycoside is typified by allyl β-D-glucopyranoside. 2,3,4,6-Tetra-O-acetyl-α-D-glucopyranosyl bromide (1.5 g) was added to a mixture of 10 ml dry allyl alcohol, 10 ml alcohol-free chloroform, 1.0 g "Drierite", 0.65 g HgO and 0.05 g $HgBr_2$, and stirred for 48 hours. The mixture was filtered through a layer of Celite, and evaporated to dryness. The sugar was extracted into dry chloroform; any remaining mercuric salts were precipitated and removed by filtration. The filtrate was evaporated to dryness and the product crystallized from an ethanolic solution at -4°, in 70% overall yield. M.Pt. 86° (Lit. 86/88°).

The ozonolysis was performed as follows. The sugar was dissolved in methanol (unprotected) or $MeOH/CH_2Cl_2$, 4:1 (protected sugar) at a concentration of 1 mmole per 5 ml solvent. The solution was cooled to -60° (acetone/dry ice) and ozone-enriched oxygen bubbled through (5-10 min/mmole) until the methanolic solution went pale blue, indicating an excess of ozone. The solution was flushed with N_2 to remove this ozone, and excess dimethyl sulphide (DMS; > 2 mole/mole sugar) added. The solution was removed from the coolant and allowed to reach room temperature, where it was stirred for 2 hours. Excess DMS, methanal and methanol were removed under reduced pressure. With blocked sugars, the

sirup was dissolved in methylene chloride and washed several times with water to remove DMSO.

In a typical reductive amination reaction, BSA (18 mg; 0.015 mmole lysine), aldehydo sugar (16.2 mg; 0.074 mmole) and NaCNBH$_3$ (22.8 mg; 0.38 mmole) were dissolved in 6 ml water, and the pH adjusted to 9.0 with 0.1 M NaOH. The solution was left overnight, and then passed down a Sephadex G-25 column (0.02 % sodium azide eluant), where the excluded volume was collected. This was freeze-dried and the neoglycoprotein analyzed by the phenol-sulphuric acid method, measuring the absorption at 490 nm.

With a blocked sugar, the procedure was identical except that the reaction solution was H$_2$0/MeOH, 3:1. The blocked aldehydo sugar (in MeOH/H$_2$0, 2:1) was added over 10 min. Methanol was removed under reduced pressure taking care to minimize frothing. If any solids were suspended in the solution, they were filtered off prior to desalting, usually by dialysis (3 days against distilled H$_2$0). Note that 2-acetamido-3,4,6-trio-O-acetyl allyl-β-D-glucopyranose is moderately soluble in water, and methanol was not necessary in the reaction solution.

I.4.2 ^{13}C NMR

Most neoglycoprotein spectra were recorded on solutions (ca. 150 mg/1.8 ml D$_2$0) at 308 K. The spectrometer used was a Bruker WH-400, equipped with a single-frequency probe for ^{13}C (100.6 MHz). The spectral width was 200 ppm and the recycle time ca. 0.8 s. An excitation pulse (18 μs for neoglycoproteins or 12 μs for

monosaccharides; $90° = 22$ μs) was followed by the acquisition of 16 K

data-points, while broad-banded ^1H decoupling was employed.

Signal-averaging generally took place overnight (ca. 160 000 scans).

For the enzyme studies, galactose oxidase (Sigma or Worthington)

was added (ca. 20 U/150 mg neoglycoprotein) together with 5 μl catalase

(Sigma; 60,000 U) to ca. 150 mg of neoglycoprotein. The solution was

left open to the atmosphere (O_2) overnight at room temperature, and the

^{13}C NMR spectrum was recorded. Where specified, sodium borohydride

reduction was performed (2 mg, from MCB).

I.4.3 ^1H SEAS Experiments

For the ^1H NMR (SEAS) experiments, samples were prepared by

dissolving in D_2O and freeze-drying several time, to remove H_2O and

exchangeable protons. The spectra were recorded at 270 MHz using a

home-built spectrometer, based on an Oxford superconducting magnet ($\underline{B}_o$

6.35 T), a Bruker WP-60 console, and Nicolet 1180 computer and 293B

pulse-programmer. The deuterium lock, quadrature detection, and proton

decoupler units were manufactured in the Department of Chemistry,

U.B.C. (Dr. G.A. Morris and Mr. T. Marcus). Spectral widths were 3012

Hz, with 8K data-points collected. Presaturation at the HOD resonance

frequency was for 3 seconds; no relaxation delay was used. Typically,

400 spectra were acquired for each tau value. Data-processing involved

the use of a trapezoidal window (NTCFTB "T1 = 55") and 1.2 Hz

exponential line-broadening. Magnitude-calculation spectra were

recorded. The $90°$ and $180°$ pulses were checked before each experiment,

and typical values are 10 μs and 21 μs, respectively.

SECTION II

CHAPTER II.1

INTRODUCTION

High-resolution nuclear magnetic resonance (NMR) spectroscopy has deservedly earned a place as one of the most universal and powerful tools in organic structural determination. The NMR phenomenon was first reported for bulk solids by Bloch and coworkers[1] and Purcell and coworkers[2] in 1945, who were jointly awarded in 1952 the Nobel prize for their discovery. Improvements in magnetic field homogeneity soon resulted in measurement of higher resolution spectra, which revealed first the chemical shift, and then the spin coupling phenomena. In 1966 Ernst and Anderson[3] demonstrated the application of Fourier transformation (FT) of pulse responses, and along with signal averaging this led to further increases in sensitivity. With the concomitant integration of digital computers, insensitive but important nuclei such as ^{13}C and ^{15}N could be routinely observed.

The next major land-mark in the development of high-resolution NMR was the application of super-conducting materials to magnet construction. Starting in the late 1960's the then common 100 MHz instruments were soon superceded by 200-360 MHz devices, and by the late 1970's, 400 MHz instruments were common, and 500 and 600 MHz instruments were being described at NMR congresses. These high field instruments gave the anticipated increases in dispersion and inherent signal-to-noise.

At the conceptual level, perhaps the most startling development came in 1971, when Jeener suggested[4] the possibility of two-dimensional

(2D) NMR experiments. Interestingly, although it was five years before the detailed quantum-mechanical theory of the experiment was presented,[5] many other experiments were described in the literature, most from the research groups of Ernst, in Switzerland, and Freeman, in England.

Although the technological capability to perform most of these experiments has been commercially available for at least five years (since 1978), surprisingly few reports on their applications have appeared. In the biolgical area, the collaborative efforts of Ernst and Wüthrich have amply demonstrated the potential for studies of small proteins.[6] Hall's group in Canada had an early interest in the evaluation of the technology as applied to structural organic chemistry; this thesis forms a part of that tradition.

In this work, the author has undertaken a systematic, objective appraisal of some of the available 2D NMR experiments, in the light of their application to structural investigations in organic and natural-products chemistry. It became evident early on that 2D experiments were not a panacea to all the problems associated with the investigation of complex molecules, and modified forms of certain 1D experiments found an important place in the general protocols which emerged. In all cases, the fundamental objective was the efficient integration of spectroscopic methods, the most expeditious route to the required answers, and the conditions to which each experiment was best suited.

It was decided that before attempting to apply the methods to complex molecules, a thorough assessment of each experiment using a

single simple exemplar would prove beneficial. This lengthy
investigation is detailed in Chapter II.2, where the data are presented
along with theoretical aspects. A simple protected α-glucopyranoside
was chosen, since it is conformationally rigid and has a reasonably
simple, first-order spectrum at 270 or 400 MHz. As will be seen, these
experiments are an important, integral component of the research of the
thesis, since an equivalent array of experiments has not previously been
systematically applied to a single molecule. Furthermore, because this
initial investigation of the procedures so successfully provided a broad
base of expertise and experience, all subsequent studies could be
performed rather efficiently, and the descriptions of subsequent
chapters are correspondingly concise. This was a very welcome
development.

Chapter II.3 describes a protocol[7] based on NMR for the de novo
sequencing of oligosaccharides. Vliegenthart's[8] and Dabrowski's[9] groups
have already exposed some of the power of NMR in the structural analysis
of glycopeptides and ceramide oligosaccharides, respectively, where they
found great utility. Dabrowski's more recent work has elements in
common with our procedures in that reliance on chemical shifts implicit
in Vliegenthart's approach as a basis for assignment was avoided. The
intention was to develop a general procedure whereby the complete
primary structure of an oligosaccharide could be determined by NMR with
only reliance on typical vicinal coupling constants for the carbohydrate
ring protons. As will be seen, the combination of 1D and 2D methods
found suitable proved more than adequate for the disaccharide glycoside,
which was used as a model. A more complex biological material, digoxin,

was studied in Chapter II.5.

Chapter II.4 deals with the assignment and structural investigation of brucine. The main objective here was to find the most expeditious route to the assignment of its ^{1}H and ^{13}C NMR spectra, and conformational information on the molecule. Further, the author also attempted to place himself in the position of a professional applied spectroscopist to evaluate the performance of the required experiments under "survey conditions". This required the minimum knowledge of the molecule's spectroscopic characteristics before performing experiments under "routine" conditions where demands on instrument time is a major consideration. This is in sharp contrast to the developmental situation in Ch. II.2, which is conceptually akin to a spectroscopy research study.

The final study in Chapter II.5 is on a steroidal glycoside, digoxin. Here again, the object was to assign the ^{1}H and ^{13}C NMR spectra using the currently available techniques. The glycone is considered as a critical test of the oligosaccharide sequencing methodology described in Ch. II.3. Although it consists of only three sugars, the situation is complicated by the fact that they are identical in nature and linkage, and are 2-deoxy sugars with methylene resonances overlapping with the bulk of the steroid protons. The cardenolide (steroid genin) is equally intractable because of its low extent of substitution and conformation. As will be seen, these complexities are compounded by the fact that the molecule self-associates in a polar solvent, giving broad lines for the steroid moiety, especially

troublesome in the ^{1}H NMR spectrum. the molecule was studied at 500 MHz and, for the first time in this work, significant limitations became evident in some 2D experiments.

Anticipating somewhat the conclusions of Section II, the author believes that this thesis points to an increasingly bright future for NMR spectroscopy. It is clear that certain protocols for structure determination are extremely powerful under certain regimes; thus, rapidly tumbling, medium molecular weight molecules can most certainly be studied under "survey conditions", demanding comparatively little instrument time. However, although some larger molecules can definitely benefit from use of the highest obtainable static field and a modified approach, some intrinsic limitations exist.

REFERENCES

1. F. Bloch, W.W. Hansen, and M. Packard. <u>Phys. Rev.</u> 69, 127 (1946).

2. E.M. Purcell, H.C. Torrey, and R.V. Pound. <u>Phys. Rev.</u> 69, 37-38 (1946).

3. R.R. Ernst and W.A. Anderson. <u>Rev. Sci. Instr.</u> 37, 93-102 (1966).

4. J. Jeener. Ampere International Summer School, Basko Polje, Yugoslavia. 1971.

5. W.P. Aue, E. Batholdi, and R.R. Ernst. <u>J. Chem. Phys.</u> 64, 2229-2246 (1976).

6. G. Wagner, A. Kumar, and K. Wüthrich. <u>Eur. J. Biochem.</u> 114, 375-384 (1981), and others in the series.

7. M.A. Bernstein and L.D. Hall. <u>J. Amer. Chem. Soc.</u> 104, 5553-5555 (1982).

8. J.F.G. Vliegenthart, H. van Halbeek, and L. Dorland. <u>Pure Appl. Chem.</u> 53, 45-77 (1981), and references therein.

9. J. Dabrowski, P. Hanfland, and H. Egge. <u>Methods Enzymol.</u> 83, 69-86 (1981), and references therein.

CHAPTER II.2

HIGH RESOLUTION NMR METHODS

II.2.1 General Theory

Although some understanding by the reader of pulsed Fourier

Transform (FT) high resolution NMR[1-4] will be assumed, it is necessary

to briefly review a few relevant concepts to ensure that the reader has

access to the relevant nomenclature. In what follows below, we

introduce three models, each of which gives different insight to the

effect of a pulse of radiofrequency energy on an ensemble of nuclear

spins.

We consider an ensemble of identical spin-1/2 nuclei in a static

magnetic field, $\underline{B}_0$. Two energy levels, α and β, will exist, differing

in energy by ΔE:

$$\Delta E = \gamma \hbar \, \underline{B}_0 \qquad [II.2.1]$$

γ is the magnetogyric ratio of the nuclide, and $\hbar$ is the reduced

Planck's constant $(h/2\pi)$. At thermal equilibrium, nuclei are

distributed between the two energy levels by a Boltzmann distribution,

with the resultant net macroscopic magnetization termed $\underline{M}_0$.

It is convenient to define a frame of reference as shown in

Fig. II.2.1A. The applied magnetic field, $\underline{B}_0$ is defined to lie parallel

to the z-axis. Magnetic moments (vectors), μ, are required to precess

about $\underline{B}_0$ at the Larmor angular velocity, ω_0:

$$\omega_0 = -\gamma \, \underline{B}_0 \qquad [II.2.2]$$

Expressed in frequency units, the Larmor precessional frequency, ν_0,

is given by:

$$\nu_0 = -\gamma \underline{B}_0/2\pi \qquad\qquad [II.2.3]$$

There is no phase coherence in the x-y plane and consequently no resultant magnetization; the resultant magnetization, $\underline{M}_0$, lies on the z-axis.

To induce resonance, a second radio frequency (RF) field, $\underline{B}_1$, must be applied in the x-y plane. Resonance is attained when the frequency of $\underline{B}_1$ exactly matches ν_0.

It is now convenient to redefine the terms of reference in Fig. II.2.1.A.; now the reference frame itself is rotating about the z axis with the same sense and frequency, ν, as the RF field, $\underline{B}_1$. When $\nu \approx \nu_0$, magnetic moments are effectively motionless, or moving slowly ($\nu_0 - \nu$). The x and y axes are re-labelled x' and y' to make the distinction, as in Fig. II.2.1.B (where $\nu = \nu_0$). This is the "rotating reference frame".

Let us now consider the effect of $\underline{B}_1$ on $\underline{M}_0$, placed along the x' axis, with the resonance condition met. $\underline{B}_1$ exerts a torque on $\underline{M}_0$, tipping it away from the z axis. If $\underline{B}_1$ is applied for a time, $\underline{t}_p$* (the "pulse length"), $\underline{M}_0$ rotates about x' by an angle θ, defined by:

---

*A square pulse of length $\underline{t}_p$ (time domain) of frequency ν_0 corresponds, in frequency space, to a range of frequencies centred at ν_0 and extending from $\nu_0 - \underline{t}_p^{-1}$ to $\nu_0 + \underline{t}_p^{-1}$. Hence, with $\underline{t}_p$ typically of the order of microseconds, a range of frequencies extending over tens or hundreds of KHz will exist.
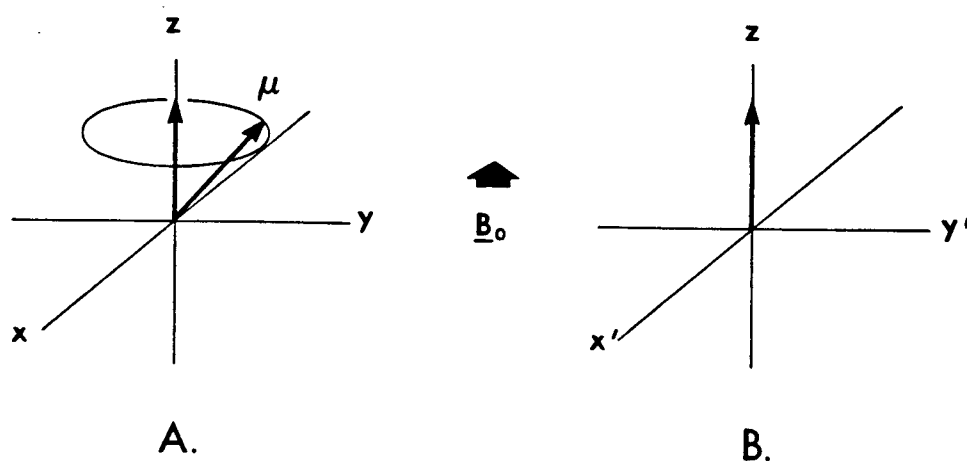
Fig. II.2.1. The laboratory (A) and rotating-reference frame (B)
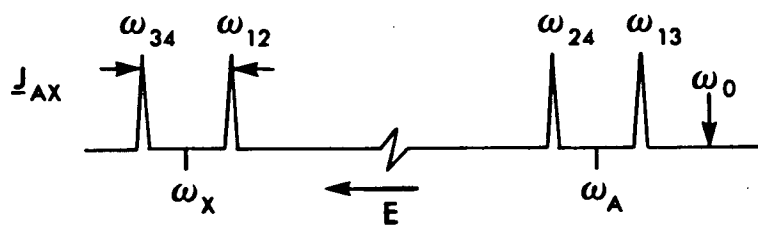
Fig. II.2.2 A stylized AX spin system

$$\theta = \underline{B}_1 \ \underline{t}_p \ \gamma/2\pi \qquad\qquad [II.2.4]$$

There is now a component of $\underline{M}$ along the y' axis, $\underline{M}_y$. This perturbs

the spin system from its thermal equilibrium with respect to its

surrounding (the lattice).

The Boltzmann equilibrium state is re-established by leakage of

magnetization into the lattice; the first-order rate-constant for this

process is $\underline{T}_1$, the spin-lattice (longitudinal) relaxation rate. A

second rate constant, $\underline{T}_2$ (the spin-spin, or transverse relaxation rate)

describes the exponential decay of transverse magnetization in the x'-y'

plane.

Following application of the perturbing pulse, measurement of

the magnetization in the x'-y' plane as a function of time produces the

free-induction decay (FID) – this measure of $\underline{M}_y$ vs. time, has the form

$\underline{M}_0 \cos(\omega\underline{t}) \exp(-\underline{t}/\underline{T}_2)$. Fourier-transform (FT) of this time-dependent

function yields the frequency-space spectrum as a single Lorentzian

line. This is the key to pulsed FT NMR spectroscopy.

Let us now briefly look at a homonuclear AX system, in the

rotating reference frame, with the spectrometer frequency, ω, placed

close to that of the high-field transition of spin A; the four line,

frequency-domain spectrum is stylized in Fig. II.2.2.

Fig. II.2.3 follows the behavior of the magnetization vectors in

the x-y plane, ignoring $\underline{T}_1$ relaxation. At thermal equilibrium, all four

vectors are aligned along the z-axis (Fig. II.2.3A). After application
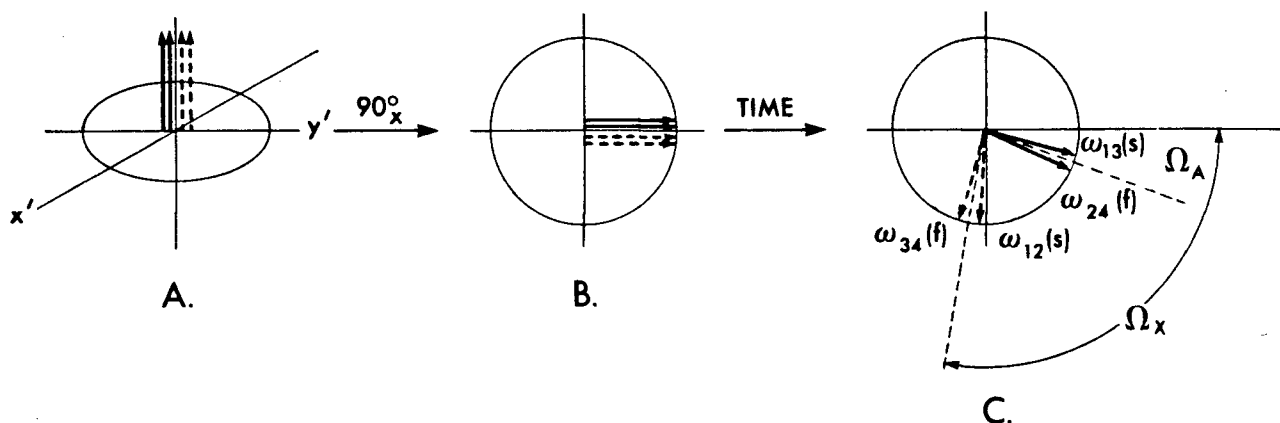
Fig. II.2.3 The action of an AX spin system's vectors, (A) at equilibrium, (B) after a 90° pulse and (C) after some time to allow dephasing. (Solid line denotes A spin vectors and broken lines, X).
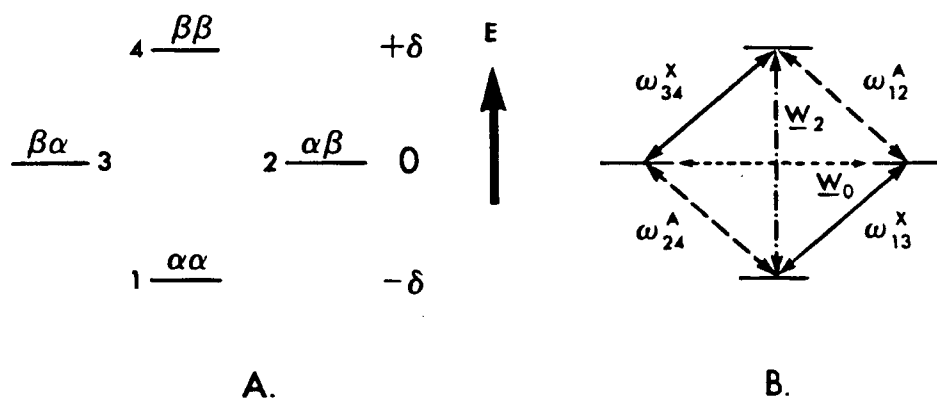
Fig. II.2.4 Energy Level diagrams of AX spin-system (A) showing transition probabilities (B). 0 and ±δ represent relative equilibrium populations.

of a perfect 90°_x pulse to <u>all</u> spins, the vectors lie along y' (Fig.

II.2.3B). Since all four vectors have a different angular velocity than

that (ω) of the rotating reference frame, with time these precess in the

x'-y' plane (Fig. II.2.3C), and dephase with respect to each other. The

average of lines ω_{12} and ω_{34} will precess at angular velocity, Ω_x

(the difference between ω and ω_x) and similarly, ω_{13} and ω_{24}

precess slower at Ω_A. Each doublet will have a relatively slow (s)

and fast (f) precessing component. As we shall see later, this model

provides a convenient description of the concepts of spin precession and

phase coherence.

We now consider the same spin system using the "energy-level"

model. The homonuclear AX system has four energy levels: $\alpha\alpha$ ($\alpha\beta$, $\beta\alpha$)

and $\beta\beta$ in increasing energy,* as depicted in Fig. II.2.4A. In this

model, the 90° pulse induces the four single-quantum transitions, (Fig.

II.2.4B) and it is these which are detected. Note that the zero- and

double quantum transitions ($\underline{W}_0$ and $\underline{W}_2$ respectively) are not induced by

this single pulse experiment.

Although the rotating reference frame and energy level models

discussed above are simple and provide reassuring, pictorial

explanations for many NMR experiments, they are often ill-suited for

explanations of many processes. For that reason, the density matrix

formalism, which is more complicated but exact in all cases, will now be

---

*In the heteronuclear case, the $\alpha\beta$ energy state does not have
the same energy as $\beta\alpha$. In the homonuclear case their energies are
almost equal, as indicated by their equal equilibrium populations.

briefly introduced. For simplicity, it is worthwhile using a diagrammatic formalism. We will ignore relaxation effects, as this simplifies the discussion.

An AX system is generally represented by a four-by-four matrix, σ, constituting all the possible products of the four energy states:

$$\sigma = \begin{array}{c|cccc} & \alpha\alpha & \alpha\beta & \beta\alpha & \beta\beta \\ \hline \alpha\alpha & \sigma_{11} & \sigma_{12} & \sigma_{13} & \sigma_{14} \\ \alpha\beta & \sigma_{21} & \sigma_{22} & \sigma_{23} & \sigma_{24} \\ \beta\alpha & \sigma_{31} & \sigma_{32} & \sigma_{33} & \sigma_{34} \\ \beta\beta & \sigma_{41} & \sigma_{42} & \sigma_{43} & \sigma_{44} \end{array} \qquad [II.2.5]$$

At thermal equilibrium, the density matrix, $\sigma(0)$, will have unequal Boltzmann population terms (P^0) along the diagonal, as in Eq. II.2.6a. Inserting the relative populations (see Fig. II.2.4A) gives the matrix Eq. II.2.6b, in which δ is the population difference between the $\alpha\beta$ or $\beta\alpha$ state, and $\alpha\alpha$ or $\beta\beta$.

$$\sigma(0) = \begin{bmatrix} P^0 & 0 & 0 & 0 \\ 0 & P^0 & 0 & 0 \\ 0 & 0 & P^0 & 0 \\ 0 & 0 & 0 & P^0 \end{bmatrix} \qquad [II.2.6a]$$

$$\sigma(0) = \begin{bmatrix} \delta & 0 & 0 & 0 \\ 0 & 0 & 0 & 0 \\ 0 & 0 & 0 & 0 \\ 0 & 0 & 0 & -\delta \end{bmatrix} \qquad \text{[II.2.6b]}$$

Consider now the effect of the pulse (rotation) on $\sigma(0)$. The new density matrix, σ', is given by:

$$\sigma' = R_- \ \sigma(0) \ R_+ \qquad \text{[II.2.7]}$$

where $R_{\pm}$ are rotational matrices. For a 90° pulse, $R_{\pm}^{90}$ will take on a special form and, omitting the details, we obtain, explicitly, Eq. II.2.8a which may be stylized as in Eq. II.2.8b.

$$\sigma' = \begin{bmatrix} 0 & 2i\delta & 2i\delta & 0 \\ -2i\delta & 0 & 0 & 2i\delta \\ -2i\delta & 0 & 0 & 2i\delta \\ 0 & -2i\delta & -2i\delta & 0 \end{bmatrix} \qquad \text{[II.2.8a]}$$

[II.2.8b]

If the reader compares Eq. II.2.8a with Eq. II.2.5, it will be clear that only single-quantum transitions have non-zero values, and hence are excited. The zero- (σ_{23}, σ_{32}) or double- (σ_{14}, σ_{41}) transitions have zero values.

Consider now the behaviour of these components as the matrix is allowed to "evolve" with time, $\underline{t}$. The σ_{12} term, for example, previously $2i\delta$ now becomes $2i\delta \exp (i\ \omega_{12}\ \underline{t})$. The exponential term contains sin and cos contributions and we may loosely represent the "detected" matrix, $\sigma'(\underline{t})$, as:

$\sigma'(t)=$

[II.2.9]

In 2D experiments at least 2 pulses are necessary and where necessary, these will be discussed in light of the density matrix formalism introduced in its stylistic form here.

II.2.2 Spectral Simplification

The purpose of this section is to introduce some of the methods which are available to "simplify" otherwise complex NMR spectra.

II.2.2.1 Via T_1 in ^1H NMR Spectroscopy[5,6]

Spectra can often by simplified by taking advantage of the fact that different types of protons in a molecule frequently have widely different spin-lattice relaxation times. For example methylene signals can quite easily be "separated" from methine, when overlap causes complications and impedes spectral assignment. The concept rests on the fact that methylene protons will relax faster than methine protons, and will all relax at approximately the same rate, since their mutual relaxation is so dominant.

Consider the inversion recovery[7] T_1 experiment (T1IR); the pulse sequence is:

$$(RD - 180° - t - 90° - AQN)_n,$$

where RD is a relaxation delay which is set $\geq 5 * T_1$ (longest). According to the rotating reference frame model (Fig. II.2.5), the 180° pulse inverts all spin populations, placing the M_0 vector along the -z axis. During the delay time, t, M_z returns towards its equilibrium
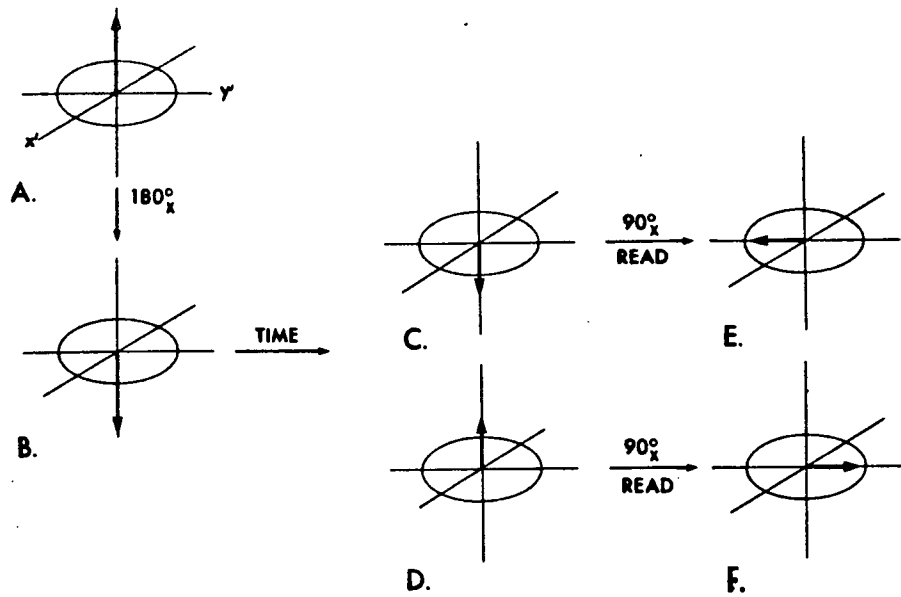
Fig. II.2.5 The rotating reference frame vector model of the T_1 inversion-recovery experiment. Vectors are shown for a short t value (A,B,C,E) and a relatively long one (A,B,D,F).
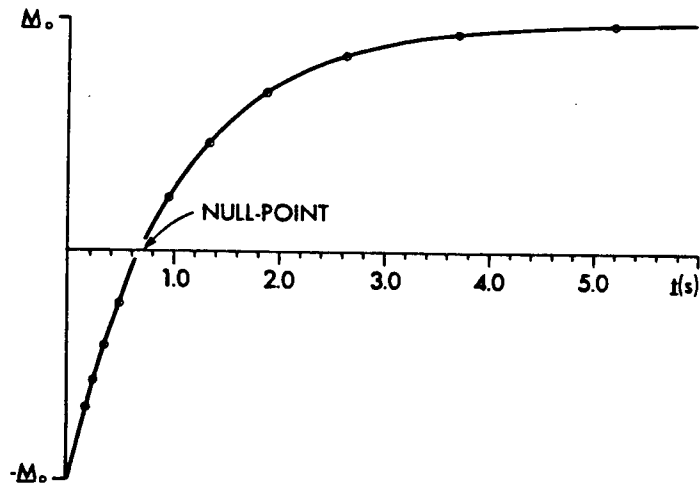
Fig. II.2.6 Plot of z-magnetization vs time in a T_1 inversion recovery experiment, indicating the null point.

position at the rate, $\exp(-t/T_1)$. Since only x'-y' magnetization can be detected, a second 90° ("read") pulse is applied to determine the magnitude of M_z, the z magnetization. This two-pulse sequence is performed for a number of different t values. Results for trideuteriomethyl 2,3,4,6-tetra-O-(trideuterioacetyl)-α-D-glucopyranoside (1) are given in Fig. II.2.7.* We can see that for short t values the peaks are negative-going (Figs. II.2.5C, E) eventually
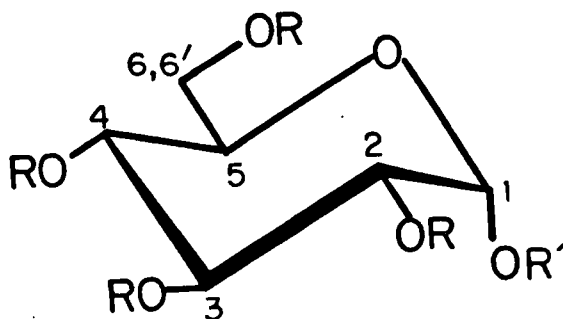
1 : R = CO.CD₃, R' = CD₃

2 : R = CO.CH₃, R' = CH₃

becoming positive-going (Figs. II.2.5D,F). A t value exists where M_z = 0 at the time when the "read" pulse is applied, i.e. the "null condition" (Fig. II.2.6). This is the basis for this form of "spectral

---

*At this stage we are not concerned with the quantification of T_1 although it is worth mentioning that these data may be used to gain useful information concerning inter-proton distances for molecules in solution[8] (vide infra).
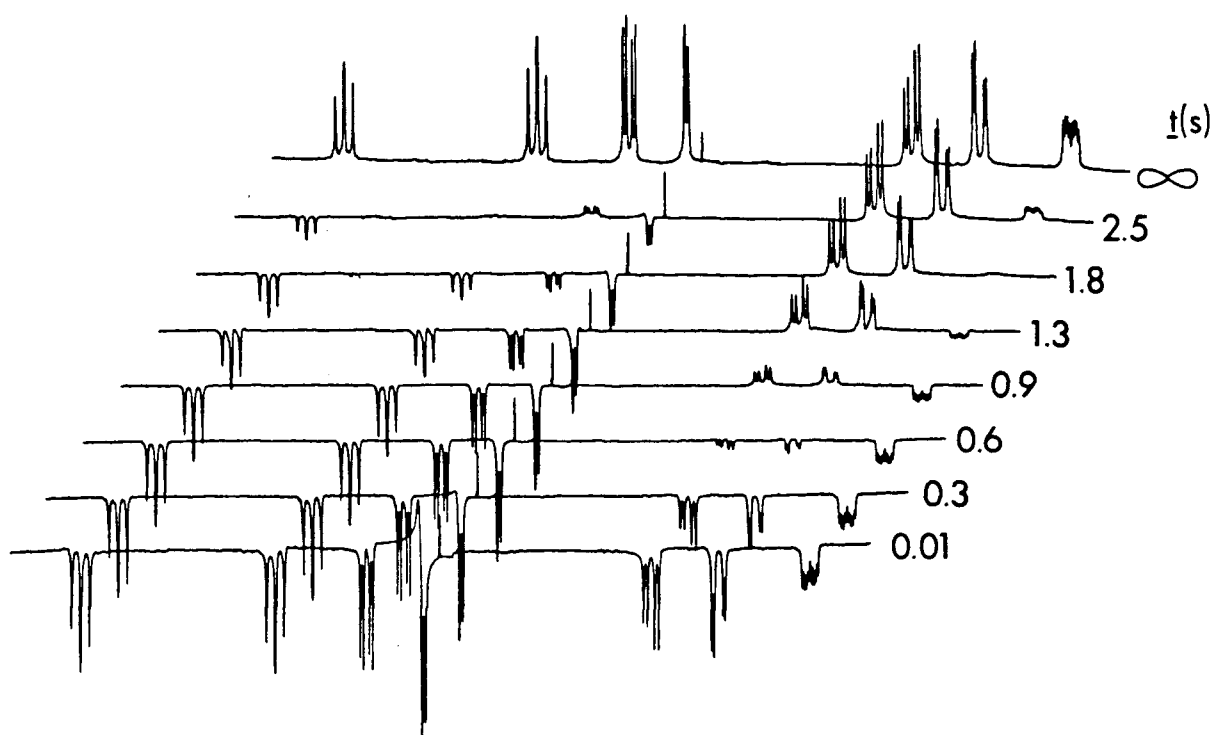
Fig. II.2.7 400 MHz TlIR experiment on 1 (0.1 M in C_6D_6). The
relaxation delay was 12 s, and t values noted next to
each spectrum.
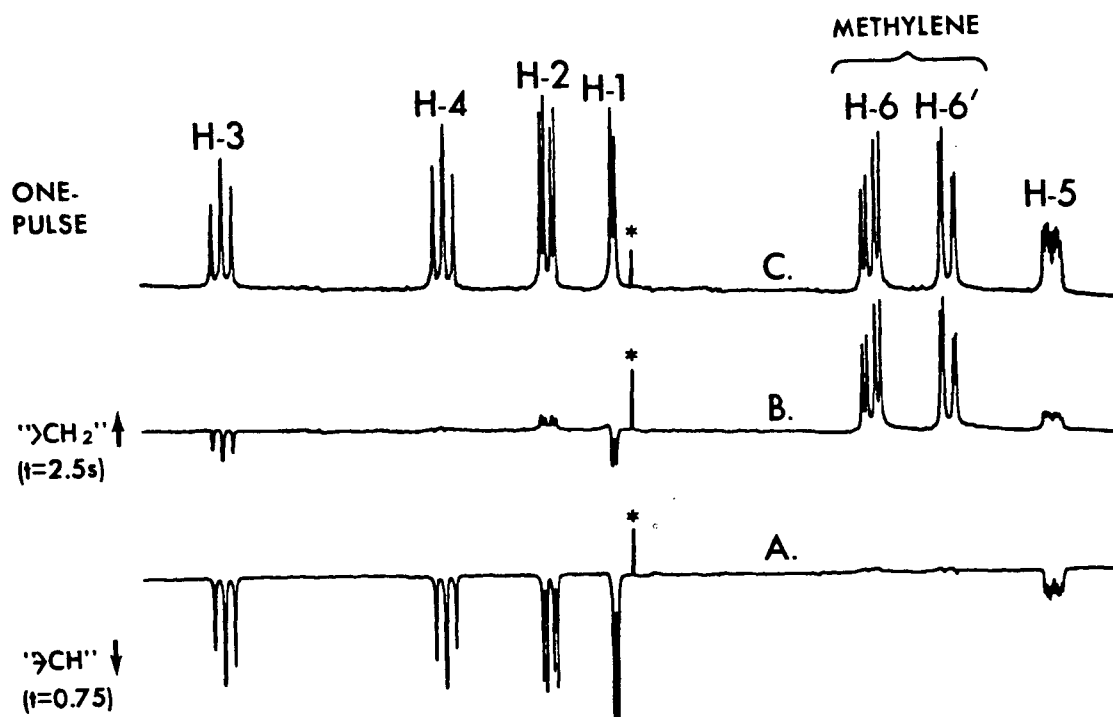
Fig. II.2.8 Spectral editing of 1 by TlIR. The control spectrum is C.
t = 0.7s is a "methine sub-spectrum", with methylene
signals nulled. t = 2.5s gives the "methylene
sub-spectrum", with methine signals partially nulled.
Other parameters as in Fig. II.2.7. The asterisk marks an
artifact at the carrier position.

editing". A preliminary TlIR experiment with a series of arbitrarily selected $\underline{t}$ values is performed to determine the null time for the $-CH_2$ resonances, for example. One of the resultant spectra might accidentally give a good nulling of the $-CH_2$ resonances under consideration. If not, a single experiment may be performed to achieve good nulling; under these conditions the more slowly relaxing $-CH$ resonances will then have negative amplitudes. An attempt to edit methine peaks is not as easy, since their $\underline{T}_1$'s may vary considerably. Fig. II.2.8 illustrates these statement. The normal spectrum of $\underset{\sim}{1}$ is shown in Fig. II.2.8C. Choosing $\underline{t} = 0.7s$ gives a "methine sub-spectrum", with methylene signals nulled (Fig. II.2.8A). With $t = 2.5s$, both methylene protons are almost fully relaxed whilst methine protons are either nulled (H-4) partly inverted (H-1, H-3) or partly upright (H-2), (H-5) (Fig. II.2.8B).

Thus, a suitable choice of $\underline{t}$ allows the creation of a spectrum lacking methylene peaks. This procedure has been used effectively in the assignment of the complex spectrum of a steroid. Although it is generally impossible to null all methine signals simultaneously, it is possible to do a number of separate experiments and choose the $\underline{t}$ values which null overlapping resonances. This method constitutes a simple and easy, yet little-used solution to the hidden resonance problem.

With ^{13}C NMR, this approach may be used to determine the number of attached protons to a carbon[9] (Chapter II.4).

II.2.2.2 Via $\underline{J}_{CH}$ in ^{13}C NMR Spectroscopy

Although broad-band proton decoupled ^{13}C NMR spectra are attractive in their simplicity, a price is paid for the removal of the ^{13}C-^1H coupling information in that the spectra are difficult to assign. The first steps towards assignment of ^{13}C NMR spectrum involves determining the chemical shifts, and the number of protons attached to each carbon. Single-frequency-off-resonance-decoupling[10] (SFORD)* is widely used to achieve the latter purposes; however, it has serious limitations in crowded regions of a spectrum, is inherently insensitive and can produce misleading results.[11]

Fortunately, a number of multi-pulse experiments exist[12-18] which are easy to use, are not as time consuming as SFORD and give a much clearer representation of the information. The first of these is "refocussed INEPT[12]" (insensitive nuclei enhanced by polarization transfer); although this works well with decoupled spectra, the observed transitions are distorted when the $^1\underline{J}_{CH}$ couplings are preserved. A number of other variants have been described; however, the author has had the opportunity to try only one of these, dubbed DEPT[13,19,20] (distortionless enhancement by polarization transfer). This experiment gives undistorted coupled spectra, as well as good editing.

"Polarization transfer" is a process in which magnetization from the protons, which are high natural abundance and sensitive nuclides, is

---

*SFORD employs a single ^1H decoupler frequency placed (usually) to high-field of the ^1H spectrum. This causes suppression of the one-bond ^{13}C-^1H couplings.

transferred to the relatively insensitive ^{13}C nuclei. The maximum intensity enhancement is $\gamma_H/\gamma_C \approx 4$; compared with the maximum nOe attainable by broad-band ^1H decoupling $(1 + (1/2) \gamma_H/\gamma_C = 3)$ this may not seem to be a significant improvement. However, a further advantage lies in the fact that the repetition rate for the experiment is governed by the spin-lattice relaxation rates of the protons rather than of the ^{13}C spins; given that ^1H relaxation rates are typically faster than those of ^{13}C, 2-3 times as many scans can be obtained in unit time. Other advantages of DEPT over INEPT are that the former is unhindered by overlap of solute and solvent peaks (which is particularly important when working at high dilution) and that it has a reduced dependence on the magnitude of $^1J_{CH}$. Hence, an "average" value for $^1J_{CH}$ may be chosen which produces good results for all carbon sites in a molecule.

The pulse sequence for the DEPT experiment is presented below. Proton pulses are applied through the ^1H decoupler coils of the ^{13}C probe, at the normal offset frequency for broadband (BB) decoupling (i.e. near $\delta_H = 5$). An average value of the ^1J coupling is used in the calculation of the $(2J)^{-1}$ value, giving 3.6 ms. All pulses, and the

^1H: $90°(\Phi_1) - (2J)^{-1} - 180°(\Phi_2) - (2J)^{-1} - \theta(\Phi_3) - (2J)^{-1} - (BB)$

^{13}C: $90°(\Phi_3)$ $180°(\Phi_4)$ $AQN(\Phi_5)$

[II.2.10]

Phase cycling:

Cycle	1	2	3	4	5	6	7	8	9	10	11	12	13	14	15	16
Φ_1	x	x	x	x	x	x	x	x	-x	-x	-x	-x	-x	-x	-x	-x
Φ_2	x	-x	x	-x	x	-x	x	-x	x	-x	x	-x	x	-x	x	-x
Φ_3	y	y	y	y	y	y	y	y	y	y	y	y	y	y	y	y
Φ_4	x	x	-x	-x	y	y	-y	-y	x	x	-x	-x	y	y	-y	-y
Φ_5	x	x	-x	-x	y	y	-y	-y	x	x	-x	-x	y	y	-y	-y

[II.2.11]

receiver are phase-cycled. $(\Phi_1 - \Phi_5)$ through sixteen steps for the best cancellation of artifacts. This appears complex on paper, but is quite simple to programme on most modern spectrometers. Acquisition of the ^{13}C FID ("AQN") is often with broad-band proton decoupling ("BB").*

Spectral editing is achieved by acquiring three spectra, for (1) $\Theta_1 = 45°$ ($\pi/4$), (2) $\Theta_2 = 90°(\pi/2)$ and (3) $\Theta_3 = 135°$ ($3\pi/4$). If $\underline{n}$ scans are acquired for Θ_1 and Θ_3, $2\underline{n}$ should be acquired for Θ_2. The free induction decay signals are Fourier transformed, phased, and the edited spectra obtained by linear combinations of the three spectra:

$$-CH \quad : \quad \Theta_2$$

$$-CH_2 \quad : \quad \Theta_1 - \Theta_3$$

$$-CH_3 \quad : \quad \Theta_1 + \Theta_3 - 0.707 \; \Theta_2 \qquad [II.2.12]$$

---

*The abbreviations "AQN" (acquisition), BB (broad-band proton decoupling) and Φ_x (phase-cycling programme) will be freely used in pulse schemes in the rest of this chapter.
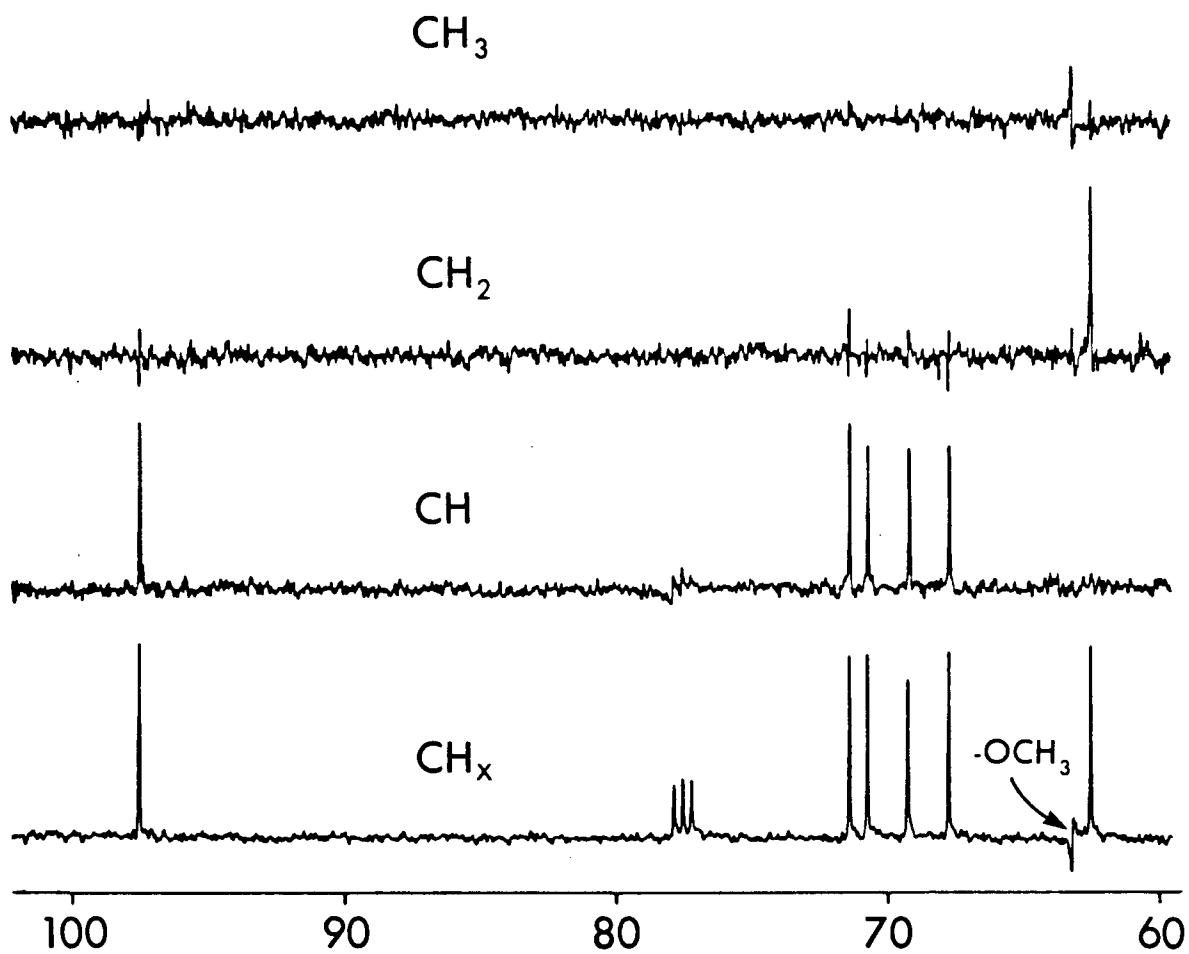
Fig. II.2.9 DEPT performed on 2 (0.4 M; CDCl₃) at 100 MHz.

These additions/subtractions may not be totally exact;[19] for example, the $-CH_2$ subspectrum is more correctly given by $\theta_1 - a. \theta_3$, where "a" varies between 1.00 and 1.10. Most modern spectrometers have a "real time" subtractive routine which allows the operator to "fine-tune" these values to achieve most efficient editing. One instrument manufacturer boasts an iterative routine which finds the best subtracted specta.[20]

Although the question of proton-pulse calibration is deferred until Section II.2.5.4, it is important to point out the $-CH$ sub-spectrum (θ_2) is reasonably sensitive to misset in the proton flip angles (vide infra) and as a result can be used to determine ^1H pulse lengths with reasonable accuracy. In practice, the experiment is repeated for a number of pulse lengths close to the approximate value, and the transformed spectra inspected for the most efficient cancellation of all but methine carbon peaks.

Results are presented in Fig. II.2.9 for DEPT performed for a ≈ 0.4 $\underline{M}$ solution of methyl 2,3,4,6-tetra-$\underline{O}$-acetyl-α-D-glucopyranoside, $\underset{\sim}{2}$ in $CDCl_3$. The $-OMe$ peak appears as a weak, aliased peak at δ 63.2. However, we see that it is clearly visible in the $-CH_3$ sub-spectrum; nulling is excellent.

II.2.3 Spin Decoupling-Difference Spectra[6,21-23] (SDDS)

This is a variant of the well known spin decoupling experiment, in which responses are observed only from those resonances directly

involved in spin coupling; all others are "nulled" by the "difference"
method. The advantages of this mode of presentation only become obvious
when one considers crowded spectra, which have overlapping resonances.
In general, interpretation is limited to observation of spectral
changes; detailed analysis of the decoupled difference peaks may not be
easy by inspection, but may be computer-simulated for verification.

In practice two spectra are acquired for each decoupling
experiment, one with the decoupler set to the precise resonance
frequency and the other, the "control", with it set just off resonance.
To minimize instrumental drift over a long period of time, the data are
collected in blocks, which may be repeated if long-term signal-averaging
is necessary to build up adequate signal-to-noise. This process is
termed "interleaving". If a series of separate experiments are to be
performed at one time, the appropriate decoupling frequencies are listed
in the computer memory, together with decoupler power settings adequate
for homonuclear decoupling.

A typical sequence of events would be:

1. Where n resonances require decoupling, create on disc $2n$
   blank files, specifying decoupler frequencies and power
   settings.

2. Read into core memory file number 1.

3. Perform 2-4 "dummy" scans (discarded), to establish a
   steady-state.

4. Acquire l scans (8 or 16) with the decoupler on resonance.

5. Save the (on-resonance) decoupled free induction decay on disc.

6. Read into core memory file 2.

7. Acquire $\underline{\ell}$ scans with the decoupler set just off resonance.

8. Save the (off-resonance) "control" free induction decay on disc.

9. Repeat steps 2-8 ($\underline{n}$-2) times, reading in each appropriate file.

10. Repeat 2-9 $\underline{m}$ times, so as to build up sufficient signal-to-noise. The total number of scans for each difference spectrum is 2($\underline{\ell}$ * $\underline{m}$).

Note that the total number of scans ($\underline{\ell}$ * $\underline{m}$) need only be equal or slightly more than that required to obtain a normal spectrum with adequate signal-to-noise. All free induction decays are then exponentially weighted (line broadening, 1.5 - 2.0 Hz), Fourier transformed, phased, and the frequency-domain spectra subtracted. The phase of the subtracted spectrum may require minor alteration before plotting.

Figure II.2.10 illustrates SDDS on $\underset{\sim}{1}$. Several points arise. We see that in crowded regions (H-1, -2, -4, and H-5, -6 and -6') the results are not always clear-cut, due to Bloch-Siegert effects.*

---

*In the presence of the decoupling field $\underline{B}_2$, all resonance frequencies are shifted from their "true" frequency by an amount which is proportional to the decoupler power ($\gamma \underline{B}_2/2\pi$), and inversely proportional to their frequency separation. This is part of the Bloch-Siegert effect.
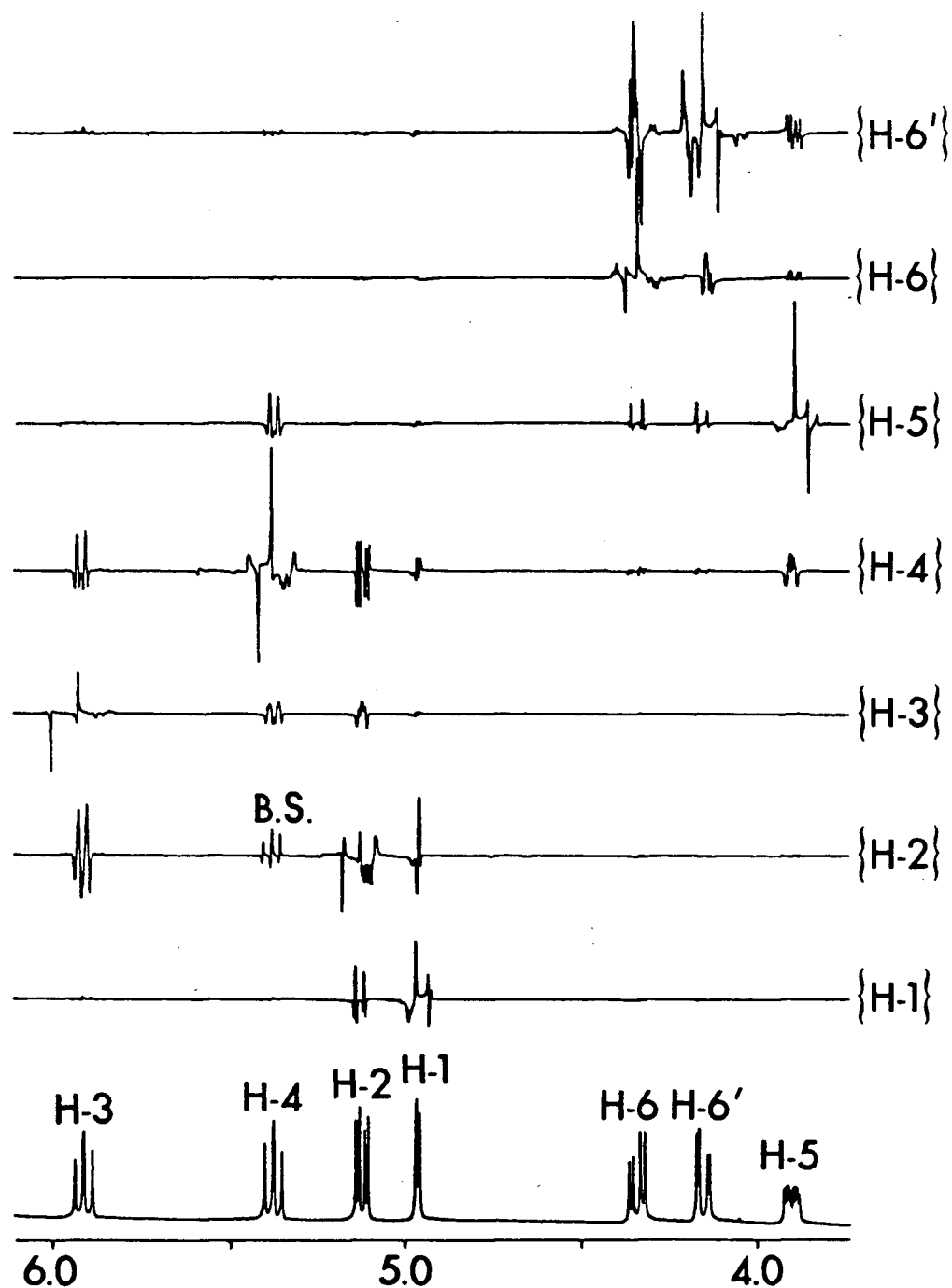
Fig. II.2.10 SDDS on 1 at 400 MHz. The irradiated proton is indicated
in each case. False responses arising from Bloch-Siegert
effects are labelled "B.S."

Computational solutions to these problems have been proposed.[24] With
{H-2}, for example, the calculated shift in H-4 is 0.87 Hz with the
decoupler on-resonance. In general, the decoupler can be moved either
to high or low field for measurement of the control spectrum. In this
case it was moved to low field as H-4 is farther from H-2 than H-1 and
this minimized Bloch-Siegert distortions. For the control experiment,
the decoupler was 285.4 Hz from H-4 and now the induced Bloch-Siegert
shift is 0.93 Hz. The difference, 0.06 Hz between these two values,
accounts for the false "response" at H-4 in the SDDS spectrum. We note
that a false response due to this phenomenon is very different from the
genuine decoupling-difference response (c.f. H-3). Having made this
point, consider now the {H-6'} experiment (top trace). Protons 6' and 5
are coupled ($\underline{J}$ = 2.3 Hz), yet the "response" at H-5 looks more like a
Bloch-Siegert artifact than a decoupling difference peak; in contrast,
the {H-3} experiment is entirely unambiguous.

We conclude then that SDDS is a powerful tool, but that it
should be approached with caution in spectrally crowded regions. If
this method alone is used to establish $\underline{J}$-connectivity, several
experiments may be necessary, varying decoupler pulse power and/or
control spectrum frequency. An illustration is given in Fig. II.2.11
where, with a constant decoupler power ($\gamma \underline{B}_2 / 2\pi$ = 17 Hz), the control
offset is sequentially moved from 50 to 10 Hz from ν_{H-1} ($\nu_{control}$ -
ν_{H-1} is termed $\Delta\nu$). With $\Delta\nu$ = 50 Hz, Bloch-Siegert effects are seen
for every proton; in the top trace ($\Delta\nu$ = 10 Hz), Bloch-Siegert shifts
are insignificant. The line-shape of H-2 is poorer than with $\Delta\nu$ = 15
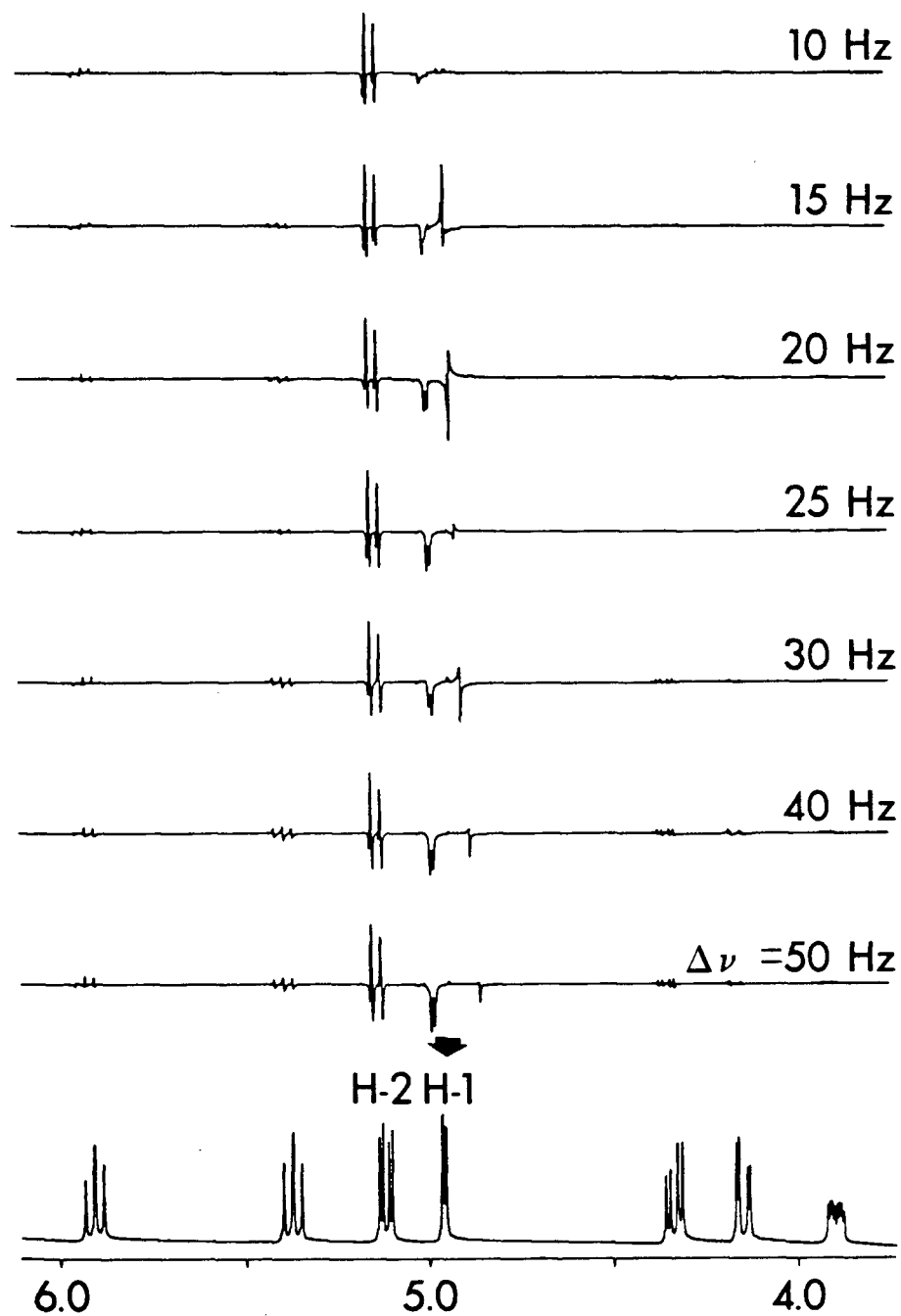
Fig. II.2.11   SDDS irradiating H-1 [$(\gamma \underline{B}_2/2\pi) = 17$ Hz], and varying the frequency difference ($\Delta\nu$) between the decoupler on resonance (fixed) and the control, off-resonance (varied).

Hz; H-3 is long-range coupled to H-1 and the response is probably genuine.

II.2.4 Nuclear Overhauser Effect[25-28]

The nuclear Overhauser effect (nOe) is of great utility in routine ^1H and ^{13}C NMR spectroscopy. Classically, one considers a saturating RF field, $\underline{B}_2$, and two spins, I and S.* The nOe specifies a variation in intensity ($\equiv$ integrated area) of spin I when spin S is saturated. In this section, discussion is restricted to a homonuclear steady-state experiment involving intramolecular nOe's between weakly coupled (or coupled) spins (such as $^1H\{^1H\}$ in rigid molecules, in the absence of chemical exchange phenomena).

The nOe, defined as the fractional change in intensity of the signal of spin i when spin j (or group of spins j) is saturated, is given by:

$$f_i(j) = \frac{\langle I_{zi} \rangle - I_{oi}}{I_{oi}}. \qquad [II.2.13]$$

$\langle I_{zi} \rangle$ is the average magnetization of i in the presence of saturation of spin(s) j, and I_{oi} the equilibrium magnetization in the absence of $\underline{B}_2$.

The nOe phenomenon involves population transfer resulting from relaxation effects between spins. If $\underline{R}_i$ is the total direct relaxation rate of spin i, it may be considered as:

---

*In keeping with the literature nomenclature, the two spins are designated I and S (with S irradiated), rather than A and X.

$$\underline{R}_i = \sum_{i \neq j} \rho_{ij} + \rho_i^* \qquad\qquad [II.2.14]$$

where ρ_{ij} is the dipolar relaxation rate of spin i with j, and ρ_i^* is the direct relaxation rate due to mechanisms other than dipolar (which for small molecules is often negligible in comparison with ρ).

At this stage a feel for the populations and transition probabilities is useful. Consider the energy level diagram for the
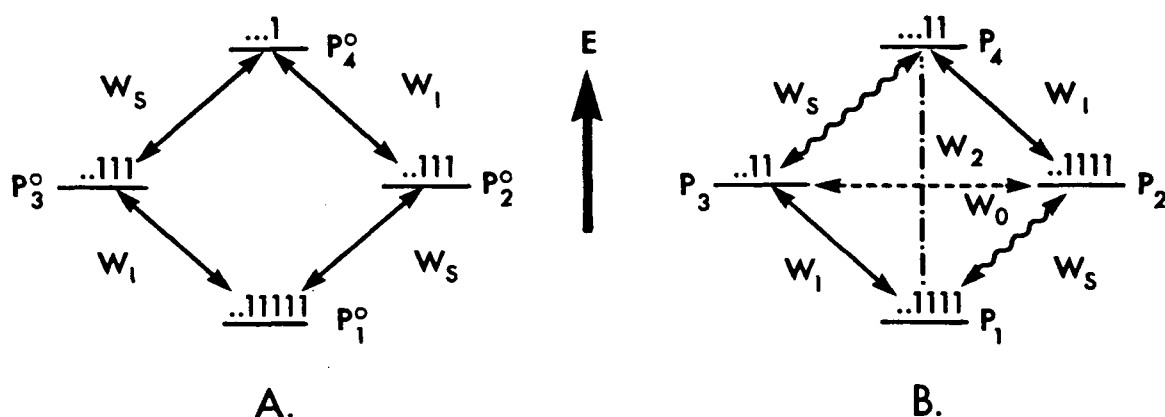
Fig. II.2.12 Energy levels, transition probabilities and relative populations (A) for an IS system at equilibrium, and (B) for an I{S} situation (where S is saturated).

weakly coupled IS spin system at equilibrium (Fig. II.2.12A). $\underline{P}_x^0$ is the equilibrium population of the x-state, and $\underline{W}$ the transition probability. The intensity of the I spins will be proportional to $(\underline{P}_3 - \underline{P}_1) + (\underline{P}_4 - \underline{P}_2)$. Measurement of single-quantum $\underline{W}_1$ transitions has no information on dipolar-relaxation and, hence, distances; this information is in the zero - $(\underline{W}_0)$ and double-quantum $(\underline{W}_2)$ transition

probabilities and can only be determined when the spin populations have been prepared in some suitable fashion (e.g. saturation or population inversion). When S is saturated (Fig. II.2.12B), populations of levels 1 and 2, 3 and 4 are equalized: $(\underline{P}_3 - \underline{P}_1) = (\underline{P}_4 - \underline{P}_2)$, and $(\underline{P}_4{}^0 - \underline{P}_1{}^0) = 2(\underline{P}_4 - \underline{P}_1)$. This change in the energy level populations will be negated by the "cross-relaxation" processes: $\underline{W}_2$ will attempt to re-establish equilibrium by increasing $\underline{P}_1$ and decreasing $\underline{P}_4$. The effect of $\underline{W}_0$ will be to increase $\underline{P}_3$ and decrease $\underline{P}_2$.

These cross-relaxation terms contribute to a cross-relaxation rate, σ_{ij}:

$$\sigma_{ij} = \underline{W}_2^{DD}\ (ij) - \underline{W}_0^{DD}\ (ij) \qquad\qquad [\text{II.2.15}]$$

For the totally dipole-dipole (DD) relaxation mechanism, ρ_{ij} can be written in terms of transition probabilities:

$$\rho_{ij} = \underline{W}_0^{DD}\ (ij) + 2\underline{W}_1^{DD}\ (ij) + \underline{W}_2^{DD}\ (ij) \qquad\qquad [\text{II.2.16}]$$

Eq. II.2.13 can be expressed in terms of σ and ρ:

$$f_i(j) = \sigma_{ij}/\rho_{ij} \qquad\qquad [\text{II.2.17}]$$

Expressions may also be derived for ρ_{ij} and σ_{ij} which interest us more, as they contain the dipolar distance information for the homonuclear experiment (as mentioned). Under extreme narrowing conditions, the frequency terms in the fuller expressions can be ignored

and it can be shown that:

$$\rho_{ij} = \gamma_i^2 \; \gamma_j^2 \; h^2 \; \tau_c \; r_{ij}^{-6} \qquad\qquad [II.2.18]$$

$$\sigma_{ij} = (1/2) \; \gamma_i^2 \; \gamma_j^2 \; h^2 \; \tau_c \; r_{ij}^{-6} \qquad\qquad [II.2.19]$$

where r_{ij} is the internuclear separation between spins i and j, τ_c is the motional correlation time* and n, Planck's constant divided by 2π.

We now return to the measurable fractional nOe, $f_i(j)$, and relate this to the concepts introduced above as we work towards a practical use for the experiment. The measured $f_i(j)$ has (the first) direct polarization of spin i by spin j, minus the indirect polarization of spin i by spin j through the other spins, n, in a multispin system:

$$f_i(j) = \frac{\sum\limits_{j} \gamma_j \; \sigma_{ij}}{\gamma_i R_i} - \frac{\sum\limits_{n} \gamma_n \; \sigma_{in} \; J_n(j)}{\gamma_i R_i} \qquad\qquad [II.2.20]$$

The second term in Eq. I.2.20 accounts for the "three-spin effect" which is the indirect interaction between i and j, mediated by n. This is discussed later.

The next stage requires developing a working protocol for the determination of internuclear distances involves consideration of a three-spin AMX system. From Eq. II.2.14 we get:

---

*Very roughly, the motional ($\equiv$ rotational) correlation time is the time taken for the molecule to tumble in solution and rotate by one radian.

$$\underline{R}_A = \rho_{AM} + \rho_{AX} + \rho_A^*$$

$$\underline{R}_X = \rho_{AS} + \rho_{MX} + \rho_X^* \qquad [II.2.21]$$

$$\underline{R}_M = \rho_{MX} + \rho_{AM} + \rho_M^*$$

Assuming $\rho_A^* \approx \rho_M^* \approx \rho_X^*$, and given that $\underline{R}_A$, $\underline{R}_M$ and $\underline{R}_X$ were measurable

quantities, the three unknowns in these three equations can explicitly

be determined, and internuclear distances calculated from Eq. II.2.18.

This involves a further assumption that the correlation times of the AM,

AX and MX vectors (which could be quantified from ^{13}C relaxation data[29])

are equal, Hence, we arrive at a master equation of this form:

$$\left[\frac{r_{AX}}{r_{AM}} \right]^6 = \frac{f_A(M) + f_A(X) \; f_X(M)}{f_A(X) + f_A(M) \; f_M(X)} \qquad [II.2.22]$$

With the two-spin approximation, only the first terms $[f_A(M)$

and $f_A(X)]$ are used. If one of the two distances is either known or

can be assumed, the other can be calculated. Also, if the location of A

is sought, it should not be irradiated, but the A{M} and A{X}

experiments should be performed. In terms of experimental practice, the

power levels have to be carefully set to ensure the same percentage

saturation of each spin(s), or normalized. These are the fundamental

tenets of the process of determining internuclear distances in small

organic molecules.[30]

As described in some detail by Mersh and Sanders,[31] it is well

known that the 3-spin case can lead to the observation of negative nOe's

in roughly linear systems[32] when long (2-3 T_1) irradiation times are used. The authors explain the phenomenon and its potential diagnostic uses. In such cases, more explicit equations (e.g. Eq. II.2.20) are used which take into account the positive "direct effects" and "indirect" negative ones. It is interesting to note that, under some conditions, these two contributions can almost cancel, leading to a small induced nOe in a proton which is geometrically close in space to the one being irradiated; this is an unpleasant possibility.

II.2.4.1 Steady-State nOe

This is the simplest nOe experiment and has been alluded to in the preceding remarks. With two spins I and S, radiofrequency field (B_2) is applied to one resonance long enough (≈ 3 T_1) for the nOe to build up in the other. Immediately prior to acquisition, the decoupler is turned off so as to retain spin-spin coupling and preclude Bloch-Ziegert effects. Schematically:

$$\left[\begin{array}{c} 5T_1 \text{ (RD)} - 3T_1 - 90° - \text{AQN} \\ B_2: \underline{\hspace{1.5cm}}\sqcap\underline{\hspace{2cm}} \end{array} \right] \qquad [\text{II.2.22}]$$
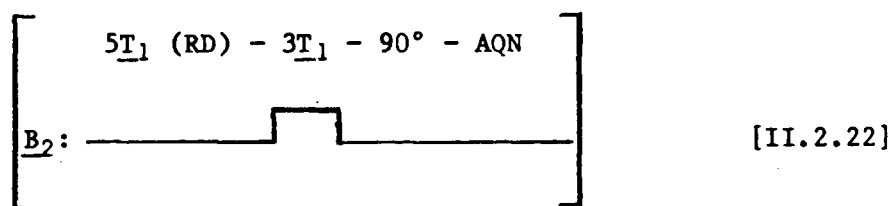
The experiment is repeated to obtain a good signal-to-noise ratio and is then repeated with B_2 placed off resonance, and the integrals of the two spectra compared.

Several practical considerations warrant expansion. When the

frequencies of I and S are close (say, < 1 ppm) it is difficult to saturate one spin without radiation leakage into the other. In order to maintain the required frequency selectivity the strength of the irradiating field ($\gamma B_2/2\pi$) should be reduced so as to effect 60-80% saturation. A less than saturating decoupler field does not invalidate the measurement since the magnitude of the induced nOe for a particular spin is proportional to the extent of saturation of its neighbour.[34] Use of a weaker B_2 field reduces the magnitude of induced nOe's and this could demand a significantly larger signal-to-noise ratio if these (small) changes in intensity are to be reliably measured.

In practice, the frequency selectivity can be checked by performing a number of experiments varying the decoupler power. To minimize nOe build-up, the decoupler is left on for a short period of time (ca. 0.01s). Comparison of peak intensities of resonances close to the decoupler frequency with those in a "control" experiment (decoupler off-resonance) will ascertain whether the desired frequency selectivity is achieved.

It is invariably convenient to perform the experiment in the difference mode[34] (nOe difference spectroscopy ≡ NOEDS). For n irradiation experiments, (n + 1) experiments are required, including one "control" where the decoupler frequency is chosen distant from the spectral region - say, 5 or 10 p.p.m. to high field of the highest-field resonance. Again, the signal acquisition[6] is interleaved:

1. Create on disc (n + 1) blank files, with the decoupler frequencies and power settings specified.

2. Read into core memory file number 1.

3. With the decoupler set to ω_1, obtain 2-4 "dummy" scans (discard), to establish a steady-state.

4. Acquire $\underline{\ell}$ scans (8 or 16).

5. Save the spectrum on disc.

6. Repeat 2-5, now with file number 2 (ω_2).

7. Continue until ($\underline{n}$ + 1) spectra have been saved on disc, reading in the appropriate file each time.

8. Repeat 2-7, $\underline{m}$ times so as to build up a good signal-to-noise.

The total number scans for each experiment = $\underline{\ell}$ * $\underline{m}$. Again, the FID's are exponentially weighted (using 1.5 - 2.0 Hz line-broadening), Fourier transformed and phase corrected. Each spectrum is then subtracted from the "control", and plotted.* Overhauser enhancements are best measured by digital integration of signals (and not by measuring peak heights). Subtraction errors, usually obvious with intense singlets, may be reduced by small (0.001 Hz) shifts of the spectra.[24]

When plotted with the irradiated peak negative-going in intensity, positive going peaks indicate a positive nOe (fast molecular tumbling) and negative peaks indicate a negative nOe (usually indicating slow tumbling). Care should be exercised in applying this rule, since radiation leakage into a nearby signal may falsely indicate a negative

---

*Small phase adjustments in the difference spectrum may improve its quality.

nOe, and, as has been discussed previously, certain linear spin-systems can produce negative nOe's in the extreme narrowing limit.

We reiterate that, in practice, excellent signal-to-noise ratios are required for each spectrum, especially when (a) one is using significantly less than a saturating decoupling field, and (b) the expected nOe's are small. With care, enhancements down to 0.5% are measurable, as seen in later chapters.

It is not always necessary to attempt all the nOe experiments which are possible for the molecule of interest. Choice of which signals to saturate is important. It is difficult (but not impossible) to induce and detect nOe's into a methyl resonance because the methyl protons relax one another efficiently without requiring significant relaxation pathways from other protons in the molecule; furthermore, induced nOe's are difficult to detect since methyl signals are often sharp singlets and, therefore, readily show small frequency offsets when displayed in the difference mode. In short, for qualitative data one should irradiate the proton having the fewest alternative relaxation pathways, since this will be dominated by dipole-dipole relaxation from the smallest number of protons and therefore show maximal nOe's. It has been noted[6,31] that irradiation of steroid methyl groups is useful in providing information on β-axial protons in the vicinity. Finally, we note that tailored excitation sequences[35,30] could prove useful in (a) their frequency selectivity and (b) the ability to "irradiate" simultaneously serveral chosen multiplets in a spectrum.

Fig. II.2.13 illustrates a series of NOEDS(SS) experiments
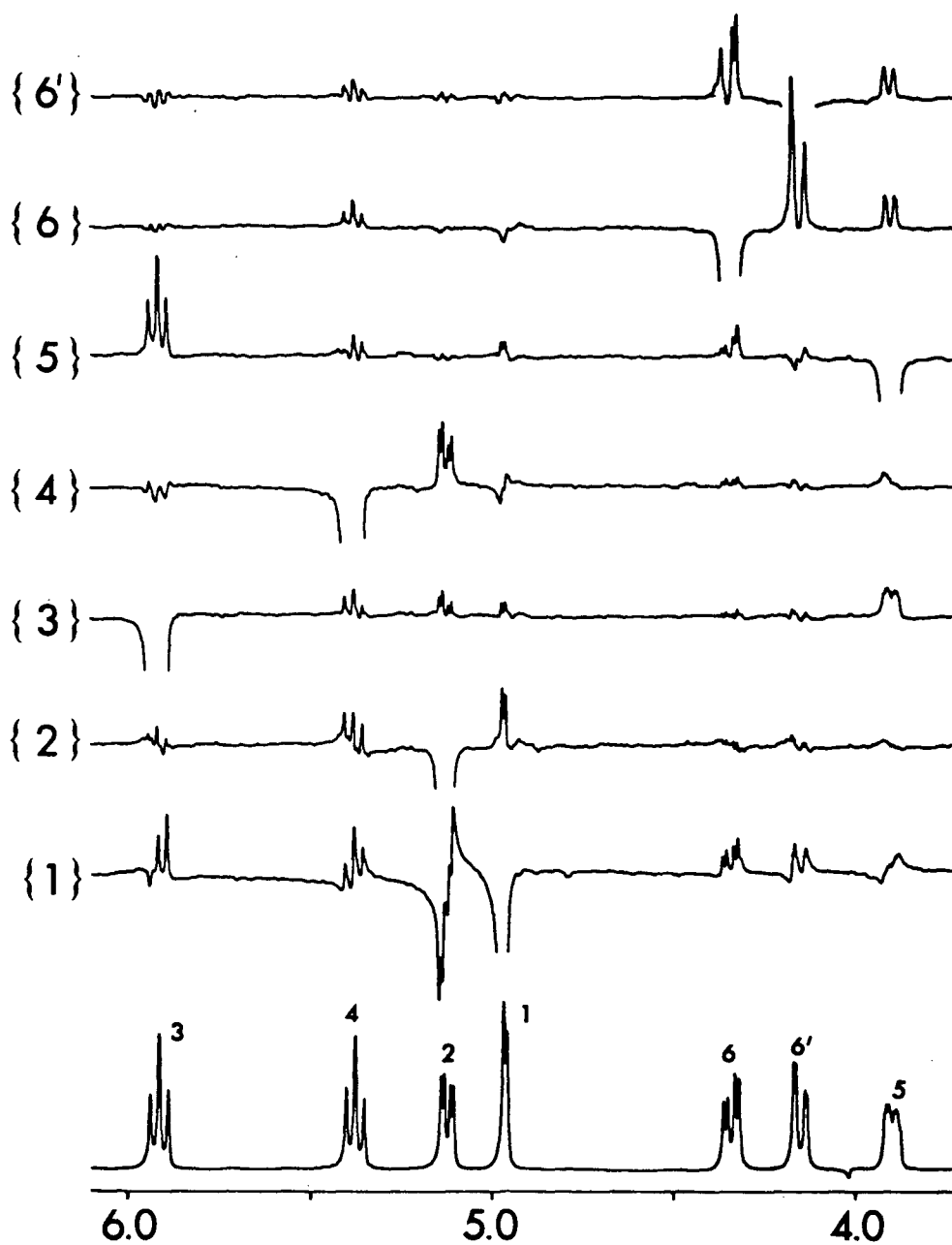
Fig. II.2.13 SSNOEDS on 1 (400 MHz). The irradiated proton is
indicated next to each difference spectrum. The
irradiation time was 6s.

performed on $\underset{\sim}{1}$. It is clear that it is difficult to get the required

frequency selectivity given the small frequency separation (Δv) between

H-1 and H-2 (75% saturation; $\Delta v = 64$ Hz). $\{5\}$ is an interesting

experiment as it illustrates both the strong nOe induced in its 1,3

trans diaxial neighbour (H-3), and the comparatively small nOe into the

methylene protons (which have an efficient, mutual relaxtion patheway).

II.2.4.2 Transient Overhauser Effect[28],[36],[37] (TOE)

This experiment is similar to the steady-state nOe experiment

in that the populations of one spin multiplet are selectively inverted

(using a selective 180° pulse) and the recovery of the spin system is

followed. To obtain frequency selectivity, the duration of the

decoupler pulse is, typically, 0.01 to 0.03 s. The experiment is

depicted below:

$$\left[\begin{array}{c} 5\underline{T}_1(RD)\text{-} \quad \text{-}\underline{t} - 90° - AQN \\[2mm] \underline{B}_2: \text{————————} \prod \text{————————} \\ \omega_s \end{array} \right]_{\underline{n}} \qquad [II.2.23]$$
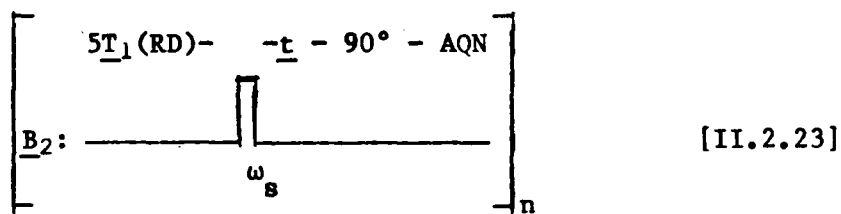
An initial relaxation delay is ended by the selective 180° pulse, which

is applied through the decoupler channel. A variable time-delay ($\underline{t}$)

follows (cf. T1IR experiment), with a non-selective 90° "read" pulse and

data acquisition. For each $\underline{t}$ value, $\underline{n}$ scans (8-16) are initially

collected, and the cycle repeated in a fashion analogous to the SSNOEDS

and SDDS experiments. To achieve a more selective 180° pulse, a

composite pulse[38] comprising a "sandwich" of three pulses, $90°_{\pm x}$

$240°_{\pm y}$ $90°_{\pm x}$ is highly recommended, as this gives excellent

population inversion and removes errors caused by resonance offset. A

comparison of the effect of using a single selective 180° pulse vs. the

composite pulse is given in Fig. II.2.14.

A.   B.   C.
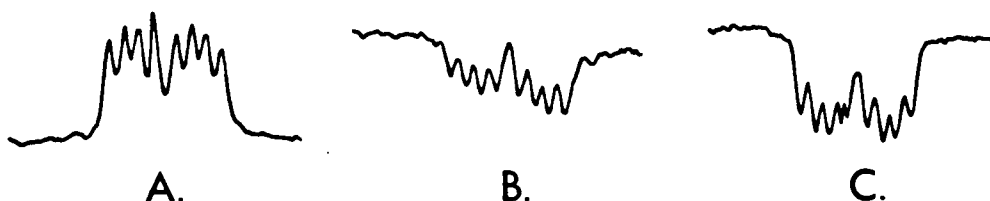
Fig. II.2.14 (A) The equilibrium z-magnetization of 1 (H-5). The
z-magnetization immediately after (B) a single
selective 180° pulse, and (C) a compositive 180°
pulse.

Conceptually, the TOE experiment can be explained by invoking

similar arguments to those proposed in II.2.4.1. In general

magnetization of the inverted resonance will follow a multiexponential

recovery, while the unperturbed spin suffers a transient change in

intensity, which depends on the extent of its relaxation with the one

perturbed. Attention is directed to the growth in intensity of the

unperturbed spin (displayed in the difference mode) as a function of time, $\underline{t}$. As we shall see, comparisons of absolute nOe's for different protons do not necessarily give the correct distance information; a more precise evaluation comes from the initial slope[26,28] of the TOE build-up curve, which is approximately equal to σ. Using a two-spin approximation and assuming $\rho_{ij} = \rho_{ji}$, $\sigma_{AM}/\sigma_{AX} = (r_{AX}/r_{AM})^6$. Although not absolutely precise, this gives us a maximum figure for r, the internuclear separation.

Fig. II.2.15 illustrates a difference TOE experiment conducted on $\underset{\sim}{1}$; H-5 is selectively inverted by a composite pulse (180° = 20 ms). $\underline{t}$ values are in seconds. A relatively fast build-up of nOe in H-3 is observed, while, for example, H-1 builds up a smaller nOe at a slower rate. Fig. II.2.16 shows plots of the nOe build-ups for H-3 and H-1.

Consider now the nOe build-ups in H-3 and H-1. The ratios $f_{H-1}(H-5)/f_{H-3}(H-5)$ vary from 0.25 - 0.41 and cannot be used for distance calculations. From the initial slopes, $\sigma_1/\sigma_3 = 0.26$. Knowing that $(\sigma_1/\sigma_3) = (r_{5-3}/r_{5-1})^{+6}$, and assuming a typical H-3, H-5 internuclear separation of 2.64Å, we calculate $r_{5-1} = 3.32$ Å ($\pm.1$Å).
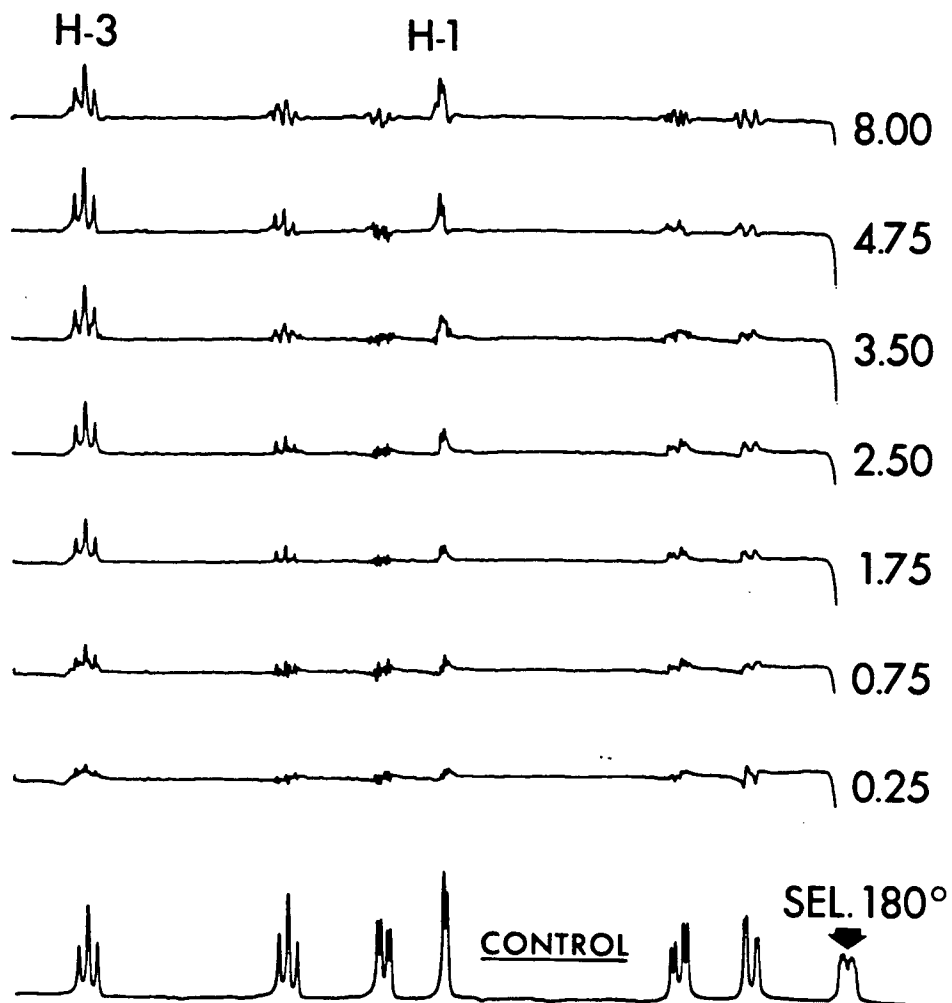
Fig. II.2.15 Difference TOE on $\underset{\sim}{1}$ (400 MHz), selectively inverting H-5
with a composite pulse (see text). The time, $\underline{t}$, between
selective population inversion and total signal
acquisition is given with each spectrum.
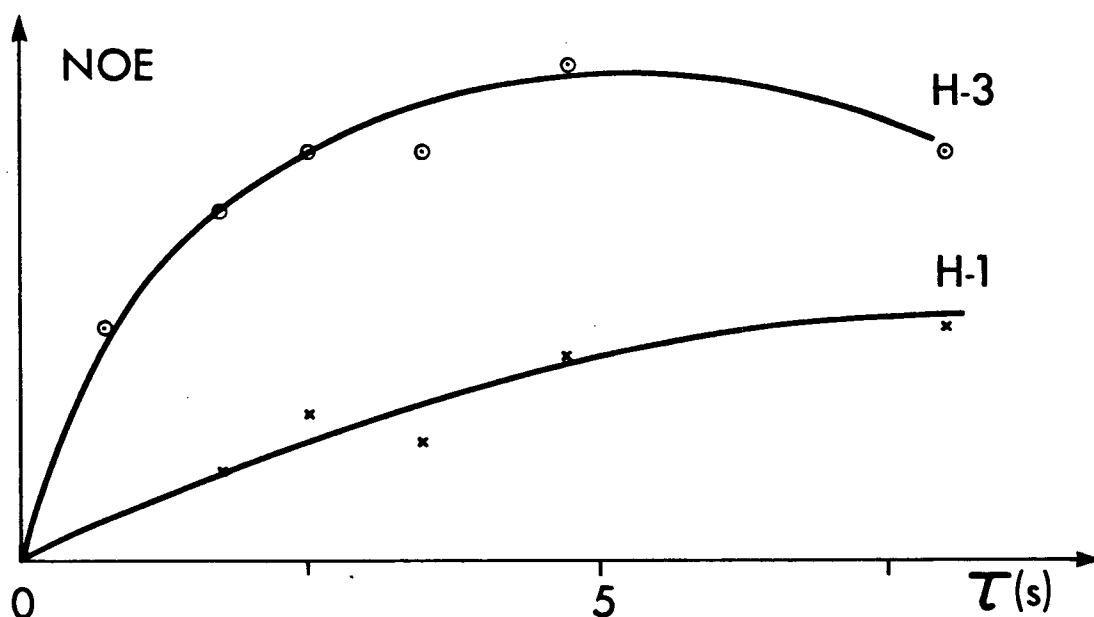
Fig. II.2.16 Data from Fig. II.2.15, showing the nOe build-ups of H-1 and H-3 with time.

Considering the small size of σ_{H-1} and the resultant error in its calculation, we note a close agreement to the distance obtained by neutron-diffraction for a similar system[8], of 3.33 Å. Note also that errors in the measurement of σ translate to sixth-root of errors in distances. This example illustrates the ease with which approximate distance measurements may be obtained for rigid systems. The interested reader is referred to a thesis on this subject.[8]

Distance information derived from dynamic methods such as TOE is much more useful than SSNOEDS, since the method automatically gives a

feel for the <u>rate</u> at which these population transfer processes occur, and this gives a better picture of the system. TOEDS eliminates the guess-work involved with choice of the irradiation time in the SSNOE experiment. Results are found in build-up rates, rather than SSNOE peak integrals. We also draw attention to the potential frequency selectivity through the use of a selective 180° pulse. If further selectivity is demanded, one may make use of a tailored excitation pulse sequence[35] or DANTE[41]. For the author's purposes, the composite 180° pulse has proved satisfactory.

In conclusion we note the potential of the experiment with slowly tumbling molecules[37,39,40] (spin-diffusion limit; <u>vide infra</u>).

II.2.4.3 <u>Truncated Driven NOE Difference Spectroscopy</u>

For studies of molecules outside of the extreme narrowing limit, the results from steady-state NOE measurments no longer bear a direct relation to interproton distances; instead, the behaviour depends on "spin diffusion".

It is general practice to study biologically important molecules – even as small as an octapeptide – dissolved in viscous solvents (e.g. DMSO-$\underline{d}_6$) and observed at as high a field-strength as possible (to obtain maximum dispersion). These two factors combine to place the system in the spin diffusion regime where a maximum nOe of –1 is attainable. Two alternative, one-dimensional experiments may be used to study molecules in this regime: transient nOe experiment (<u>vide supra</u>) and the more

useful truncated driven nOe experiment[29,42-44] ("driven nOe").

The pulse sequence for driven nOe requires a selective, near-saturating $\underline{B}_2$ to be applied at ω_S for varying times, $\underline{t}$.* This is followed by a "read" pulse and signal acquisition. Again, the experiment is collected in blocks, together with a blank, and the data presented in the difference mode. At each frequency, a number of

$$\left[\begin{array}{c} RD(5\underline{T}_1) - \quad -90° - AQN \\[2em] \underline{B}_2:\underline{\hspace{0.2cm}}\sqcap\underline{\hspace{0.2cm}}\underline{\hspace{1.5cm}} \\ \underline{t} \end{array} \right]_{\underline{n}}$$

[II.2.24]

experiments is performed, varying $\underline{t}$.

For each experiment the induced nOe is plotted against $\underline{t}$, for each spin showing an nOe. The nOe curve for each proton builds up to a maximum value and then levels off. Again, it is the initial slope of each curve which gives the distance information. If spin i is irradiated and the nOe build-up curve for spin s plotted, the initial slope of the curve = $-\sigma_{ij}$. This can be translated into distance information using the comparative methods discussed earlier.

If one is familiar with the system under investigation and knows that for a particular irradiation time one is in the approximately linear, "rising" portion of the build-up curve, one may perform just one experiment, with this irradiation time and compare single nOe's rather

---

*$\underline{t}$ is short compared with the irradiation times used in SSNOEDS (< 0.5 s).

than the slopes, to obtain the distance information.

Examples of this experiment appear in Chapter II.5.

II.2.5 Two-Dimensional Experiments[45-47]

II.2.5.1 Basic Concepts

Most readers are familiar with the concept of normal pulse FT NMR. A pulse is applied to the system and a signal is detected as a function of time, $\underline{s}(\underline{t})$. The process of Fourier transformation converts this time-dependent function into a frequency-dependent one, $\underline{S}(\underline{F})$ - which is the familiar display of absorption $\underline{vs}$ frequency. With two dimensional ("2D") NMR spectroscopy the magnetization is detected as a function of $\underline{two}$ time intervals; one a $\underline{linearly\ incremented\ time\ delay}$, $\underline{t}_1$, and detection occurring during the acquisition time, labelled $\underline{t}_2$, resulting in a two dimensional data array, $\underline{s}(\underline{t}_1, \underline{t}_2)$. Usually, $\underline{n}$ experiments are performed, each with an increasing value of $\underline{t}_1$, and the $\underline{n}$ data sets saved on a mass data storage device, such as a hard disc.

Each signal detected in $\underline{t}_2$ corresponds basically to a normal single-quantum spectrum of the molecule. However, each resonance has a "memory" of processes occurring during $\underline{t}_1$ and this will result in a $\underline{modulation}$ of the signals - either by phase or amplitude. The analogy has been drawn between 2D NMR and two-dimensional paper chromatography. Chromatographic separation of similar compounds is improved by using one solvent system to disperse components along one axis of the paper which is then turned 90° and developed with a different solvent system in the second dimension to provide enhanced dispersion. If the paper is
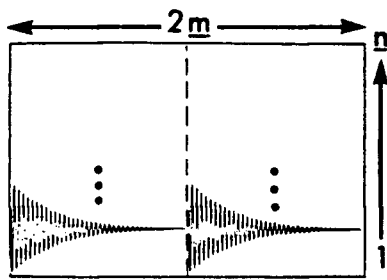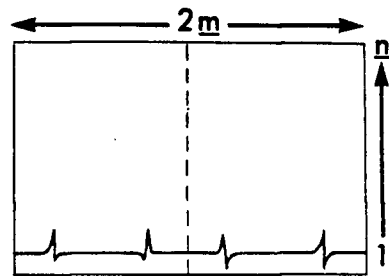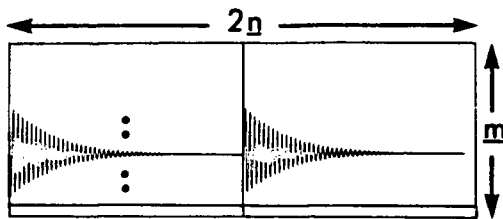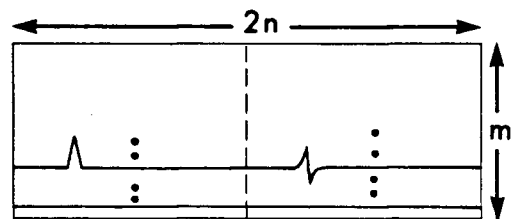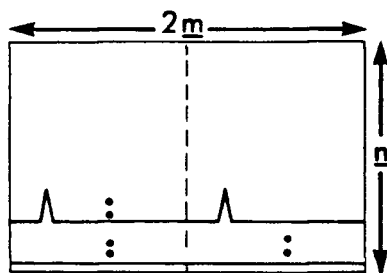
Fig. II.2.17 Schematized data matrices illustrating the stages of processing of a 2D data-set.

sprayed to visualise the compounds, a plot of colour intensity over the eluted area would produce diagrams similar to those presented in this chapter! With 2D NMR, the NMR responses are spread over two <u>frequency</u> axes to improve dispersion. The "solvent" used in F_2 is almost always chemical shift, but F_1 may characterise a variety of parameters (e.g. homonuclear $\underline{J}$'s), depending on the pulse-sequence used to elicit the NMR responses.

As mentioned, $\underline{n}$ experiments are performed and the FID's ($2\underline{m}$ words) sequentially stored on disc (Fig. II.2.17.A.). This data matrix of $\underline{n}$ rows and $2\underline{m}$ columns is denoted $\underline{s}(\underline{t}_1,\underline{t}_2)$. Next, all FID's are Fourier transformed, yielding (Fig. II.2.17.B.) the $\underline{s}(\underline{t}_1,\underline{F}_2)$ matrix; this comprises a set of spectra, the signals of which are modulated in either their amplitude or phase. Next, a <u>transposition</u> is performed giving a data-set which indicates the dependence of the magnetization at a particular point in $\underline{F}_2$, as a function of $\underline{t}_1$; $\underline{S}(\underline{F}_2,\underline{t}_1)$ in (Fig. II.2.17.C). This generates a series of interferograms* - one for each absorption frequency in $\underline{F}_2$. These are traces of columns taken from the $\underline{s}(\underline{t}_1,\underline{F}_2)$ data set and indicate the "spectrum" of amplitude or phase modulation in $\underline{t}_1$. The interferograms are Fourier transformed, to give $\underline{S}(\underline{F}_2,\underline{F}_1)$ in Fig. II.2.17.D.; these signals are often displayed in a phase-insensitive mode (<u>vide infra</u>) since phasing in both frequency dimensions is difficult. Finally, this matrix is transposed again to give a $\underline{S}(\underline{F}_1,\underline{F}_2)$ data set (Fig. II.2.17.E.). This process is simpler in

---

*An interferogram is essentially an "FID" of magnetization as a function of $\underline{t}_1$, given another name to differentiate it from $\underline{t}_2$ signals.

practice than it may appear here, and can be performed relatively easily with standard soft-ware packages included in most modern spectrometers. Some programmes require the operator first to specify all parameters and then with a single command, the above steps are performed automatically, transparent to the operator, while others require operator intervention at each step.

As mentioned previously, 2D spectra are normally presented in either power- or magnitude-mode (i.e. phase insensitive,* as this obviates the necessary complex phase adjustments required over two dimensions). Unfortunately this procedure creates a problem, since the phase-insensitive display of a Lorentzian line has very wide "wings" - intensity distant from the resonance frequency. These dramatically reduce the base-line separation between individual signals, and can give rise to artifacts - false signals arising from interference between the wings of two peaks. Fig. II.2.18 illustrates the problem and some of the solutions. The first column shows the appearance of several weighting (apodisation) functions,[4] the second shows the derived phase-sensitive frequency-domain spectra and the last is the magnitude calculation of the absorptions in the second column on the same frequency scale. Fig. II.2.18A shows the exponential filter

---

*Fourier transformation of a time-domain signal yield a "real" (u) and imaginary (v) component. Usual (phase-sensitive) detection requires observation of the "real" component, with some phase adjustments. The "magnitude" (or "absolute") display calculates the modulus of the signal, $(u^2 + v^2)^{1/2}$, and the "power" mode is its square $(u^2 + v^2)$.
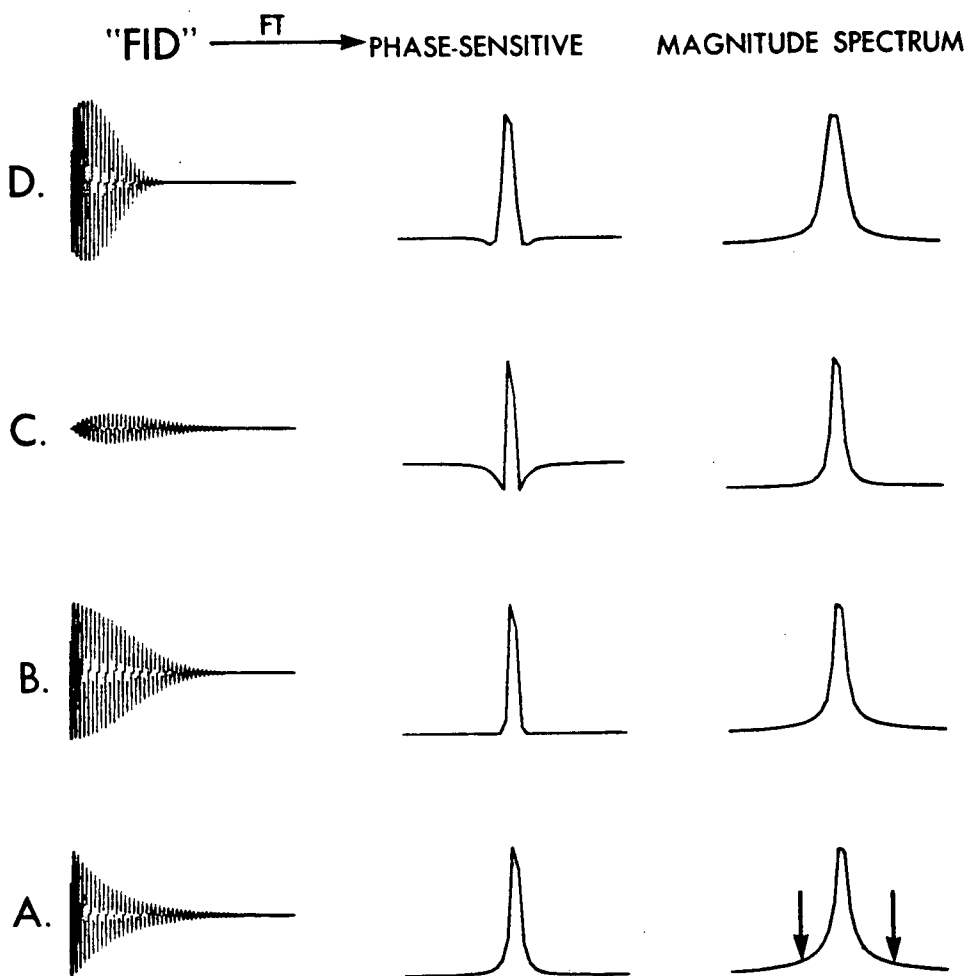
Fig. II.2.18 Effect of apodization functions on line-shapes in phase-sensitive (column 2) and magnitude mode (column 3).

(line-broadening of 0.75 Hz) applied to a sine-wave. FT yields a
Lorentzian absorption line-shape which, when subjected to magnitude
calculation yields the very broad "wings" ($\equiv$"tailing"), indicated with
arrows. Converting the sine-wave into a Gaussian function, as in Fig.
II.2.18B, yields an improved situation in both regimes. Fig. II.2.18C
illustrates the use of the "sinebell" function. An exponential-shaped
FID (Fig. II.2.18A) is apodised with a sine-function of period twice the
acquisition time, and zero phase shift (i.e. zero at $t=0$ and $t=AT$). Its
phase-sensitive FT shows decreased line-width accompanied by significant
distortion at the base of the peak. A significant loss in
signal-to-noise is incurred, not obvious from the second frame.
Magnitude calculation produces a line-shape which approximates to an
absorption line and is comparable with the phase-sensitive Lorentzian
signal. This form of modulation is termed a "pseudo-echo", as it is
roughly symmetical about AT/2 and zero at both start and finish.[49] The
pseudo-echo shaping may be further improved by first multiplying the
decaying exponential function by a rising exponential to artificially
eliminate the decay, and then applying the sinebell function (or a
similar symmetrical Guassian envelope).

A similar protocol, less drastic in its attenuation of
signal-to-noise is the "double exponential" filter, shown in Fig.
II.2.18D. Here, the FID is weighted with a rising exponential filter
and a falling function for Gaussian line shape. The result is a
compromise - the resolution enhancement is poorer, but there is less
peak-base distortion and degradation of signal-to-noise. The magnitude

calculation spectrum shows less tailing.

The display of 2D data sets is a non-trivial problem. Early experiments were invariably displayed as a "stacked plot"; this consists of a series of conventional $S(F_2)$ spectra, one for each regular interval of F_1 (or, _vice_ _versa_). The three-dimensional impression is further enhanced by use of the "white-wash" routine, whereby peaks from previous traces are not overwritten (the pen lifts up and skips over them). Although the three-dimensional effect is excellent and the plots are aesthetically very pleasing, it is often difficult to extract the scientific information. Furthermore, the process is unecessarily time-consuming because the majority of the traces only display noise. A far more efficient routine employs the "contour plot" display which is similar to that used for geographical maps; contour lines link loci of, say, equal elevation. With 2D NMR, the F_1/F_2 plane is viewed from above, along the amplitude axis; contours join points with the same amplitude. Data are easily extracted from such displays. Problems arise in choosing the contour levels when a large dynamic-range exists between different peaks; in fact, a series of peaks could be entirely missed if the threshold level were set too high - hence, caution should be exercised. Fig. II.2.19 illustrates the benefit of the contour plot over the stacked plot. The diagrams are from the 2D homonuclear J-correlated spectrum of a derivatized disaccharide.

The relevant parameters can often be extracted from the data set without the need for the 3D representation. Here, use is made of projections[50,51] (or sums) either taken over the entire frequency
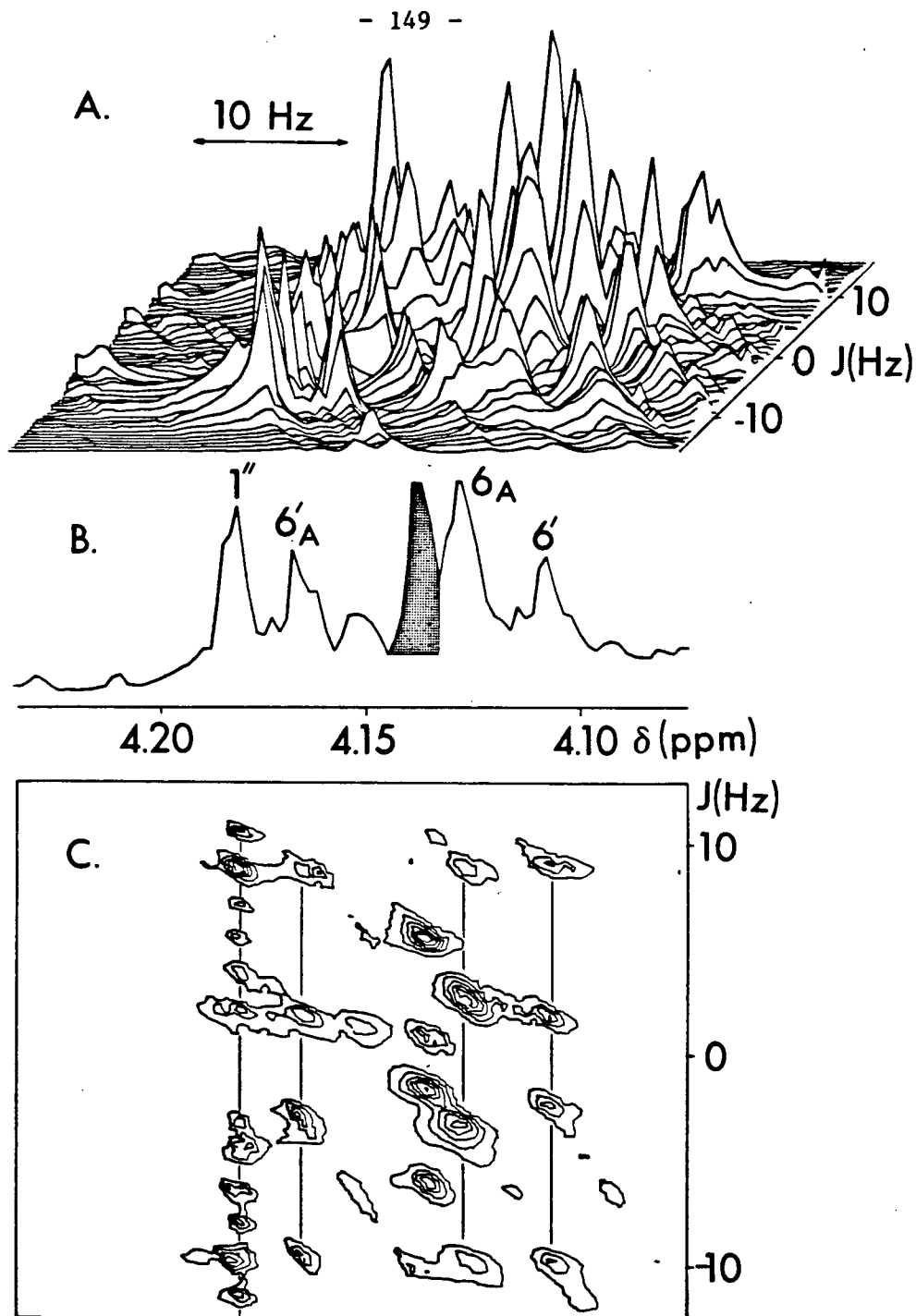
Fig. II.2.19 Comparison of stacked (A) and contour plots (C). B.
The F_1 projection of the tilted data-set. The stipled
peak arises through strong coupling between 6' and $6'_A$.

Data are from the same region of a 2D J-resolved
experiment of a disaccharide.

A.

B.

0° PROJECTION

90° PROJ.

$\underline{F}_1$

$\underline{F}_2$

$\underline{F}_1$

$\underline{F}_2$
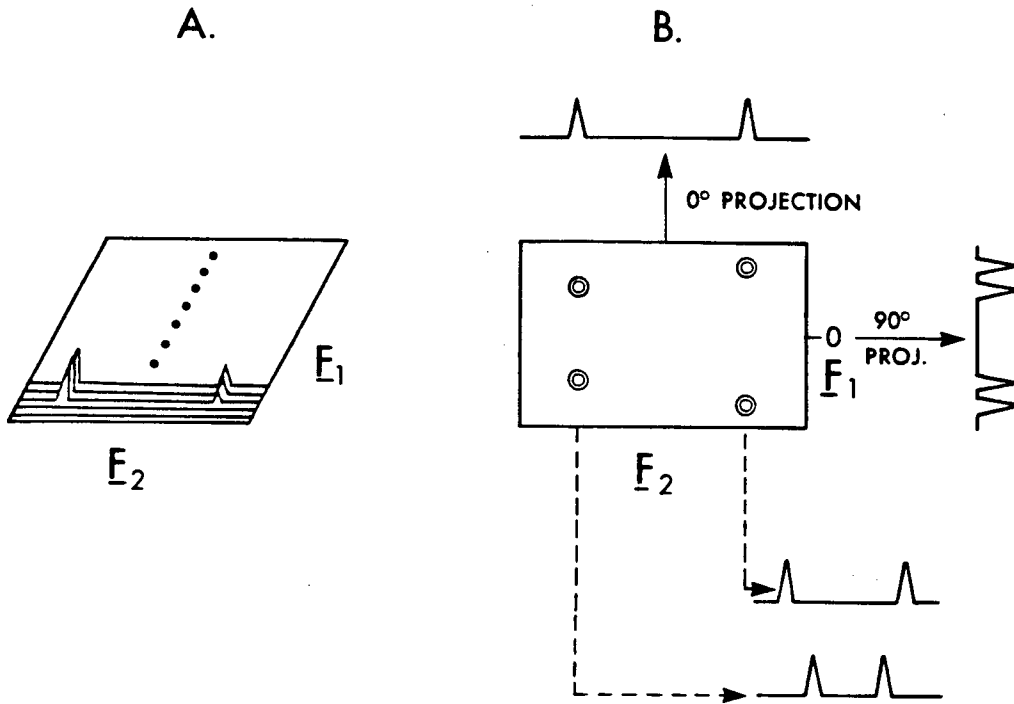
Fig. II.2.20 A. Stacked-plot of schematized 2D data set. B. Contour plot illustrating full 0° and 90° projections (top and right), and "partial" 90° projections (bottom).

range in F_2 or F_1 (0° or 90° projection, respectively) or a single trace, or "slice" may be taken out at a particular F_2 value and viewed at 90° (Fig. II.2.20). The latter are called F_1 traces and generally contain all the information needed.

An almost overwhelming variety of 2D experiments has already been published and all indications are that this rapid proliferation will continue. An objective inspection of the recent literature indicates that the major experiments have already been developed; what is now evident is a second generation of pulse sequences in which existing ones are either refined (see, for example, ref. 46, pp. 50-65) or two experiments are combined to either yield additional information (e.g. Section II.2.5.3.4) or improve the experiment (e.g. ref. 52). It is useful at this juncture to broadly classify the available 2D experiments:

A. <u>Resolved NMR</u>

In this case, F_2 is the chemical shift axis of the observed nucleus and F_1 may represent a variety of "resolving" parameters such as homonuclear J-coupling (<u>vide infra</u>), heteronuclear J-coupling, heteronuclear chemical shift (<u>vide infra</u>) or dipolar coupling.

B. <u>Correlated NMR</u>

Also termed "autocorrelation" the same chemical shift axis is plotted along both dimensions and spins are correlated either through J-coupling (<u>vide infra</u>) or spin exchange (nOe or chemical exchange).

C. Indirect Detection

Multiple quantum transitions (MQT) cannot be observed
directly, but experiments have been developed to allow for
their indirect detection. Indirect detection of rare nuclei
also falls in this category.

D. Combination of A, B and C, and Others

Before commencing with more detailed comments on some selected
experiments, a few general points are appropriate. A major experimental
restriction is often digitization, since one is often limited by
available data storage space and time. As a result, the minimum
sweep-widths in F_1 and F_2 should be selected. Any aliasing in F_2, due
to insufficient sweep-width can usually be chosen so that these peaks
fall into a blank region of the spectrum. They can be attenuated by use
of the frequency filter if they have no information.* It is not
possible to perform frequency filtering in F_1 and the experimenter is
advised either to avoid aliasing by choosing a suitable sweep-width, or
exercise caution by being aware of the way in which this occurs.

The number of experiments performed, n, is usually a binary
number (64, 128, 256, etc). The smaller n, the less machine time will
be required to obtain $s(t_1, t_2)$. Digitization in F_1 can usually be
improved by zero-filling, but caution should be exercised in trying to

---

*Solvent signals, impurities and acetate singlets can often be
treated in this way.

let a very small $\underline{n}$ suffice, since this may lead to severe truncation of the interferograms, and associated line-shape distortions. Having chosen a suitable block-size and sweep width (in $\underline{F_2}$), one can calculate the acquisition time and set up the experiment such that the effective acquisition time in $\underline{F_1}$, ($\underline{n}$ * $\Delta\underline{t}_1$) is of similar duration.

The incremental delay-time, $\Delta\underline{t}_1$ is easily calculated from the required SW in $\underline{F_1}$. 0.5 $\Delta\underline{t}_1$ used in spin-echo experiments is given by expression II.2.24, and $\Delta\underline{t}_1$ is given by II.2.25:

$$0.5 \ \Delta\underline{t}_1 = (4 \ * \ \pm \ SW_{\underline{F}_1})^{-1} \qquad [II.2.24]$$

$$\Delta\underline{t}_1 = (2 \ * \ \pm \ SW_{\underline{F}_1})^{-1} \qquad [II.2.25]$$

Finally the total experimental time may be estimated from equation II.2.26.

$$\text{Total time} = \underline{n} \cdot NA[1/2 \ (\underline{t}_1)_{max} + AT + RD] \qquad [II.2.26]$$

$\underline{n}$ is the number of increments in $\underline{t}_1$, AT is the acquisition time ($\underline{t}_2$), RD is the relaxation delay between acquisition and the first pulse in the sequence, and NA is the number of acquisitions for each $\underline{t}_1$ value (including dummy scans).

Finally, we address the topic of signal-to-noise in 2D experiments, which has been explicitly formulated by Ernst and co-workers.[53] It happens that the overall demands of the method are reasonable, since both the signals and the noise are spread over the ($\underline{F_1},\underline{F_2}$)-plane. Obviously a loss in signal-to-noise is incurred as a

result of signal decay during $\underline{t}_1$, but this only becomes critical when dealing with molecules with very short $\underline{T}_2$'s (see Chapter II.5). Some autocorrelation experiments suffer a further degradation in sensitivity because each conventional resonance generates $-2^{\underline{m}-1}$ components, where $\underline{m}$ is the number of weakly-coupled non-equivalent spins. This is offset by an increase in sensitivity resulting from symmetrization procedures (discussed in II.2.5.3.1). The author's "working rule" is that if signals can be seen upon FT of the first of the $\underline{n}$ intervals (blocks) of the $\underline{s}(\underline{t}_1,\underline{t}_2)$ data-set, the overall experiment stands a good chance of succeeding. Of course, if resolution enhancement is necessary for the resolution of closely spaced peaks, the signal-to-noise requirements of the original data set will be correspondingly higher.

II.2.5.2 Homonuclear J-Modulated Spectroscopy[54] (2D J-resolved)

The key to this experiment is the basic Hahn spin-echo, which has been documented[55] for over 30 years. Hahn used a 90°-τ-180°-τ-AQN pulse-sequence; he noted the narrower line widths attainable and used this very early on in making some of the first scalar $\underline{J}$ measurements. He analysed plots of echo-amplitude $\underline{vs}$ τ in the frequency domain and came to some anticipatory conclusions. A modulation of the echo envelope which depends on both $\underline{J}$ and the chemical shift separation was observed. Further, he noted that "...if only one of two coupled nuclei is subjected to resonance (e.g. between ^{19}F and ^1H) no echo envelope modulation will appear for either of such coupled nuclei, although the steady state resonance will still reveal the $\underline{J}$ splitting."

Herein lie the concepts of 2D $\underline{J}$-resolved spectroscopy, albeit without the complex two-dimensional FT. The above quotation has also been documented in the light of 2D $\underline{J}$-resolved spectroscopy.[56]

The basic 2D $\underline{J}$-resolved pulse-sequence is:

$$RD - 90°(\Phi_1) - 0.5\underline{t}_1 - 180°(\Phi_2) - 0.5\underline{t}_1 - AQN(\Phi_3) \qquad [II.2.27]$$

Phase cycling of the pulses and receiver is important. The EXORCYCLE scheme proposed by Bodenhausen, Freeman and Turner[57] (II.2.28) eliminates so-called "ghosts" and "phantoms" arising[58] from pulse imperfections and residual transverse magnetization.

Further improvements in the quality of the final spectrum may be achieved by (a) using a composite 180° refocussing pulse[38] ($180°_{\pm x} \equiv 90°_{\pm x}$ $180°_{\pm y}$ $90°_{\pm x}$; $180°_{\pm y} \equiv 90°_{\pm y}$ $180°_{\mp x}$ $90°_{\pm y}$ and (b) extending the phase-cycling to 16 steps by incorporating the well known CYCLOPS scheme (II.2.29) to reduce quadrature images in $\underline{F}_2$.

Cycle	1	2	3	4
Φ_1	x	x	x	x
Φ_2	x	y	-x	-y
Φ_3	x	-x	x	-x

[II.2.28]

Cycle	1	2	3	4	5	6	7	8	9	10	11	12	13	14	15	16
Φ_1	x	x	x	x	y	y	y	y	-x	-x	-x	-x	-y	-y	-y	-y
Φ_2	x	y	-x	-y	y	-x	-y	x	x	-y	x	y	-y	x	y	-x
Φ_3	x	-x	x	-x	y	-y	y	-y	x	-x	x	-x	y	-y	y	-y

[II.2.29]

The 16-cycle scheme is preferable should one require much signal-averaging, especially for studies of dilute solutions. If only four pulses yield sufficient signal-to-noise, then phase-cycling according to II.2.28 with a composite 180° pulse should be sufficient, but one should be aware of very strong signals which may still show quadrature images in $\underline{F}_2$[57] (vide infra).

The 2D $\underline{J}$-resolved experiment may be explained in terms of vector diagrams. Consider the X nucleus of an AX spin system. The relaxation-delay (RD) is terminated by the application of a 90°_{x} pulse, which tips the equilibrium magnetization onto the $\underline{y}'$-axis (Fig. II.2.21A). The X magnetization has a fast ($\underline{f}$) and slow ($\underline{s}$) vector*, corresponding to the two possible spin states of A to which it is coupled. With time, the vectors will precess in the $(\underline{x}'-\underline{y}')$-plane (Fig. II.2.21B) (as depicted previously in Fig. II.2.3) mainly under the influences of chemical shift and $\underline{J}$. A 180°_{y} (refocussing) pulse is now applied which takes the vectors to their mirror-image positions about the y'-axis in the rotating reference frame. Consider the situation where both A and X experience the 180° pulse, which gives the situation in Fig. II.2.21C. As well as changing the position of the vectors

---

*Here, we are using the terms "fast" and "slow" to describe two different transitions, as in Fig. II.2.3. Note that in discussions on the removal of magnetic inhomogeneity effects by this experiment, these terms pertain to a single resonance and have a different meaning.
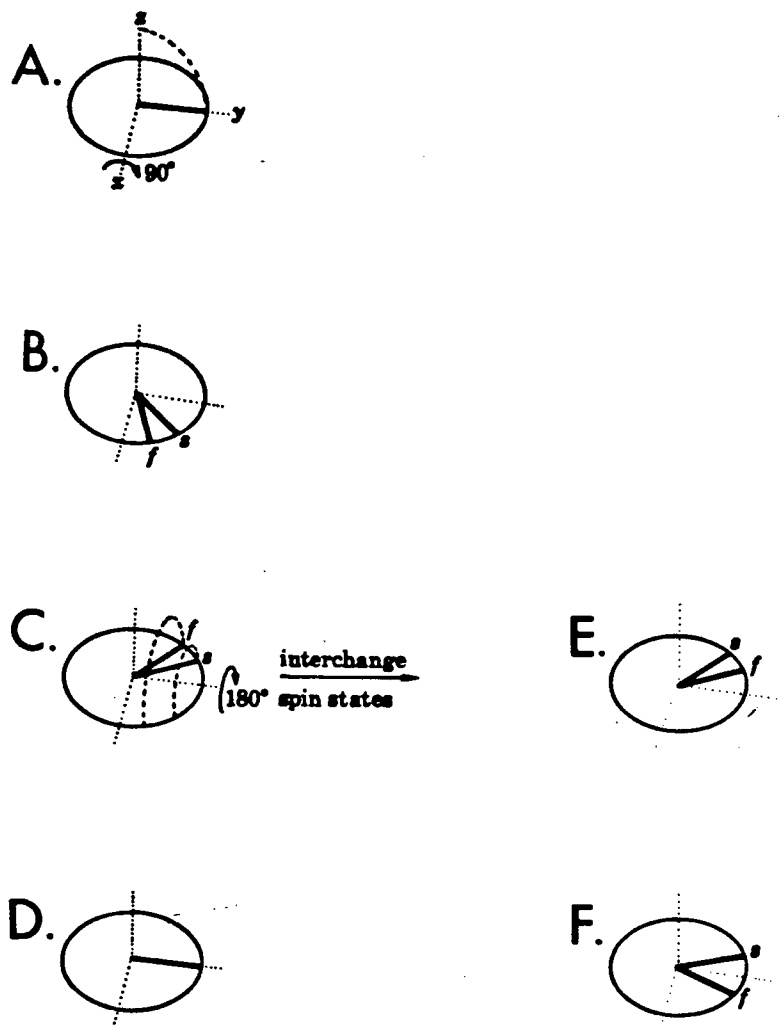
Fig. II.2.21 Vector diagram model of the 2D J-resolved experiment.
With the X transitions in an AX spin system (A,B,E,F),
both spins feel both pulses; in A-D, only spin X is
subjected to the refocussing pulse (From Freeman[45]).

representing X, the labels of the two X transitions are changed (F <->
S) as A changes its spin state (α <-> β). Thus, during the second 0.5
t_1 period the vectors continue to diverge and the echo consists of two
components (Fig. II.2.21F); that is, only the chemical shift effects are
refocussed and not spin-spin coupling. The overall result is a
modulation in phase of the signals by J, as a function of t_1. The phase
of a signal will be a function of $\pi J\ t_1$.

A second situation is possible when A is a heteronuclear species
(^{19}F, for example), for the 180° pulse affects the X spins but not A.
Under these conditions the X vectors are flipped through 180°, but their
"labels" remain unchanged (Fig. II.2.21C). Therefore, after 0.5t_1 both
the X transitions will be exactly refocussed (Fig. II.2.21D); the echo
is modulated by neither chemical shift nor J effects, and would be seen
to decay in amplitude due to transverse relaxation effects (T_2) only.

We have seen that the usual 2D J experiment (Figs.
II.2.21A,B,E,F) leads to a J-modulated spin echo. With the step-wise
incrementation of t_1 one builds up a data matrix which can be handled in
the usual way (Section II.2.1) and the FT in t_1 will be a function of
J. Hence, this is called the "J-dimension". One further point not
apparent from the above discussion is that line-widths in the 2D
J-resolved experiment will approach the natural line-width ($T_2^* \rightarrow T_2$),
i.e. the contribution of magnetic inhomogeneities to line-widths will be
very small, compared with a normal FT experiment. This arises from the
fact that magnetic field inhomogeneity effects also refocus at t_1, the
time of the echo.

A generalized out-put is given in Fig. II.2.22A, depicted in the contour mode. Well resolved 2D peaks hold a one-to-one correspondence to the resonance lines observed in 1D NMR, in the absence of strong coupling effects. One notes that a line drawn through a multiplet is at 45° to F_2, when F_1 and F_2 are drawn to the same scale. It is mandatory to remove the δ contribution from F_2 by "shearing", or "tilting" the data matrix according to $(\omega_1, \omega_2') = (\omega_1, \omega_2 - \omega_1)$,[59] to give the plot shown in Fig. II.2.2.22B. Now F_2' is a function of δ only and F_1 (the J-dimension) encodes only the scalar $^1H - ^1H$ couplings.

$$F_2(\delta, J)$$

A.

$$F_2(\delta)$$

B.
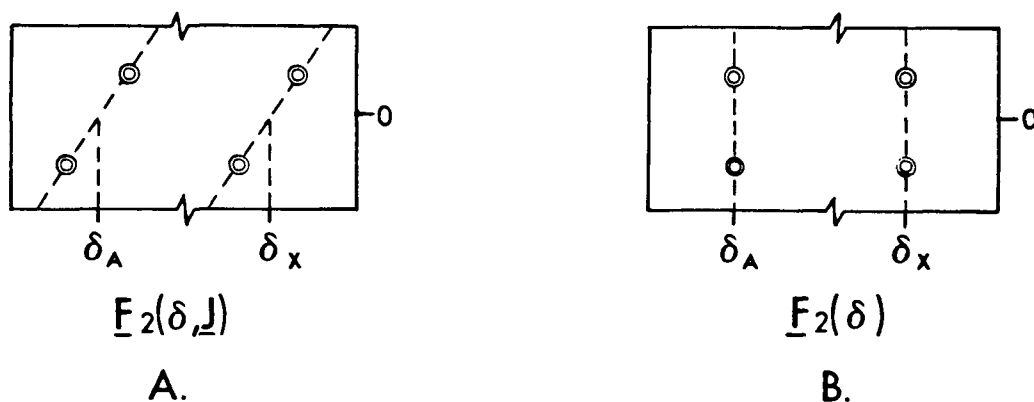
Fig. II.2.22 Schematized 2D J-resolved contour plot output of AX spin system without (A) and with (B) tilting.

The utility of this experiment becomes apparent when one considers projections and slices taken[51] as outlined in Fig. II.2.20. The 0° projection (onto F_2') of the complete data matrix will given one line for each spin-multiplet - this has the appearance of a "broad-band decoupled" proton spectrum and gives the ^1H shifts. "Slices" taken at

the frequency corresponding to each shift, and viewed at 90°, will give
the "J-spectrum" for each resonance. These are referred to as "partial
J" spectra. In the absence of either strong coupling or very short
T_2's, homonuclear 2D J-resolved spectroscopy must be the ultimate answer
to the "hidden resonance" problem. Resonances need only be removed from
one another by a few Hz ($\simeq$ 0.01 ppm at high field) for their J-spectra
to be completely resolvable.

The question of line-shapes in the 2D J-resolved experiment has
received much attention. Because the method is based on phase
modulation, the resonance lines have a phase-twisted shape[48] which is
very difficult to phase correct[60] in two dimensions. With a
phase-sensitive $\underline{S}(\underline{F}_1,\underline{F}_2)$ matrix one can almost always phase correct
individual partial J-spectra using the conventional A and B
phase-corrections. A phase-sensitive tilted $\underline{S}(\underline{F}_1,\underline{F}_2')$ matrix will
always yield J-spectra with distortions at the base of resonance lines;
however, the resultant absorption-like spectrum is obtainable[61] with
significantly better line-width than those from the more commonly used
phase-insensitive spectrum (power- or magnitude-spectrum).

Homonuclear 2D J-resolved spectroscopy is known to produce
additional transitions for strongly coupled[62,63] spin systems, which
increases the complexity of the interpretation. Fortunately, these
effects are generally predictable; additional transitions arising from
strong coupling will often lie midway between the coupled resonances and
usually (but not always) appear as a broad hump in the 0° projection of

the tilted data-set. As such, they actually have diagnostic utility in

the sense that they provide warning of the presence of strong coupling.

A note of caution should be sounded in the interpretation of such

strongly-coupled systems, since the observable resonances may not be

truly depicted in F_1. Of course, one can make use of a two-dimensional

spectral simulation program[63] as a check, but this is unlikely to be a

routine procedure. Strong coupling effects in the J-resolved spectra of

amino acids have been studied in detail,[64] as have other spin systems.[63]

The question of digital filtering (apodization) deserves special

mention. The use of a pseudo-echo filter[65] will produce absolute value

lines with absorptive Gaussian character; that is, narrower lines than

what one would obtain using an exponential envelope (giving Lorentzian

lines in the frequency domain). However, this is not ideal as it

attenuates signal-to-noise, causes severe intensity distortions and is

particularly destructive when a many-lined multiplet resonates close to

a strong signal. In a situation where signal-to-noise is at a premium,

the usual exponential filter may be used in t_2. If possible, it is

recommended to use a pseudo-echo filter in the t_2 dimension.

Line-narrowing in t_1 may then be effected by a Lorentzian-to-Guassian

transformation (a double-exponential function). If one is optimising

the experiment for resolution in F_1, a large number of experiments (n)

should be performed to yield an acquisition time in F_1 of several T_2's.

Tilted proton 2D J-resolved spectra should obviously be

symmetrical about $F_1 = 0$, and a symmetrization procedure has been

proposed[66] which improves spectral quality and signal-to-noise by
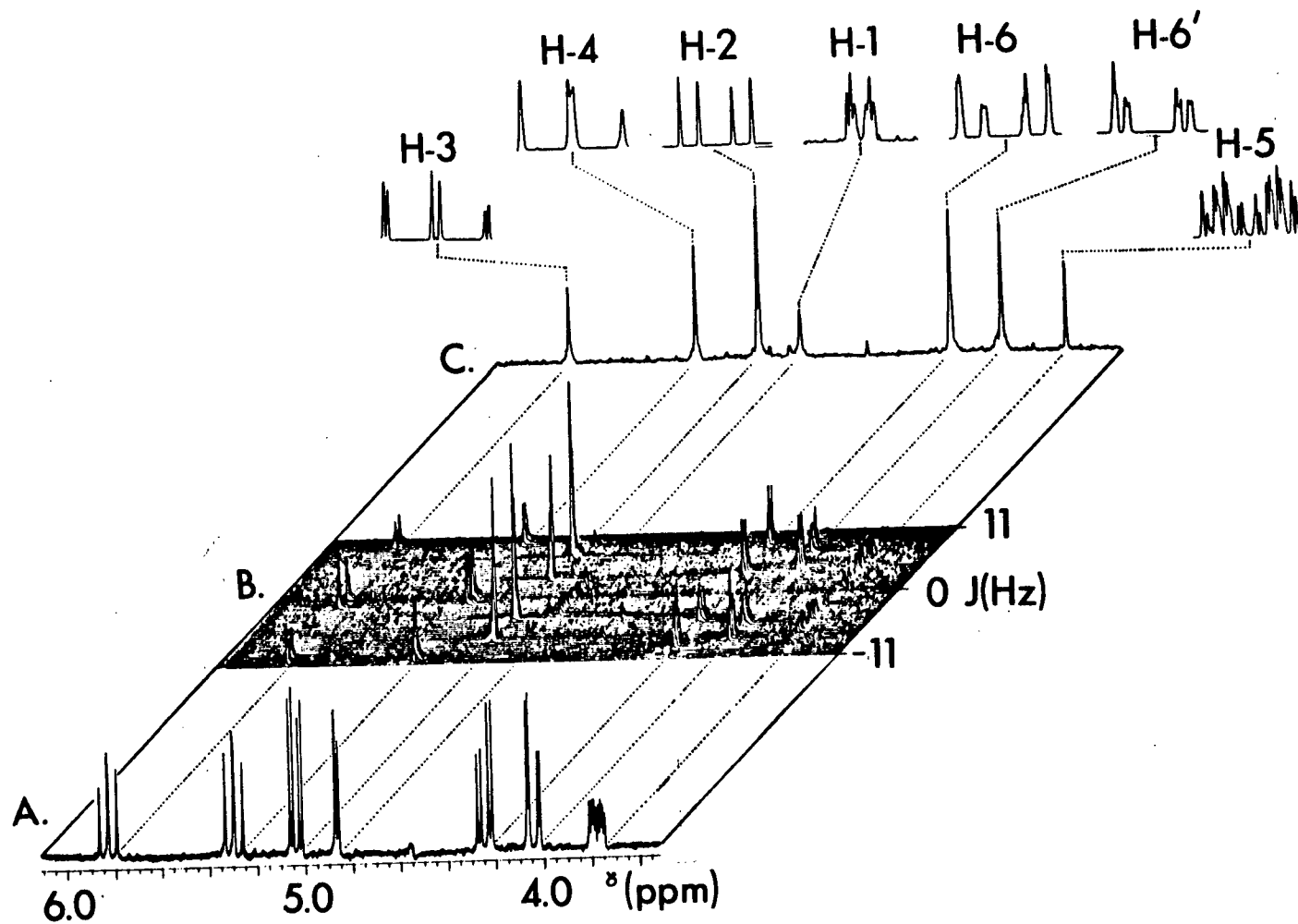
Figure II.2.23 270 MHz 2D J-resolved experiment on 1. See text for details.
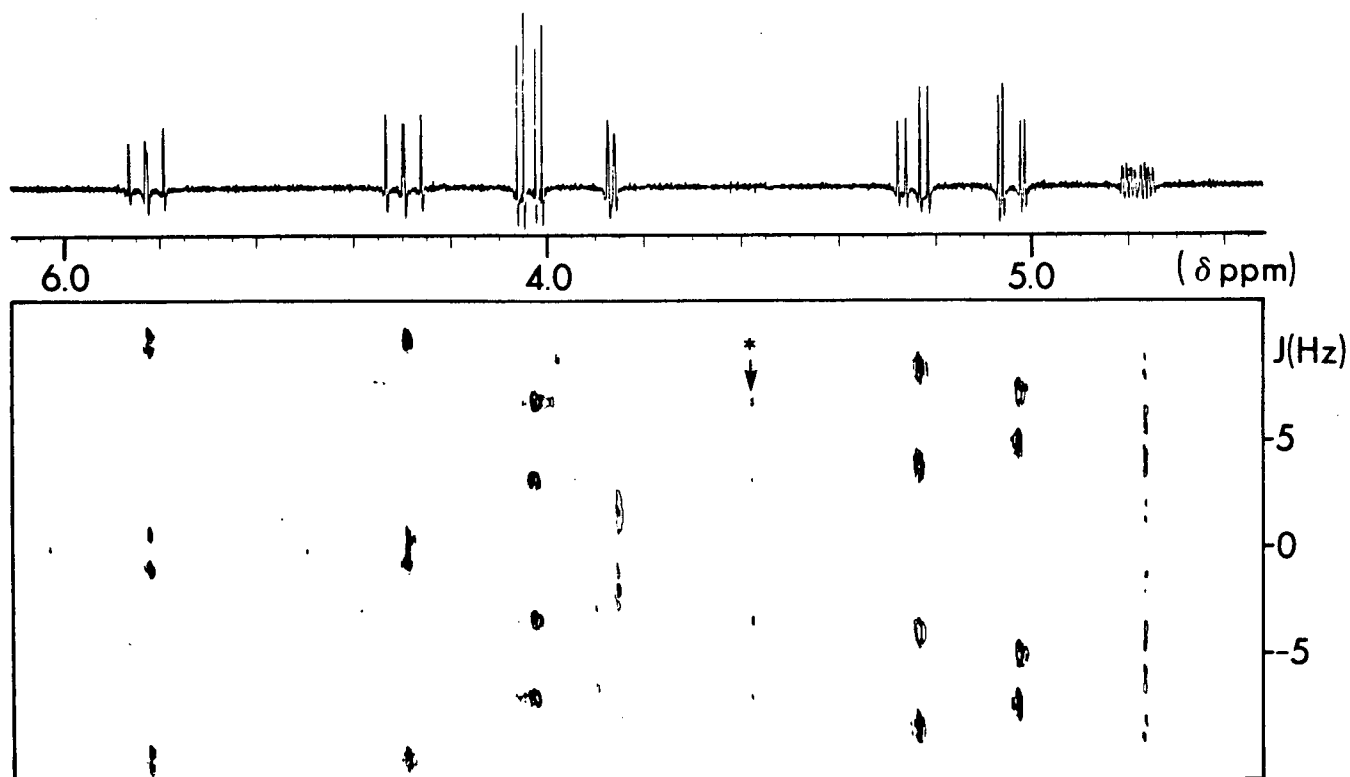
Fig. II.2.24 Data taken from Fig. II.2.23B, now plotted in the
contour-plot mode. Quadrature images for the intense
H-2 resonance are marked with an asterisk.

elminating much of the "tailing" in $\underline{F}$, and is especially useful in the case of strong singlet resonances.

Fig. II.2.23 contains phase-insensitive displays of the homonuclear 2D $\underline{J}$-resolved spectrum of $\underline{1}$. Fig. II.23A is the 1D spectrum, showing seven multiplets. Fig. II.2.23B is the stacked plot representation of the 2D $\underline{J}$-resolved experiment, performed with Exorcycle phase cycling and a single 180° pulse. Sinebell resolution enhancement was used in both dimensions. Fig. II.2.23C is the 0° projection of the tilted data matrix - the "proton-decoupled" proton spectrum. From this the chemical-shifts are measured and the seven corresponding partial $\underline{J}$-spectra are displayed. Their enhanced resolution is evident, especially for the H-1 and H-5 resonances which are long-range coupled to one another, and other protons.

Alternately, one may use a contour mode of display, as demonstrated in Fig. II.2.24. The resolution-enhanced ("sinebell") 1D spectrum is above the contour plot. Most of the splittings are clearly discernable in the contour-plot and $\underline{J}$ measurements may be made directly from it with adequate accuracy.

II.2.5.3 Jeener Experiment: J-Correlated 2D NMR

The "autocorrelation" 2D experiment was one of the first to be mathematically explained[67] and documented, yet did not gain wide acceptance until relatively recently when it was improved to allow quadrature detection in both dimensions.[68] Now it is perceived as a very useful experiment, which is quick and easy to perform, and whose
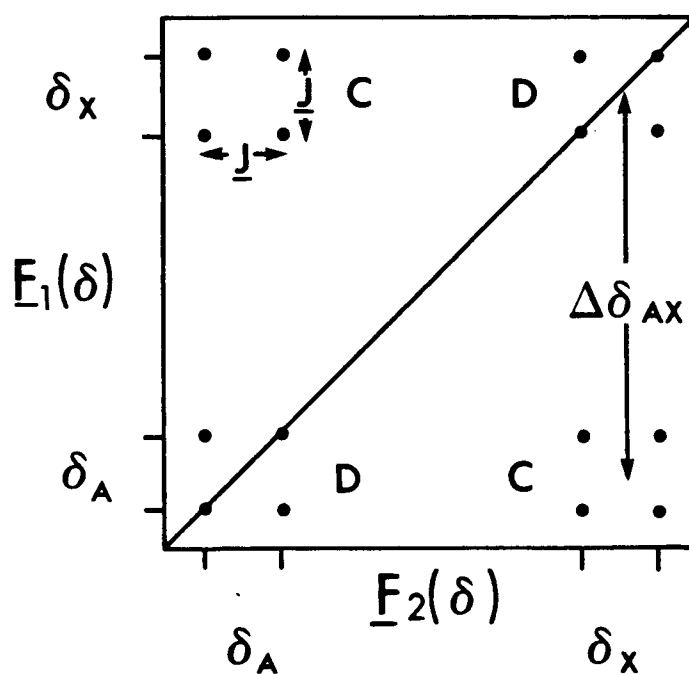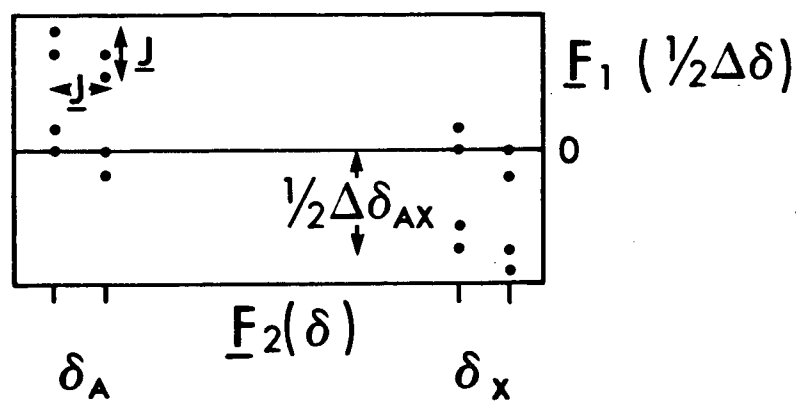
Fig. II.2.25 Stylized $\underline{S}(\underline{F}_1,\underline{F}_2)$ contour-plot output of an AX spin system
(A) with COSY and (B) with SECSY experiments.

informational content is high and predictably extractable.

Two major variants on the experiments exist, which will be discussed separately. The 2D correlation spectroscopy (COSY) experiment involves a $(90° - t_1 - 90° - t_2)$ pulse sequence and the idealized out-put (AX spin-system) is given in Fig. II.2.25A. The spin-echo correlation spectroscopy (SECSY) variant involves a $(90° - 0.5 t_1 - 90° - 0.5t_1 - t_2)$ pulse sequence,[69] and its stylized output is shown in Fig. II.2.25B. The COSY experiment displays both chemical shift and couplings along both frequency axes, and gives rise to two types of peaks: "diagonal" peaks (8) along the line $F_1 = F_2$ (labelled "D") and "correlation", or "cross" peaks (8) between pairs of spins which are scalar coupled (labelled "C"). The latter are symmetrically disposed with respect to the principal diagonal. The SECSY experiment displays chemical shift and scalar couplings along F_2, and $\Delta\delta/2$ along F_1. Thus, the informational content is the same as COSY in that diagnoal- and cross peaks are both present – but the display is slightly different.

For both experiments, optimum magnetization transfer in t_1 between coupled spins (AX) occurs at the maximum of $\sin(\pi J_{AX} t_1)$ $\exp(-t_1/T_2)$, while optimum detection of the transferred magnetization occurs at the maximum of the corresponding expression for t_2. The expression is plotted for a typical T_2 (1.5s) and J's of 0.5 and 4 Hz in Fig. II.2.26. This topic will be raised later in Section II.2.5.3.3.

A final general note concerns apodisation. With the Jeener experiment a pseudo-echo shaping function (e.g. "sinebell") is recommended for use in both dimensions. As usual, absolute value mode
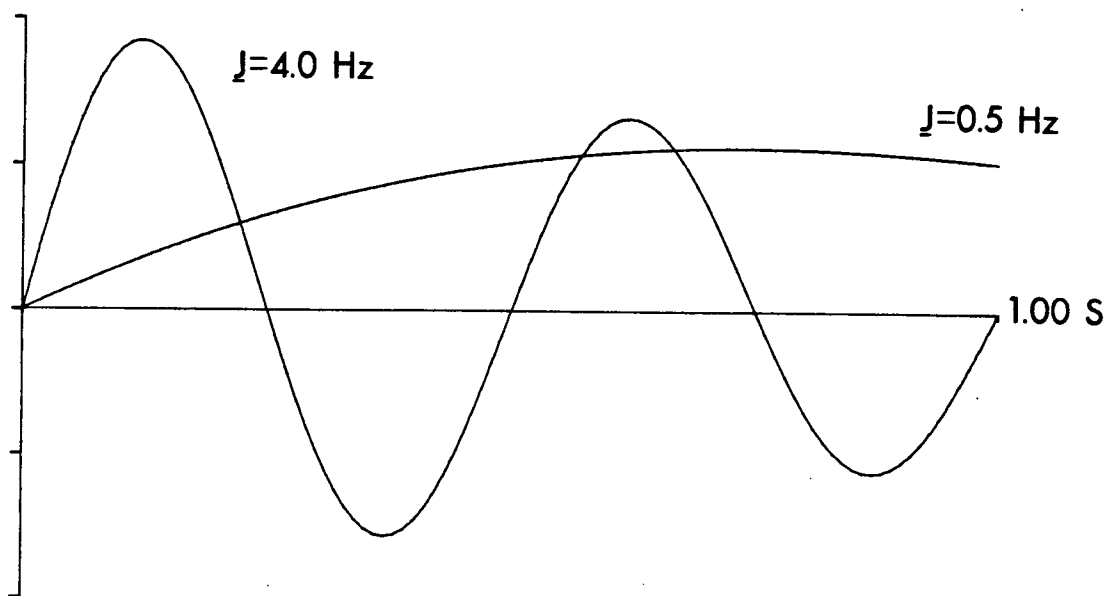
Fig. II.2.26 Plot of $\sin(\pi J_{AX} t_1) \exp(-t_1/T_2)$ vs. t_1 for $J = 4.0$ and 0.5 Hz.

display is chosen and the reader interested in phase-sensitive line-shapes is referred to the literature.[67,68]

II.2.5.3.1 COSY

The basic COSY experiment uses the pulse sequence given below, and the phase-cycling of II.2.31. The latter is required to differentiate between the so-called N-type (echo) and P-type (anti-echo) signals which must be differentiated when quadrature detection is used.

$$RD - 90°(x) - \underline{t}_1 - 90°(\Phi_1) - AQN\ (\underline{t}_2;\ \Phi_2\ or\ \Phi_3) \qquad [II.2.30]$$

Cycle	1	2	3	4	
Φ_1	x	y	-x	-y	
Φ_2 (N)	x	-x	x	-x	[II.2.31]
Φ_3 (P)	x	x	x	x	

The first _preparatory_ _pulse_ $(90°_x)$ is followed by the _evolution_ _period_ $(\underline{t}_1)$ and the second _mixing_ _pulse_ (90°), and detection $(\underline{t}_2)$. The preparatory pulse has constant phase and the phase of the mixing pulse is incremented in 90° steps (Φ_1). The receiver phase chosen, Φ_2 or Φ_3, selects the coherence transfer echo or anti-echo, respectively, and cancels the axial peaks at $\underline{F}_1$ = 0 (which have $\underline{T}_1$ information and are relatively uninteresting). This phase-cycling scheme may be expanded to incorporate CYCLOPS, which removes images resulting from quadrature detection. The basic four-cycles are repeated three times, incrementing

all phases by 90° to give a 16-cycle scheme.

A satisfactory explanation of the experiment is not possible without a density-matrix formalism, and even this becomes rather unwieldy when considering more than two or three spins. We limit discussion here to a highly stylized density-matrix formalism (see Fig. II.2.27) for an AX spin-system, with relaxation effects ignored. States A, B and C were described at the beginning of the chapter, in equations II.2.5 – II.2.9. A rotational matrix changes the initial Boltzmann state density matrix, σ_0 into σ_1 which has eight non-zero terms from single-quantum transitions. With time, the terms in the density matrix evolve, and after t_1 may be represented by σ_2. Application of a

$$90°_x \qquad\qquad 90°_x$$

$$\underline{\quad\quad} \text{A} \sqcap \text{B} \qquad \text{C} \sqcap \text{D}$$

Preparation   Evolution (t_1)   Detection (t_2)
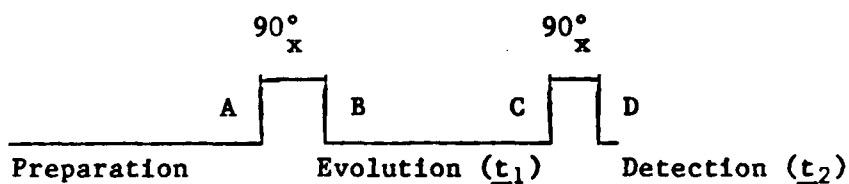
A. Boltzmann State

$$\sigma_0 = \begin{bmatrix} P^0 & 0 & 0 & 0 \\ 0 & P^0 & 0 & 0 \\ 0 & 0 & P^0 & 0 \\ 0 & 0 & 0 & P^0 \end{bmatrix}$$

B. After Preparatory Pulse

$$\sigma_1 = \begin{bmatrix} 0 & \blacksquare & \blacksquare & 0 \\ \blacksquare & 0 & 0 & \blacksquare \\ \blacksquare & 0 & 0 & \blacksquare \\ 0 & \blacksquare & \blacksquare & 0 \end{bmatrix}$$

C. After Evolution

$$\sigma_2 =$$

D. Mixing Pulse

$$
\sigma_3 =
\begin{bmatrix}
 & & () & & & & () & \\
 & & & & & & & \\
 & () & & & & & () & \\
 & & & () & () & & & \\
 & & & & & & & \\
 & () & & () & () & & () & \\
 & & & & & & & \\
 & () & & & & & () & \\
\end{bmatrix}
$$

E. Detection

$$\sigma_4 \; = \; \begin{bmatrix} & & & \\ () & & & () \\ & () & () & \\ & () & () & \\ () & & & () \\ & & & \end{bmatrix}$$
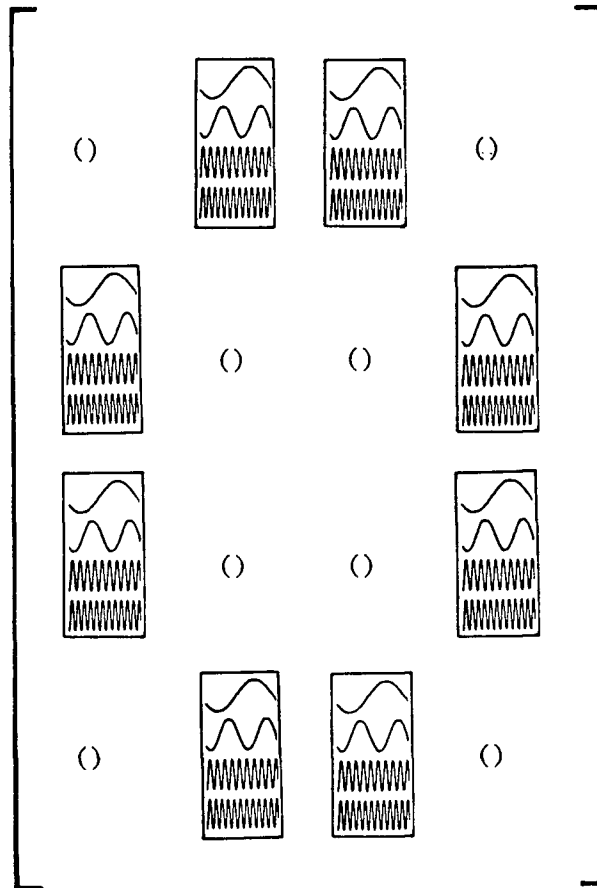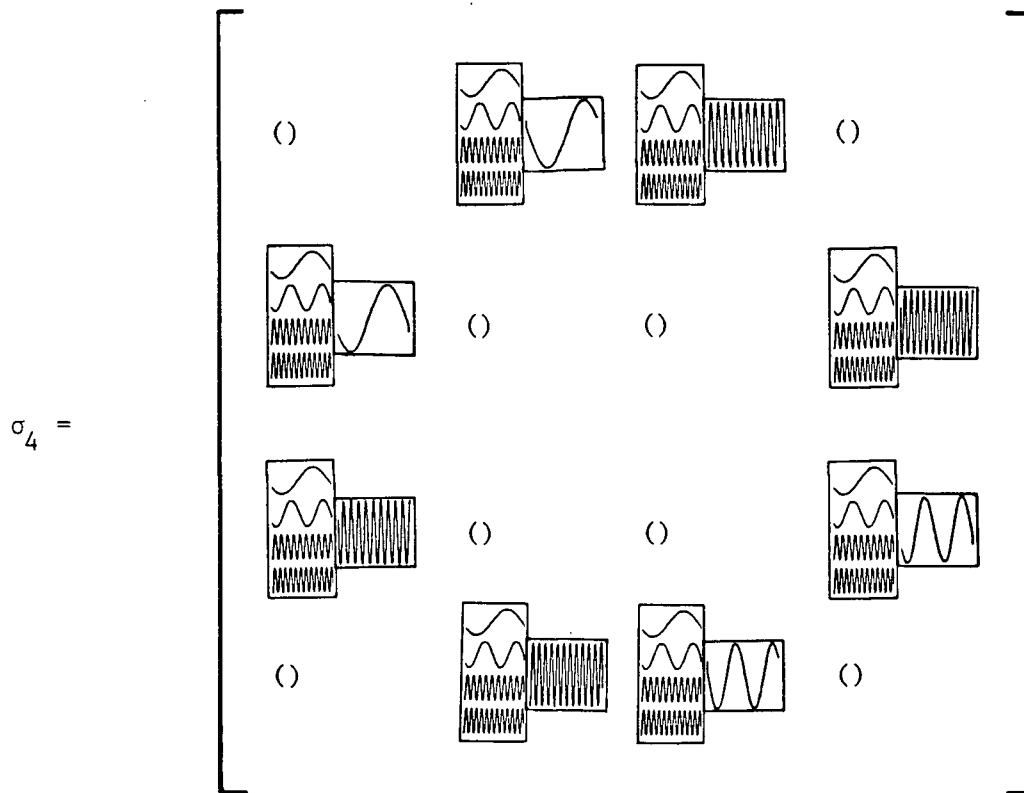
Fig. II.2.27 Schematized density matrix formalism of COSY experiment
for an AX spin-system

second rotational operator (i.e. a 90°_x pulse) on σ_2 has the effect of

mixing the elements in the two areas denoted by broken lines. Now each

element is a sum of four frequencies. The observable (single-quantum)

coherences are depicted whilst generated zero- and multiple- quantum

coherencies are ignored and indicated by parentheses. Each observable

resonance frequency will be detected during $\underline{t}_2$, modulated by events in

$\underline{t}_1$ which are due to scalar coupling.

The experiment is performed with incremental delays in $\underline{t}_1$ in the

usual way, and subjected to 2D complex FT. The diagonal and cross peaks

are symmetrical about the $\underline{F}_1 = \underline{F}_2$ axis. Noise in the $\underline{F}_1$ dimension,

especially from strong solvent peaks, is not symmetric and may be

removed by "symmetrization" procedures described by Wüthrich and

co-workers;[70,71] an increase in signal-to-noise automatically results.

For the symmetrization, each of the pairs of points in the 2D matrix

which should be identical are compared in turn; either the geometric

average of the two points is calculated and used in place of both

values, or the smaller of the two is taken as correct and is substituted

for the larger. A much "cleaner" and unambiguous display results.

Fig. II.2.28 is the 2D COSY spectrum of $\underset{\sim}{1}$. Digitization is

fairly good (2.7 Hz pt^{-1} in $\underline{F}_1$ and $\underline{F}_2$), and considerable detail is

obvious within each response. In general practice one may often have to

tolerate much coarser digitization ($\simeq$ 10 Hz pt^{-1}) but this does not

appear to significantly affect the information content;* detail within

---

*The antiphase nature of peaks in a correlation suggests that
course digitization will lead to their cancellation and poor intensity
seen; this conviction does not appear to born out in the experiments
performed in this thesis.
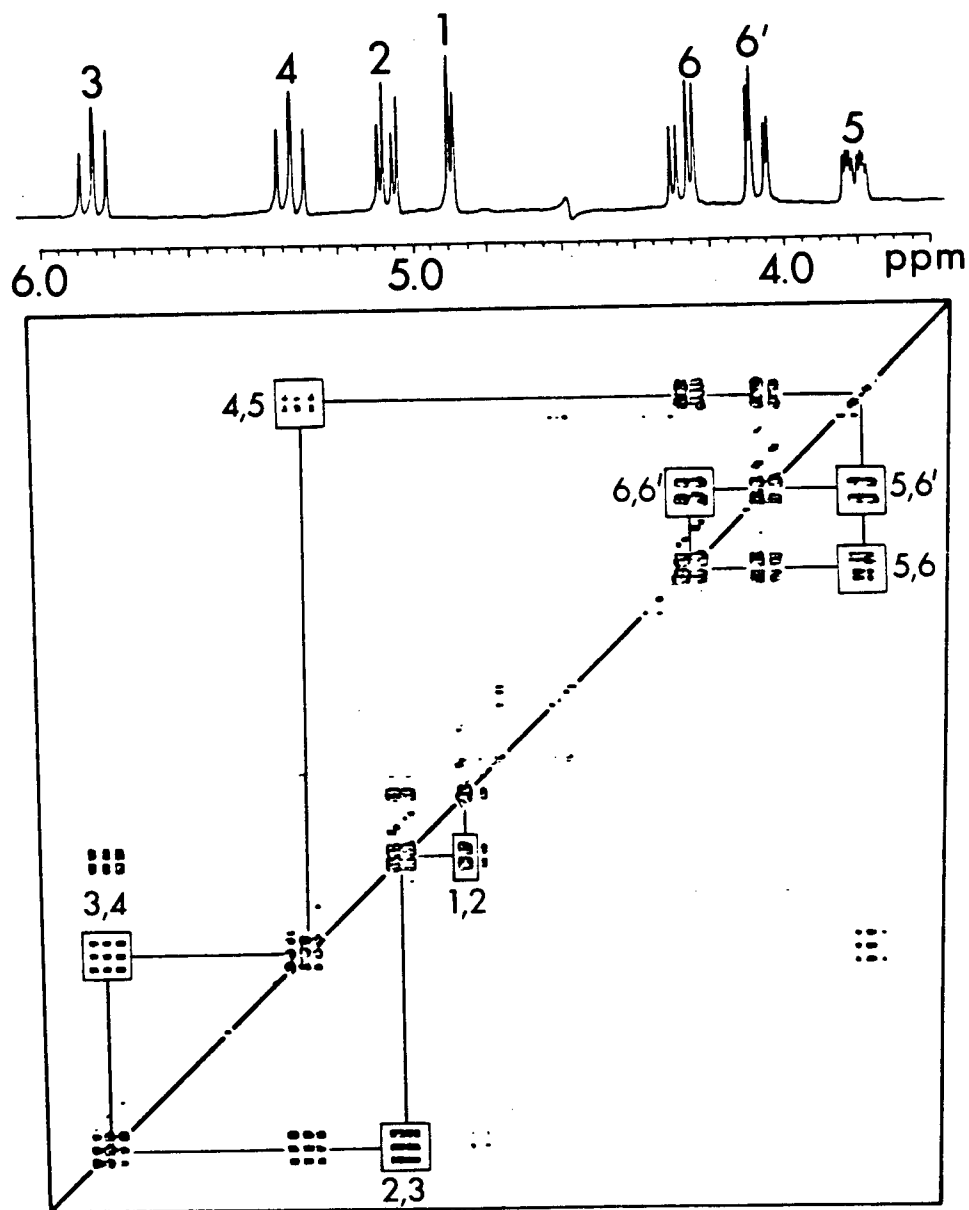
Fig. II.2.28 COSY spectrum of 1 (270 MHz).

cross-peaks may not be identifiable but "the cross peak" itself will still be clear. This point will be illustrated in later sections. The displayed data-set was collected using the four cycle sequence with anti-echo selection. The $\underline{S}(\underline{F}_2,\underline{F}_1)$ display was not symmetrized. Correlations are clear for all $^3\underline{J}$ pairs and the coupling pattern is easily mapped out.

A surprisingly short relaxation delay of $\underline{ca}$. 0.1 s is usually all that is necessary, making the data collection time quite short.

II.2.5.3.2 SECSY

The pulse sequence used for this experiment is given by Eq. II.2.32.

$$RD - 90°(x) - 0.5\underline{t}_1 - 90°(\Phi_1) - 0.5\underline{t}_1 - AQN(\underline{t}_2; \Phi_2) \qquad [II.2.32]$$

Phase cycling is as for the COSY experiment, with echo selection. The experiment has the potential advantage over COSY that the $\underline{F}_1$ dimension represents differences in chemical shift, rather than chemical shift itself. As a result, it may be possible to substantially reduce the sweep-width in $\underline{F}_1$ without aliasing, provided that the highest-field resonances are not coupled to those at lowest-field. This smaller sweep-width means that fewer data points ($\underline{n}$) in $\underline{F}_1$ are necessary, which translates into a smaller experimental time both in terms of data acquisition and computation. Although this is an attractive option, for many organic molecules it is non-viable since it is quite feasible that two resonances at different extremes of the spectrum may be coupled. Under these circumstances, the theoretical maximum sweep-width in $\underline{F}_1$ should be chosen, so as to avoid aliasing, and the potential advantages

of SECSY over COSY discussed earlier are inapplicable. This is not the

case with SECSY performed on proteins, however, and it is with this

class of compounds that the experiment shows most promise. This topic

is covered in detail in the review of Nagayama.[45]

Fig. II.2.29 shows the SECSY spectrum of 1. A slightly reduced

sweep width in F_1 was possible in this case, since the connectivities
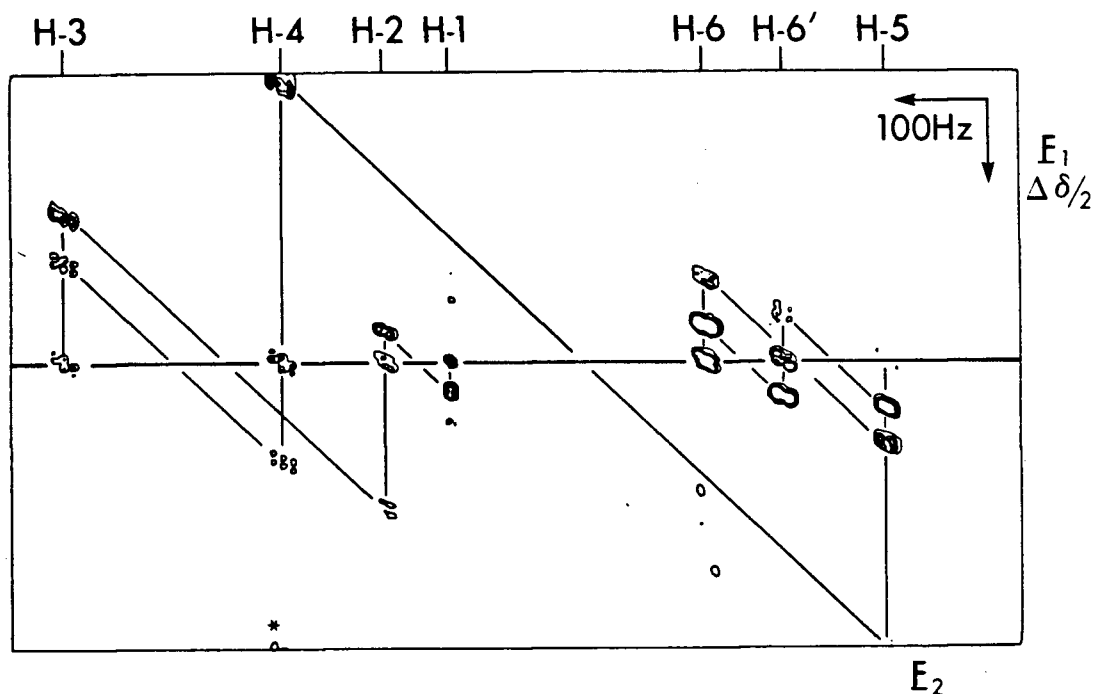
Fig. II.2.29   SECSY spectrum of 1 (400 MHz). The sweep-width in F_1
was slightly small, causing aliasing of part of the
$J(4,5)$ connectivity; the aliased portion is marked with
an asterisk.

were already known; if this were not the case, it would be inadvisable.

Data-retrieval for SECSY is marginally less convenient than with COSY.

The F_1 = 0 line corresponds to the diagonal in COSY. Lines joining

correlations lie at a constant angle with the F_1 = 0 line (135°, if

plotted to the same scale); this process is illustrated in Fig. II.2.29.

Two disadvantages of the experiment merit note. Firstly, since correlations in F_1 occur at <u>half</u> the difference in chemical shifts (<u>vs</u> the <u>full</u> chemical shift difference with COSY) the spectral resolution in F_1 is halved. As molecular complexity increases, the number of cross-peaks increase too and with SECSY the "frequency area" (F_1*F_2) is half that of COSY, increasing the likelihood of cross-peak overlap, and the resultant ambiguity.

The second point arises from considerations of transverse relaxation times, and signal-to-noise. When performing any echo experiment on a large molecule with broader lines (shorter T_2's), significant intensity loss can occur during the refocussing period and the detected signal may be severely attenuated. This is less of a limitation with SECSY than with homonuclear 2D J-correlated spectroscopy, as the following sample figures illustrate. Assume a half-height line-width ($\Delta v_{0.5}$) of 5 Hz with negligible contribution from magnetic inhomogeneity; from $T_2 = 1/\pi\Delta v_{0.5}$ we get $T_2 \approx 64$ ms. The amplitude of a signal will be attenuated by 75% after $T_2*\ell n\ 4 = 88$ ms. Now, assuming a sweep-width in F_1 of $\pm$ 1000 Hz (10 ppm for a 4.7 Tesla magnet), the incremental delay required will be 0.25 ms and the evolution period will reach 88 ms after about 350 experiments. With a 2D J-resolved experiment, the sweep-width in F_1 might be $\pm$ 20 Hz, giving an incremental delay of 12.8 ms. One T_2 period will have passed after 5 experiments. The signal will be 75% attenuated in intensity after < 7 increments which is a small number compared with the number (32) required to give a digitization of 1.25 Hz per point. Of course, this disadvantage would be offset by the fact that resonances with broad

line-widths do not require very fine digitization, and 1.25 Hz per point could be more than adequate. These arguments hold in practice, as we shall see in later chapters. This question of sensitivity losses in the spin-echo experiment is addressed briefly by Morris in his discussion on SECSY.[72]

SECSY appears to be a viable alternative to COSY when cross-peak overlap and broad line-widths are not evident. Whilst it is true that, in principle, SECSY should be faster to perform than COSY, this may not always be the case since signal degradation during the second 0.5 t_1 period may demand more scans to be collected than would be the case with COSY.

II.2.5.3.3 Delayed COSY - Detection of Long-Range Couplings

As mentioned in the introduction to this section, the observed J's in a COSY experiment are a function of t_1 and t_2. If one is interested in detecting small J's (< 1 Hz), such as those which arise from long-range coupling, the data for a COSY experiment should be sampled around t_2 = 0.5 - 1.0s after the mixing pulse. Using the pulse scheme in Section II.2.5.3.1, to have an acquisition time ≈ 1s in both dimensions would require the acquisition and storage of prohibitive amounts of data and one resorts to a variant on the COSY experiment, where a fixed delay, Δ, is inserted after each pulse.[68]

$$\text{RD} - 90°_x - \Delta - t_1 - 90°(\Phi_1) - \Delta - \text{AQN}(t_2; \Phi_2 \text{ or } \Phi_3) \qquad [\text{II.2.33}]$$

Practically, Δ is set to approximately 0.3 s, which offers the best compromise between observation of correlations between protons coupled by small J's, and loss in signal amplitude during Δ.
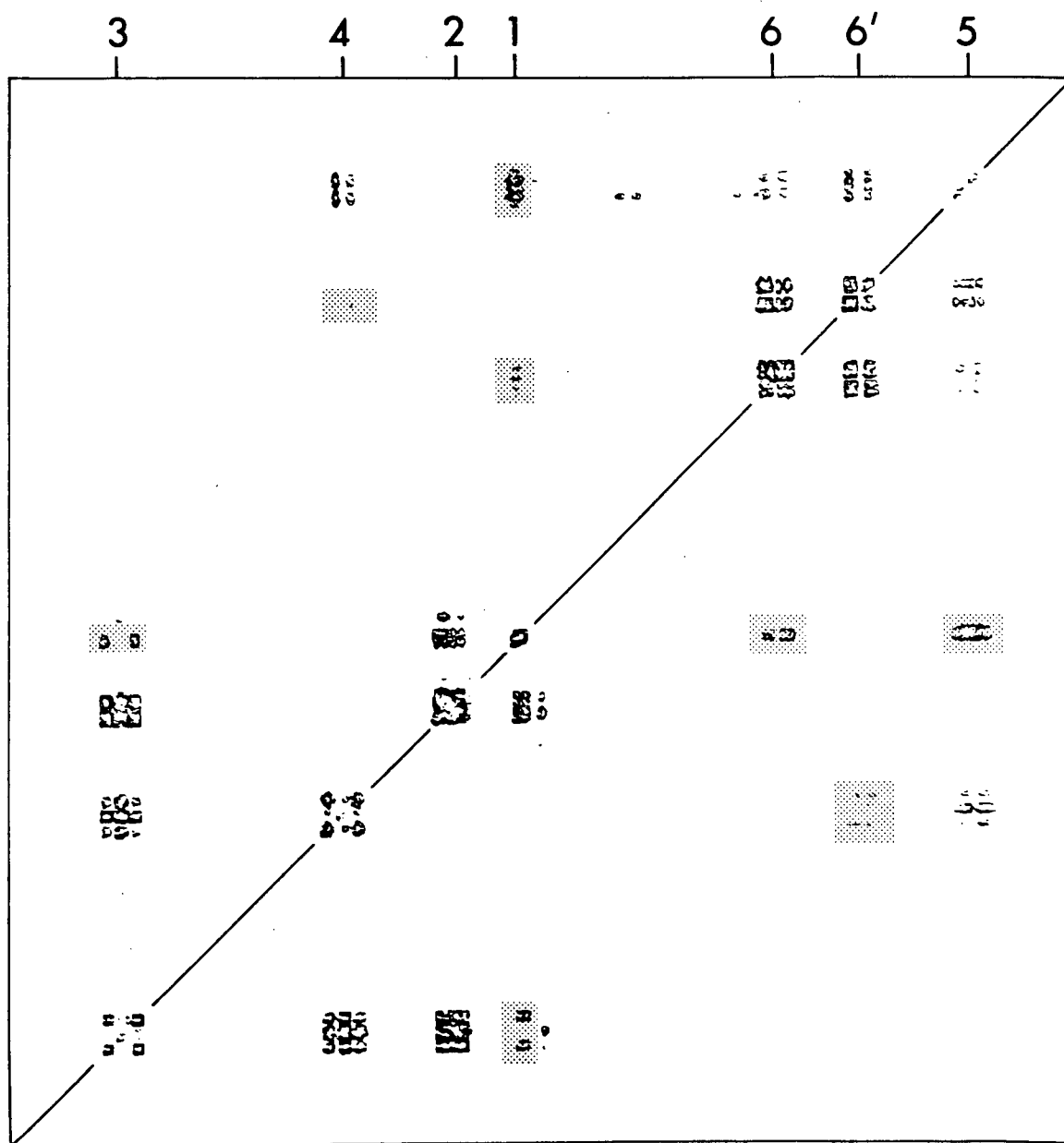
Fig. II.2.30 Delayed COSY experiment on 1 (270 MHz). Δ = 0.4 s.
Responses from long-range couplings are shaded.

Fig. II.2.30 shows this version of the COSY experiment, again using $\underset{\sim}{1}$ as the exemplar. The delay, Δ, was 0.4 s. Responses corresponding to all $^3\underline{J}$ couplings are visible, in addition to those from a wealth of long-range couplings (which are shaded in the diagram). H-1 appears to be the most richly coupled proton, showing long-range responses to H-3, H-5 and H-6. The long-range coupling, $\underline{J}$(H-1, H-6), is quite interesting and presumably indicates a reasonably "rigid orientation" of the acyclic C-6 moiety. H-2 is conservative in its coupling - only to H-1 and H-3. We draw the reader's attention to the 2D $\underline{J}$-resolved experiment, Fig. II.2.24, where in the 0° projection (a sky-line silhouette[73]) it is clear that H-2 is the most intense signal, and H-1 the weakest. We attribute this to the fact that H-2 has only four, well digitized lines, whilst H-1 must have at least sixteen, poorly digitized.

II.2.5.3.4 "Decoupled" COSY

An interesting variant on the basic COSY experiment has been suggested[48] which has the net result that all couplings in $\underline{F}_1$ are collapsed, and the autocorrelation map is considerably simplified. Its potential merits are obvious.

The experimental scheme is given in Fig. II.2.31. The 90° (preparatory) and 45° (mixing) pulses represent a variant on the 2-pulse COSY experiment and are phase-cycled in exactly the same way. Now, however, the time between these pulses is held constant $(\underline{t}_d)$ and a reduced mixing pulse of 45° is used. Increments of $0.5\underline{t}_1$ separate the preparatory pulse from the refocussing 180° pulse.* The period between

---

*Again, a composite pulse[38] is used: $180°_{\pm y} \equiv 90°_{\pm y} \; 180°_{\mp x} \; 90°_{\pm y}$
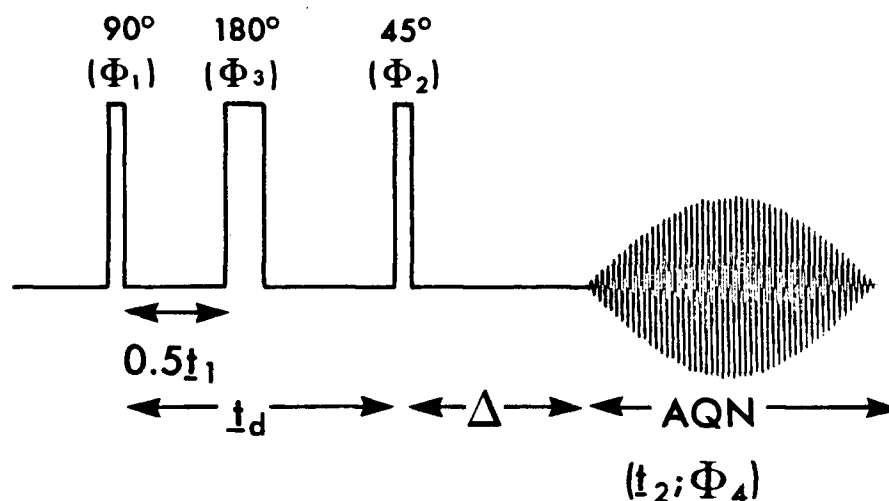
Fig. II.2.31   Pulse scheme for the COSY experiment with homodecoupling in $\underline{F}_1$.

Cycle	1	2	3	4	5	6	7	8
Φ_1	x	x	x	x	x	x	x	x
Φ_2	x	y	-x	-y	x	y	-x	-y
Φ_3^*	y	y	y	y	-y	-y	-y	-y
Φ_4	x	-x	x	-x	x	-x	-x	-x

[II.2.34]

the refocusing and mixing pulses, $\underline{t}_d - 0.5\underline{t}_1$ has to be <u>decremented</u>. At this time a decremental $\underline{t}_1$ is not available in an instrument manufacturer's standard soft-ware, and must be programmed.[74]   If

long-range couplings are of interest, a delay, Δ, is inserted prior to acquisition. The phase-cycling is according to Eq. II.2.34.

Usually the last value of $0.5 t_1$ has the composite 180° pulse just before the 45° pulse; that is, the value of t_d is determined by the sweep-width and digitization in F_1. Now, the magnitude of t_d will favour cross-peaks arising from a certain J.[75] With $t_d = 1$ s, $J = 0.25$ Hz is favoured, and with $t_d = 200$ ms, $J = 1.25$ Hz is favoured. Δ is non-zero only when long-range couplings are of interest.

Fig. II.2.32A shows a contour plot of the decoupled COSY spectrum of $\underset{\sim}{1}$. Sinebell resolution enhancement was utilized in both dimensions. A sweep-width in F_1 of $\pm$ 350 Hz, and the 256 x 512 complex point data matrix resulted in $t_d = 182$ ms. Decoupling is seen to be good; the only visible imperfections in this plot is a set of spurious responses at the mid-point between the geminal protons in F_2, which arises through strong coupling. Other smaller imperfections are not visible in the contour plot, but are seen in the F_1 projection – they are signals aliased in F_2 about $F_2 = 0$ and are called "quadrature images". These are presumably due to imperfect phase settings for the pulses and residual transverse magnetization, and could possibly be eliminated by extending the phase cycling to include CYCLOPS. Once again the $J(4,5)$ correlation is weak in this experiment, as it was in all other previous Jeener experiments.

_____

*Again, a composite pulse[38] is used: $180°_{\pm y} \equiv 90°_{\pm y} \ 180°_{\mp x} \ 90°_{\pm y}$
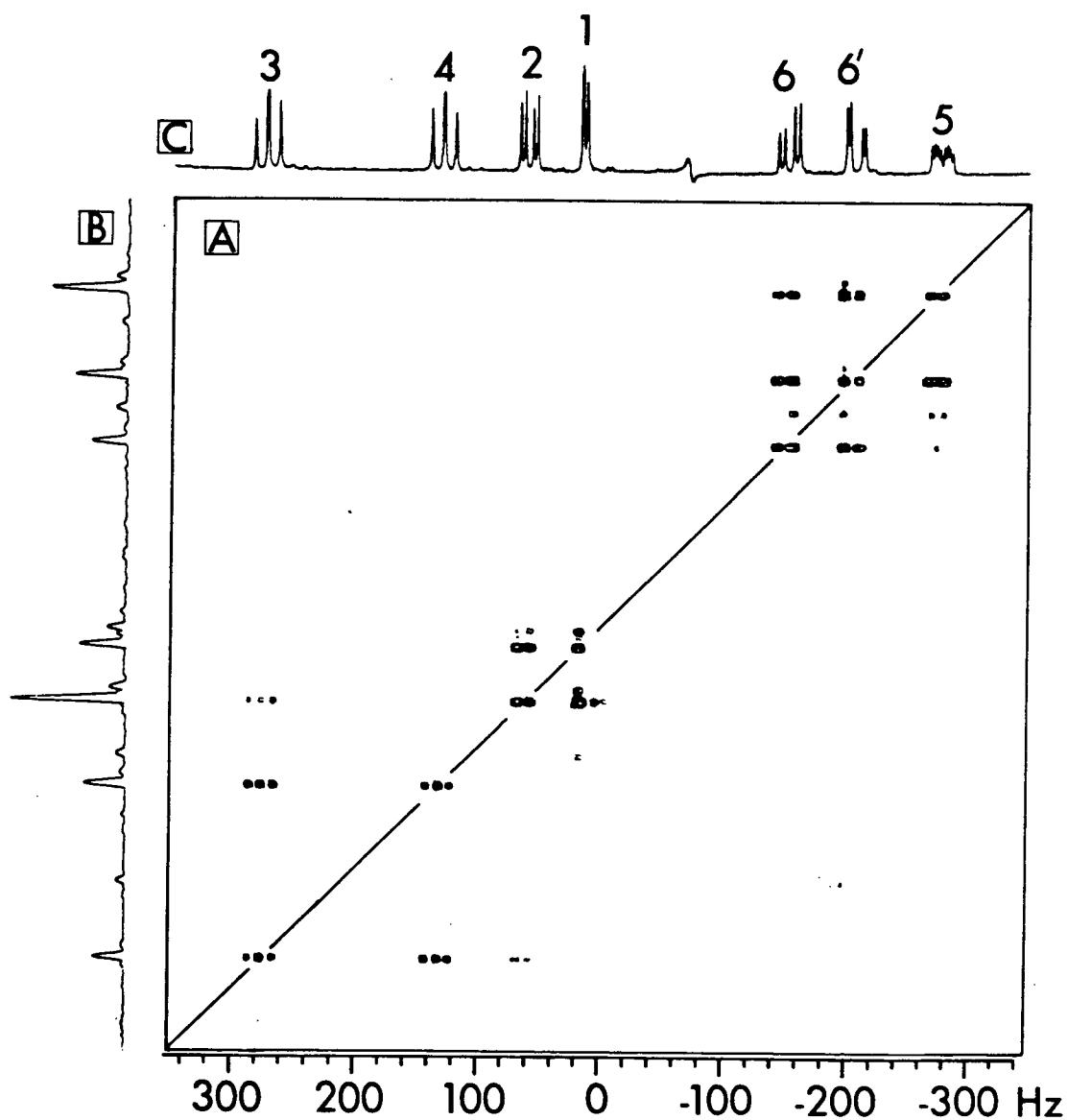
Fig. II.2.32 Decoupled COSY experiment with $\underset{\sim}{1}$ at 270 MHz. $\underline{t}_d$ = 182
ms and Δ = 0. (A), contour-plot of 2D spectrum. (B), $\underline{F}_1$
projection.(C), control spectrum.

The experiment clearly has elements of COSY and homonuclear 2D $\underline{J}$ correlated spectra, and if the digitization in $\underline{F}_2$ were fine enough, this single experiment could replace both these experiments, with the added advantage of the simplification of the COSY content. Of course, caution would have to be exercised with the detailed interpretation of line-shapes in $\underline{F}_2$.

II.2.5.4 Heteronuclear Chemical Shift Correlation

This very powerful 2D experiment correlates the chemical shifts of heteronuclei. Usually $\underline{F}_1$ is chosen as the chemical shift axis for protons, and $\underline{F}_2$ as ^{13}C. Although its uses with other heteronuclei such as ^{11}B, ^{15}N and ^{31}P have been reported,[45] we shall restrict our discussion to the ^{13}C - ^{1}H chemical shift correlation map (CSCM) experiment[76,77] which correlates carbon resonances with the directly bound proton(s), as this is the most common and diagnostically useful one. The pulse-sequence is best designed such that ^{13}C resonances ($\underline{F}_2$) are broad-band decoupled, whilst ^{1}H resonances ($\underline{F}_1$) show homonuclear coupling. These couplings turn out to be useful in interpretation of data, even though (a) a detailed examination of the proton multiplicities can lead to errors arising from infidelities inherent to the experiment, and (b) the digitization in $\underline{F}_1$ is seldom good enough to permit the observation of fine detail in homonuclear proton couplings.

The experiment involves a magnetization-transfer step (see DEPT, II.2.2.2) and is therefore inherently quite sensitive. Typically, 512 experiments are performed, collecting 2K complex data points in $\underline{t}_2$. The minimum sweep-width in $\underline{F}_2$ is chosen and one can alias quaternary signals since they will give no correlations. (Similarly, deuterated solvent peaks will be absent).

The pulse-sequence has been refined to one having quadrature detection in both dimensions and the characteristics listed above. A minimum of four phase-cycles are mandatory, but this is often extended to eight (Eq. II.2.35).

^{1}H: RD - 90°(Φ_1) - 0.5$\underline{t}_1$ -   - 0.5$\underline{t}_1$ - Δ_1 - 90°(Φ_2) - Δ_2 - BB

^{13}C: 180°(Φ_3)   90°(Φ_4)   - AQN ($\underline{t}_2$;Φ_5)

$$[II.2.34]$$

Cycle	1	2	3	4	5	6	7	8
Φ_1	x	x	x	x	-x	-x	-x	-x
Φ_2	x	y	-x	-y	-x	-y	x	y
Φ_3	x	x	x	x	-x	-x	-x	-x
Φ_4	x	x	x	x	x	x	x	x
Φ_5	x	y	-x	-y	x	y	-x	-y

$$[II.2.35]$$

The experiment may be understood by considering the populations for an isolated C-H fragment, as given in Fig. II.2.33A; the relative spin populations reflect the four-fold sensitivity difference between ^{1}H and ^{13}C, _viz._ $\gamma_H = 4\gamma_C$. Now, we may ignore the 180°, ^{13}C pulse at this stage, and concentrate on the proton pulses: 90° - t_1 - 90°. A population inversion across one of the proton transitions results in the situation in Fig. II.2.33B.

The affect of two 90° (^{1}H) pulses, separated by $\underline{t}_1$ to produce "population inversion" is shown in Fig. II.2.34A and B. The initial 90°$_x$ ^{1}H pulse creates transverse magnetization which precesses in the x'-y' plane according to $\underline{J}_{C-H}$. Depending on its position after $\underline{t}_1$, the second 90°$_x$ pulse may, in the limits, cause population inversion,

- 186 -

A.   B.

Fig. II.2.33   Energy levels of a CH fragment at equilibrium (A) and
                after a proton population inversion (B).
                (From a review by R. Freeman, Ref. 45).
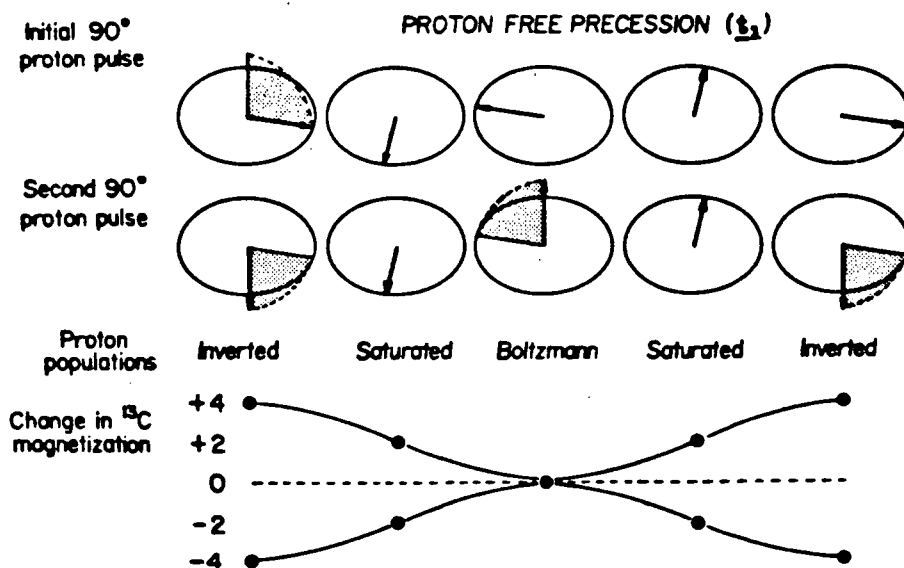
Fig. II.2.34   The affect of a proton 90° - t_1 - 90° pulse sequence on
                proton vectors, and their interpretation in terms of
                proton spin state populations is given in (A) and (B).
                (C) maps the corresponding change in population
                differences across the ^{13}C transitions.
                (Adapted from Freeman and Morris.[45])

saturation, or regeneration of Boltzmann state populations. The proton populations follow a cosine modulation after the second 90° pulse. Since the ^{13}C transitions share an energy level in common with this modulated proton transition, the population differences between ^{13}C levels are necessarily affected and this can be monitored with a 90° ^{13}C "read" pulse.

Four antiphase signals would be detected from such a pulse-sequence $(90°_H - \underline{t}_1 - 90°_H \; 90°_C - AQN)$, showing heteronuclear coupling in both frequency dimensions. It would be desirable to remove the heteronuclear coupling; this is accomplished in $\underline{F}_2$ by employing broad-band ^1H decoupling during ^{13}C acquisition, and in $\underline{F}_1$ by inserting a ^{13}C, 180° pulse halfway through the $\underline{t}_1$ period. This experiment might be expected to result in one transition for a C-H fragment,* but would actually result in no signal at all, due to the exact cancellation of the four antiphase signals. Two delays, Δ_1 and Δ_2 are inserted to allow 180° relative phase rotation between these components (which differ in frequency by $\underline{J}_{C-H}$) and this provides a practical solution to the problem described above. This is the experiment described in Eq. II.2.34. For Δ_1, a value of $(2 * \; ^1\underline{J}_{AVE})^{-1}$ effects the required phase rotation of the proton vectors. Considering the ^{13}C vectors, the situation is more complex and calls for a compromise, since the time for the phase rotation will depend on the number of attached protons. Bax has shown[46] that a good compromise is to select $\Delta_2 = 0.3/^1\underline{J}_{AVE}$.

Further, two refinements exist. To improve the ^{13}C decoupling, a composite 180° pulse[38] $(180°_{\pm x} = 90°_{\pm x} \; 180°_{\pm y} \; 90°_{\pm x})$ is recommended. It

---

*This would be located at δ_C (in $\underline{F}_2$) and δ_H (in $\underline{F}_1$).

has also been demonstrated that broad-band ^{13}C decoupling during t_1 may be effected with an MLEV-16-type procedure[78] giving good results without the problem of excessive sample heating.[79]

Let us now pause to consider the merits and shortcomings of the experiment. Its strengths lie in the relative ease with which it is performed with all variables being determinable before the 2D experiment is performed. The sensitivity is good, since one benefits from the nOe as well as the polarization transfer. Further, the repetition rate is based on _proton_ relaxation parameters as opposed to the (generally longer) ^{13}C values. A relaxation delay of _ca._ 1.3 $\underline{T}_1$ is optimal. One may find spurious peaks at δ_C when the protons attached to the carbon form a tightly-coupled AB pair. Secondly, since the experiment relies on polarization transfer, this must be efficient. Hence the condition $(1/2\underline{J}) < \underline{T}_2$ is necessary, which may restrict work with very large, conformationally rigid macromolecules. Still, one major factor makes the experiment very attractive; one uses the very high dispersion of the ^{13}C spectrum as a lever for the ^{1}H spectrum.

Fig. II.2.35 shows the result of an experiment performed on a 0.5 $\underline{M}$ solution of $\underset{\sim}{2}$ in C_6D_6, displayed in the contour plot mode. Details of the proton spectrum are not clear even when these are taken out as slices (not shown). In that the assignment of the proton spectrum is known, the ^{13}C assignment immediately follows (going from low- to high-field: C-1, C-2, C-3, C-4, C-5, C-6).

We conclude with a few remarks addressed to some practical considerations and suggest a general protocol. The experiment may be performed with a ^{13}C probe, using the ^{1}H decoupler coil to pulse the proton spectrum.

1. Tune the ^{13}C and ^{1}H coils and shim the magnet carefully, since proton spinning side-bands can be bothersome.

2. Record the ^{13}C spectrum (quadrature detection; broad-band ^{1}H decoupling, with the minimum sweep-width necessary - quaternary peaks may be folded over). Select a block size which gives an acquisition time (AT) $> 1\underline{T}_2$ and adequate digitization for closely spaced ^{13}C resonances. Save a sample spectrum on disc, with very good digitization and signal-to-noise.
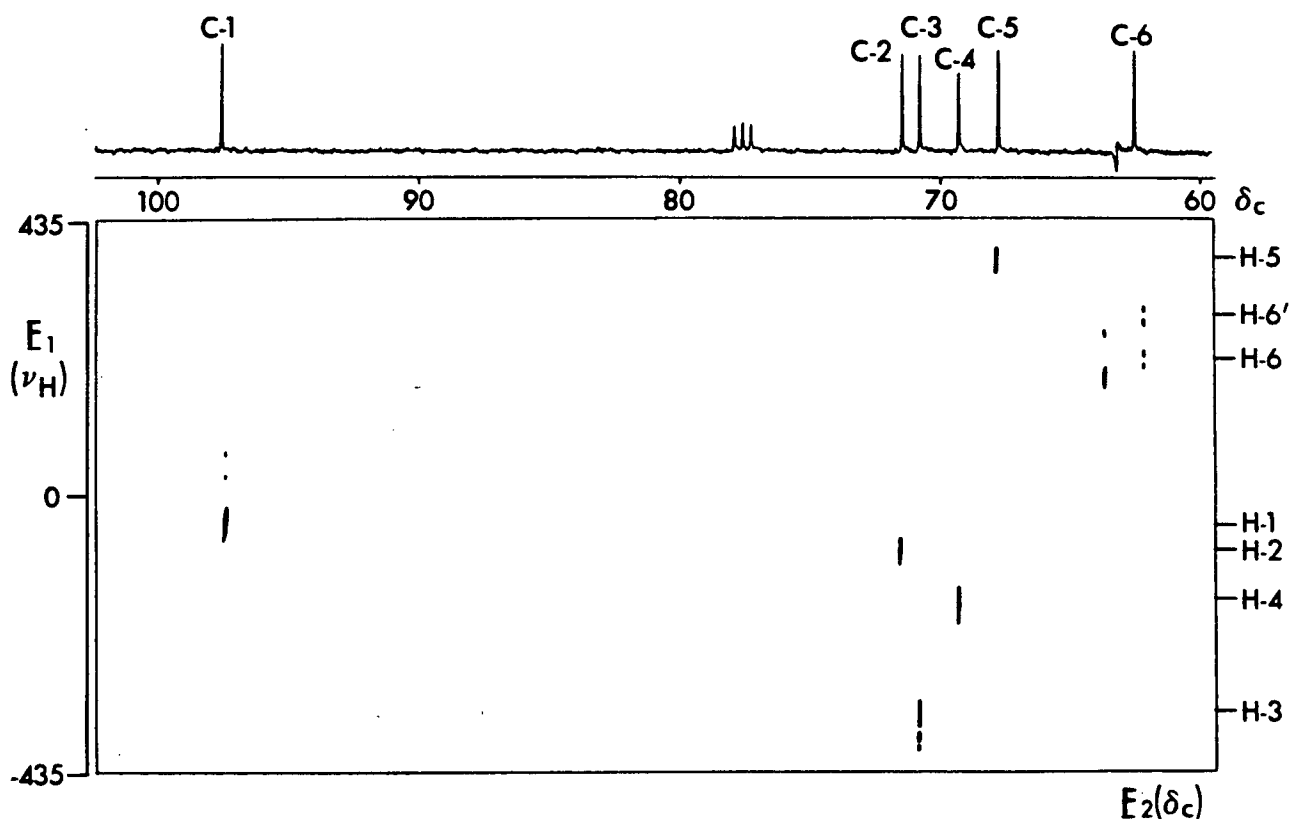
Fig. II.2.35 CSCM on a 0.5 $\underline{M}$ solution of $\underset{\sim}{2}$, at 100.3 MHz for ^{13}C.

3. Determine ^{13}C pulse-lengths.* If these measurements are made on the sample itself, it may be best to observe the fastest relaxing carbon (e.g. $-\underline{C}H_3$).

4. Set up the spectrometer to observe protons, pulsing and observing with the decoupler coil. Set the decoupler offset to the middle of the ^1H spectrum and choose a minimum sweep-width without introducing aliasing. Save a sample spectrum on disc. Note the dwell-time (DW) for the particular sweep-width.

5. Measure the ^1H $\underline{t}_{90}$ (90° pulse-length), observing ^1H.

6. Change back to ^{13}C observe.

7. Determine an accurate ^1H 90° pulse length:

   a. By residual coupling in a single frequency off-resonance decoupled (SFORD) experiment.

   $$(\gamma \underline{B}_2)^2 = \Delta\nu(\frac{\underline{J}_0^2}{\underline{J}_{RES}^2} - 1) \text{ Hz} \qquad [II.2.36]$$

   $$\underline{t}_{90} = 1/4(\gamma\underline{B}_2) \quad s \qquad [II.2.37]$$

   $\Delta\nu$ = distance (Hz) the decoupler is placed from the proton resonance frequency.

   $\underline{J}_0$ = $\underline{J}$(C-H) for the attached carbon in the absence of continuous-wave decoupling.

   $\underline{J}_{RES}$ = residual $\underline{J}$(C-H) for the attached carbon with continuous-wave decoupling during acqusition.

---

*For determination of all pulse lengths, one may choose to use a simpler sample at higher concentration, such as methanol.

With this experiment it is necessary to know at least

one $^{13}C - ^{1}H$ assignment and determine the ^{1}H frequencies

before returning to ^{13}C observe. Two experiments are

performed, one with the decoupler off during acqusition

(to give J_0) and one with it on at its highest power

level during acqusition (to give J_{RES}). Knowing Δv,

t_{90} is now easily calculated. (Eqns. II.2.36,37).

b. By a simple coherence-transfer experiment.

^{13}C: RD - 90° - 1/2J -   - AQN

^{1}H: θ - BB   [II.2.38]

This simple pulse scheme is performed after any J(C-H)

has been measured. When θ = 90°, no signal is seen for

this ^{13}C resonance.

8. The CSCM experiment is now set up.

9. Δ_1, Δ_2 are selected for a typical J_{CH}, e.g. 135 Hz.*

10. The incremental delay in t_1 is set to half the proton dwell

time (see 4) or calculated from II.2.24. The number of

experiments to be performed (typically, 512) should give an

acquisition time in t_1 of ca. 100 ms.

11. The number of scans at each t_1 value should be set to the

value which gives "reasonable" signal-to-noise in the 1D ^{13}C

experiment.

12. A relaxation delay of ca. 1.3 * T_1 (^{1}H) is chosen.

_____

*Δ_1 = 3.7 ms and Δ_2 = 2.2 ms.

13. Data are now collected (minimum time for experiment = <u>ca</u>. 1 hour).

14. The data are processed with as much resolution-enhancement in both dimensions as the signal-to-noise permits. A double-exponential or shifted sinebell multiplier should be used in the data manipulation.

II.2.5.5 Relayed Coherence Transfer

This 2D experiment was suggested by Bolton[80] as an assignment aid, having elements of CSCM and homonuclear correlation experiment. A CSCM-like display having, in addition, correlations when the attached protons are scalar coupled. Consider an AMX fragment as in Fig. II.2.36A. The first stage of the experiment involves transfer of coherence between H_A and H_M. This may then be relayed to the heteronucleus, C_X in a CSCM experiment.
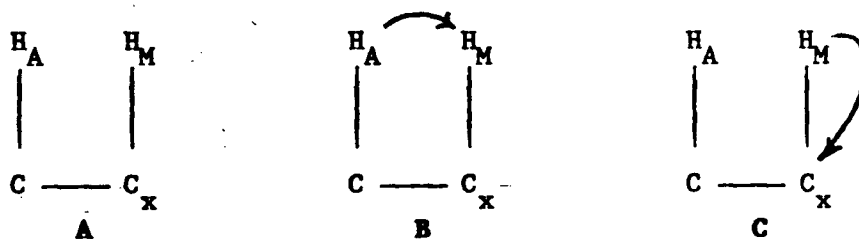
Fig. II.2.36   Steps of magnetization transfer in the relayed coherence transfer experiment.

The pulse sequence and phase-cycling are as <u>per</u> II.2.39 and II.2.40, respectively:

^{1}H: RD-90$^\circ_x$-0.5$\underline{t}_1$-   -0.5$\underline{t}_1$-90°(Φ_1)-0.5t_m-180°-0.5$\underline{t}_m$-Δ_1-90°(Φ_2)-Δ_2-BB

^{13}C: 180° 90°(Φ_2)-   AQN
                                                                                    ($\underline{t}_2$)

[II.2.39]

Cycle	1	2	3	4	5	6	7	8	9	10	11	12	13	14	15	16
Φ_1	x	-x	y	-y	x	-x	y	-y	x	-x	y	-y	x	-x	y	-y
Φ_2	x	x	x	x	-x	-x	-x	-x	y	y	y	y	-y	-y	-y	-y

[II.2.40]

The free induction decays are co-added and ($\underline{t}_m$ + Δ_1) = ca. 33 ms, favouring $^3J_{AM}$ = 7.7 Hz (1/4J_{AM}).

The experiment was first performed on a concentrated sample of n-propanol, displayed as a stacked-plot in Fig. II.2.37. Peaks arising from heteronuclear correlations are labelled (*) and the other symmetrical correlations identify neighboring carbons/protons. Hence, the one experiment has the potential to act as a tool in determining heteronuclear correlations and coupling pathways within a molecule. The ^{13}C and ^{1}H assignments are obvious.

The experiment will not be dealt with at any length, since it was observed in the author's hands to be limited to simple molecules having weakly-coupled proton spectra. When solutions of sucrose and 2 were tried, the results were less than satisfactory. An analogous homonuclear correlation experiment which has a COSY-like display identifies[81] a family of scalar coupled spins. The output is quite

messy even for the single AMQ$_3$X system illustrated, and one is led to speculate that even two such overlapping systems would be difficult to decipher.
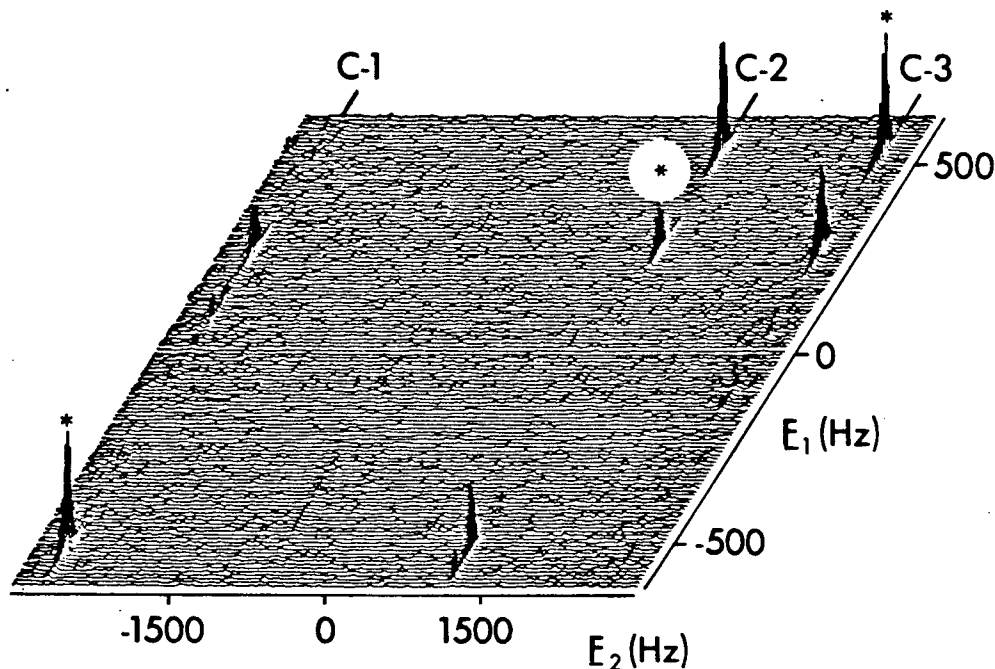
Fig. II.2.37 Relayed coherence transfer experiment performed on n-propanol (^{1}H frequency 400 MHz). Peaks present in the CSCM experiment are labelled with an asterisk.

II.2.5.6 2D Nuclear Overhauser Enhancement Spectroscopy[82,83]

A 2D experiment exists which explores magnetization transfer (via chemical exchange or nOe) and, in the nOe sense, is called 2D nuclear Overhauser enhancement spectroscopy or "NOESY". The experiment bears many similarities to COSY/SECSY; it involves a three-pulse

sequence and is an autocorrelation experiment, correlating spins involved in magnetization transfer, such as nOe.

The display of the experimental output may be chosen as COSY-like (II.2.47A) or SECSY-like (II.2.41B).

$$RD - 90°(\Phi_1) - \underline{t}_1 - 90°(\Phi_2) - \tau_{mix} - 90°(\Phi_3) - AQN(\underline{t}_2;\Phi_4) \qquad [II.2.41A]$$

$$RD - 90°(\Phi_1) - 0.5\underline{t}_1 - 90°(\Phi_2) - \tau_{mix} - 90°(\Phi_3) - 0.5\underline{t}_1 - AQN(t_2;\Phi_4)$$

$$[II.2.41B]$$

For sequence II.2.41A the display shows a plot of δ vs δ with the normal spectrum along the diagonal, and cross-peaks indicating magnetization transfer (c.f. COSY). With sequence II.2.41B, $\underline{F}_1$ represents $\Delta\delta/2$ and the normal spectrum lies at $\underline{F}_1 = 0$ (c.f. SECSY).

Phase-cycling is important in this experiment and achieves two purposes: (a) quadrature detection in $\underline{F}_1$ with quadrature image supression and (b) elimination of multiple quantum coherence (MQC) contributions to cross-peaks (see later). Hull proposed[84] the following scheme.

Cycle	1	2	3	4	5	6	7	8	9	10	11	12	13	14	15	16
Φ_1	x	x	x	x	x	x	x	x	x	x	x	x	x	x	x	x
Φ_2	x	y	-x	-y	x	y	-x	-y	-x	-y	x	y	-x	-y	x	y
Φ_3	x	-y	x	-y	y	x	y	x	-x	y	-x	y	-y	-x	-y	-x
Φ_4	x	x	-x	-x	y	y	-y	-y	x	x	-x	-x	y	y	-y	-y

$$[II.2.42]$$

Since the experiment was first suggested, several detailed papers have emerged from the same group concentrating on theoretical aspects,[82,83,85] refinements[86-89] and applications.[90-92] A brief description is given in Fig. II.2.38.

$$90^\circ_x \qquad 90^\circ_x \qquad 90^\circ_x$$

Preparation | Evolution | Mixing (τ_{mix}) | Detection ($\underline{t}_2$)

•A   B• •C   D• •E

A.   B.   C.   D.   E.
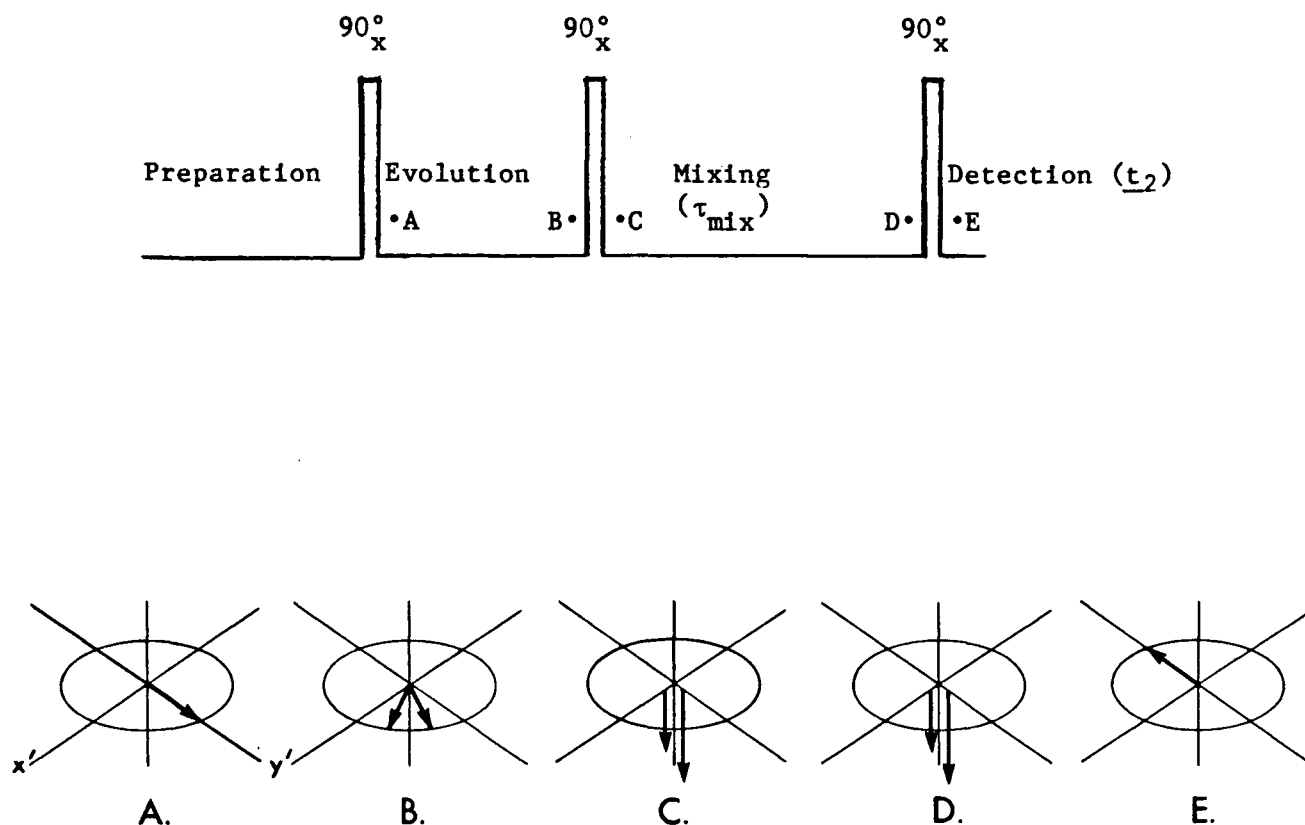
Fig. II.2.38 Schematized NOESY experiment and vector model.

We consider two (homonuclear) spin-1/2 nuclei, close in space and not
scalar coupled. The "preparation" period is terminated by the first 90°
"preparatory" pulse, which creates transverse magnetization (Fig.
II.2.38A). The "evolution" period (t_1)* serves to frequency-label the
vectors (c.f. COSY) and at the end of this period they may be
represented by Fig. II.2.38B. A second "mixing" pulse now generates
z-magnetization (Fig. II.2.38C); transverse magnetization also exists at
this stage but is undesirable and removed by phase-cycling and,
therefore, omitted from the diagram. During the "mixing" period,
τ_{mix}, magnetization transfer (e.g. dipole-dipole or cross relaxation)
processes occur where possible. The end of the mixing period (Fig.
II.2.38D) is marked by a final 90° "detection" pulse, which recreates
detectable transverse magnetization (Fig. II.2.38E) which is sampled
during the "detection" period, t_2. Normal 2D FT yields a COSY-like plot
with a diagonal bearing the 1D spectrum and cross-peaks arising where
magnetization transfer processes occurred during τ_{mix} (ideally).

We now look at the experiment in the light of the motion of the
molecule. A rapidly tumbling, low molecular weight molecule
(extreme-narrowing limit) will behave differently from a large, high
molecular weight molecule at high-field (spin diffusion limit). In the
extreme-narrowing limit, the dipole-dipole relaxation mechanism often
dominates and NOESY cross-peaks would be negative going compared to the
diagonal peaks (if phase-sensitive display were used) and small - a
maximum of ca. 10% of diagonal peak height ($\tau_{mix} = 0$). The critical
case of $\omega_0 \tau_c = 1.12$ leads to zero cross-peak intensity. In the spin

---

*t_1 is systematically incremented in the usual fashion.

diffusion regime, cross relaxation dominates and cross peaks have the same phase as diagonal peaks. Moreover, cross- and diagonal-peak intensities can be quite comparable under favourable conditions. The degree of intragroup relaxation is an important factor in the two regimes. If one were considering two close methyl groups in a molecule, these protons would have strong intragroup relaxation and under extreme narrowing conditions the cross-peaks would amost certainly be undetectably small; in the spin diffusion limit, however, strong cross-peaks could be expected.

When attempting a NOESY experiment, a decision has to be made regarding the choice of τ_{mix}. The variation of nOe cross-peak intensity as a function of τ_{mix} is well understood. In the extreme-narrowing limit*, the cross-peak build up occurs as a function of τ_{mix} is roughly analogous to those seen in the TOE experiment (II.2.4.2) and nOe builds up linearly with τ_{mix} to a maximum value, and then tapers off. In such a case an optimal τ_{mix} would be $\approx 1\underline{T}_1$. In the spin diffusion limit,* the build up curve is entirely analogous to that obtained from a driven nOe experiment[93] (I.2.4.3). Generally, a mixing time can be selected by doing a trial driven nOe experiment; an irradiation time which produces a strong negative nOe can be used as τ_{mix}.

─────────────

*In the extreme narrowing limit τ_{mix} will be ca. 1s, and in the spin diffusion limit, ca. 100 ms.

A complication with the NOESY experiment, alluded to earlier, is that more than one mechanism can give rise to cross-peaks. Zero (Z-) and MQC give rise to cross-peaks with scalar coupled spins, analogous to COSY. These are referred to as $\underline{J}$ cross-peaks and arise from coherent magnetization transfer (vs. incoherent magnetization transfer in the case of nOe). Several schemes have been put forward to supress these contributions. First-, second- and third order MQC may be easily removed by phase-cyling.[83,86] The problem remains with ZQC. Several ideas have been suggested[85,87] in this respect but have not been systematically evaluated:

a. Digital apodization can be used to discriminate against $\underline{J}$ cross-peaks.

b. Randomized τ_{mix}. Instead of using exactly the same τ_{mix} in each experiment, τ_{mix} is randomly varied 10-20% (e.g. $0.9 \leq \tau_m \leq 1.1$ is a 10% randomization of τ_{mix} = 1.0 s). NOe cross-peaks are hardly affected by this, but $\underline{J}$ cross-peak intensity behaves in an oscillatory fashion during τ_{mix} and the randomization causes a smearing of $\underline{J}$ cross-peaks in the $\underline{F}_1$ axis, resulting in an additional noise band significantly reduced in intensity and, hopefully, below the contour level threshold. The noise band could, however, obscure a small nOe response of interest.

c. Partial refocussing. Introduction of a refocussing 180° pulse placed at random positions during τ_{mix} has been suggested to result in a similar effect to (b).
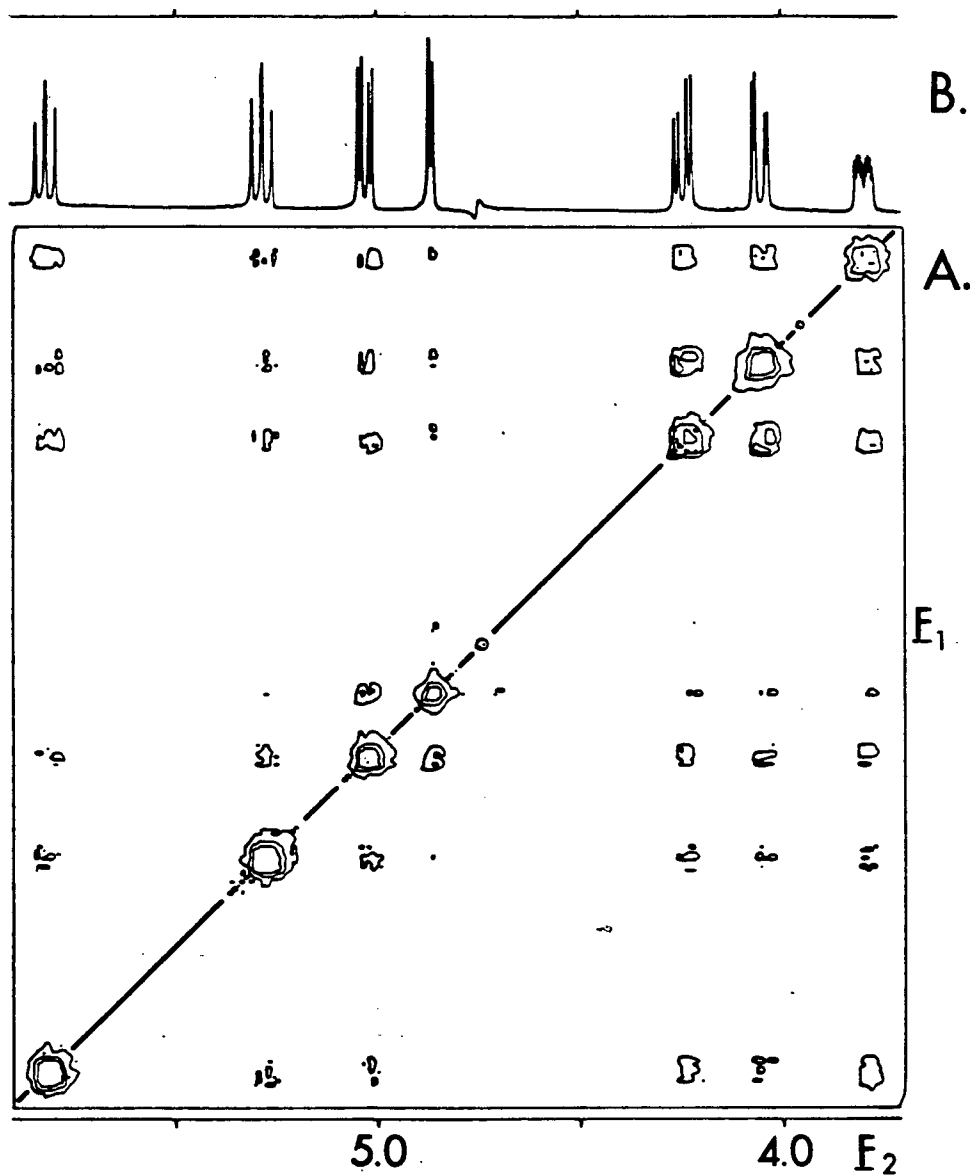
Fig. II.2.39 2D NOESY spectrum of 1 at 400 MHz. A mixing time of 0.3 s was used, randomized ± 10%.

d. <u>Sequential variation of τ_{mix}.</u> In this experiment, τ_{mix}
is progressively incremented in parallel with the evolution
time, $\underline{t}_1$. The mixing time is set $\tau_{mix} = \tau^0_{mix} + \chi \underline{t}_1$,
where τ^0_{mix} is the initial value and χ is chosen such that
$\tau^0_{mix} \gg \chi^*$ (acquisition time in $\underline{t}_1$). A symmetrization
procedure is imperative to eliminate ZQC and MQC peaks which
are not symmetrical about the line $\underline{F}_1 = \underline{F}_2$. Here, $\underline{J}$
cross-peaks are not smeared out as in the case of (b), but
it was advised that the experiment be repeated for a second
τ_{mix} to remove any doubts of ambiguities arising from
accidental symmetrical disposition of Z- or MQC peaks.

In the author's hands, the simplest procedure has been the
utilization of phase-cycling, the randomized τ_{mix} and sinebell
apodization in both $\underline{t}_1$ and $\underline{t}_2$.

Fig. II.2.39 shows a contour plot of the NOESY experiment for $\underline{1}$,
which should be compared with the $\underline{J}$-correlated spectrum (Fig. II.2.28).

II.2.6 Conclusions

The reader has been introduced to a large number of the NMR
experiments which we believe will find greater utility in the years to
come. Where possible, the theory has been explained at as pictorial a
level as possible since the assumption has been made that the reader
will not have had extensive experience in these areas.

Except where an experiment has failed (relayed coherence

transfer), these have been viewed in as impartial a light as possible, since the intention with this chapter is to identify, explain and illustrate potentially useful experiments. In the following chapters, several of these experients are used as we work our way towards a practical evaluation of the combination of experiments to yield an effective protocol for the structure elucidation of organic molecules using NMR spectroscopy.

The graph, below, shows the relative number of publications of 2D NMR related papers since its conception 1975. The first 3 or 4 years saw a steady rate of 2D NMR publication, dominated by a handful of workers concentrating on fundamental development. The incorporation by instrument manufacturers of the necessary soft-ware into standard spectrometers, and the excitement generated in the scientific community in the preceding years, led to a rapid growth phase from 1979 to 1981. Interestingly, still relatively few groups were involved with the assessment of the first experiments, and their application to "real-life" problems. In the authors's opinion, 1983 and subsequent years will witness a further explosion of literature articles drawing on 2D NMR for results. Increasing numbers of papers will have as their focus the data from the experiments, rather than their evaluation as a source of information. This thesis will hopefully assist in the acceptance of 2D NMR with a new air of confidence. This chapter, specifically, should serve as a compilation of 1D and 2D NMR experiments which an organic chemist or spectroscoptist should find useful when considering a particular experiment.

Year	Relative Number of Publications
1975	*
1976	*
1977	***
1978	***
1979	*********
1980	***********
1981	*******************
1982	********************

Table II.2.1 An indication of the relative number of publications relating to 2D NMR in the literature, categorized by year.

REFERENCES

1. M.L. Martin, J.-J. Delpeuch, and G.J. Martin. Practical NMR spectroscopy. Heyden and Son Ltd., Philadelphia. 1980.

2. T.C. Farrar and E.D. Becker. Pulse and Fourier transform NMR. Introduction to theory and methods. Academic press, N.Y. 1971.

3. D. Shaw. Fourier transform N.M.R. spectroscopy. Elsevier, New York. 1976.

4. J.C. Lindon and A.G. Ferrige. Progress in NMR Specroscopy, 14, 27-66 (1980).

5. L.D. Colebrook and L.D. Hall. Can. J. Chem. 58, 2016-2023 (1980).

6. L.D. Hall and J.K.M. Sanders. J. Amer. Chem. Soc. 102, 5703-5711 (1980).

7. Ref. 1, pp. 254-255.

8. K.F. Wong. Ph.D. thesis, University of British Columbia, 1980.

9. G.E. Martin. J. Pharm. Sci. 70, 81-84 (1981).

10. R.R. Ernst. J. Chem. Phys. 45, 3845-3861 (1966).

11. H.J. Osten and R. Radeglia. J. Magn. Reson. 49, 8-21 (1982).

12. D.P. Burum and R.R. Ernst. J. Magn. Reson. 39, 163-168 (1980).

13. D.T. Pegg, D.M. Doddrell, W.M. Brooks, and M.R. Bendall. J. Magn. Reson. 44, 32-40 (1981).

14. S.L. Patt and J.N. Schoolery. J. Magn. Reson. 46, 535 - 539 (1982).

15. J.-C. Beloeil, C. Le Cocq, and Y.-V Lallemand. Org. Magn. Reson. 19, 112-115.

16. D.M. Doddrell, D.T. Pegg, and M.R. Bendall. J. Magn Reson. 48, 323-327 (1982).

17. H.J. Jakobsen, O.W. Sorensen, W.S. Brey, and P. Kanyha. J. Magn. Reson. 48, 328-335 (1982).

18. F.-K. Pei and R. Freeman. J. Magn. Reson. 48, 318-322 (1982).

19. M.R. Bendall, D.M. Doddrell, D.T. Pegg, and W.E. Hull. High resolution multipulse NMR spectrum editing and DEPT. Bruker Spectrospin note. 1982.

20. R. Richarz, W. Amman, and T. Wirthlin. XL-200/300 in DEPT: A new experiment for the ADEPT spectroscopist! Varian Associates note Z-15. 1982.

21. C.D. Barry, C.M. Dobson, D.A. Swiegart, L.E. Ford, and R.J.P. Williams. NMR shift reagents. Edited by R.E. Sievers. Academic Press, New York. 1973. pp 173-195.

22. M. Kuo and W.A. Gibbons. J. Biol. Chem. 254, 6278-6287 (1979).

23. L.D. Hall and J.K.M. Sanders. J. Chem. Soc. Chem. Commun., 368-370 (1980).

24. J.D. Mersh and J.K.M. Sanders. J. Magn. Reson. 50, 289-298 (1982).

25. J.H. Noggle and R.E. Schirmer. The nuclear Overhauser effect. Chemical applications. Academic Press, New York. 1971.

26. B.P. Roques, R. Rao, and D. Marion. Biochimie 62, 753-773 (1980).

27. A.A. Bothner-By. Biological applications of magnetic resonance. Edited by R.G. Shulman. Academic Press, New York. 1979. pp 177-219.

28. I.D. Campbell, C.M. Dobson, R.G. Ratcliffe, and R.J.P. Williams. J. Magn. Reson. 19, 397-417 (1978).

29. Ref. 26, pp. 26-31; ref. 1, p. 18.

30. R. Freeman, H.D.W. Hill, B.L. Tomlinson, and L.D. Hall. J. Chem. Phys. 61, 4466-4473 (1974).

31. J.D. Mersh and J.K.M. Sanders. Org. Magn. Reson. 18, 122-124 (1982).

32. Ref. 26. pp. 57-69.

33. H. Thogersen, R.U. Lemieux, K. Bock, and B. Meyer. Can. J. Chem. 60, 44-57 (1982).

34. R. Richarz and K. Wüthrich. J. Magn. Reson. 30, 147-150 (1978).

35. B.L. Tomlinson and H.D.W. Hill. J. Chem. Phys. 59, 1775-1784 (1973).

36. Ref. 26, pp. 116-117.

37. A.A. Bothner-By and J.H. Noggle. J. Amer. Chem. Soc. 101, 5152-5155, (1979).

38. M.H. Levitt. J. Magn. Reson. 48, 234-264 (1982), and references cited therein.

39. N.M. Szeverenyl, A.A. Bothner-By, and R. Bittner. J. Phys. Chem. 84, 2880-2883 (1980).

40. S.L. Gordon and K. Wüthrich. J. Amer. Chem. Soc. 100, 7094-7096 (1978).

41. G.A. Morris and R. Freeman. J. Magn. Reson. 29, 433-462 (1978).

42. G. Wagner and K. Wüthrich. J. Magn. Reson. 33, 675-680 (1979).

43. F.M. Poulsen, J.C. Hoch, and C.M. Dobson. Biochem. 19, 2597-2607 (1980).

44. C.M. Dobson, E.T. Olejniczak, F.M. Poulsen, and R.G. Ratcliffe. J. Magn. Reson. 48, 97-110 (1982).

45. Recent reviews: G.A. Morris. Fourier, Hadamard, and Hilbert transforms in chemistry. Edited by A.G. Marshall. Plenum Press, New York. 1982. pp. 271-305. K. Nagayama. Adv. Biophys. 14, 139-204 (1981). R. Freeman. Proc. R. Soc. Lond. A. 373, 149-178 (1980). R. Freeman and G.A. Morris. Bull. Magn. Reson. 1, 5-26 (1979).

46. A. Bax. Two-dimensional nuclear magnetic resonance in liquids. D. Reidel, Holland. 1982.

47. S. Sukumar. Ph.D. Thesis, University of British Columbia. 1981.

48. G. Bodenhausen, R. Freeman, R. Niedermeyer, and D.L. Turner. J. Magn. Reson. 26, 133-164 (1977).

49. Ref. 46, pp. 41-43.

50. S. Brownstein. J. Magn. Reson. 42, 150-154 (1981).

51. K. Nagayama, P. Bachman, K. Wüthrich, and R.R. Ernst. J. Magn. Reson. 31, 133-148 (1978).

52. D.L. Turner. J. Magn. Reson. 49, 175-178 (1982).

53. W.P. Aue, P. Bachmann, A. Wokaun, and R.R. Ernst. J. Magn. Reson. 29, 523-533 (1978).

54. Ref. 46, pp. 99-101.

55. E.L. Hahn and D.E. Maxwell. Phys. Rev. 88, 1070-1084 (1952).

56. L.D. Hall and S. Sukumar. J. Amer. Chem. Soc. 101, 3120-3121 (1979).

57. G. Bodenhausen, R. Freeman, and D.L. Turner. J. Magn. Reson. 27, 511-514 (1977).

58. G. Bodenhausen and D.L. Turner. J. Magn. Reson. 41, 200-206 (1980).

59. L.D. Hall, G.A. Morris, and S. Sukumar. Carbohydr. Res. 76, C7-C9 (1979).

60. M. Levitt and R. Freeman. J. Magn. Reson. 34, 675-678 (1979).

61. L.D. Hall and S. Sukumar. J. Magn. Reson. 38, 555-558 (1980).

62. A. Kumar. J. Magn. Reson. 30, 227-249 (1978).

63. G. Bodenhausen, R. Freeman, G.A. Morris, and D.L. Turner. J. Magn. Reson. 31, 75-95 (1978).

64. G. Wider, R. Baumann, K. Nagayama, R.R. Ernst, and K. Wüthrich. J. Magn. Reson. 42, 73-87 (1981).

65. A. Bax. R. Freeman, and G.A. Morris. J. Magn. Reson. 43, 333-338 (1981).

66. J.D. Mersh and J.K.M. Sanders. J. Magn. Reson. 50, 171-174 (1982).

67. W.P. Aue, E. Bartholdi, and R.R. Ernst. J. Chem. Phys. 64, 2229-2246 (1976).

68. A. Bax and R. Freeman. J. Magn. Reson. 44, 542-561 (1981).

69. K. Nagayama, A. Kumar, K. Wüthrich, and R.R. Ernst. J. Magn. Reson. 40, 321-334 (1980).

70. R. Bauman, G. Wilder, R.R. Ernst, and K. Wüthrich. J. Magn. Reson. 44, 402-406 (1981).

71. R. Bauman, A. Kumar, R.R. Ernst, and K. Wüthrich. J. Magn. Reson. 44, 76-83 (1981).

72. Morris' review, ref. 45.

73. B. Blümich and D. Ziessow. J. Magn. Reson. 49, 151-154 (1982).

74. S. Sukumar, personal communication.

75. A. Bax, personal communication.

76. A. Bax and G.A. Morris. J. Magn. Reson. 42, 501-505 (1981), and others in the series.

77. Ref. 46, pp. 50-65, and references cited therein.

78. J. S. Waugh. J. Magn. Reson. 49, 517-521 (1982).

79. P.H. Bolton. *J. Magn. Reson.* 51, 134-137 (1983).

80. P.H. Bolton. *J. Magn. Reson.* 48, 336-340 (1982).

81. G. Eich, G. Bodenhausen, and R.R. Ernst. *J. Amer. Chem. Soc.* 104, 3731-3732 (1982).

82. J. Jeener, B.H. Meier, P. Bachman, and R.R. Ernst. *J. Chem. Phys.* 71, 4546-4553 (1979).

83. S. Macura and R.R. Ernst, *Molec. Phys.* 41, 95-117 (1980).

84. W.E. Hull. Two-dimensional NMR. Aspect 2000. Bruker Report (1982).

85. S. Macura, Y. Huang, D. Suter, and R.R. Ernst. *J. Magn. Reson.* 43 259-281 (1981).

86. G. Bodenhausen and R.R. Ernst. *Molec. Phys.* 47, 319-328 (1982).

87. S. Macura, K. Wüthrich, and R.R. Ernst. *J. Magn. Reson.* 47, 351-357 (1982).

88. S. Macura, K. Wüthrich, and R.R. Ernst. *J. Magn. Reson.* 46, 269-282 (1982).

89. G. Bodenhausen and R.R. Ernst. *J. Amer. Chem. Soc.* 104, 1304-1309 (1982).

90. A. Kumar, R.R. Ernst, and K. Wüthrich. *Biochem. Biophys. Res. Comm.* 95, 1-6 (1980).

91. A. Kumar, G. Wagner, R.R. Ernst, and K. Wüthrich. *Biochem Biophys. Res. Comm.* 96, 1156-1163 (1980).

92. G. Wagner, A. Kumar, and K. Wüthrich. *Eur. J. Biochem.* 114, 375-384 (1981).

93. A. Kumar, G. Wagner, R.R. Ernst, and K. Wüthrich. *J. Amer. Chem. Soc.* 103, 3654-3658 (1981).

CHAPTER II.3

OLIGOSACCHARIDE CHARACTERIZATION USING NMR

Complex carbohydrates are widely dispersed in Nature where they play a variety of roles. Often in polymerized form, they constitute structural materials (e.g. cellulose, bacterial cell-walls), or energy storage molecules (e.g. starch, glycogen). With bacterial cell-walls they can serve the additional purpose of coding the immunogenicity the organism presents. An equally important role is played by carbohydrates conjugated to protein or lipid - glycoproteins or glycolipids respectively. Again these serve the gamut of functions, as structural molecules (e.g. collagen), the "letters" of the blood-group substance's "alphabet", lubricants (e.g. gastro-intestinal tract mucins), "anti-freeze" agents (in Arctic fish) and bound to a host of proteins (e.g. some enzymes and the immunoglobulin proteins). It has even been speculated that in time, all proteins will be found to contain some carbohydrate!

The ubiquity and importance of complex carbohydrates in biological systems has, not surprisingly, attracted much attention. Initial investigations tended to focus on primary structure - which sugars are present and the details of the ordering. However, in the last few years people have begun to try to relate structure with function, and to this end knowledge of the secondary, three-dimensional picture is sought.

Prior to this study, a wide range of technologies existed for sequencing complex carbohydrates, which will be briefly reviewed below.

The last few years has seen a demonstration of the tremendous potential of NMR in this field and this chapter discusses the development of one such protocol which we believe to be of some potential. Pivotal to the procedure is the use of recently developed techniques detailed in the preceding chapter; an understanding of these will henceforth be assumed. NMR has the broad advantages of being a non-destructive technique with several extractable parameters, each with its own information content. As a counterpoint, the method is inherently insensitive and demands on sample quantity may totally preclude its use for many biologically important systems.

Before the 1970's, almost all structural studies hinged on classical "wet" chemical analyses.[3] These demand relatively large amounts of sample, are labour intensive and have even been found to be incorrect when re-examined.[4] The early seventies saw the infusion of spectroscopic techniques and at this time, such methods must be considered indispensable. Although the focus here is primarily on NMR, the utility of mass-spectroscopy cannot be overlooked, especially in light of its signal-to-noise sensitivity.

^{13}C NMR spectroscopy has been of great utility in the area, (often in conjunction with "wet" methods), and recent reviews have been presented by Gorin[5] and Barker et al.[6] Nevertheless ^{13}C NMR spectra remain difficult to fully assign and structural assignments are totally convincing only when a series of molecules is synthesized[7,8] (or produced by degradation) and a systematic investigation is pursued. Anomeric configuration may confidently be assigned on the basis of

either ^{13}C chemical shifts or $^1J_{C1-H1}$. The potential exists for the extraction of conformational information, based on inter-ring ^{1}H-^{13}C couplings.[9] However, these are often small ($\leq$ 6 Hz), unresolved and one may have to synthesize[10] the molecule enriched in ^{13}C; as a result this approach has limited potential. Nevertheless, the overall simplicity of ^{13}C NMR spectra is appealing and the technique is finding a larger place as superior experiments and protocols are designed. In the limit though, the fact that ^{13}C NMR is impractical with sub-milligram quantities may serve to limit its utility.

A number of European and Canadian groups have already dedicated some considerable effort to the application of ^{1}H NMR to oligopeptides and cerebrosides. The Franco-Dutch group of Vliegenthart and Montreuil has focussed on the structurally related oligomannoside glycopeptides,[2] isolated from the urine of patients with mannosidosis. The mannose anomeric and H-2 protons resonate down-field from the bulk of the ring protons. Their chemical shifts and coupling constants were accurately measured and, by reference to data from known compounds, assignments were made.[11] In a broader study by Carver and Grey[12], useful conclusions were drawn and the method extended. Although this approach is probably wholly appropriate for molecules of this type, we draw attention to its lack of generality because of its reliance on a "library" of reference data. Furthermore, virtual coupling may complicate anomeric proton signals.[13] Dabrowski's group in Germany has concentrated on glycosphingolipids and his work has recently been reviewed.[14] Compounds were dissolved in DMSO-$\underline{d}_6$ and proton measurements

made on sub-milligram quantities. Extensive 1D NMR measurements, together with catalogue data, allowed almost complete assignment of cerebrosides having up to ten sugar residues. At the time our study was performed, no 2D NMR had been used in such structural studies, and the developments are presented chronologically.

Hall and co-workers have put some considerable effort[15-18] into the use of proton $\underline{T}_1$'s as a measure of inter-proton distances in carbohydrate molecules. These, together with nOe methods described earlier,[19] have been capitalized on by Lemieux and co-workers in the complex carbohydrate area. An elegant study[7] used such NMR techniques to validate carbohydrate secondary structures determined by hard-sphere molecular modelling calculations, taking into account the exo-anomeric effect (HSEA). A series of blood-group determinant oligosaccharides were synthesized and systematically studied by ^1H and ^{13}C NMR. This paper represents a land-mark in both spectral assignment and conformational analysis of complex oligosaccharides.

Cerebrosides have been derivatised and studied in organic solvents by NMR. Martin-Lomas and Chapman made per-O-acetylated galactocerebrosides[20] and noted large chemical shift changes upon varying solvents; this allowed them to make partial first-order assignments and confirm the anomeric configuration, and conformation of the pyranose ring. Falk et al. studied[21] more complex Lewis-like cerebrosides as their O-methyl ethers. Six compounds were considered, including a heptaglycosylcerebroside. The fact that the O-CH3 resonances resonate at roughly the same chemical shift as the other ring

protons restricted their study mainly to anomeric protons at $\delta > 4.0$. A method was developed for differentiating Type I and Type II saccharide chains.
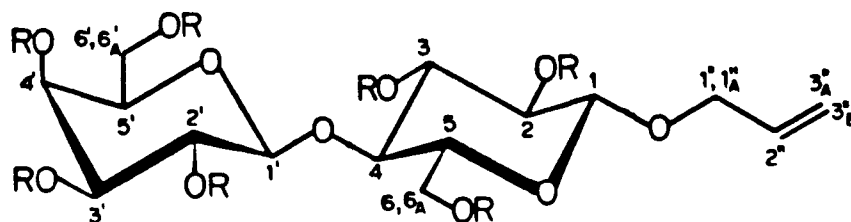
$\underset{\sim}{1}$ R = H

$\underset{\sim}{2}$ R = CO.CD$_3$

We now propose a protocol for the structure elucidation of complex oligosaccharides, using NMR.[22] As a model compound we chose allyl β-D-galactopyranosyl-β-(1→4)-D-glucopyranoside ("β allyl lactoside"), 1, which we prepared using standard procedures.[23]

The oligomer is initially considered as a mixture of glycosides of the constitutent monosaccharides, and we aim for the full assignment of carbohydrate ring protons, and the determination of linkage order by inter-ring nOe measurements. Our protocol is as follows:

1. Maximize signal dispersion. Use of a very high-field spectrometer with the parent compound may be adequate, but most times derivatization will be necessary. Preferably the

derivatization reagents should be fully deuterated and, hence, spectroscopically silent, to preclude introduction of additional resonances which may overlap with those of the parent solute resonances.

2. A solvent, pure or mixed, should be found which minimizes signal overlap.

3. The assignment process is begun with 1D techniques, such as partially T_1 relaxed spectra,[24] SDDS[25] and NOEDS.[26] Should these prove sufficient to complete the assignment, steps 4 and 5 are omitted.

4. The 2D J-resolved experiment[27] is used to locate the resonance frequencies of all ring protons. Partial J spectra allow the measurement of all coupling constants.

5. Next, the J connectivities are established by the 2D J correlation experiment, COSY (or SECSY); each ring acts as an isolated spin system oblivious to its partners, since inter-ring coupling will be indetectably small or zero.

6. A few very specific 1D experiments (3) may be necessary to resolve any outstanding ambiguities in assignment.

7. Next, each unit is identified (e.g. β-galactopyranosyl) by comparison of the measured J-values with reference values.[29] This identifies the sugars, their anomeric configurations and ring sizes.

8. The final task is the determination of the sequence along the chain; this is done by determining the specific inter-ring relaxation effects. With 1D nOe experiments it is necessary

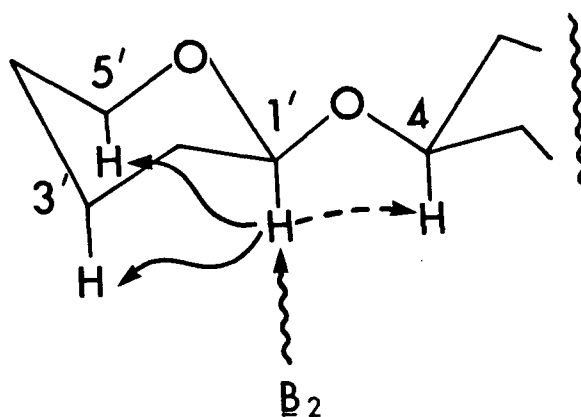Fig. II.3.1 With a β(1-4) glycosidic linkage, irradiation of the glycosidic proton (H-1') induces intra-ring (——) and a single inter-ring (---) nOe.

that all the anomeric protons be separately resolved (which may be possible by changing solvent). Aside from known intra-ring nOe's (1,3 diaxial protons, e.g.), each
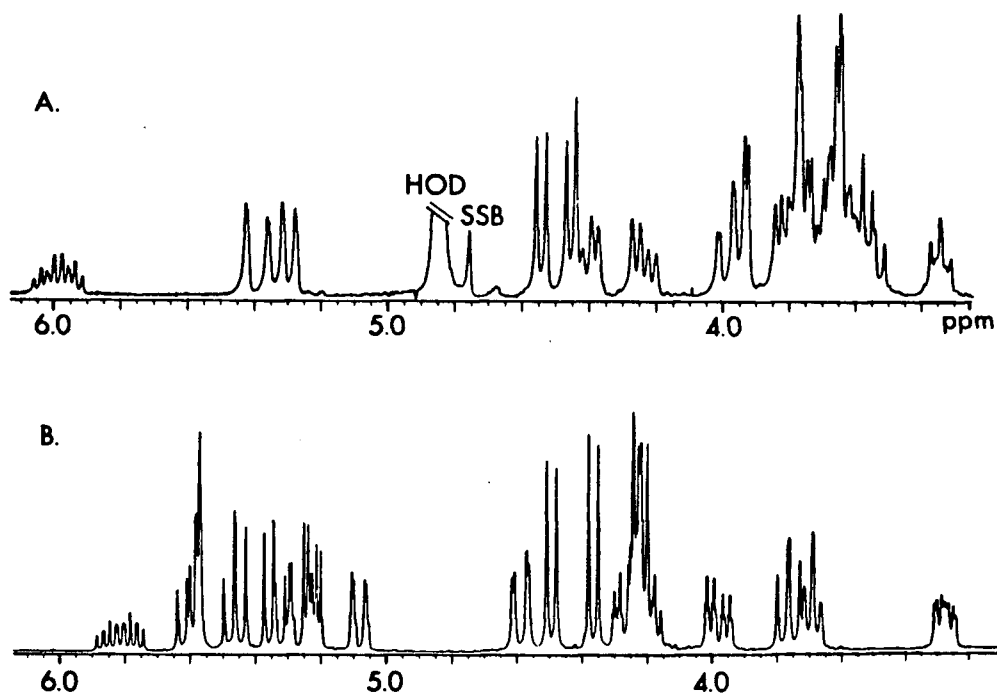

Fig. II.3.2. 270 MHz spectra of (A) β-allyl lactoside in D₂O, and (B) β-allyl aceto(d₃) lactoside.

irradiation should induce a unique inter-ring nOe (see

Fig. II.3.1). Since all protons have been assigned, the

linkage can be easily deduced. The same information may be

obtained from a 2D NOESY experiment.[30] In this case the

advantage is that the anomeric signals may be hidden; this

may be of greatest utility with more complex structures.

We illustrate this approach using β-allyl lactoside, 1, as the

exemplar. The 270 MHz ^{1}H NMR spectrum of a D_2O solution of the molecule

is shown in Fig. II.3.2.A. The anomeric protons are clearly discernable

as the doublets near δ 4.5. The bulk of the ring protons all resonate

between δ 3.9 and 3.5 and only a few are separately discernable. The

corresponding per-O-trideuterio-acetylated derivative, 2, was

synthesized by standard methods[31] using perdeuterio-acetic anhydride.

Its spectrum (0.2 M in C_6D_6*) is shown in Fig. II.3.2B. As expected,

many signals (arising from O-acetylated centres) are deshielded and the

spectrum is considerably simplified. In this simple instance,

spin-decoupling experiments almost sufficed to determine the full

assignment.

2D NMR investigations began with the 2D J-resolved experiment

which allowed the detection of ten carbohydrate ring protons and the

five allyl protons. A contour plot of the 2D J-resolved experiment is

given in Fig. II.3.3; their chemical shifts and coupling constants were

recorded. Next, the COSY experiment was performed at 400 MHz; the data

are shown in Fig. II.3.4, in the contour-plot mode again. It is

---

*In this case, this balance of concentration and solvent was
found to minimize signal overlap.
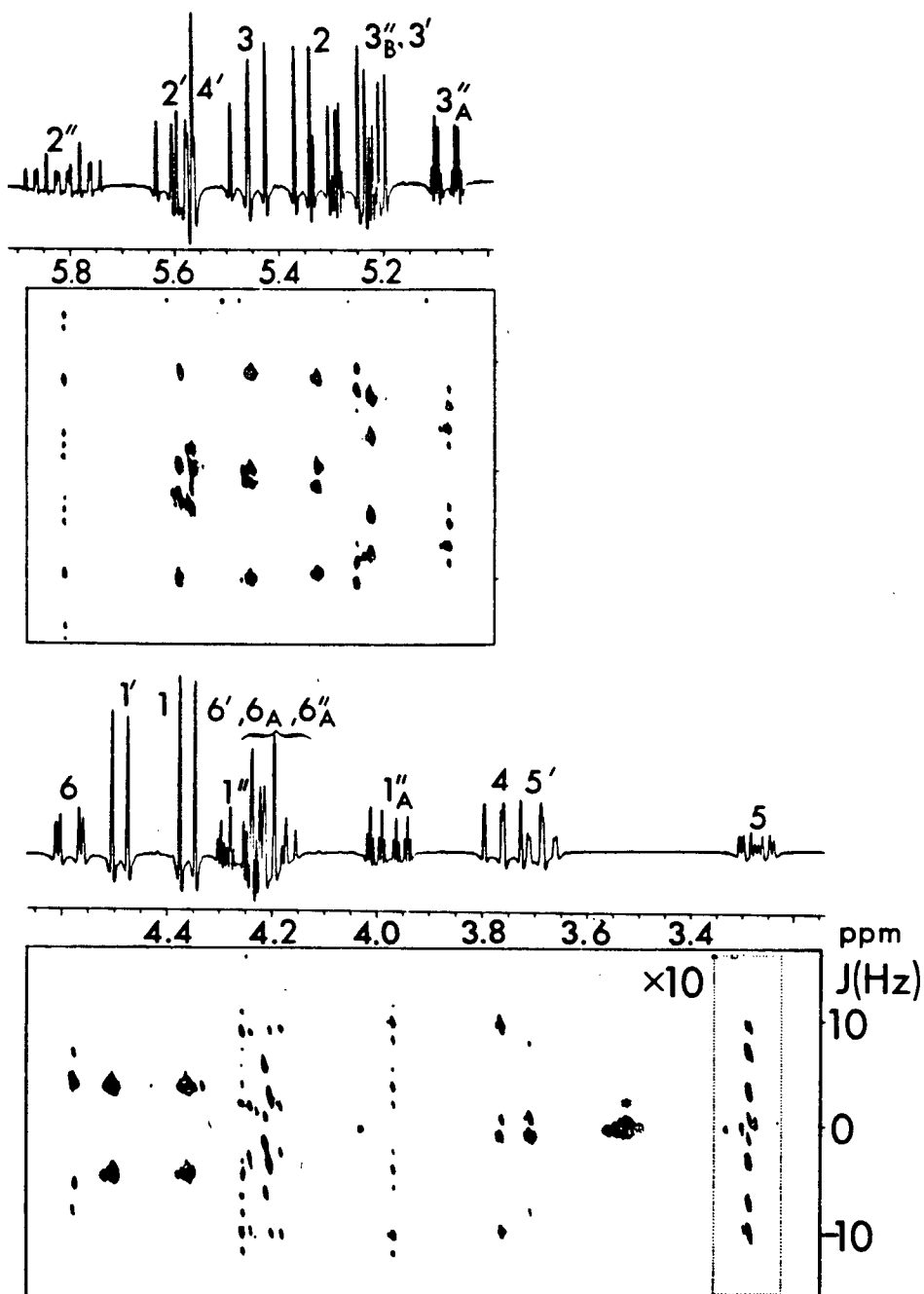
Fig. II.3.3 Contour plot of 2D J-resolved NMR spectrum of 2 (270 MHz; 0.2 M in C_6D_6). The assigned, resolution-enhanced spectrum is plotted above.

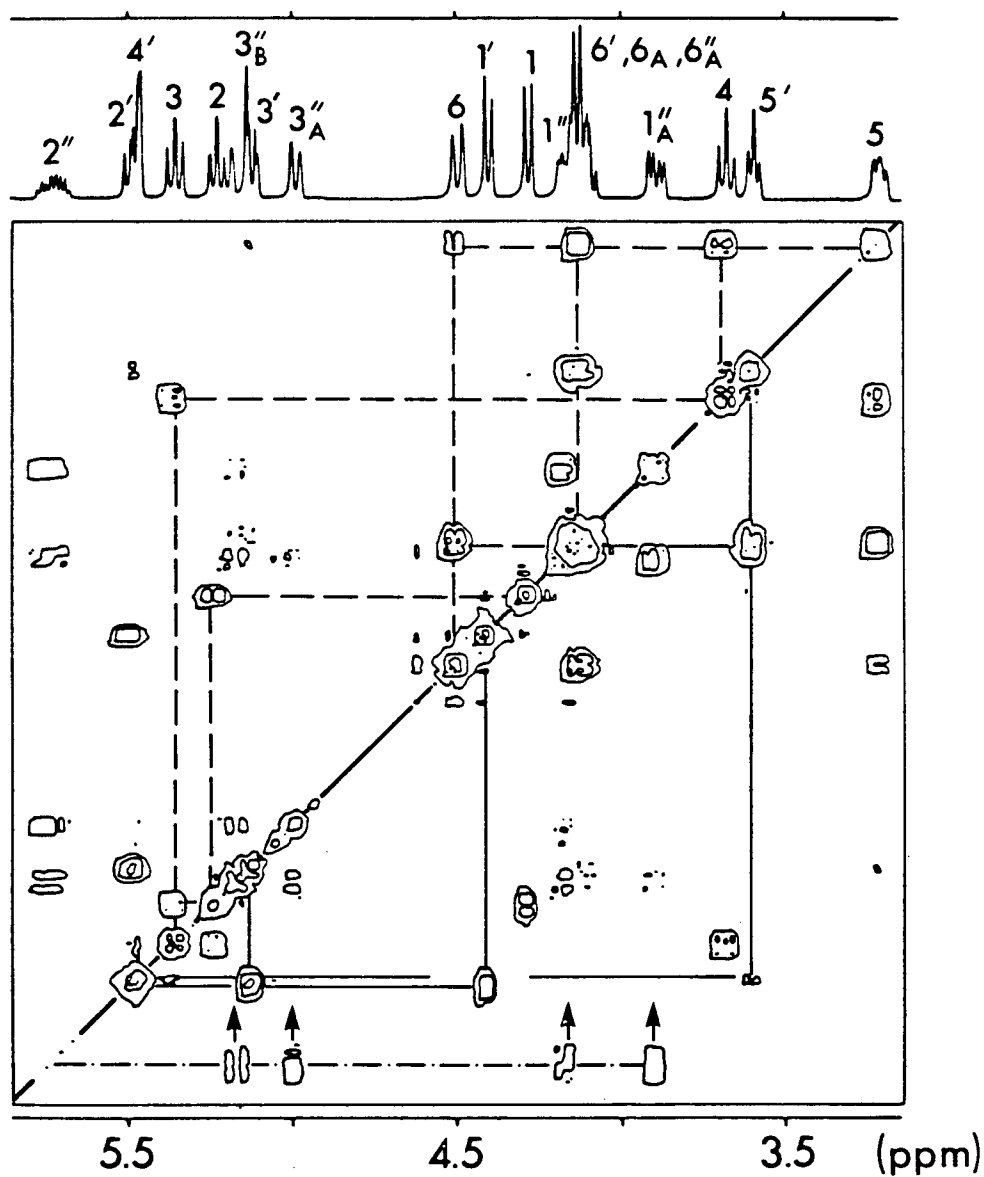Fig. II.3.4 400 MHz COSY spectrum of 2 (0.2 M in C6D6). Connectivities
within the glucopyranosyl ring are shown (---) in the top
left half, and the galactopyranosyl (——) in the bottom
right half. Allyl connectivities are shown (—•—•—).

convenient to begin tracing connectivities with the anomeric protons.
For example, starting with H-1, the connectivities to the other glucosyl
ring protons are clear from an inspection of Fig. II.3.4. In this way,
it was now possible to trace out all connectivities. The only ambiguity
arose from the galactosyl H-2', H-3' and H-4' where cross-peak contour
overlap resulted from H-2' and H-4' resonating very close to one another
and both being coupled with H-3'. The assignment was made after careful
inspection of an expansion of this region of the COSY plot, and
confirmed by matching coupling constants from the 2D $\underline{J}$-resolved data.
Comparison of these coupling constants with standard literature values
in Table II.3.1, confirmed the existence of a β-galactopyranoside and a
β-glucopyranoside moiety. The identification of the constituents
monosaccharides and their anomeric configuration was complete.

Next, the linkage sequence was determined from the nOe
experiments involving the anomeric protons. The SSNOEDS experiment was
just feasible at 400 MHz with adequate decoupler-frequency selectivity.
The results, shown in Fig. II.3.5, clearly indicate a single
"inter-ring" nOe in each case. As expected, irradiation of the
galactosyl H-1' resonance induces an nOe into the glycosyl H-4 proton
(as well as some intra-ring nOe's), and irradiation of the glucosyl H-1
resonance induces an nOe into the allyl methylene pair, H-1$_A^{''}$ and H-1".
Similar information is obtained from the 2D NOESY experiment, shown as
the contour plot in Fig. II.3.6. The unique inter-ring nOe between H-1'
and H-4 ($\eta_{1'-4}$) is clear, but the nOe into the methylene pair is small
and below the contour level threshold.

Table II.3.1 - Comparison of expected and obtained vicinal ring proton
coupling constants for (A) a β-glucopyranoside, and (B)
β-galactopyranoside ring.

		Expected $\underline{J}$(Hz)[29]	Measured $\underline{J}$(Hz)
A:	(1,2)	7.8	8.0
	(2,3)	9.6	9.9
	(3,4)	8.8	8.9
	(4,5)	9.5	10.4
B:	(1'-2')	7.8	8.1
	(2'-3')	9.8	11.0
	(3'-4')	3.4	3.7
	(4'-5')	1.0	1.7
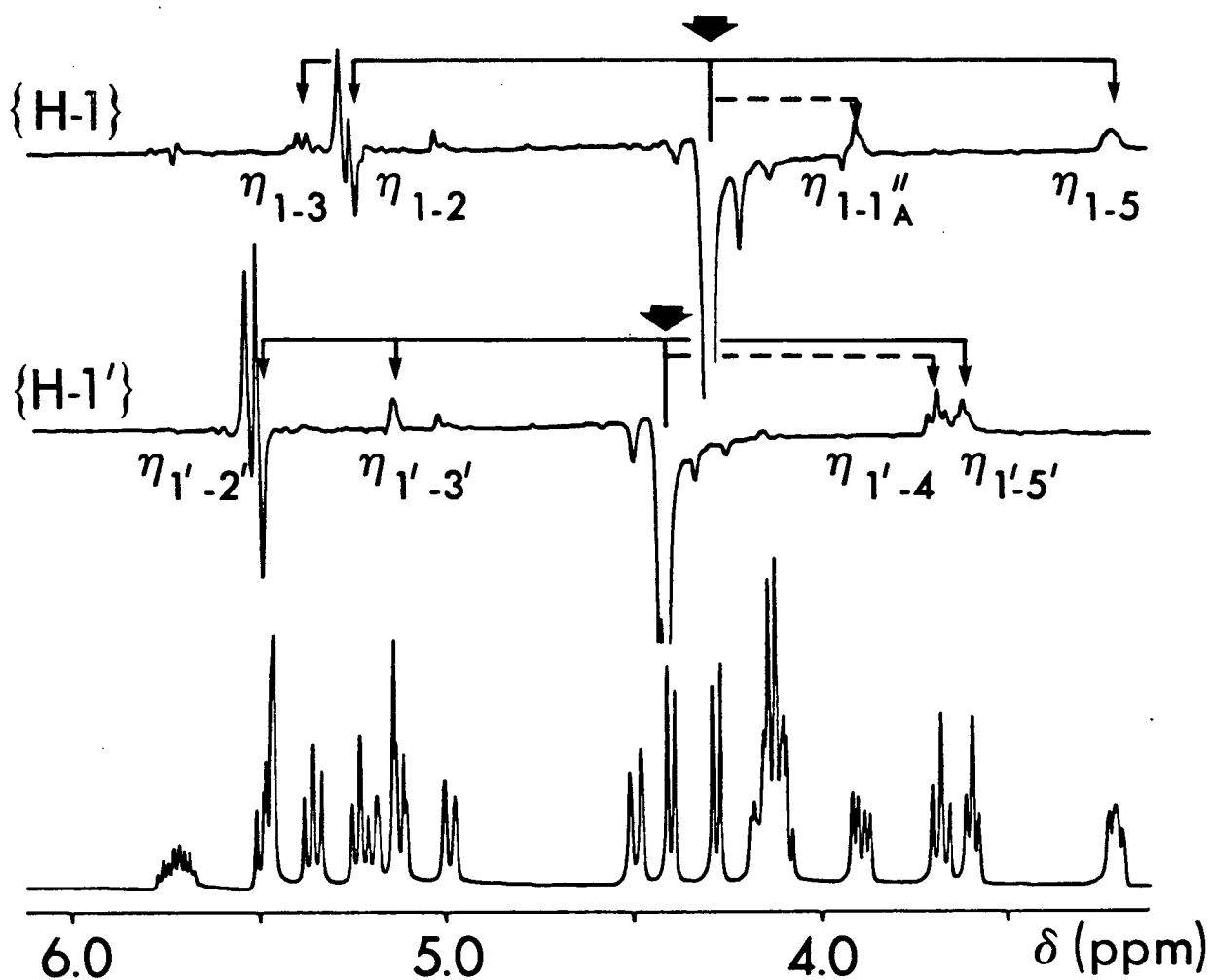
Fig. II.3.5 400 MHz SSNOEDS of 2 (0.2 M in C_6D_6). Intra-ring nOe's are shown with a solid line (——) and inter-ring nOe's with a broken line (---).
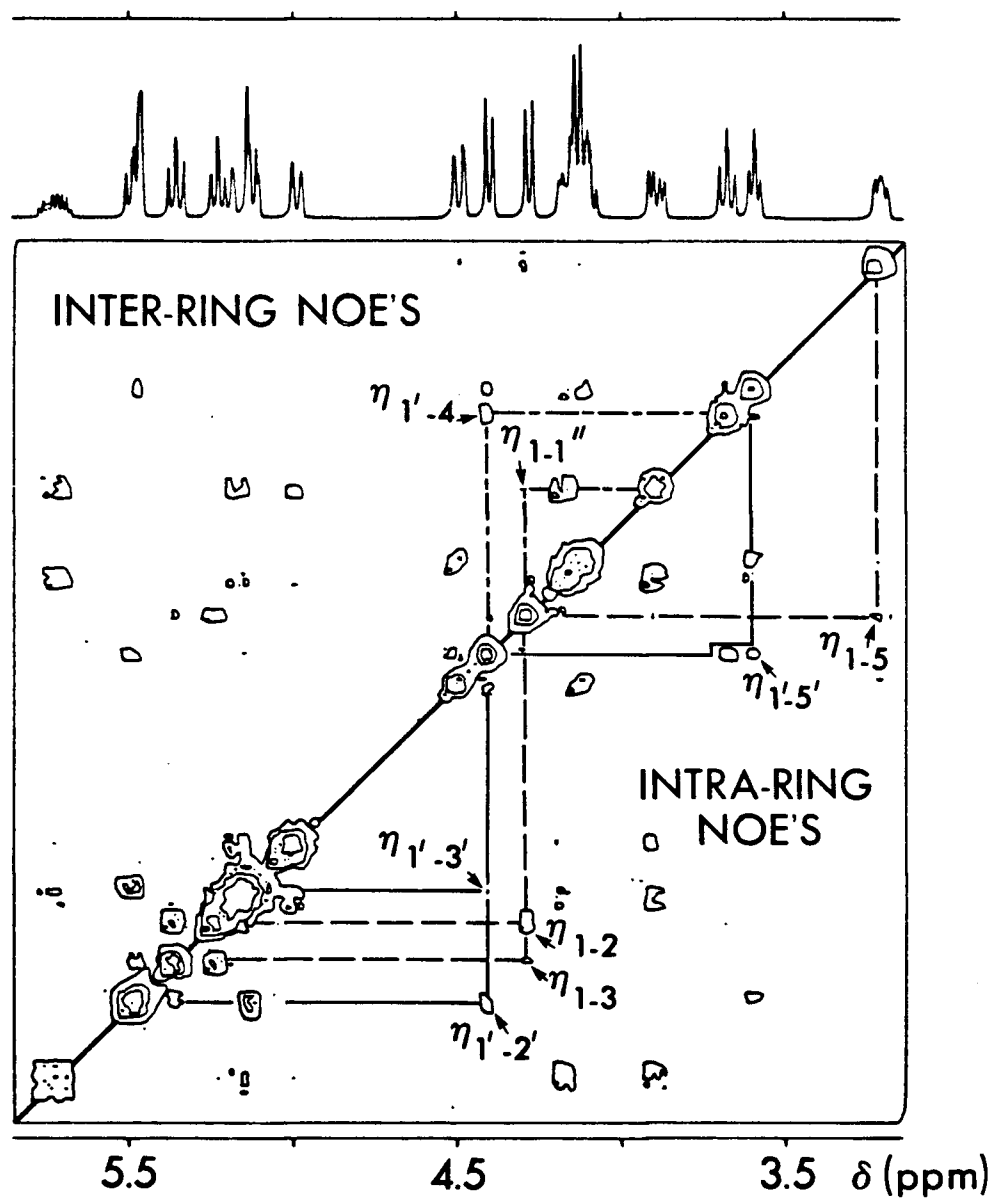
Fig. II.3.6 NOESY of 2 (0.2 M in C_6D_6) at 400 MHz. The mixing time, $\tau_{mix} = 0.\tilde{7}5$ s ± 15%. Intra-ring nOe's for the glucosyl (---) and galactosyl (——) rings are drawn in the bottom right half, and inter-ring (— — ——) in the top left half.
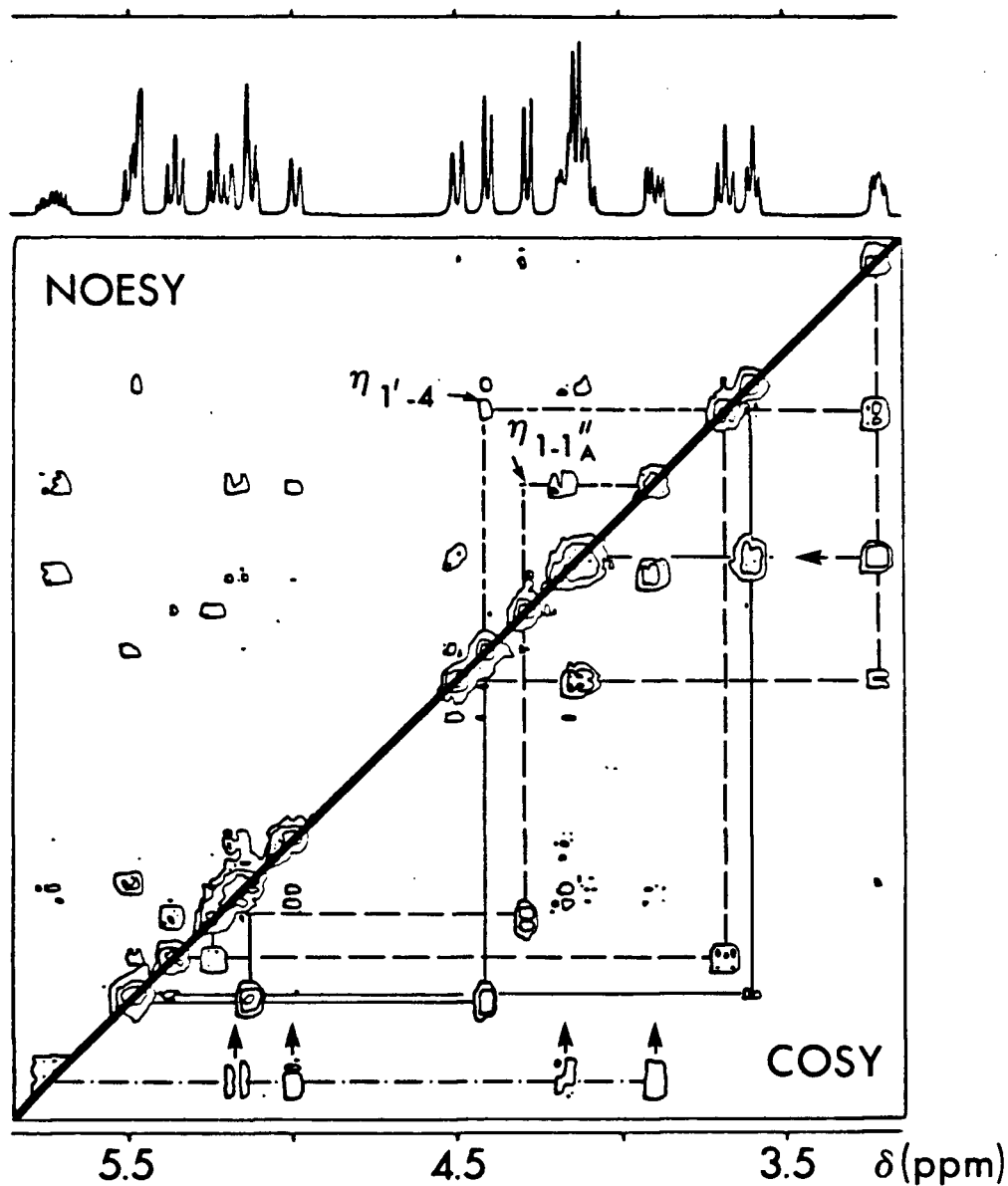
Fig. II.3.7 Combined NOESY (top left) and COSY (bottom right) data
taken from Figs. II.3.4. and II.3.6, respectively.

Since both the COSY and NOESY displays are similar and
symmetrical about the principal diagonal, they can be combined into a
single display[32] which has all the information. This is shown in Fig.
II.3.7.

A number of points warrant discussion. Although this protocol
does not use any new NMR experiments, their integration into this scheme
provides an approach which will find application with many complex
molecules of biological interest. We feel the fact that the approach
has a minimal reliance on reference data will make it applicable to a
wide array of molecules. It is important to note that to the author's
knowledge, no instances in Nature have been reported where sugar rings
exist in unusual conformations - however, if such a situation were to
occur, it would be immediately obvious from the vicinal couplings, and
extra steps could be necessary to resolve such an anomaly.

By restricting the protocol to ^{1}H experiments, demands on sample
should not prove excessive. Both O-methylation and O-acetylation are
efficient reactions. COSY and 2D J-resolved spectroscopy are relatively
easy experiments to set up in that most parameters (delays,
sweep-widths etc.) can be reliably chosen before performing the
experiment and the need of repetition is small; furthermore, neither of
these experiments has demanding signal-to-noise prerequisites. The nOe
experiments demand considerably more machine time. The SSNOEDS
technique requires careful calibration of the decoupler power and
position, and has high signal-to-noise demands; because it is a
"difference" technique, the demands on instrument stability are
unusually high over what may be a period of up to 2 days, if one were

working with extremely small (microgram) quantities. NOESY has, in addition to signal-to-noise demands, a variable - the mixing time, τ_{mix}. As mentioned in Section II.2.5.6, the choice of τ_{mix} depends on the rate at which the molecule is tumbling and nOe build-up occurs. Although not necessary every time a new molecule is encountered, the experimenter may wish to perform some exploratory 1D nOe experiments before venturing into the 2D field. We observed in our experiments a strong nOe between H-1' and H-4, but a weaker one between H-1 and the allyl methylene pair. This is in accord with what might be expected, since the methylene protons will relax one another quite efficiently to the exclusion of "external" contributions. NOESY appeared to fail in this respect, although a cross-section taken at the chemical shift of H-1 (not shown) did show evidence for a small nOe into H-1" and H-1".

There is ample precedent in the literature for using chemical means to improve spectral dispersion. The question of whether or not to derivatize the molecule rests on a number of factors. An ideal situation arises when the "natural" molecule itself gives sharp, well dispersed resonances since, in addition to the information on primary structure, $\underline{T}_1$ or nOe experiments have the potential to yield the desirable secondary structure information. In the event that such data have to be obtained instead from the "derivatized" molecule, it is fact that the extrapolation of any conformational information about the derivatized back to the unprotected material introduces uncertainties. In spite of this, the case for derivatization is still a strong one

because, in addition to the increased spectral dispersion, derivatization of amphipathic molecules can often reduce the tendency of the unprotected molecules to associate in polar solvents to form micelles, thereby decreasing the effective molecular weight and narrowing the lines observed (lengthening T_2).

In the case of oligosaccharides, it is difficult to decide whether the O-acetylated or O-methylated derivative should be chosen for study. If mass spectrometric analyses are planned, the O-methyl derivative will probably have to be made in any case. However, if the parent material bears O-acetate groups, difficulties with O-acetyl migration may arise during the derivatization procedure. Furthermore, since O-methyl groups resonate in the region of interest, the deuterated methyl iodide used for the derivatization should be of the highest isotopic purity obtainable. Experience in this laboratory has shown that full O-acetylation of polysaccharides[33] is non-trivial and demands that conditions be optimised for each substrate.[34] On this basis, O-methylation of polysaccharides may be a more general procedure,[35] but this is not substantiated with experimental evidence.

Since the completion of this study, other groups have found utility for 2D NMR in structural studies on complex oligosaccharides. More recently two dimensional J-resolved spectroscopy and SECSY have been integrated into Dabrowski's studies (vide supra) to allow the extension of the work to a ceramide pentadecasaccharide.[36] Conceptually, resonance frequencies are determined from the 2D J-resolved experiment, and J-connectivities established by taking

sections through the SECSY data-set. Whilst Dabrowski draws attention

to the utility of the 2D experiments, he also cautions they are "...by

no means a panacea for all signal overlap problems...". This is in

agreement with our convictions. Finally, we draw attention to the

broadness of some of the signals (short T_2) which we know to present

problems in spin echo-type 2D experiments (see II.5).

An independent study by Prestegard et al. found utility for the

2D chemical shift - and nOe correlated experiments (SECSY and NOESY) in

the elucidation of primary structure of a glycolipid at 500 MHz.[37] It

is known that cellulose can be "fully" O-acetylated and yield a spectrum

in $CDCl_3$ with discernable vicinal couplings.[38] Gagnaire's group in

France has reported[39] 2D J-resolved spectroscopy on intact and

derivatized polysaccharides. This experiment is not easy to perform,

due to the rapid T_2 relaxation during the refocussing period. We

suggest that such 2D NMR analyses on polysaccharides may be improved by

partial or complete depolymerization either by mild acid hydrolysis[40] or

bacteriophage degradative[41] procedures. If partial depolymerization

yields adequately narrow line-widths, this would be preferable since one

could effectively disregard the terminal reducing sugar unit which would

complicate the analysis of the single repeating oligosaccharide unit.

Bruch and Bruch have also reported[42] the application of 2D

J-resolved spectroscopy to glycopeptides; several broad anomeric signals

responded poorly to the analysis. Patt has described the use of 2D

INADEQUATE[43] to assign the ^{13}C spectra of a monosaccharide[44] and a

disaccharide,[45] but the punitive demands on sample concentration make

the experiment of little more than academic interest in the present context.

One final point on the generality of our sequencing protocol is that we believe it to be extendable to almost any complex molecule consisting of units of coupled spins. Whilst coupling through a peptide bond is measurable at 500 MHz[46] it is still small (^5J=ca. 0.5 Hz) and one can speculate on the application of such technology to oligopeptides.

REFERENCES

1. N. Sharon. Complex carbohydrates - their chemistry, biosynthesis and functions. Addison-Wesley Reading, Mass. 1975.

2. J. Montreuil. Adv. Carb. Chem. Biochem. 37, 157-223 (1980), and references cited therein.

3. G.O. Aspinall and A.M. Stephen. In MTP International reviews of science. Organic chemistry, series one. Edited by G.O. Aspinall. University Park Press, Baltimore, Maryland. 1973. Vol. 7, pp. 285-317.

4. G.G.S. Dutton and E.H. Merrifield. Carbohydr. Res. 105, 189-203 (1982).

5. P.A.J. Gorin. Adv. Carbohydr. Chem. Biochem. 38, 13-104 (1981).

6. R. Barker, H.A. Nunez, P. Rosevear, and A.S. Serianni. Methods Enzymol. 83, 58-69 (1982).

7. R.V. Lemieux, K. Bock, L.T.J. Delbaere, S. Koto, and V.S. Rao. Can. J. Chem. 58, 631-653 (1980).

8. L.O. Sillerud, R.K. Yu, and D.E. Schafer. Biochem. 21, 1260-1271 (1982).

9. J.A. Schwarcz and A.S. Perlin. Can. J. Chem. 50, 3667-3676 (1972).

10. P.R. Rosevear, H.A. Nunez, and R. Barker. Biochem. 21, 1421-1431 (1982).

11. J.F.G. Vliegenthart, H. van Halbeek, and L. Dorland. Pure Appl. Chem. 53, 45-77 (1981), and references therein.

12. J.P. Carver and A.A. Grey. Biochem. 20, 6607-6616 (1981).

13. J-R. Brisson and J.P. Carver. J. Biol. Chem. 257, 11207-11209 (1982).

14. J. Dabrowski, P. Hanfland, and H. Egge. Methods Enzymol. 83, 69-86 (1982), and references therein.

15. J.M. Berry, L.D. Hall, D.G. Welder, and K.F. Wong In Anomeric effect, origins and consequences. Edited by W.A. Szarek and D. Horton. ACS Symposium Series, No. 87. 1979. pp. 30-49.

16. K.F. Wong, Ph.D. Thesis, University of British Columbia (1979), and references therein.

17. L.D. Hall and C.M. Preston. Carbohydr. Res. 29, 522-524 (1973).

18. L.D. Hall and H.D.W. Hill. J. Amer. Chem. Soc. 98, 1269-1270 (1976).

19. See section II.2.4.

20. M. Martin-Lomas and D. Chapman. Chem. Phys. Lipids. 10, 152-164 (1973).

21. K-E. Falk, K-A. Karlsson, and B.E. Samuelsson. Arch. Biochem. Biophys. 192, 191-202 (1979).

22. M.A. Bernstein and L.D. Hall. J. Amer. Chem. Soc. 104, 5553-5555 (1982).

23. V. Horejsi and J. Kocourek. Biochim. Biophys. Acta. 336, 338-343 (1974); H.M. Flowers. Methods Carbohydr. Chem. 6, 474-480 (1972).

24. See section II.2.2.1.

25. See section II.2.3.

26. See section II.2.4.

27. See section II.2.5.2.

28. See section II.2.5.3.

29. C. Altona and C.A.G. Haasnoot. Org. Magn. Reson. 13, 417-429 (1980).

30. See section II.2.5.6.

31. M.L. Wolfrom and A. Thompson. Methods Carbohydr. Chem. 2, 211-215 (1973).

32. K. Nagayama and K. Wüthrich. Eur. J. Biochem. 114, 375-384 (1981).

33. J. Hoffman and B. Lindberg. Methods Carbohydr. Chem. Biochem. 8, 117-122 (1980).

34. K.R. Holme, private communication,

35. H.E. Conrad. Methods Carbohydr. Chem. 7, 361-364 (1972), and references cited therein.

36. J. Dabrowski and P. Hanfland. FEBS Lett. 142, 138-142 (1982).

37. J.H. Prestegard, T.A.W. Koerner, Jr., P.C. Demou, and R.K. Yu. J. Amer. Chem. Soc. 104, 4993-4995 (1982).

38. H. Friebolin, G. Keilich, and E. Siefert. Angew. Chem. Int. Ed. 8, 766-767 (1969).

39. D.Y. Gagnaire, F.R. Taravel, and M.R. Vignon. Macromol. 15, 126-129 (1982).

40. M.L. Wolfram and M.E. Franks. Methods Carbohydr. Chem. 5, 276-280 (1965), and others in the same section.

41. G.G.S. Dutton, J.L. DiFabio, D.M. Leek, E.H. Merrifield, J.R. Nunn, and A.M. Stephen. Carbohydr. Res. 97, 127-138 (1981).

42. R.C. Bruch and M.D. Bruch. J. Biol. Chem. 257, 3409-3414 (1982).

43. A. Bax, T.A. Frenkiel, R. Freeman, and M.H. Levitt. J. Magn. Reson. 43, 478-483 (1981).

44. S.L. Patt, Carbohydr. Res., in press.

45. S.L. Patt, F. Sauriol, and A.S. Perlin. Carbohydr. Res. 197, C1-C4 (1982).

46. H. Kessler, W. Bermel, A. Friedrich, G. Krack, and W.E. Hull. J. Amer. Chem. Soc. 104, 6297-6304 (1982).

CHAPTER II.4

NMR SPECTROSCOPIC ASSIGNMENT OF BRUCINE

Interest in the <u>Strychnos</u> alkaloids, of which strychnine (1) and brucine (2) are members, dates from their isolation in 1819, and 1946 when the correct skeletal structure was finally proposed. Although of "medium" molecular weight, the skeleton is disproportionately complex, having six chiral centres in a 24 atom skeleton. NMR spectroscopists have also been interested in these alkaloids for some time, and the relevant literature is reviewed below.
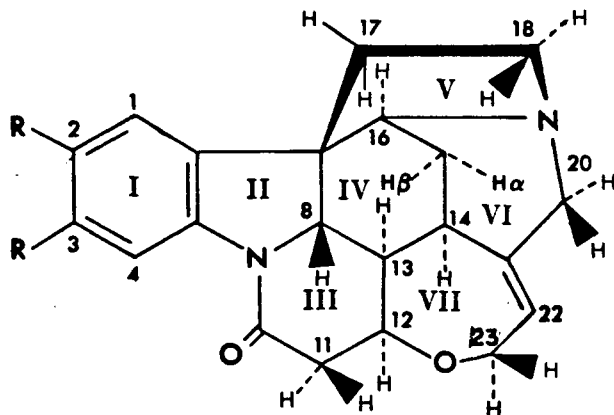
1 : R = H

2 : R = OCH$_3$

The object of the exercise detailed in this chapter is to determine the generality of the NMR methods presented in Chapter II.2, and to determine which is the most expeditious route to the final assignment of the ^{1}H and ^{13}C spectra of complex molecules. An important aspect of this study was an evaluation of the time required to perform the experiments, and optimum ways to integrate data-acquisition and processing. It should be stressed that the experiments were intentionally carried out using the minimum of literature data; thus, only brucine's skeletal structure and configuration, and an early (erroneous) table of ^{13}C chemical-shift assignments[1] was used as reference data. No data that could lead to subtle chemical shift arguments were sought, since the intention was to keep the reliance on such tacks to a minimum. Wherever possible, spectra were acquired under "survey conditions", that is, using the fullest possible sweep-widths in both dimensions for the 2D experiments, with "typical" delays. In this way, an attempt was made to simulate conditions which an "applied" spectroscopist might encounter when analyzing the structure of a molecule for which little or no prior spectroscopic knowledge was available. The questions are: which experiments should be performed, in what order and how much instrument time will they demand?

The considerable body of classical chemistry performed on the Strychnos alkaloids has been reviewed.[2] After uncountable man-hours of degradative analyses by numerous groups the correct skeletal structure was proposed in 1946 by R. Robinson and colleagues.[3] The absolute configuration at the asymmetric centres was determined by X-ray

diffraction analysis,[4] and Woodward succeeded[5] in synthesizing

strychnine in 1954.

The initial NMR spectroscopic interest focussed on the ^{13}C

spectrum, probably because of the complexity of the ^{1}H spectrum at the

field strength of the then common magnets ($\leq$ 100 MHz for ^{1}H). Since the

initial report by Wehrli,[6,7] some considerable controversy has

occurred in the literature over the ^{13}C assignments, which has only

recently reached full consistency.

In 1973, Wehrli described[6] the assignment of the seven

quaternary carbons in brucine. This was based on chemical shift

additivity rules and $\underline{T}_1$ relaxation data. In that the relaxation pathway

is dipolar, quaternary carbons are relaxed by protons on α carbon

atoms. The $\underline{T}_1$'s vary from 2.62 to 11.75 sec. Shortly thereafter,

Wehrli published the complete ^{13}C assignment of brucine.[7] Again, much

attention was focussed on ^{13}C $\underline{T}_1$ relaxation rates. Single frequency

off-resonance decoupling (SFORD) was used to determine ^{13}C

multiplicities and further assignments were based on chemical shift and

residual splitting ($^1\underline{J}_{CH}$) arguments, and comparisons with related

molecules. This assignment was correct, but numerous "reassignments"

were made over the following years. Srinivasan and Lichter,[1] and Singh[8]

et al., followed with some erroneous "reassignments," later summarized

and clarified by Verpoorte[9] and coworkers.[10] Leung and Jones reported[11]

on the ^{13}C NMR spectrum of strychnine, which needed only one

reassignment. Wenkert et al., reported[12] the ^{13}CNMR (and some ^{1}H NMR)

assignments of a number of related alkaloids of this genre, which were

in agreement with Verpoorte.[9] The above workers relied on SFORD to provide the information on the number of attached protons, various derivatives, chemical shift arguments, and (reduced) $^1J_{CH}$ values for their assignments.

Many of the discrepancies between the various assignments can be traced to the data from the SFORD experiment. In the case of an $\{AB\}X$ experiment with a methylene carbon, complexities may arise and this is well documented by Roth and Bauer,[13] using strychnine as an exemplar. Depending on the decoupler position and power, C-15 is seen to show 3 or 4 lines (6 transitions, maximum). Careful analysis can yield $^1J_{AX}$, $^1J_{BX}$ and $^2J_{AB}$. This was extended in Roth's description[14] of NORD (noise-modulated off-resonance decoupling) which is similar in concept and potential information-yield. Difficulties can arise in the interpretation of the SFORD spectrum where lines are crowded; Wehrli has published the SFORD spectrum of brucine,[7] and the complexity is evident.

Martin suggested[15] an extension of Wehrli's T_1 relaxation ideas. In that the relaxation mechanism is predominantly dipole-dipole (even at 1.3 M) and mediated by the directly attached protons, carbons bearing two protons will relax at about twice the rate of those bearing one. Quaternary carbons, as mentioned, relax at a rate proportional to the number of α protons. Methyl carbons do not always conform because they can have additional internal reorientation, but still relax much faster than methine or methylene carbons. These concepts are similar to those presented in II.2.2.1. Additionally, SFORD experiments were

performed with selective excitation of the ^{13}C signals. This is one way around the sometimes misleading {AB}X system discussed above. In this way, Martin was able to correctly determine the multiplicity of each carbon in the molecule, and assign them using the tactics outlined previously.

The 250 MHz ^{1}H NMR spectrum of strychnine was fully assigned by Carter et al. in 1974.[16] Specifically deuterated analogues were prepared and this, in conjunction with double-resonance experiments, spectral simulation and solvent induced shifts, resulted in the total assignment. Wenkert et al. substantiated the assignments with some small modifications[12] - reversal of assignment within each pair of geminal protons at C-15, C-18 and C-20.* Their work was based on conformational arguments using coupling constants; however the results were not compared with solid-state conformational data. Carter et al., made these assignments based on solvent induced shifts. In a proton relaxation study by Colebrook and Hall,[17] the aromatic protons of brucine were assigned. Finally, a ^{1}H nOe study by Bothner-By and co-workers[18] used brucine dissolved in a viscous solvent as a model compound for the driven nOe experiment (See II.2.4.2).

Before presenting the spectroscopic studies of this thesis, a number of points should be reiterated. The majority of the considerable literature detailed above was deliberately consulted post facto, and in

---

*A recent study by Colebrook and co-workers[21] confirms this reassignment, and corrects that of H-17α and β. NOEDS and T_1 measurements, along with spectral simulation were used.

our reasoning, a minimal reliance was made on chemical shift arguments. As the emphasis was on the spectroscopic aspects, access to derivatized materials and data on analogues were also excluded.

The overall strategy chosen was firstly to fully assign the proton NMR spectrum and then use this to assign the non-quaternary signals in the carbon-13 spectrum. The former was achieved primarily using COSY (II.2.5.3.2), with some assistance from 2D J-resolved spectroscopy (II.2.5.2), and 1- and 2-D nOe experiments. With this completed, the ^{13}C NMR spectrum was easily assigned using the CSCM experiment (II.2.5.4), with spectral editing performed using DEPT (II.2.2.2).
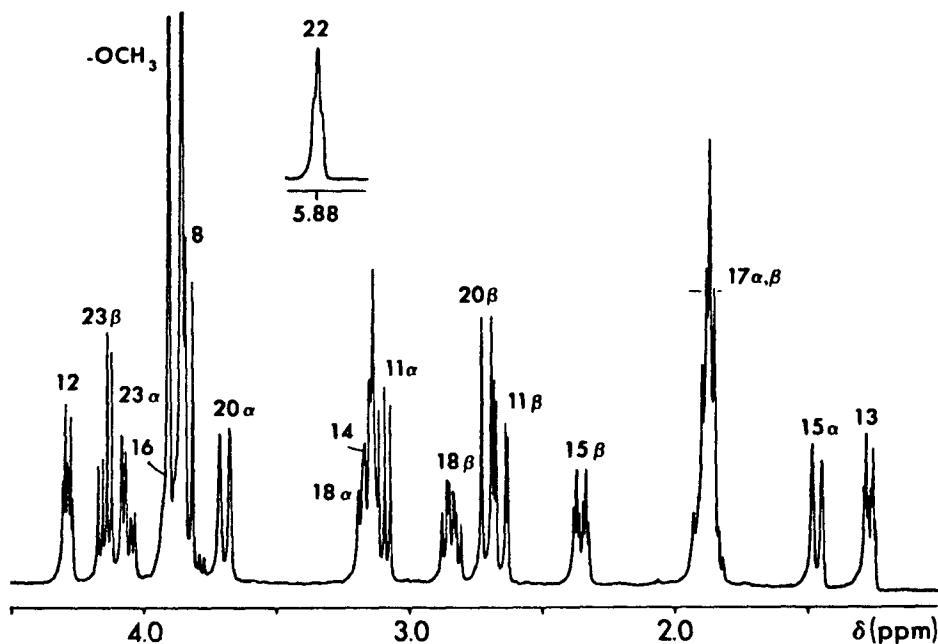
Fig. II.4.1   400 MHz ^{1}NMR spectrum of brucine (ca. 0.02 M in CDCl₃), showing the assignment of non-aromatic protons.

Portions of the ^{1}H NMR spectrum of brucine are presented in Fig. II.4.1. Two singlets in the aromatic region are omitted, and the multiplet in the vinyl region is shown in an inset. Analysis at 360 MHz began with the COSY spectrum. The experiment was performed with coherence transfer echo selection, on a ca. 0.01 M solution in CDCl$_3$. A relaxation delay of only 0.2s, and the minimum of 4 acquisitions per t$_1$ interval meant that 20 min was required for the collection of a 512 * 1K data-set; the sweep-width was 10 ppm in both dimensions. Next, a 2D J-resolved experiment was set up; this experiment required ca. 45 min for collection of the data - this was somewhat longer than that of the COSY due to the necessarily longer relaxation delay and more scans. Whilst these J-resolved data were being collected, the COSY data-set was processed and plotted. At this stage, acquisition of the 2D J-resolved data set was complete, and data processing was performed. All the above operations were performed automatically in a MACRO program on the Nicolet system.* Minimal operator intervention was required, except at the plotting stage, where decisions were made to expand certain spectral regions. Details of the "survey-condition" parameters are in Table II.4.1.

The COSY spectrum of brucine is shown in Fig. II.4.2. Only the region between δ4.5 and 1.0 is plotted here, for the sake of clarity. The analysis began with the realization that four "pockets" of coupled spins exist in the molecule, with little or no coupling between them

---

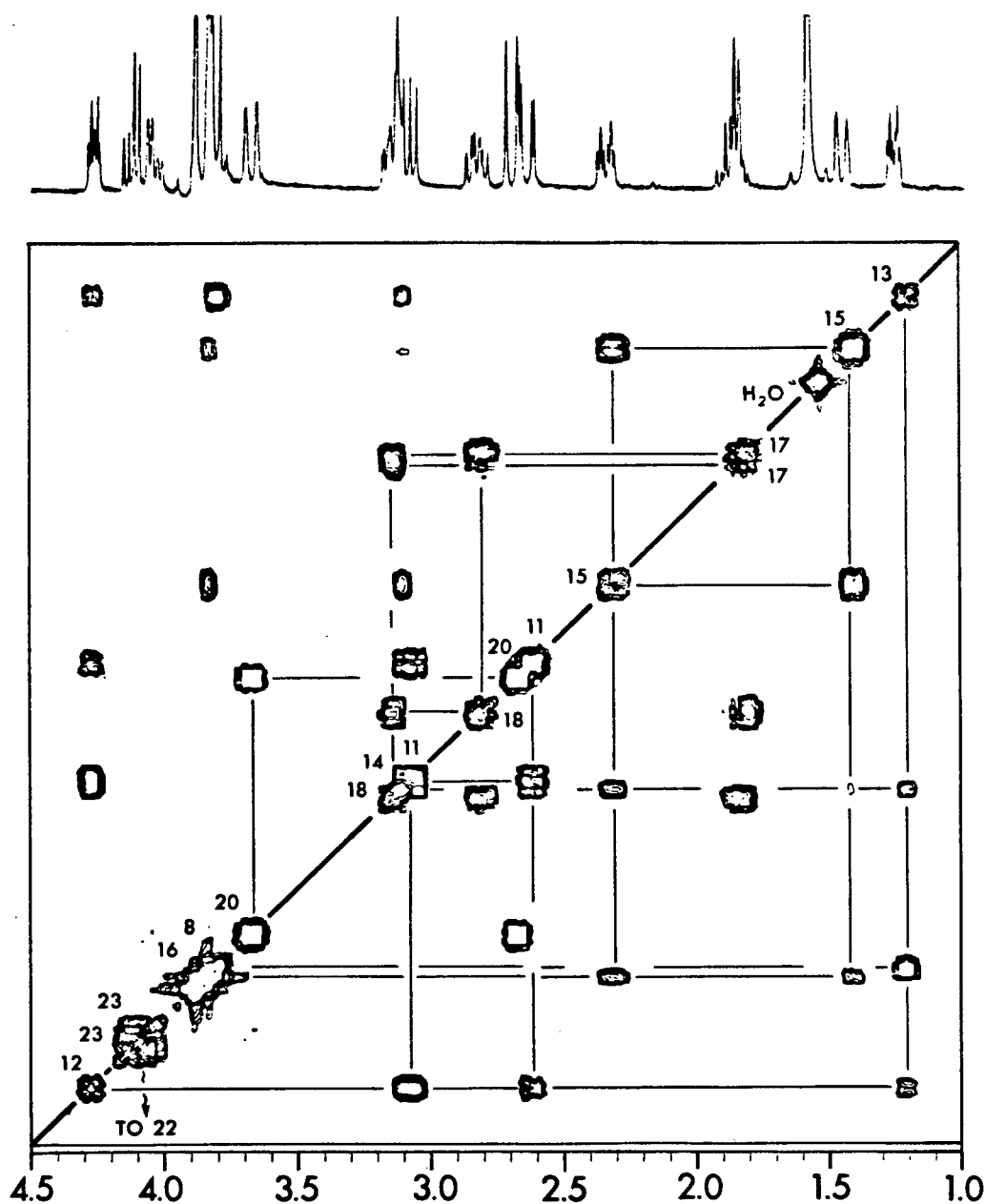*All 360 MHz experiments were performed at Nicolet Magnetics Corp., Fremont, Ca. USA.

Fig. II.4.2   360 MHz COSY spectrum of brucine in the region
between δ 4.5 and 1.0.   Connectivities to the
vinylic proton are indicated, though they are
not on the diagram.

Table II.4.1. Parameters used in automated "survey conditions" collection and processing of ^{1}H COSY and 2D J-resolved experiments at 360 MHz. [a]Full sweep-width (Hz). [b]Block-sizes (words). [c]Relaxation delay (s). [d]Apodization function: EM = exponential multiplier; DM = double exponential multiplier; MS = sinebell multiplier. With the J-resolved experiment, the strongest resolution enhancement function is chosen for t_2 which the signal-to-noise permits. [e]Symmetrization was not possible with the 2D J-resolved data, but would be recommended.

Total Time (min)		Sweep Width[a]		Block Size[b]		Relax Delay[c]	No. Scans Per t_1	Apodization[d]		Zero-fill t_1?	Symm.[e]
		F_2	F_1	F_2	F_1			t_1	t_2		
–	Collect 1D spectrum			16K							
–	Calibrate pulse widths										
0	Begin collecting COSY data	3,600	3,600	1,024	512	0.2	4				
20	Begin collecting 2D	3,600	29	4,096	64	1.0	16				
–	Process and plot COSY							MS	MS	No	Yes
65	Commence processing and plotting of 2D J-resolved experiment							EM DM MS	DM MS	Yes	No
120	END										

(cf. II.3):namely (a) H-20α and H-20β, (b) H-17α, H-17β, H-18α and

H-18β, (c) H-22, H-23α and H-23β, and (d) H-11α, H-11β, H-12, H-13, H-8,

H-14, H-15α, H-15β and H-16. COSY succeeded in assigning all 18 of

these protons, although it was not possible at this stage to

differentiate α from β geminal protons.* The connectivities are

indicated along with the assignments in the Figure; these were made

without ambiguity. The large −OCH$_3$ peaks which resonate very close to

H-8 and H-16 could have hindered the assignment had H-8 and H-16 been

scalar coupled as they might then have obscured a set of cross−peaks;

this was not the case. Special considerations were required for the

tightly coupled geminal protons, which were assigned to the H-23 and

H-17 pairs. Distortion of peak intensities indicated tight coupling,

especially in the case of the H-17 pair. To assess the reliability of

the COSY spectrum, it is interesting to consider H-15β (ca. δ 1.4),

which shows one large splitting and several smaller ($\leq$ 1.5 Hz) ones. In

the COSY spectrum, the expected three connectivities are clear, even

though the digitization is less than 7 Hz per point.

The 2D J−resolved experiment did not prove very useful and these

data are not included here. It would have been particularly useful in

the −OCH$_3$ signal region. However, the overlapping H-16 resonance

remained obscured by the familiar "tailing" in F$_1$ from the intense −OCH$_3$

singlets. The partial J−spectrum of the hidden H-18 resonance was not

---

*The molecule is not planar and hence, an upper (β) and lower
(α) face is not clear. For this reason, geminal protons are defined
(See 1 and 2) for the purpose of this study.

useful, since it suffered from the same virtual coupling effects as the other H-18 resonance at δ 2.83, making the extraction of accurate coupling constant data impossible without spectral simulation. (The geminal H-17 protons, to which they are vicinal, are tightly coupled).

The assignment of the aromatic, geminal and O-methyl protons was now sought. The solid-state conformation as determined by X-ray crystallography was used to build a molecular model having the correct configuration. This was found to be a rigid structure, suggesting that the solution conformation might be very similar to that in the solid-state. The experiments required to complete these ^{1}H assignments also served to corroborate this postulated solution conformation.

In the determination of conformation, techniques relying on "through-space" phenomena (e.g. $\underline{T}_1$, nOe) prove very useful, often in conjunction with (through-bond) coupling-constant information. Axial protons take on unusual importance in an nOe experiment. The 1,3 diaxial interaction provides important information in a six-membered ring, and with a boat conformation, the "flagpole" protons are close to one another in spite of their being 5 bonds removed; an nOe experiment will also detect this.

The SSNOEDS results are presented in Fig. II.4.3. No special effort was made to optimise the experiment and the data were collected in approximately three hours. A single decoupler power setting was used (which resulted in 40-80% saturation, depending on the total multiplet width). In all cases a check was made for decoupler power leakage into
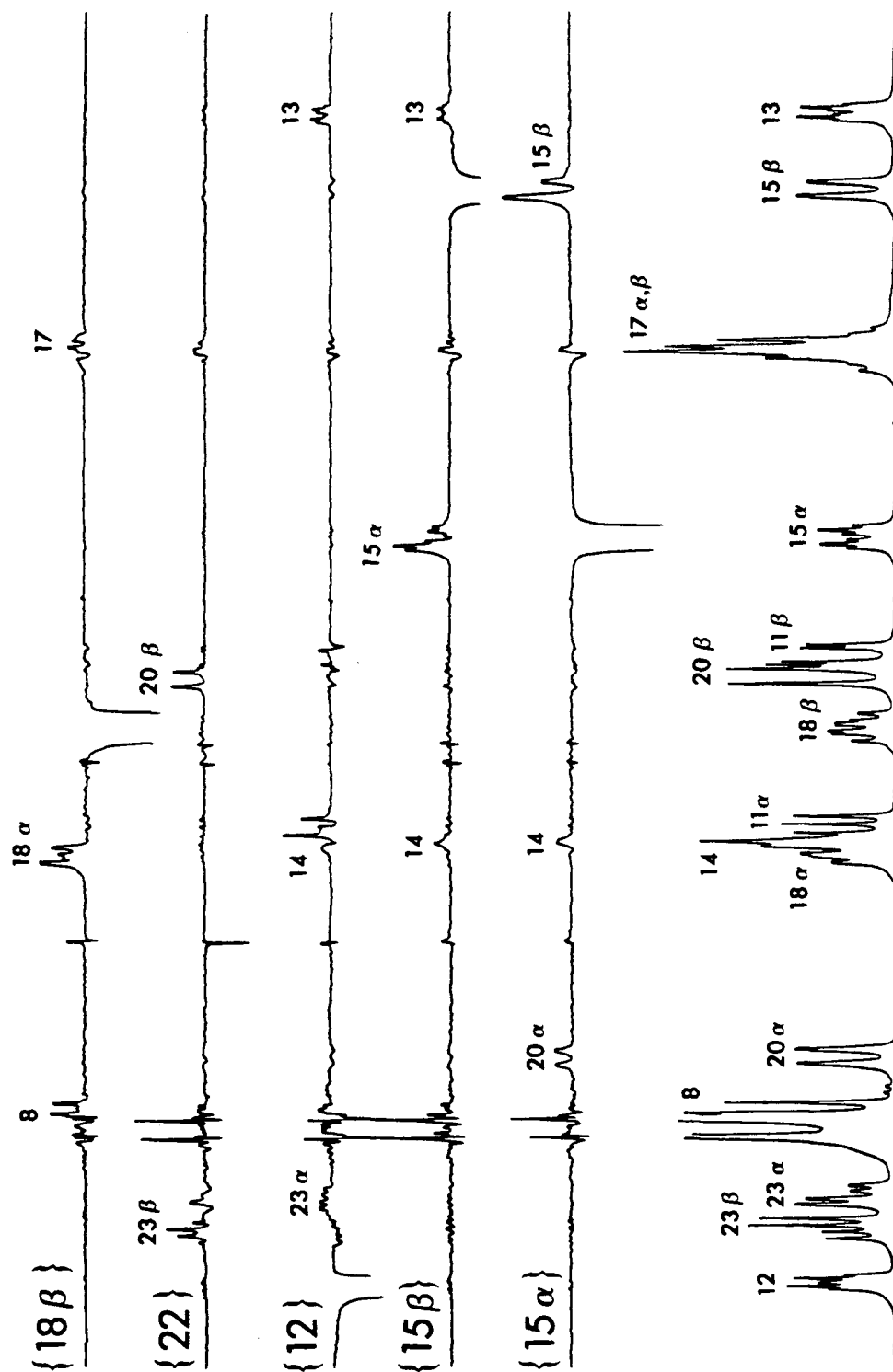
Fig. II.4.3. SSNOEDS experiments performed on brucine at 400 MHz.

neighbouring resonances ("spillover"), and was found to be absent. The irradiation time was set at 0.5 s*, and the experiments "interleaved" by collecting scans in blocks of 16, repeated 30 times.

Let us consider ring IV, which is in a chair conformation in the solid-state (Fig. II.4.4.A). Evidence for this also being so in solution comes from a consideration of coupling-constants, and nOe experiments. $\underline{J}$ (8, 13) = 10.5 Hz, which indicates a trans or cis arrangement of the two protons. In keeping with the chair conformation, H-14 and H-16 are judged to be roughly co-planar since $\underline{J}$ (14, 15α) ≈ $\underline{J}$ (16, 15α), and $\underline{J}$ (14, 15β) ≈ $\underline{J}$ (16, 15β).** Strong confirmatory evidence for the proposed conformation comes from the SSNOEDS experiment where H-15 (δ 1.46) was irradiated, inducing an nOe in H-13; the two protons must assume axial orientations in a ring having a chair conformation, and the irradiated proton is accordingly assigned to H-15β. Irradiation of the higher-field of the two H-18 protons induced an nOe in H-8, thereby identifying the proton irradiated as H-18β and H-8 to be axial, as depicted in Fig. II.4.4A.

Consider now ring VI. Since the H-20 protons have no vicinal neighbours, no conformational information can be sought from arguments based on vicinal coupling-constnts. The nOe experiment where H-15α was

---

This is far less than the time usually used for nOe build-up (ca. 3 T_1), and was chosen to minimize the experimental acquisition time and "three spin effects", without jeopardizing the observation of "direct" interactions.

**The H-15 protons are assigned here to allow the reader to check the statement with the reported data in Table II.4.2, but the absolute assignment of the H-15 protons is not necessary at this stage.
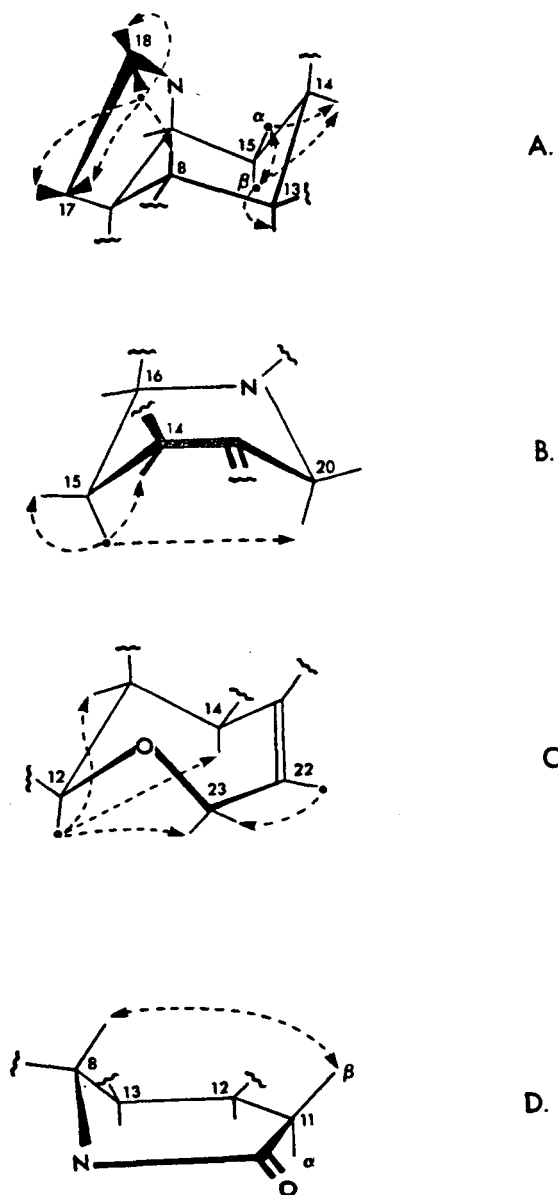
Fig. II.4.4 Conformations of rings IV and V (A), VI (B), VII (C)
and III (D) in brucine, indicating some of the results
from the SSNOEDS experiments. The irradiated proton is
indicated with (•) and nOe's (---).

irradiated induced a strong nOe in the lower-field of the two H-20 resonances. This confirms the approximate "boat" conformation of this ring (Fig. II.4.4.B), which places the "flagpole" protons, H-15α and H-20α, close to one another; this is a "bowsprit-flagpole" interaction. Hence, this single experiment confirms the expected conformation of ring VI, and identifies H-20α (and H-20β, by default).

The analysis of ring VII was complicated somewhat by the fact that it is a seven-membered ring, with a double bond and ring hetero-atom.* Two nOe experiments were performed to support the structure shown in Fig. II.4.4C. Irradiation of the vinylic H-22 induced an nOe into the pseudo-equatorial proton H-23β, the lower-field of the two H-23 protons. Additionally, an nOe is induced in H-20β. Although not depicted in this diagram, H-22 and H-20β are close to one another and this confirms the assignment of the geminal H-20 protons based on the irradiation of H-15α. Irradiation of H-12 induced an nOe into other axial or axial-like protons: H-14 and H-23α.** The assignment of the H-23 protons is now confirmed.

The conformational analysis of ring III is more complex. Here the H-11α and H-11β protons must be assigned. The molecular model favours a boat-like conformation. A pure boat conformation would make H-12 and H-11β _trans_ diaxial, and one would anticipate a large vicinal coupling constant here on the basis of the Karplus relationship; using

---

*This is a tetrahydrooxepin ring.

**Here, a negative nOe is induced in H-23 β due to the "three-spin effect".

this argument, the lower field of the two H-11 protons would be assigned to H-11β. The geminal coupling constant $\underline{J}$ (11α, 11β) is, at 17.4 Hz, unusually large. This suggests that the carbonyl on C-10 roughly bisects the angle between the geminal protons and C-11,[19] and this would not be the case if ring III were to be in the pure boat conformation considered above. Satisfying the condition of the relationship between the carbonyl and geminal protons "flattens" one end of the boat, placing N-9, C-10, C-11, C-12 and C-13 approximately co-planar. In this situation H-12 and H-11α have a small dihedral angle (ca. 10°), and, hence, a large vicinal coupling constant would be anticipated. This argument assigns the lower field of the two H-11 protons as H-11β - a reversal of assignment. It is clear that in both cases H-8 and H-11β are close in space, and an nOe experiment would not suffer from these ambiguities. The H-11 protons could be assigned, and on this basis the ring conformation determined from the coupling-constant arguments.

The SSNOEDS experiment (vide supra) was not possible here, since all three protons - H-8, H-11α and H-11β - overlap with other resonances, precluding irradiation selectivity. A 2D NOESY experiment was performed, and the data are given in Figs. II.4.5 and .6.* Fig. II.4.5 shows the NOESY spectrum over the entire spectral width, and Fig.II.4.6 shows the high-field portion of this data in more detail; we concentrate on the latter, for the moment. Before searching for the

---

*Here, the principal diagonal runs from the top left-hand corner to the bottom right; a mirror image of the displays previously shown, but entirely analogous.
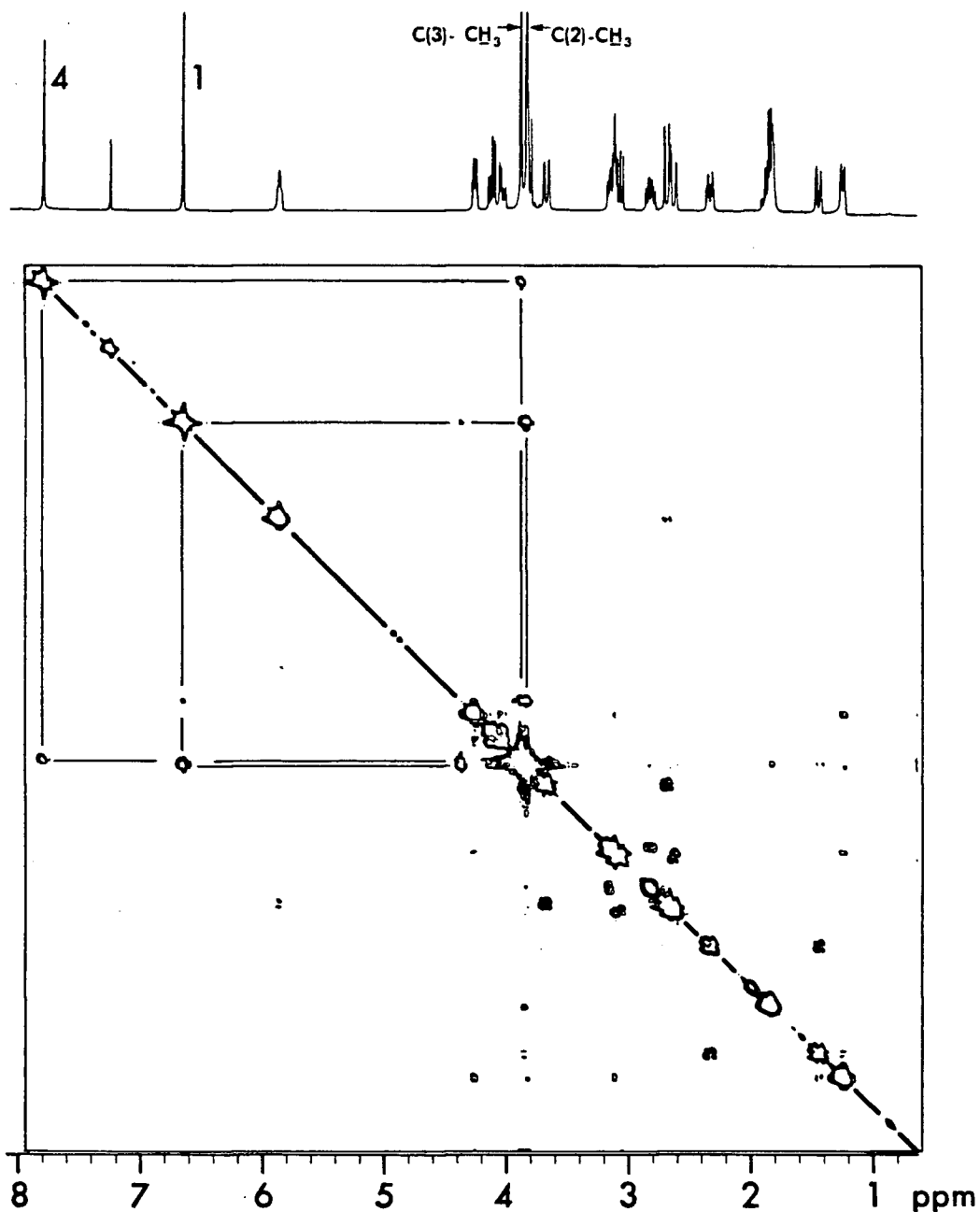
Fig. II.4.5 400 MHz NOESY spectrum of brucine. The 256 * 1K
data-matrix was collected in ca. 8 h, with relaxation
delay 3.0 s, mixing time 0.6 s ± 10% and 32 scans per
t_1 interval. The data were processed and plotted
using a Nicolet 1280 computer and Zeta 8 recorder.
The final digitization was 5.8 Hz pt^{-1} in both
dimensions, after zero-filling F_1; the "sinebell"
multiplier was used in both dimensions, and magnitude
spectra calculated.

Fig. II.4.6 The high-field region of the NOESY plot in Fig. II.4.5

8-11β nOe, it is worth checking the experiment by looking for the nOe's determined previously using SSNOEDS. These are all clearly discernable and are indicated in the upper h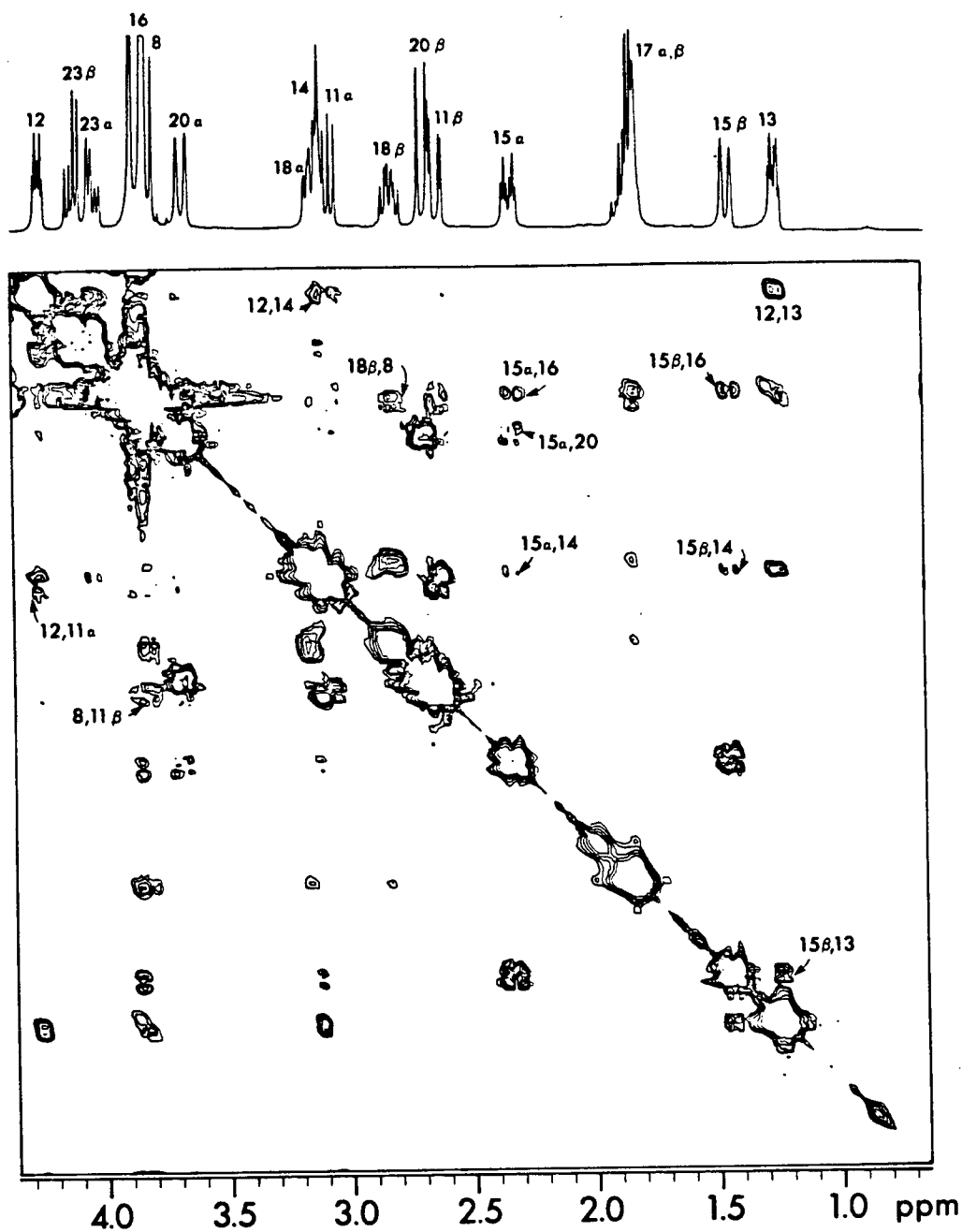alf of Fig. II.4.6. A number of nOe's with H-16 are clear here which were not in the 1D experiments, as a result of being obscured by subtraction errors with the overlapping sharp O-CH₃ singlets.

The 8-11β nOe correlation is discernable, assigning H-11β as the higher field of the H-11 resonances. This is in accord with the second argument above using vicinal and geminal J-coupling magnitudes and suggests a boat-like conformation, flattened at C-11 (See Fig. II.4.4.D). This is confirmed by the observation of a larger nOe between H-12 and H-11α than H-12 and H-11β.

The NOESY spectrum also provides the means for the assignment of the aromatic and O-methyl signals. The relaxation of H-4 must be dominated by the O-CH₃ protons on C-3, and H-1 by those on C-2. H-1 has additional relaxation contributions from H-16 and H-17α. Fig. II.4.5 shows the nOe between the aromatic and the O-methyl protons. Correlations between an aromatic proton and protons on ring V are below the contour threshold; slices taken at each aromatic proton's chemical shift (not shown) identify the higher field of the two aromatic resonances as that of H-1, by the above reasoning. The nOe with H-17 is not clear, as it overlaps with the strong correlation to the O-methyl resonance. Further, the O-methyl resonances are easily assigned; the higher field of the two singlets corresponds to the O-methyl on C-2 and the lower field to that on C-3.

Table II.4.2 Summarized ^{1}H NMR chemical shift assignments and coupling constants of brucine in CDCl$_3$ (ca. 0.02 M). ^{a}strong coupling. ^{b}Coupling pattern complicated by virtual coupling.

Proton	δ (ppm)	J (Hz)
1	6.66	-
4	7.80	-
8	3.83	(8-18) = 10.5
11α	3.09	(11α, 11β) = 17.4 (11α, 12) = 8.5
11β	2.64	(11β, 12) = 3.3
12	4.27	(12,13) = 3.3
13	1.26	(13, 14) = 3.2
14	3.14	(14, 15α) = 4.0 (14, 15 β) = 1.0
15α	2.34	(15α, 15β) = 14.2 (15α, 16) = ca. 4.9
15β	1.46	(15β, 16) = 2.1
16	3.9	
17α, β^a	1.9, 1.8	(17α, 17β) = ca. 12.0
18α^b	3.15	
18β^b	2.83	
20α	3.68	(20α, 20β) = 14.8 (20α, 22) = 1.6
20β	2.70	
23α	4.05	(23α, 23β) = 13.8 (23α, 22) = 6.3
23β	4.13	(23β, 22) = 6.9
(C-2)-OCH$_3$	3.85	-
(C-3)-OCH$_3$	3.89	-

The final assignments of the ^{1}H NMR spectrum of brucine are compiled in Table II.4.2. These data are in complete accord with those of Wenkert et al., for strychnine.[12]

We have seen that the COSY experiment was sufficient to perform the bulk of the analysis of the ^{1}H NMR spectrum of brucine. The 1D and 2D nOe experiments assigned individual geminal protons and provided valuable conformational information.

Now, the ^{13}C spectrum was analysed. A ca. 0.3 M solution of brucine in $CDCl_3$:CD_3OD (10:1) was prepared. First, the number of protons attached to each carbon was determined using DEPT. This might have been redundant because a CSCM experiment was planned; however in this case not all methylene protons had very different chemical shifts (vide infra). The CSCM experiment required 45-60 min. for data collection. The CSCM spectrum of the interesting regions of δ_C 22-80 and δ_H 1.0-4.5 is shown in Fig. II.4.7. (All assignments outside this region are unambiguous). The DEPT information is included. Knowing the proton assignments, the indicated carbon assignments were made. In only two cases was there any uncertainty. H-8 and H-16 resonate very close to one another making the assignment of the carbon signals around δ 59 difficult. The carbon signals around δ 41 are very close and insufficiently digitized in this case. Hence, C-11 and C-16 cannot be distinguished.

No attempt was made to assign quaternary carbons since this would not fall within the scope of the present design protocol. The data from the CSCM is compared with that of Srinivasan and Lichter[1] -
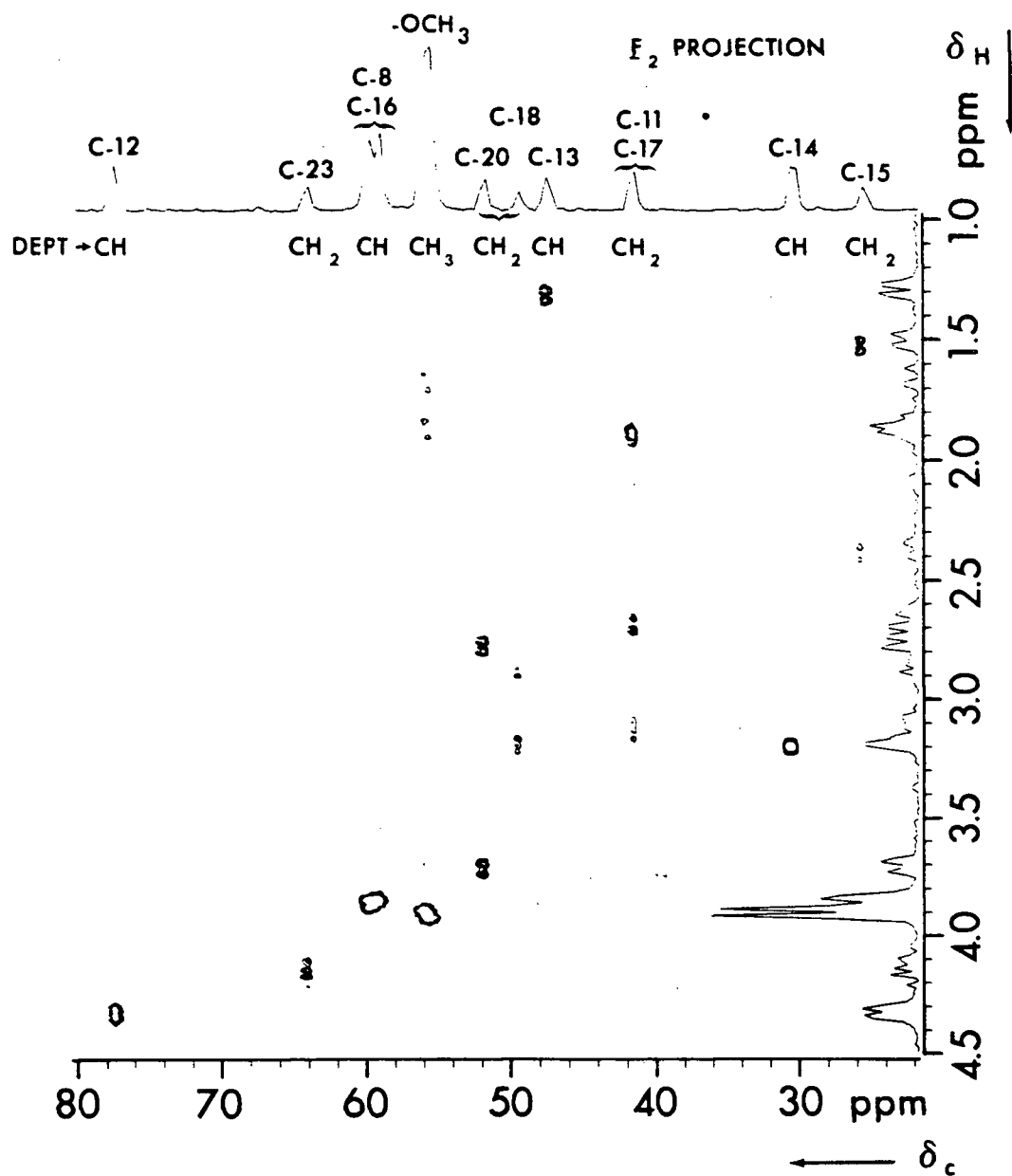
Fig. II.4.7 360 MHz (^{1}H) CSCM experiment with brucine (ca. 0.3 M
in C_6D_6/CD_3OD, 10:1). δ_C 22–80 and δ_H 1.0–4.5 is
plotted in the contour mode. F_1 and F_2 projections
are on the abcissa and ordinate, respectively.

Table II.4.3 Table of assigned ^{13}C chemical shifts for brucine, compared with the literature. Chemical shifts are referenced to the central transition of CDCl$_3$ (δ 77.0). The solution was <u>ca.</u> 0.3 <u>M</u> in CDCl$_3$:CD$_3$OD (10:1) and the instrument a Bruker WH-400, operating at 100.6 MHz for ^{13}C. [a,b]may be interchanged.

Carbon	Ref. 1	Ref. 10	This Study
1	105.78	105.7	106.4
4	101.00	101.1	101.5
8	59.84	60.3	60.2[a]
11	50.09	42.3	42.2[b]
12	77.64	77.8	77.5
13	48.18	48.3	48.1
14	31.50	31.5	31.4
15	26.73	26.8	26.5
16	60.28	59.9	59.6[a]
17	42.28	42.3	41.9[b]
18	52.57	50.1	49.9
20	42.28	52.7	52.4
22	127.14	127.2	127.6
23	64.47	64.6	64.4
OCH$_3$	56.43; 56.08	56.4; 56.2	56.6; 56.0

that referred to whilst the work was in progress - and the now accepted assignments of Verpoorte.[9] Our data are in complete agreement with the latter.

Several conclusions can be drawn from this study. First, only modest amounts of spectrometer time are necessary for the partial assignment of the ^{1}H NMR spectrum of a medium sized molecule such as brucine; in this case a total of ca. 2 hours for the 2D J-resolved and COSY experiments and an additional 3-8 hours for the complete spectroscopic and conformational assignment. Additional conformational information, plus the assignment of individual geminal protons results from nOe experiments. Where the selective irradiation experiments can be performed, the SSNOEDS experiment is probably the most expeditious route. In the case of signal overlap, the 2D NOESY experiment will provide all the necessary information in a single experiment, but with greater demands on spectrometer time. This investment of time is offset by the fact that all possible nOe experiments are "simultaneously" performed, resulting in a high return being realized in terms of information yield.

With the proton spectrum assigned at least to the point before nOe experiments are performed, non-quaternary sites in the ^{13}C NMR spectrum can be routinely assigned providing their resonances are not too close (ca. > 1ppm) and the attached proton resonances are not badly overlapping.

We believe that the 2D J-resolved and COSY experimental data can be collected and processed in a highly efficient, integrated fashion,

with the prior knowledge of the chemical system. NOe data might require some educated guess-work in the selection of an irradiation time (SSNOEDS experiment) or the mixing time (NOESY), or a series of exploratory experiments could be performed. All the experiments described in this chapter provided the required information from the data collected the first time it was performed.

Hurd[20] has independently reported on the utility of the combination of COSY with the CSCM experiment. It is advantageous to use a ^{13}C probe to measure both the ^{13}C and ^{1}H spectra, the latter _via_ the ^{1}H decoupler coil. In this way the COSY assignment (and NOESY, if required) is for the molecule at the same concentration as for the CSCM experiment and no time is expended changing probes. This approach has the further merit that if it were possible to automate changeover of the probe circuits, it would be possible to automate the acquisition and processing of all ^{1}H and ^{13}C data into a simple (overnight) run. Given its high efficiency, it seems probable that the mode of analysis described in this chapter will find a place in organic structural investigations which warrant more than a few, unrelated NMR measurements.

REFERENCES

1. P.R. Srinivasan and R.L. Lichter. Org. Magn. Reson. 8, 198-201 (1976).

2. G.F. Smith. The alkaloids. Edited by R.H.F. Manske. Academic Press, New York, Vol. 8, 1965, pp. 591-671.

3. L.H. Briggs, H.T. Openshaw, and R. Robinson. J. Chem. Soc. 903-908 (1946), and others in the series.

4. A.F. Peerdeman. Acta Cryst. 9, 842 (1956).

5. Ref. 2, pp. 642-647, and references therein.

6. F.W. Wehrli. J. Chem. Soc. Chem. Commun. 379-380 (1973).

7. F.W. Wehrli. Adv. Mol. Relaxation Processes. 6, 139-151 (1974).

8. S.P. Singh, V.I. Stenberg, S.S. Parmar, and S.A. Farnum. J. Pharm. Sci. 68, 89-92 (1979).

9. R. Verpoorte. J. Pharm. Sci. 69, 865-867 (1980).

10. R. Verpoorte, P.J. Hylands, and N.G. Bisset. Org. Magn. Reson. 9, 567-571 (1977).

11. J. Leung and A.J. Jones. Org. Magn. Reson. 9, 333-337 (1977).

12. E. Wenkert, H.T.A. Cheung, H.E. Gottieb, M.C. Koch, A. Rabaron, and M.M. Plat. J. Org. Chem. 43, 1099-1105 (1978).

13. K. Roth and H. Bauer. Org. Magn. Reson. 15, 331-332 (1981).

14. K. Roth. J. Magn. Reson. 42, 132-140 (1981).

15. G.E. Martin. J. Pharm. Sci. 70, 81-84 (1981).

16. J.C. Carter, G.W. Luther, III, and T.C. Long. J. Magn. Reson. 15, 122-131 (1974).

17. L.D. Colebrook and L.D. Hall. Can. J. Chem. 58, 2016-2023 (1980).

18. N.M. Szeverenyl, A.A. Bothner-By, and R. Bittner. J. Phys. Chem. 84, 2880-2883 (1980).

19. R.R. Fraser and B.F. Raby. J. Amer. Chem. Soc. 94, 3458-3463 (1972).

20. R.E. Hurd. Relaxation Times, January 1982. An in-house publication of Nicolet Magnetic Corp., Fremont, California, U.S.A.

21. W.J. Chazin, J.T. Edward, and L.D. Colebrook. Submitted for publication.

CHAPTER II.5

DIGOXIN

The studies on oligosaccharide sequencing (Ch. II.3) and brucine (Ch. II.4) suggested to us that the NMR spectroscopic methods detailed in Ch. II.2 are effective for molecules which tumble rapidly in solution. These encouraging results prompted us to see if specific problems might be associated with the analysis of NMR spectra of more complex, higher molecular weight molecules.

Our laboratory's experience with carbohydrates and steroids led us to the naturally occurring steroidal glycosides.[1] Of the extensive group of such plant natural products,[2] we chose digoxin (1) - first isolated from the leaves of <u>Digitalis lanata</u> by Smith[3] in 1930. The molecule is of more than academic interest due to its important pharmacological place as the most frequently prescribed digitalis steroid for heart congestion therapy.

1
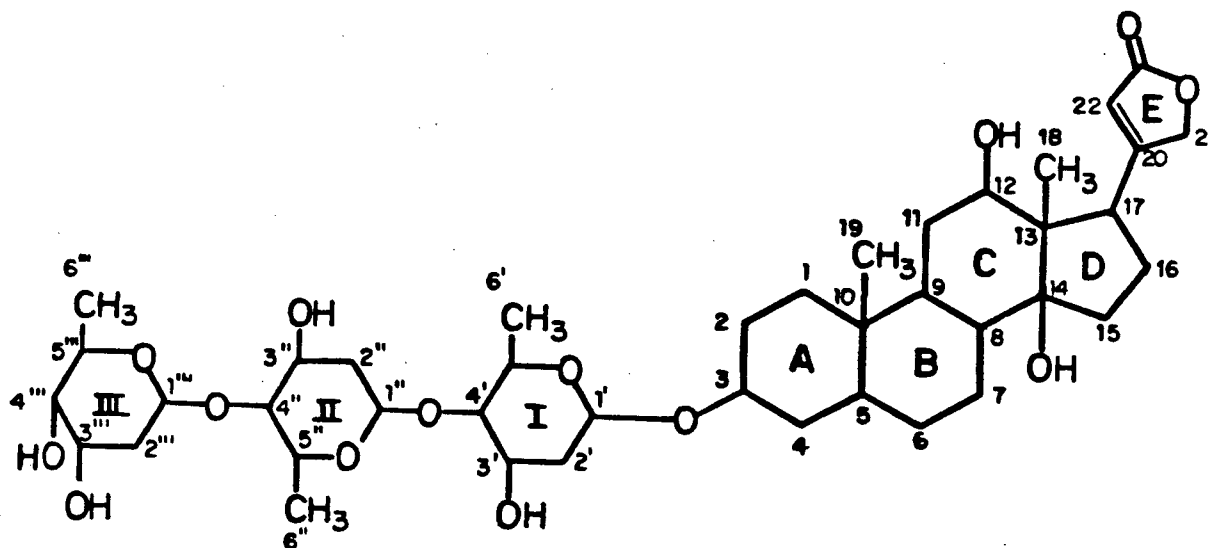
The molecule is highly complex. The glycone consists of three β-D-digitoxose units, identically linked (1 → 4). From the NMR viewpoint one could anticipate in advance of any experiment, that this molecule poses some stringent tests. Thus, the steroid moiety (viz. digoxigenin) is substituted by hetero-atoms at only three positions (C-3, C-12 and C-14), which implies that only a few steroid protons will resonate outside the "methylene hump". (It is advantageous to have as many steroid protons deshielded from this region as possible, since they are of tremendous assistance in assignment). Furthermore, digoxin is amphipathic and would be expected to aggregate (form micelles) in polar solvents such as DMSO (which is one of the few good solvents for digoxin). This would increase the effective molecular weight, adding to the already broader lines resulting from the high monomer molecular mass of 780 ($C_{41}H_{64}O_{14}$). Owing to the higher viscosity of DMSO (cf. $CDCl_3$), molecules dissolved therein are expected to display broader lines, even in the absence of molecular aggregation.

All ^{1}H NMR investigations* were performed at 500 MHz, and ^{13}C at 90 MHz (360 MHz for ^{1}H), using Nicolet spectrometers. As in previous chapters, reliance on chemical shift arguments was kept to a minimum, and little chemical derivatization was performed. Our goals were to assign as many of the ^{1}H and ^{13}C resonances as possible, draw conformational conclusions and, most importantly, determine the limits

---

*The findings of this chapter resulted from a collaborative study with Dr. R.E. Hurd of Nicolet Magnetics Corp., Fremont, Ca. U.S.A.

of the procedures hitherto extensively relied upon. If an experiment

were to fail, could a shift in emphasis make up for this?

The proton NMR spectrum was investigated first using the

procedures found useful in Chaps. II.3 and II.4. As the assignments

progressed, the emphasis was allowed to find its balance; the chapter is

presented largely chronologically.

The digitoxose rings have the $^4\underline{C}_1$ conformation, with the $-CH_3$

substituents equatorial. The conformation of the glycoside and genin

are depicted below.
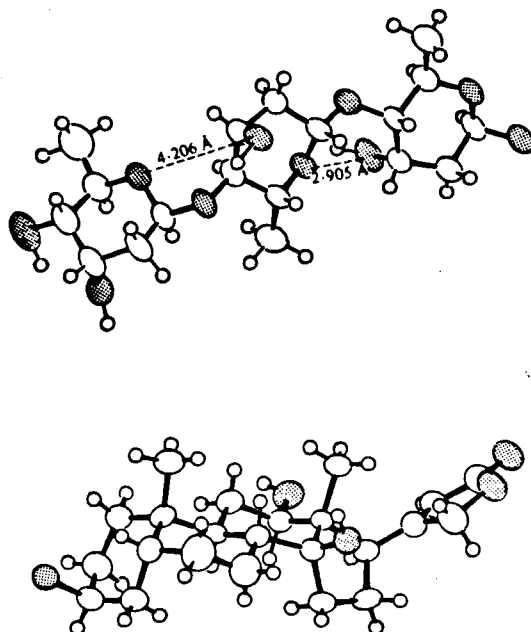

Fig. II.5.1 Solid-state conformations of digoxigenin (lower)
and the digoxin glycone (upper). (From Go et al.[4]).
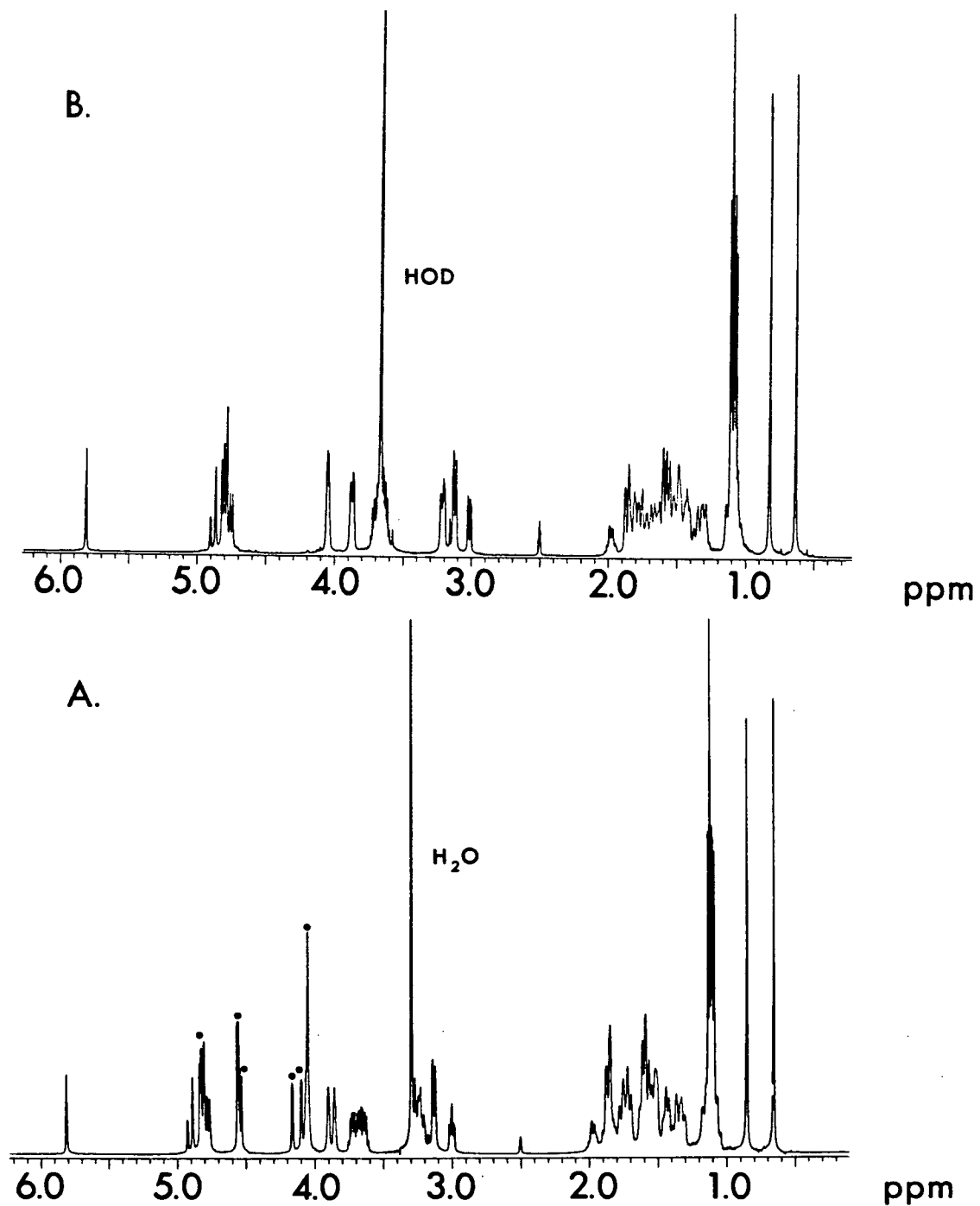
Fig. II.5.2 A. 500 MHz ^{1}H NMR spectrum of digoxin in DMSO-$\underline{d}_6$.
B. Same molecule following a D_2O exchange. Hydroxy protons are marked (•) in A.

A solution of 19 mg digoxin in 0.4 ml DMSO-d_6 was used throughout the ^{1}H NMR studies. Some line-narrowing was induced by heating the sample to ca. 70°C and allowing to cool to room temperature. We assume that this treatment results in the molecules forming a more homogeneous solution. The spectrum reveals a low-field region with relatively sharp, overlapping lines, whereas those in the the methylene region appear broader and little detail is evident. This line-width (T_2) phenomenon can be postulated to result from micelle formation, with the lipophilic steroid moieties in the aggregated phase, and solvated, more mobile, pendant sugars. If this were the case, of the sugar rings one would expect ring III to have the greatest mobility, and ring I the least; conclusions to support this hypothesis appear later.

The original spectrum in DMSO-d_6 required some simplification, and a D_2O exchange was performed. The spectrum of the parent compound is shown in Fig. II.5.2 A with the -OH resonances marked (•), and that of the -OD compound shown in Fig. II.5.2 B; the latter was used for all subsequent studies.

At the outset, the probable vicinal coupling constants for the digitoxose groups were estimated,[5] and these are listed in Table II.5.1.

Protons	Expected $\underline{J}$ (Hz)
(1,2a)	10.0
(1,2e)	2.5
(2a,3)	2.6
(2e,3)	3.1 - 3.6
(3,4)	2.6 - 3.1
(4,5)	9.3 - 9.6
(5,6)	6.2

Table II.5.1 Expected $^3\underline{J}$ values for a β-digitoxose sugar residue.

These data enabled a surprising number of assignments to be made by direct inspection of the spectrum. We concentrate first on the region corresponding to δ > 2, where twelve carbohydrate and six steroidal protons are expected to resonate. Five groups of resonances can be distinguished in this region, and these are shown expanded in Fig. II.5.3 (after resolution enhancement with a double-exponential time-domain filter). "Ladder" assignments indicate the resonances which require assignment.*

On the basis of its chemical shift, we assign the most low-field proton (δ 5.81) to H-22 on ring E of the steroid, which has a small (1.83 Hz) long-range coupling to the geminal H-21 protons. Inspection of the region δ 4.92 - 4.72 (Fig. II.5.3. B) reveals, amongst other resonances, the AB portion of an ABX system; a large (geminal) coupling

---

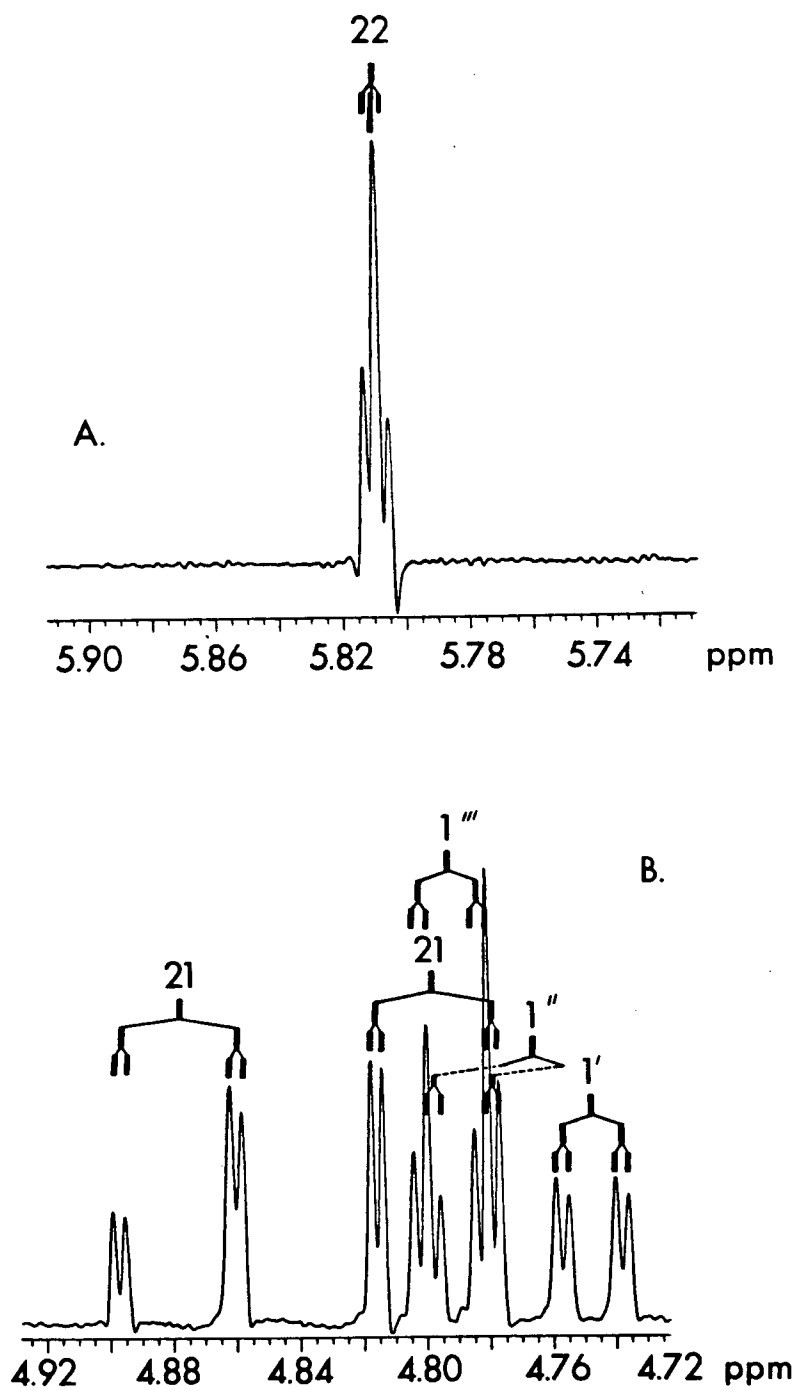*The final assignments are included, for reference later in the chapter.

Fig. II.5.3 Expansions of the low-field region of the 500 MHz
^{1}H NMR spectrum of digoxin in DMSO-$\underline{d}_6$, with a drop
of D_2O added.
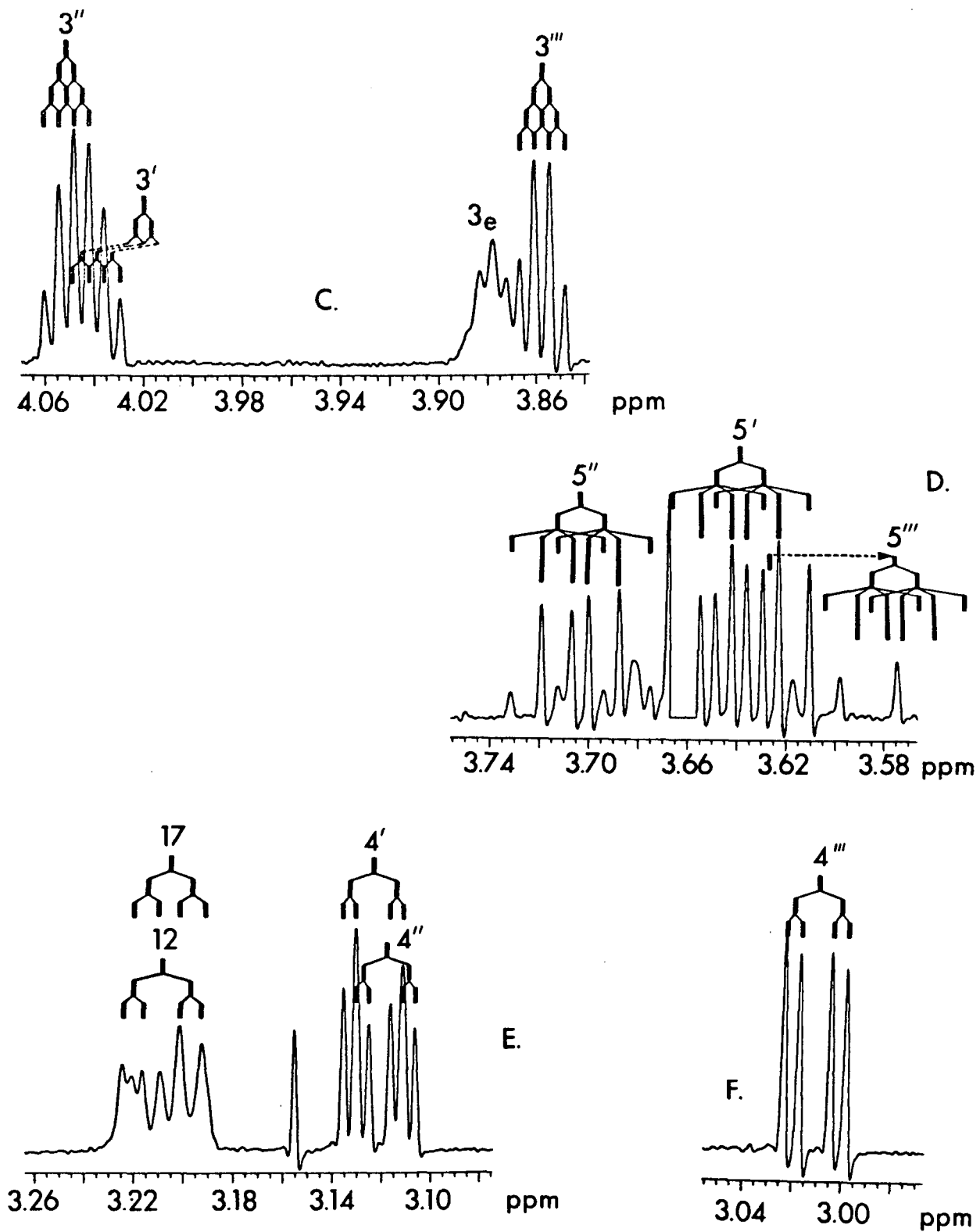
Fig. II.5.3 cont.

constant $\underline{J}$ (A,B) is indicated by the intensity build-up and direct measurement. The smaller coupling constant matches that in H-22. Accordingly, these protons are assigned to the geminal H-21 protons.

Further "general" assignments of digitoxose protons may be made on the basis of a comparison of vicinal coupling constants (Table II.5.1) and the simplification effected by O-deuteration. Based on the magnitude of their two coupling constants to the geminal H-2 protons, three sets of anomeric protons are distinguishable in Fig. II.5.3 B. Between δ 4.07 and 3.84 (Fig. II.5.3 C) the almost identical digitoxose H-3 resonances occur. This is based on their three very similar coupling constants (giving rise to a coupling pattern resembling a quartet) and their simplification upon O-deuteration (data not shown). By virtue of their unique coupling to the methyl groups, the digitoxose H-5 protons can be identified to resonate between δ 3.74 and 3.57 (Fig. II.5.3 D)* Fig. II.5.3 E and F show the digitoxose H-4 protons, identified by matching coupling constants and comparison with data in Table II.5.1. Two other protons resonate in this region and, by default, must be steroidal in origin. The proton at δ3.01 can be assigned to H-4''', as ring III is the only digitoxose residue having an exchangeable hydroxyl proton at position 4 and this agrees with the results of the deuterium exchange experiment. Thus, the simple procedure of matching spectral splittings and a deuterium exchange

―――――――――――――

*The HOD peak at δ 3.66 has been eliminated by presaturation.

experiment led to significant steps being taken in the assignment of the "low-field" region of the spectrum ($\delta > 2$).

The above assignments were made on the underivatized material, and encouraged us to proceed with a full assignment of the spectrum. Although this was in apparent conflict with the conclusions of Chap. II.3, the temptation to proceed with this assignment was strong since any conformational deductions would be of considerable interest.

A proton 2D J-resolved experiment was performed in an attempt to unravel the high-field methylene/methine resonances (24 protons extensively overlapping between $\delta 1$ and 2.1). Unfortunately this failed to produce useful information for the high-field region due to the protons' short T_2's (See Discussion in II.2.5.2). With this experiment, most of the transverse magnetization had relaxed beyond the point of detection after only six or seven experimental increments ($t_1/2$) had been performed. Some data were extractable for the resonances of the low-field region, but these provided no additional information over what had been gained by straight inspection of the 500 MHz ^{1}H NMR spectrum. We believe this to be the first report of the failure of the 2D J-resolved experiment. Attempts to improve the efficacy of this experiment included the use of a much larger than necessary sweep-width in the J-dimension, to shorten $\Delta t_1/2$ and, hence, improve the digitization of the initial portion of the interferogram. Also, the experiment was attempted at elevated temperature (60°C) in an effort to lengthen T_2's; both attempts were to no avail.

Next the COSY experiment (II.2.5.3.1) was performed to establish proton coupling connectivities. (SECSY was avoided as it is a spin-echo experiment and would be expected to suffer similar limitations to those described for the 2D $\underline{J}$-resolved experiment). A contour plot of the COSY spectrum of the deuterium exchanged digoxin is shown in Fig. II.5.4. Aside from a confirmation of assignment for the lactone, ring E, not much is clear until we consider expansions of the two regions indicated. Between δ 4.2 and 2.8 the digitoxose 3,4 and 5 protons resonate, and the COSY plot for this region is given in Fig. II.5.5. With H-4''' previously assigned, H-3''' and H-5''' are readily assigned as the most high-field resonances in each group of resonances. The lowest field of the carbohydrate H-4 resonances is coupled to the lowest field of the H-5 resonances, but these cannot yet be unambiguously assigned to H-4' and H-5', or H-4'' and H-5''. The connectivities do not distinguish H-3' from H-3''.

Next, the connectivities into, and out of, the high-field region are considered in Fig. II.5.6. With H-3''' assigned, H-2$_e$'' and H-2$_a$'' and H-2''' can be identified in the overlapping high field region, and these lead in turn to the assignment of H-1''', which lies between H-1' and H-1''. The highest field anomeric proton (which we later assign to H-1') has two clear correlations into the methylene region, and those protons are coupled to the highest field of the carbohydrate H-3 protons (H-3'). Similarly, the anomeric proton at lowest-field is on the same ring as the low-field carbohydrate 3 proton (H-3''). Hence, we have now
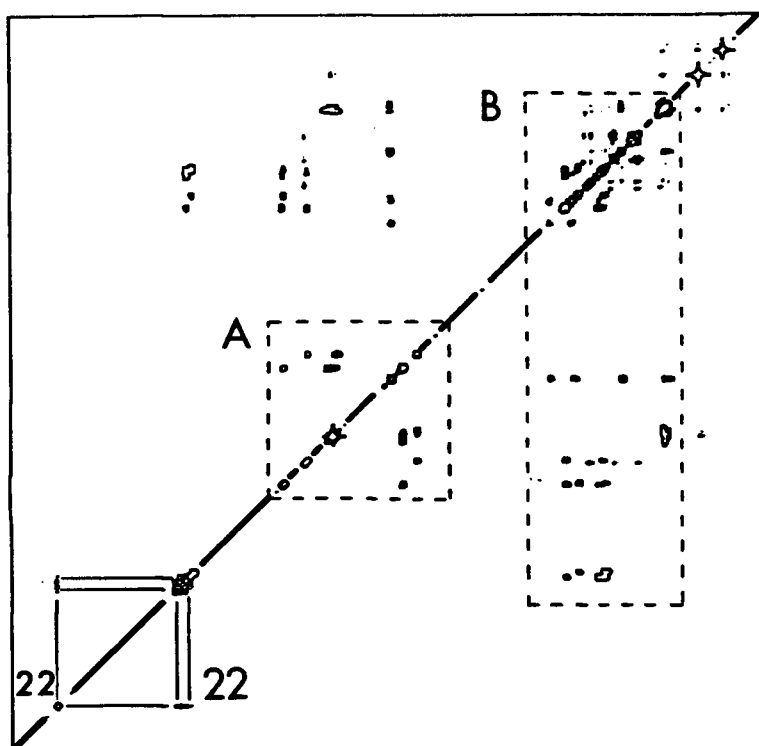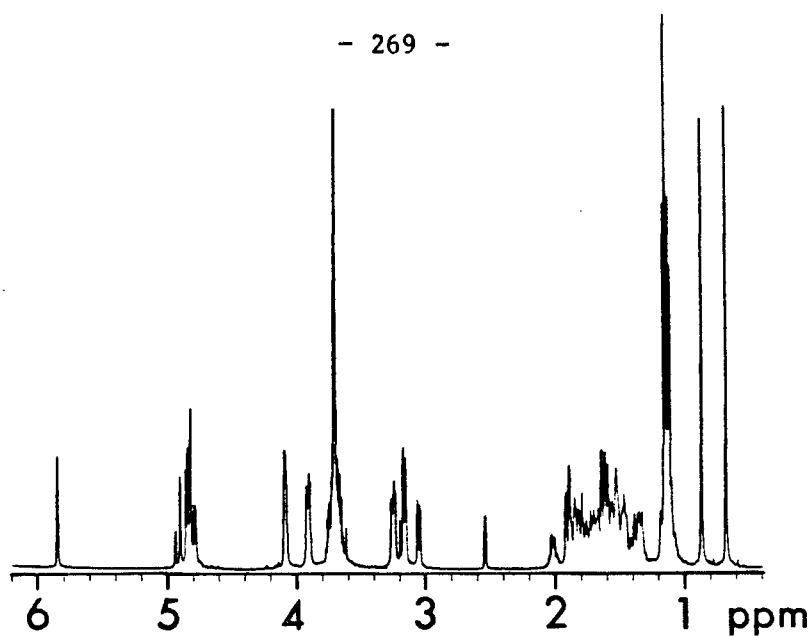
Fig. II.5.4   500 MHz COSY spectrum of digoxin (1) in DMSO-d$_6$,

after deuterium exchange. The HOD signal was
suppressed by preirradiation, and the 512 * 1024 word
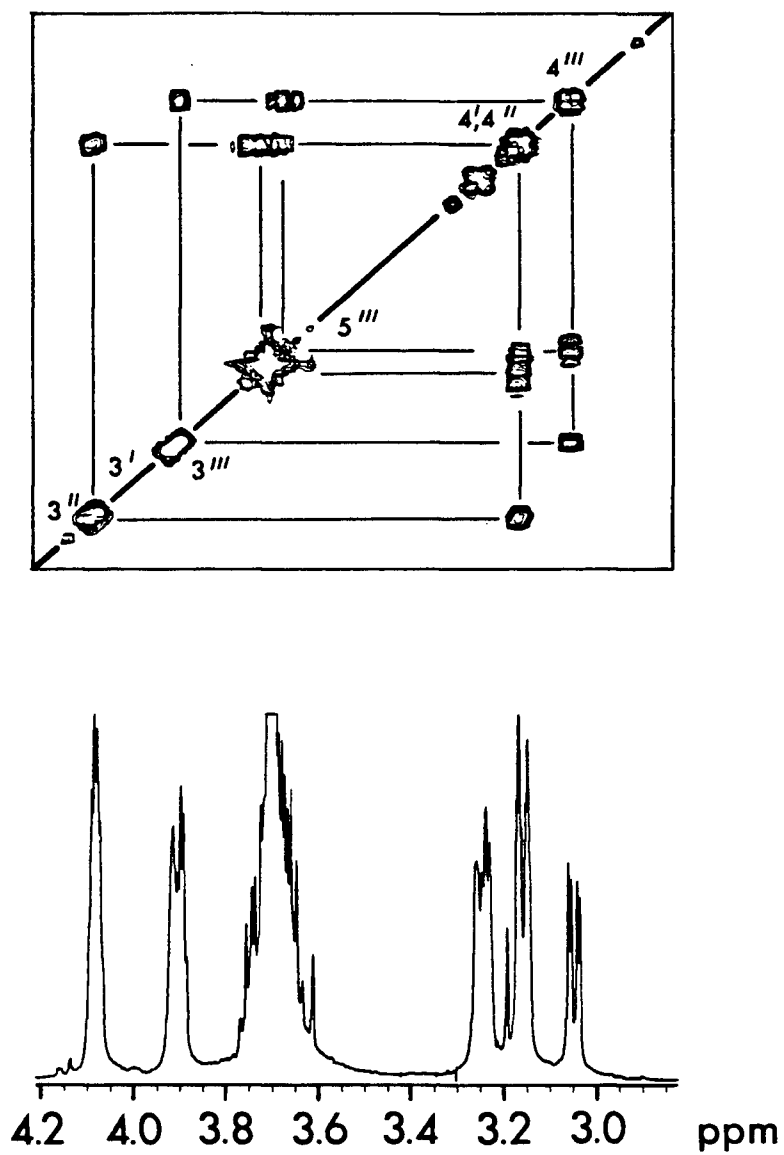data set symmetrized prior to display in the contour
mode.

Fig. II.5.5 Expansion of region A in Fig. II.5.4.
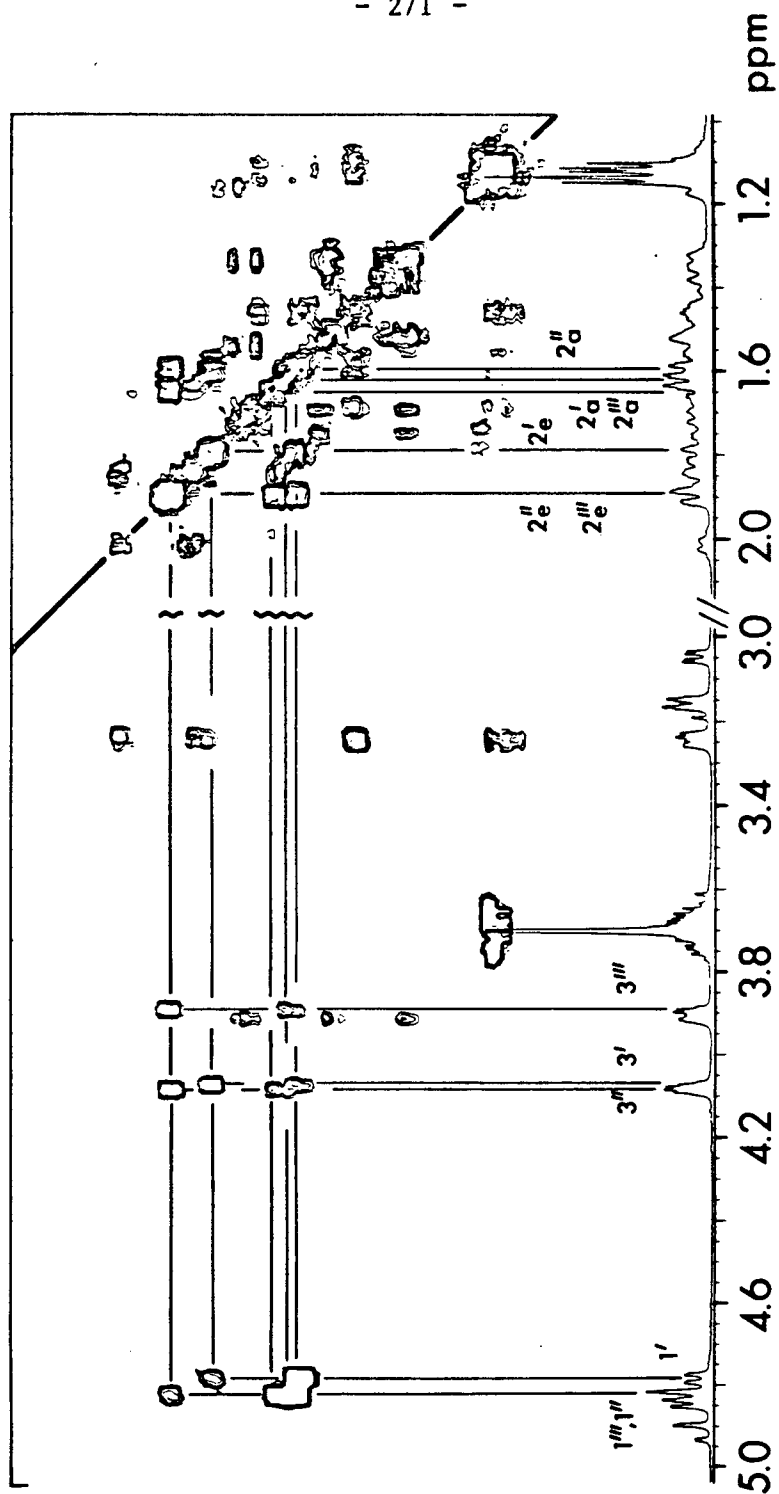
Fig. II.5.6. Expansion of region B in Fig. II.5.4.

determined all connectivities of the ring protons of the digitoxose units I and II, but we cannot assign a particular set of resonances to either unit.

Connectivities between the carbohydrate methyl-groups and the H-5 protons are present, but unassignable due to extensive cross-peak overlap. Similarly, couplings between the steroid protons (H-3, H-12 and H-17) and the methylene/methine region are evident, but not fully assignable. The H-12 and H-17 resonances are each expected to have two correlations, and H-3, four. The resonance at δ 3.88 cannot be either H-12 or H-17 and must, by default, be H-3$_e$. However, only three correlations are clear, and the fourth must either be below the contour threshold or overlap with another cross-peak.

The next stage of the assignment involved a series of "driven nOe" experiments (II.2.4.3); these proved pivotal in the differentiation of ring I and ring II protons, and several steroidal protons. It turns out that the molecule is in the spin-diffusion régime and all observed nOe's were strong and negative. The highest field anomeric proton is sufficiently far from the other two that it could be irradiated with reasonable selectivity. This induced a strong inter-ring nOe into the steroid proton at δ 3.88 (data not shown) which was thereby assigned as H-3. Since only H-1' is expected to induce an nOe into a steroid proton, this assignment provided confirmation of the assignment of H-3; numerous other nOe's were induced in the aliphatic region - presumably into the H-2 and H-4 protons. With this second critical assignment (the first being H-4''''), H-2$_e'$, H-2$_a'$, H-3', H-4' and and H-5' may be identified from the COSY connectivities. Since these resonances, and
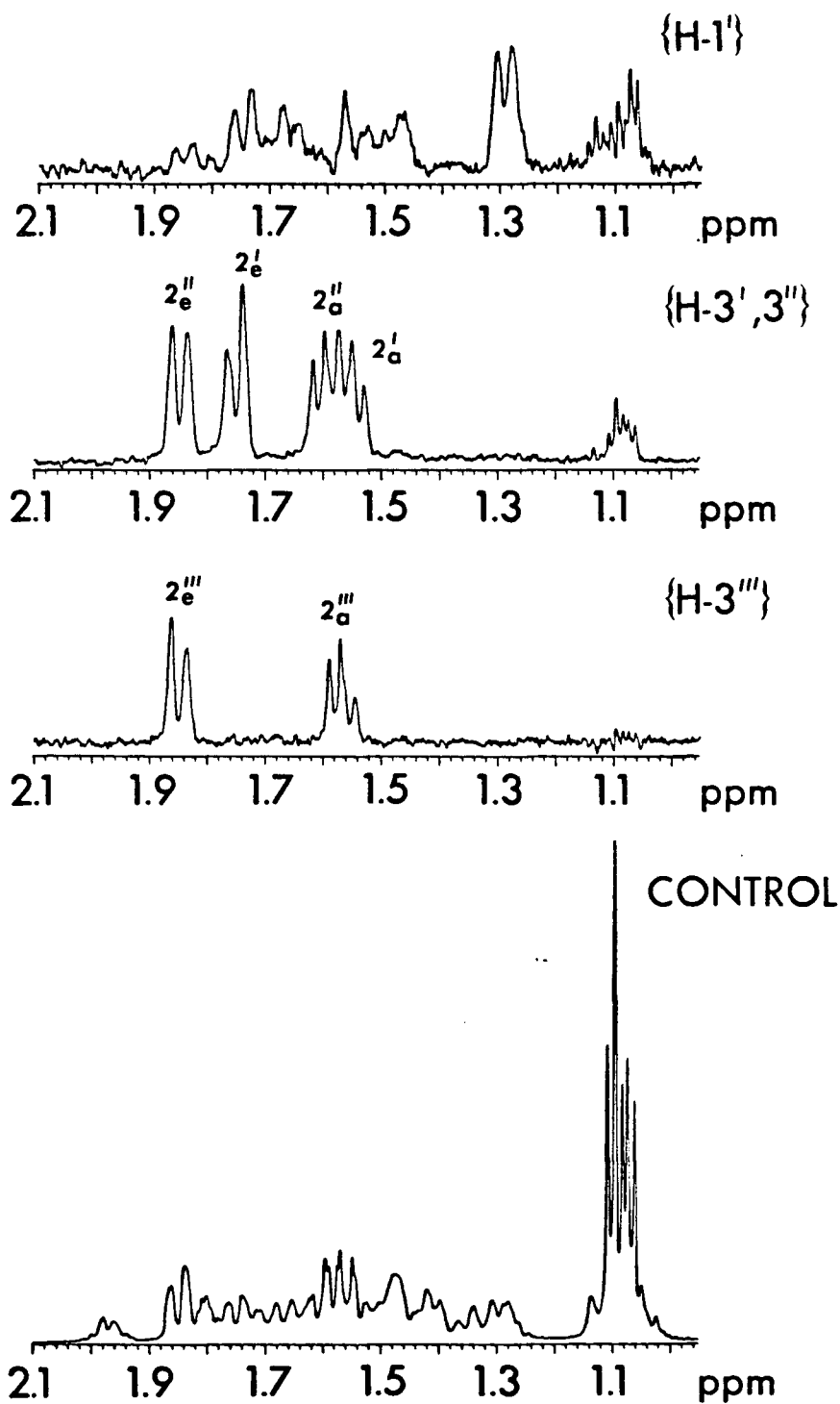
Fig. II.5.7 Driven nOe experiments performed on digoxin, showing nOe's induced into the methylene/methine region.

hence, their cross-peaks are so close, verification for these assignments was sought from the nOe experiments.

Confirmation of the digitoxose H-2 protons' assignments comes from the three nOe experiments, illustrated in Fig. II.5.7. Irradiation of (equatorial) H-3''' clearly shows H-2$_e$'' and H-2$_a$''. Irradiation of H-3' and -3'' induces nOe's in the indicated geminal protons; H-2$_e$' and H-2$_e$'', and H-2$_a$' and H-2$_a$'' are differentiated by the COSY experiment (Fig. II.5.6) which shows the connectivities from H-1' to H-2$_e$' to high field of H-2$_e$'' and H-2$_e$''' (which are coincident) and H-2$_a$' to high-field of H-2$_a$'', based on the connectivities from H-3', 3''. The experiment involving irradiating of H-1' is included (<u>vide</u> <u>supra</u>).

The carbohydrate H-5 region assignment was confirmed by the nOe experiments indicated in Fig. II.5.8. By irradiating H-1', or H-1''
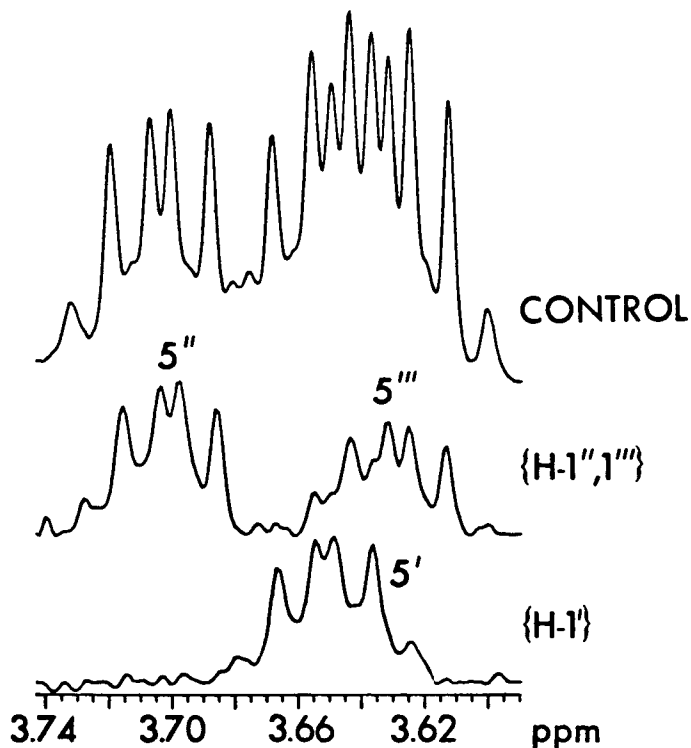
Fig. II.5.8 Driven nOe experiments showing nOe's induced into digitoxose H-5 protons by irradiating H-1', or H-1'' and H-1'''

Table II.5.2 Average interproton distances between -Me(18) and -Me(19),
and steroid ring protons.

	$\lvert r \rvert$ (Å)
C(18)-H$_3$ —— H-11$_a$	2.868
H-8	3.193
H-17	3.398
H-12	3.680
H-23$_{a,e}$	3.088, 4.410
H-22	3.982
C(19)-H$_3$ —— H-1$_{a,e}$	2.621, 2.825
H-8	2.732
H-5	2.762
H-11$_a$	2.887
H-6$_a$	2.999

plus H-1''' an nOe is induced in the corresponding H-5 with which it has a 1,3-diaxial relationship.

A number of further checks were performed which confirmed the previous assignments. Irradiation of H-5' and -5''' induced nOe's into H-4''' and the lower-field of the H-4'/H-4'' overlapping resonances, and confirmed assignments of H-1' and H-1''' (data not shown). This complemented the experiment where H-5'' was irradiated. It is clear that a carefully selected array of irradiation experiments has, in addition to providing assignments, the added bonus of enabling previous assignments to be checked or confirmed; hence, such a series of experiments provides a "network" of assignment information.

These nOe experiments shed some light on the steroid assignment, but far less than one might have anticipated. It is well known[10] that the axial methyl groups (C-18 and C-19) can act as "transmitter beacons" to induce responses from axial protons which are near them in space. When the $C(18)-H_3$ protons are irradiated, one might expect nOe's with H-11$_a$, H-8 on the β-face of the steroid, and H-12 and H-17. Further, one might expect an nOe into ring E, depending on its orientation. The cis C,D ring-fusion results in the protons on C-15 and C-16 being too far from -Me(18) to have an nOe induced. Irradiation of $C(19)-H_3$ is unlikely to be of much use in assigning protons on ring A, as a result of the cis A/B ring junction. Protons referred to in the following discussion are listed in Table II.5.2, with the internuclear separations calculated from the X-ray data[4].

Irradiation of -Me(18) induces the expected nOe's. At δ < 2.1, we note two nOe's - one into H-8 (δ 1.48) and the other, H-11β (δ
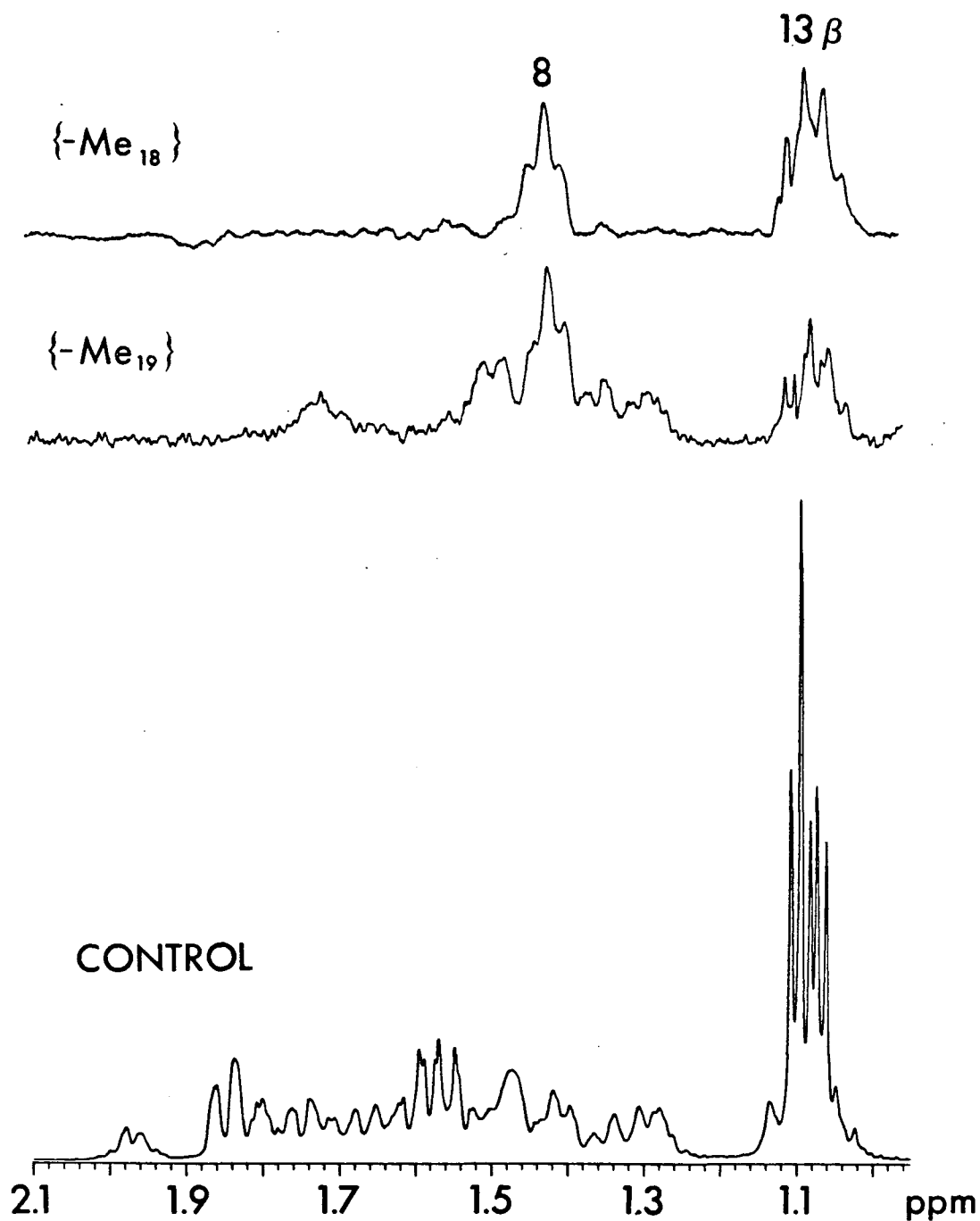
Fig. II.5.9 Driven nOe experiments with steroidal methyl peaks
irradiated; the displayed region is that of the
methylene/methine protons, although other nOe's are
evident to lower field.

1.12). This assignment is consistent with the COSY data, where a correlation exists between H-17 and H-16, but none between H-17/H-12 and H-8. Since both proton multiplets are overlapping with other signals, the enhancement factor cannot be reliably quantified. An nOe is seen at δ 3.2 where H-12 and H-17 overlap, but this is likely to include nOe's into both protons. (Based on their solid-state interproton distances, H-12 would be expected to show 70% the nOe of H-17). Significant nOe's are seen in all three protons on ring E.

Irradiation of -Me(19) also reveals significant nOe's in H-8 and H-11β. A total of six protons in the methylene/methine region display nOe's, consistent with the six protons having interproton separations < 3.0 Å, listed in Table II.5.2. No cross checks can be made, since the multiplets overlap with the signals from their closest neighbours.

Irradiation of H-22 results in an nOe in H-17, allowing it to be distinguished from H-12 (data not shown). The proton assignment is far from complete, still much information has been gleaned. With the assignments resulting from the nOe experiments, little is to be gained by returning to the COSY map for the crowded methylene/methine region. Far fewer cross-peaks are distinct than anticipated; this will be discussed later in the chapter, along with other observations relating to the performance of all the experiments described.

Before leaving the ^{1}H NMR data it is interesting to look at the digitoxose sugar assignments in the light of predictions on the self association of the molecule in solution. Such a system would have relatively mobile, solvated sugars extending from the aggregated phase.

Fig. II.5.10 CSCM experiment (^{1}H, 360 MHz) performed on digoxin.
The low-field regions are presented as a
stacked-plot.

Fig. II.5.11 The high-field region of the CSCM data-set in fig.
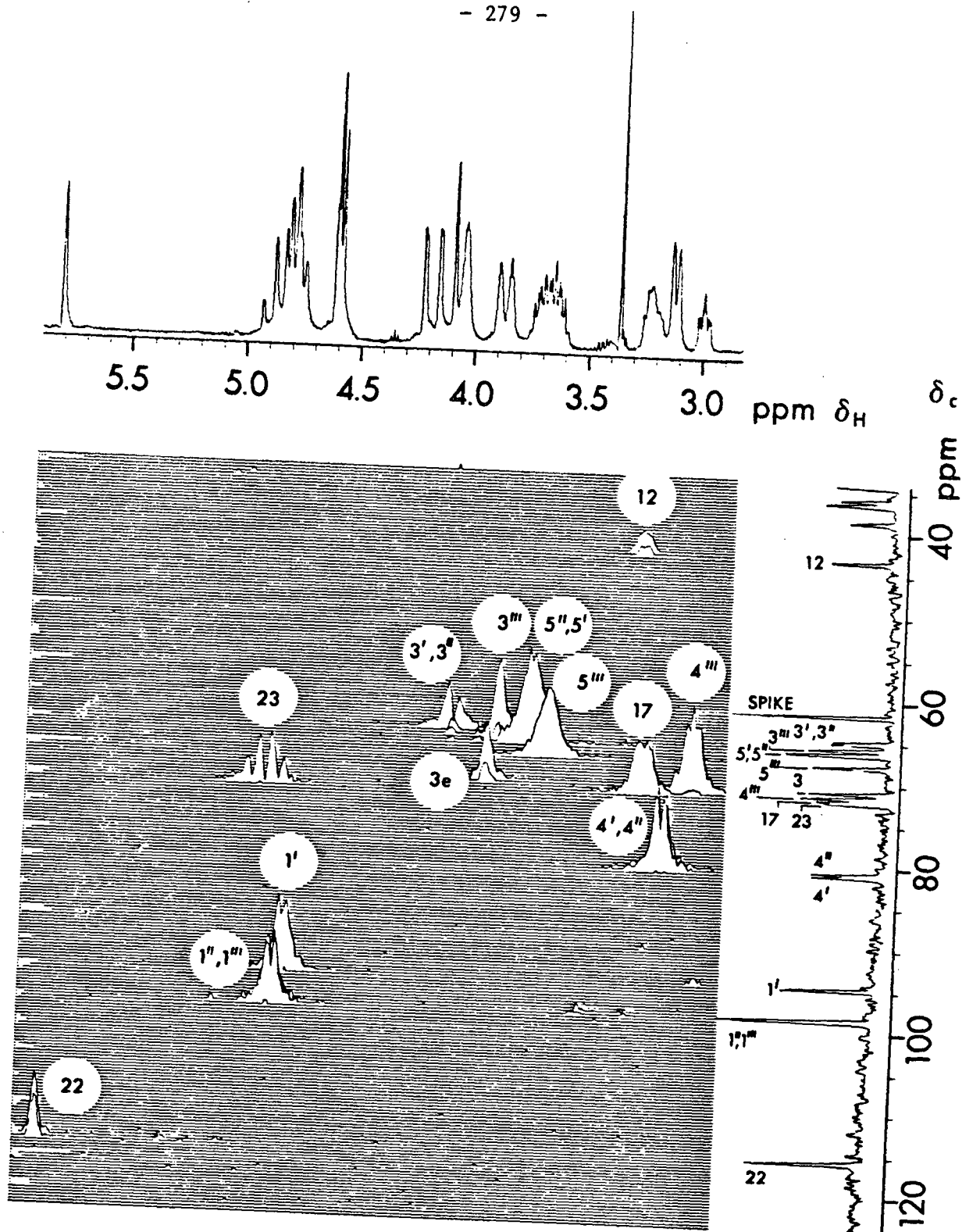II.5.10 is plotted between the frequency limits
indicated.

Hence, one might expect the terminal digitoxose ring III to have more mobility (and, therefore, narrower lines) than ring II, and likewise even more mobility than ring I. Since the coupling pattern for each proton at a particular position on all rings is the same, we can consider peak height to be a reflection of peak width (and $\underline{T}_2$). With the eye of faith, it is clear that this is so for all the observable resonances to lower field; ring III appears to have greater mobility than ring II and still greater than ring I.

We now turn our attention to the ^{13}C data. The broad-band decoupled ^{13}C NMR spectrum of digoxin in DMSO-$\underline{d}_6$ is well dispersed with few overlapping lines. The CSCM experiment was performed and parts of the resultant data-table are presented in Figs. II.5.10 and 11. Those ^{1}H assignments made were used to assign the corresponding ^{13}C signals. [13]C signals between δ_C 40 and 120 produced correlations in the ^{1}H spectrum between δ_H 2.9 and 6.0; all protons in this region were assigned. The ^{13}C NMR assignments followed smoothly provided it was not the case that both the ^{1}H signals and the ^{13}C signals were very close. The ^{13}C assignments are given in Figs. II.5.10 and 11. In the proton methylene/methine region, eleven assignments were made and the ^{13}C signals were readily correlated. The steroid methyl carbons were readily identified (data not shown). All the above assignments were checked with the literature,[5] and were in agreement.

Whilst the exercise of extracting an $\underline{F}_1$ (^{1}H) trace for each ^{13}C signal was performed, no proton assignments were made on this basis. Our spectra were run with the molecule dissolved in DMSO-$\underline{d}_6$ whilst Brown et al.[6] used $CDCl_3$:DMSO-$\underline{d}_6$ (1:2); small but sometimes significant

differences in chemical shifts were apparent, making such comparisons dangerous. It is significant to note that if the ^{13}C NMR spectrum were fully assigned, the ^1H NMR assignment would easily follow from the CSCM experiment.

The large discussion on the ^1H NMR vs. the ^{13}C NMR data in this chapter invites a few remarks. Although the ^1H spectra are more complicated (inclusion of J; smaller intrinsic dispersion) they have the higher information content. In that more parameters are represented, a wider range of experiments is possible; however, these have a limit which, in this case, is determined by the extensive overlap of T_2-broadened signals in the methylene/methine area. The ^1H NMR spectrum would have been easier to assign had the A/B and C/D ring junctions been trans, since this would have permitted considerably more information to result from the nOe experiments where methyl groups were irradiated. On the other hand, although the ^{13}C NMR spectrum is much simpler, it is equally difficult to assign in isolation, for different reasons. T_2 line broadening no longer seems to pose a serious problem, but now the difficulty in assignment seems to lie in the available procedures. We have seen that an assigned ^1H NMR spectrum can be used to assign a ^{13}C NMR spectrum (Chapter II.4) and the same is true here, where ^1H assignments are known. However, for those $^1H - ^{13}C$ pairs for which the ^1H assignment is not available, further experimentation is somewhat limited, and one is driven to consider other procedures, such as comparisons of a series of structurally related molecules.

Although it is probable that further spectroscopic aids to ^{13}C NMR assignments will emerge, there is only one contender at present.

The 2D INADEQUATE experiment[7] can undoubtedly prove useful. The obvious problem for digoxin is the preparation of a sufficiently concentrated solution to enable the experiment to be performed in a realistic time period. A less obvious problem may be associated with second order distortions resulting from the relatively small chemical shift range in which the (coupled) ^{13}C resonances occur. It has been demonstrated with carbohydrate spectra that the experiment may require compensation for such effects;[8] this is not unreasonable when one considers that $^2\underline{J}$ (^{13}C $- ^{13}$C) = $\underline{ca}$. 40 Hz, and carbon resonances from similar centres fall into fairly narrow ranges (e.g. 3', 3'', 3''', 5', 5'' and 5''' within 4 p.p.m.).

In concluding this chapter it is important to consider the limits of the various experiments actually used and the effects of those limits on the general strategy postulated in earlier chapters.

The 2D $\underline{J}$-resolved experiment worked satisfactorily for those resonances having longer $\underline{T}_2$ values which were, mostly, protons attached to heteroatom-substituted carbons. Unfortunately, these were precisely the resonances which were not difficult to distinguish in the 1D experiment, as they were deshielded and resonated out of the methylene/methine region. And unfortunately the resonances in the range δ 1.0 to 2.1 had $\underline{T}_2$ values which were too short. Thus, in contrast to earlier experiences, the 2D $\underline{J}$-resolved experiment proved to be disappointing.

The COSY experiment was very useful for the low-field region. Notwithstanding the coarse digitization ($\underline{ca}$. 10 Hz pt^{-1}), correlations

to protons only a few Hz apart could be reliably differentiated. It is critical to note that this was only possible with <u>like protons</u> (e.g. H-3' and H-3'') where the two correlation peaks have very similar patterns. By comparison, it was not possible on a first inspection to discern correlations between H-12 or H-17 and the high-field region. Also, coupling pathways to (broader) proton resonances to high field in the methylene/methine region were clear (e.g. H-3$_e$). In the high-field region, far fewer cross-peaks appeared than expected. This is probably the result of two factors, cross-peak overlap and the attenuation of the (broad) high-field signals by the necessary sinebell apodization function. Unfortunately without the latter, extensive "tailing" occurs which can lead to false "cross-peaks" where they interfere.[9] The question of attenuation by the apodization function may be partly remedied by using a less severe function (e.g. the double-exponential function), and by using a smaller block-size and zero-filling to give adequate digitization.

The driven nOe experiment proved quite useful as a qualitative rather than quantitative tool. Quantitations were limited by unfortunate signal overlap in the low-field region even at 500 MHz which made selective irradiation difficult, and overlap in the high-field region which made the determination of fractional enhancements nigh on impossible. The procedure of assigning, e.g. the irradiated methyl protons an area of 300 "units", in the difference mode, and induced intensity enhancement calculated by area relative to this, did not prove successful when compared with expected ratios based on known

distances from the solid-state. This could either be a result of the

break-down of the simplified equations, resulting from the anisotropic

motion, or the difficulty in measuring an nOe of a proton directly under

the digitoxose methyl signals. Nevertheless, qualitatively, the

experiment performed well, within the usual restrictions of

non-overlapping resonances in the 1D experiment.

The CSCM experiment worked extraordinarily well and seems well

suited to a system of this nature. Within the limits of digitization,

the ^{1}H line-shapes ($\underline{F}_1$) were easily recognizable. It is without doubt

that almost all proton assignments could be made if the ^{13}C signals were

credibly assigned. In some ways this is the most important fact to

emerge from this digoxin study. It calls for a change in the protocol

found most effective with derivatized oligosaccharides and brucine.

There the initial emphasis was on the total assignment of the ^{1}H NMR

spectrum, followed by assignment of the ^{13}C NMR spectrum on the basis of

the CSCM experiment. With digoxin, where the ^{1}H NMR spectrum is

difficult to fully assign even at 500 MHz, a more effective approach

would probably be to first assign as much of the ^{1}H NMR spectrum as

possible using the methods described above, and then concentrate on the

total assignment of the ^{13}C NMR spectrum. To this end, the 2D

INADEQUATE experiment should be performed, but a paucity of instrument

time prevented this in a reasonable time period. With this information,

completion of the ^{1}H NMR assignment would be trivial.

In conclusion, this study on digoxin indicates that not all the

procedures described in previous chapters can be relied upon for studies

of molecules which have broad, strongly overlapping resonances. In particular, the homonuclear 2D experiments appear to be less than optimal in this regard. Of the alternative experiments, CSCM operates best in this milieu, with the fundamental limitation that the ^{13}C NMR spectrum must be assignable. To this end, the 2D INADEQUATE experiment should be performed to complete this chapter.

REFERENCES

1. L.F. Fieser and M. Fieser. Steroids. Reinhold Publishing Corporation, New York. 1959. pp. 752-754.

2. J.H. Hoch. A survey of cardiac glycosides and genins. University of South Carolina Press. 1961.

3. S. Smith. J. Chem. Soc. 508-510 (1930).

4. K. Go, G. Kartha, and J.P. Chen. Acta Cryst. B36, 1811-1819 (1980).

5. C. Altona and C.A.G. Haasnoot. Org. Magn. Reson. 13, 417-429 (1980).

6. L. Brown, H.T.A. Cheung, R. Thomas, T.R. Watson, and J.L.E. Nemorin. J. Chem. Soc., Perkin Trans. 1. 1779-1781 (1981).

7. A. Bax, T.A. Frenkiel, R. Freeman, and M.H. Levitt. J. Magn. Reson. 43, 478-483 (1981).

8. S.L. Patt. Carbohydr. Res. In press.

9. A. Bax and R. Freeman. J. Magn. Reson. 44, 542-561 (1981).

II.6   EXPERIMENTAL FOR SECTION II

In general, all spectra reported at 270 MHz were recorded on a home-built spectrometer based on an Oxford Instruments superconducting magnet ($\underline{B}_o$ 6.35 T), a Bruker WP-60 console, and Nicolet 1180 computer and 293B pulse-programmer. Unless stated otherwise, standard NTCFTB soft-ware was used with this instrument. Spectra at 400 MHz (^{1}H) were recorded on a Bruker WH-400 instrument, having a 9.4 T magnet. The operating program in routine use was DISNMRP. Five hundred and 360 MHz spectra were performed using Nicolet spectrometers at the factory in California.

It is the author's opinion that a detailed documentation of all parameters for each experiment would not be useful, since these will vary widely depending on the instrument being used. It is useful, however, to document any extra pieces of information which are relevant to a particular experiment, and not mentioned in the text.

For ^{1}H experiments, the 180° pulse-length was determined (zero intensity cross-over), and all pulse-lengths calculated from this. For ^{13}C observe the procedure was the same, often using a reasonably concentrated "dummy" sample in a similar solvent to that in which the molecule of interest was dissolved. Proton pulses through the decoupler channel on the ^{13}C probe were determined by the methods outlined in the text.

When attempting an experiment for the first time, it is common to begin with a very simple molecule at high concentration. Knowing the molecule's geometry, $\underline{T}_1$ parameters, etc. can greatly assist in the

initial evaluation, or "debugging" of an experiment. With heteronuclear correlation experiments in this thesis, for example, a concentrated solution of n-propanol was used to familiarize the operator with important parameters and experimental set-up.

For DEPT (II.2.2.2), the ^{13}C parameters were selected in the usual manner, and ^{1}H pulse-lengths "fine-tuned" by performing the experiment with $\theta = 90°$. When perfect cancellation of $-CH_2$ and $-CH_3$ peaks was achieved, the proton pulse lengths were correctly set.

With all homonuclear decoupling experiments (including nOe), a critical factor is the choice of decoupler power and position. Even with sufficient decoupler power, incomplete decoupling may result from the resonance frequency of the saturated spin changing while the decoupler is on. In most cases this is not too important a consideration, but it may be necessary to slowly move the decoupler frequency (in 0.5 Hz steps) to find the optimal position to effect perfect decoupling. This is particularly a consideration in spectrally crowded regions where decoupler selectivity is difficult to achieve. To achieve this selectivity is most difficult with the SDDS experiment (II.2.3) and it is fortunate that reliable two-dimensional experiments having none of these problems (e.g. COSY) may be resorted to.

With nOe experiments it is important to come as close to 100% saturation as possible, without leakage (or "spill-over") of decoupler power into spectrally close spins. This is easily checked before the experiment is done: the irradiation of the spin in the most crowded spectral region is used to determine the maximum permissible power,

without spill-over. No excessive time-averaging is necessary here, as one is not looking for very small (< 1%) changes in peak height. Such checks not only give the experimenter a degree of confidence, but the percentage saturation in each experiment may be useful information if certain comparisons are to be made.

This practice of collecting only the FID comprising the difference spectrum, and not both spectra individually, is not recommended, since (a) information is needlessly discarded, and (b) where multiple nOe experiments are necessary, more machine time will be required to accumulate the same data. With the procedure for SSNOEDS (II.2.4.1) in the text ($\underline{n}$ + 1) experiments are necessary for $\underline{n}$ nOe irradiations; if only the difference FID is collected, 2$\underline{n}$ experiments would be necessary to derive the same information.

When the sample concentration is low, demanding a very large number of scans to build up signal-to-noise, the author has found it useful to increase the repetition rate by (a) using no relaxation delay (b) decreasing the period of irradiation to $\underline{ca}$. 1 or 2 $\underline{T}_1$, and, to compensate for these alterations in the experimental scheme, (c) decreasing the tip-angle (from $\underline{ca}$. 80° to 60°). In such a way, four nOe experiments were possible in an overnight run with $\underline{ca}$. 2 mg of sample on a Bruker WH-400, allowing the detection of < 1% nOe's with confidence.

With the one-dimensional experiments discussed above, data storage space on hard disc is seldom limiting, and spectra can be acquired with good digitization. In the case of two-dimensional (2D) NMR experiments the reverse is often the case: long "acquisition times"

in t_1 may require large amounts of instrument time to acquire, large blocks of data to store, and long computation times for data-processing. It is therefore common to restrict the sweep-widths in both dimensions to the minimum possible value. If, for example, acetate peaks to high field have no information, they may be "folded" into the spectrum where they do not overlap with any other peaks. With this approach, the minimum block-size can be chosen in both dimensions and experimental times reduced.

With the 2D J-resolved experiment (II.2.5.2), fine digitization is not necessary in F_2, and the experiment should be optimized for digitization in F_1, the "J-dimension". In the interest of minimizing instrument time, it is common to collect data for 32 t_1 increments and zero-fill in F_1 to give the necessary digitization to resolve small couplings. Although the author has not had opportunity to assess symmetrization procedures in this experiment, it is quite likely they will be extremely useful since second-order artefacts are seldom symmetrical about $F_1 = 0$ and such a procedure should prove useful in identifying such peaks and simplifying the spectrum. Other advantages of this procedure are mentioned in the text.

We have had cause to use the COSY experiment (II.2.5.3) quite extensively in this study, and have found it remarkably resistant to abuse. Pulse-angles need only be set to ± 10%, and coarse digitization (e.g. 5 Hz/pt) is often sufficient. The data may be acquired quite rapidly (ca. 0.2 sec. relaxation delay) and the sinebell apodization function is almost always appropriate for both dimensions. The Jeener

experiment is so powerful that, given a state-of-the-art spectrometer, it is arguable whether SDDS methods are justifiable.

The important heteronuclear chemical shift correlation (CSCM: II.2.5.4) is described in some detail in the text and a discussion on a "typical" set-up procedure is included.

The author has not had time to thoroughly evaluate the 2D nOe experiment (NOESY: II.2.5.6). Probably the most difficult decision with this experiment is choosing an optimal mixing time. In the slow tumbling regime, a "crude" driven nOe experiment (II.2.4.3) should indicate the rate of nOe build-up and allow an optimal τ_{mix} to be chosen. In the fast tumbling regime, a valid approach might be to first perform a "crude" transient nOe experiment (II.2.4.2) in order to characterize a "typical" nOe build-up curve and facilitate the choice of a useful τ_{mix}. Cross-peaks are small in this latter experiment, and symmetrization of the data-set will almost certainly be necessary. As is the case with COSY, coarse digitization will often suffice, thereby reducing the time required to collect the data for this somewhat long experiment.